Australian Government
Geoscience Australia

Uranium ore-forming systems of the Lake Frome region, South Australia:

Regional spatial controls and exploration criteria

Roger G. Skirrow (editor)

Record
2009/40

GeoCat #
69697

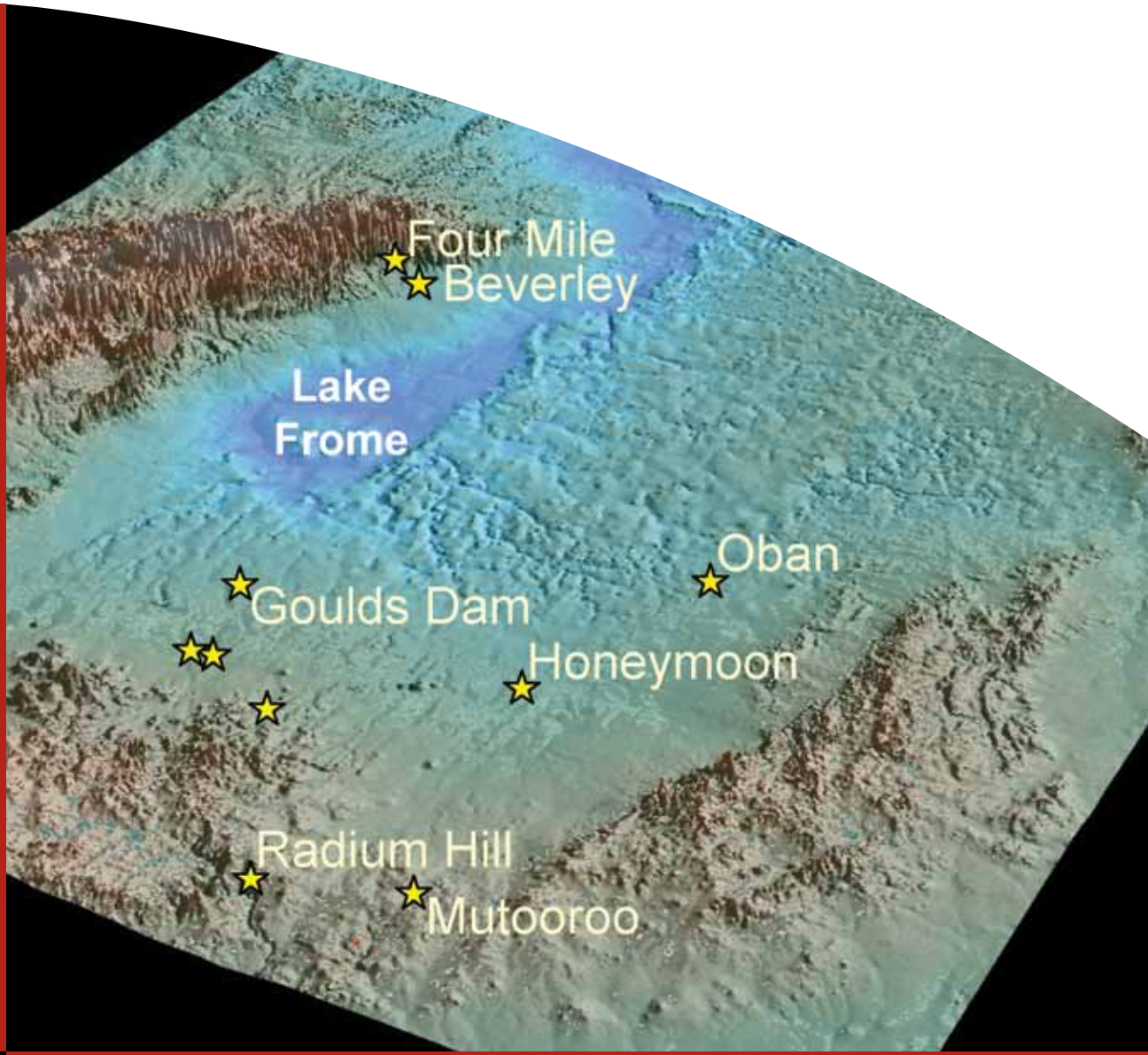

Uranium ore-forming systems of the Lake Frome region, South Australia: Regional spatial controls and exploration criteria

GEOSCIENCE AUSTRALIA
RECORD 2009/40

by

Roger G. Skirrow[1] (editor)

With contributions from Evgeniy N. Bastrakov[1], Allison F. Britt[1], Andrew Cross[1], Steven M. Hill[2], Steven B. Hore[3], Subhash Jaireth[1], Mäité Le Gleuher[1], Anthony Schofield[1], Roger G. Skirrow[1], and Simon E. van der Wielen[1]

1. Geoscience Australia
2. The University of Adelaide
3. Primary Industries and Resources South Australia

Department of Resources, Energy and Tourism
Minister for Resources and Energy: The Hon. Martin Ferguson, AM MP
Secretary: John Pierce

Geoscience Australia
Chief Executive Officer: Dr Neil Williams PSM

ISSN 1448-2177
ISBN 978-1-921672-39-2 print
ISBN 978-1-921672-37-8 web

GeoCat # 69697

Bibliographic reference:

To cite the entire Geoscience Australia Record:

Skirrow, R.G., 2009 (editor). Uranium ore-forming systems of the Lake Frome region, South Australia: Regional spatial controls and exploration criteria. Geoscience Australia Record 2009/40, 151 p.

To cite individual chapters in the Record, e.g.:

van der Wielen, S., Britt, A., and Skirrow, R.G., 2009. Chapter 3. 3D architecture and permeability. *In* Skirrow, R.G. (ed.), Uranium ore-forming systems of the Lake Frome region, South Australia: Regional spatial controls and exploration criteria. Geoscience Australia Record 2009/40, p. 20-42.

Contents

Abstract....1
1. Introduction....3
1.1 Purpose of the study....3
1.2 Mineral systems approach....3
1.3 Application of mineral systems approach to uranium in the Lake Frome region....6
1.4 Report structure....10
2. Uranium sources: lithology and stratigraphy....12
2.1 Lithostratigraphy of the Proterozoic basement....12
2.2 lithostratigraphy of phanerozoic basins....13
2.2.1 Paleozoic – Arrowie Basin....14
2.2.2 Mesozoic – Eromanga Basin....14
2.2.3 Cenozoic – Lake Eyre Basin....16
2.2.4 Quaternary....17
3. 3D architecture and permeability....19
3.1 Introduction....19
3.2 Tectonic and thermal evolution....19
3.3 Structural architecture and basin fill geometry....21
3.3.1 Data compilation for 3D geological map construction....21
3.4 Results....35
3.4 Results....36
3.4.1 3D structure....36
4. Uranium depositional gradients and chemical architecture....42
4.1 Introduction....42
4.2 Method for mapping and modelling the geological and chemical architecture....42
4.2.1 Datasets for the Lake Frome region....45
4.3 Voxet lithology model of EL5 and 6....47
4.4 3D chemical architecture....47
4.4.3 Distribution patterns of selected materials in ELs 5 and 6....50
4.5 Discussion....53
4.5.1 Reliability of the 3D chemical maps....53
4.5.2 Sediments and redox....53
5. Uranium deposits of the Lake Frome region....57
5.1 Beverley uranium deposit....57
5.2 Four Mile deposit....60
5.3 Honeymoon uranium deposit....61
5.4 Timing of uranium mineralisation: hypotheses....65
5.4.1 Maximum ages of mineralisation....65
5.4.2 Mineralisation timing constraints from uplift and cooling history....65
6. Four Mile uranium deposit: mineralogy....67
6.1 Introduction....67
6.2 Samples and analytical procedures....67
6.3 Mineralogy....67
6.3.1 Detrital phases....67
6.3.2 Post-depositional phases....69
6.3.3 Uranium-hosting mineralogy....73
6.4 Comparison with the Beverley uranium deposit....76
6.5 Discussion....77
6.6 Conclusions....79
7. Numerical modelling of regional fluid systems and uranium mineralisation....80
7.1 Introduction....80
7.2 Objectives and methodology....80

7.2.1 Objectives of the study 80
7.2.2 Geological constraints 80
7.2.3 Building simplified 2D geological models for fluid flow modelling 84
7.2.4 Representation of results – fluid flow modelling 85
7.3 Results and discussion – fluid flow modelling 86
7.3.1 Fluid flow scenarios in the Beverley – Four Mile district 86
7.3.2 Uranium mass balance calculations – Four Mile East deposit 88
7.4 Geochemical modelling of Frome uranium systems 96
7.4.1 Methodology and model setup 96
7.4.2 Granite-water interaction (modelling Paralana Hot Springs) 97
7.4.3 Modelling granite-water-sandstone interaction (formation of sandstone-hosted uranium mineralisation) 99
7.4.4 Summary of geochemical modelling results 100
7.5 Conclusions – numerical modelling 101
8. Synthesis, and implications for exploration 102
8.1 Essential components of basin-related uranium mineral systems of the Lake Frome region 102
8.1.1 Sources of ore constituents and fluids 102
8.1.2 Energy and timing 104
8.1.3 Permeability architecture and fluid flow 104
8.1.4 Depositional gradients for uranium mineralisation 107
8.2 Paleogeographic and uranium mineral system evolution 108
8.3 Exploration criteria 111
8.3 Recommendations for further work 111

References 114

Appendix 1: Field guide to the Proterozoic Mt Painter Inlier and Mesozoic to Cenozoic basins of the Lake Frome region 120

Appendix 2: Metadata for 3D geological maps, Figures 3.3-3.7. 140

Abstract

Cenozoic basins of the Lake Frome region in South Australia contain most of the nation's known resources of sandstone-hosted uranium mineralisation. In addition to the currently operating Beverley uranium mine, two other deposits have been approved for mining (Honeymoon, Four Mile East), and discoveries continue to be made in the region (e.g., Pepegoona; Heathgate Resources, announcement September 2009). While the known resources are significant, the potential of the region for very large uranium deposits has not been well understood, in part due to limited knowledge of the regional- and district-scale geological controls on uranium mineralisation.

The multidisciplinary study reported herein applies a 'mineral systems' approach to identify and map the principal geological controls on the location of known uranium mineralisation in the Lake Frome region. This new framework is aimed at providing a basis for refined exploration targeting of areas with potential for major undiscovered deposits, thus reducing risk in investment by the exploration industry.

Mineral systems approach – Major ore deposits are the product of crustal- to deposit- to micro-scale geological processes, and require the presence of (a) suitable *sources* of metals, fluids (aqueous, magmas, etc), ligands (for hydrothermal deposits), sulfur (for sulfide deposits), (b) permeable pathways or *permeability architecture* for transport of metals and for focussing and outflow of fluids, (c) *energy* sources to drive the ore-forming system, and (d) chemical and/or physical *depositional gradients* where the ore metals are precipitated. Suitable sources, permeability architecture, and physico-chemical gradients occur only in specific 'fertile' terranes that have experienced favourable geodynamic and tectonic evolution, and where the sequence of geological events permits an efficient physical link (permeability architecture) between the sources regions and the ore depositional environments. The present study aims to identify and map the geological 'proxies' (i.e., observable geological features) for each of the four mineral system components. In addition, successful exploration for major uranium or other deposits requires that the deposits are preserved at depths accessible to exploration methods.

Sources of U, fluids, ligands – It is widely assumed the uranium was sourced from the uranium-rich Proterozoic basement in the region, or from sediments derived from such basement. The Beverley deposit is hosted by sands of the Oligocene-Miocene Namba Formation, whereas the other known deposits in the region are hosted by sands of the Eocene Eyre Formation. Here we present an hypothesis for leaching of uranium from basement as it was exhumed during three major episodes of uplift since the late Mesozoic. The highly oxidised waters required to transport major quantities of uranium are assumed to have been meteoric waters and groundwaters, which in our hypothesis were maintained at high oxidation state within zones of deeply weathered and oxidised basement.

Energy and timing – The occurrence of three major uplift episodes and three periods of deep weathering since the late Mesozoic may have been crucial for uranium ore formation in the Lake Frome region. In this hypothesis, basement uplift triggered increases in gravitationally-driven fluid flow through previously deeply weathered U-bearing source rocks and into adjacent basins. Numerical modelling confirms the greater fluid fluxes expected for geometries with higher relief (greater potential energy). As a consequence, we infer development of three uranium mineral systems at different times since the late Cretaceous (see below). At least two of the periods of uplift were probably an intracontinental response to changes in motion of the Australian plate since ~40-45 Ma.

Permeability architecture – Permeable pathways for U-bearing fluids potentially include fractured and weathered basement, faults, and primary and secondary permeability within sediments and

sedimentary rocks. Previous published models depicting formation of the Four Mile and Beverley deposits within a single west-to-east fluid flow system are not supported by numerical simulations of simplified geological scenarios for this district. Either fluid flow occurred at different times to form the Beverley and Four Mile deposits, and/or the deposits formed in different west-to-east fluid flow pathways. Geological evidence from this district and elsewhere in the region points to broadly south-to-north or southwest-to-northeast direction of sediment transport in paleochannels within both the Namba Formation and Eyre Formation. Thus a viable alternative hypothesis is that known deposits in the Namba and Eyre formations formed during broadly south-to-north paleo-fluid flow, although present day groundwaters may have opposite flows in some paleochannels. Mapping of regional faults in 3D suggests that basin architecture and paleochannel orientations were controlled by broadly north-south striking faults, some of which were reactivated through the Paleozoic to Cenozoic. Hydrocarbon seeps indicate that some of these structures tap hydrocarbon reservoirs in the Arrowie and/or Eromanga basins, from which mobile reductants may have been sourced.

Depositional gradients – Reconnaissance petrography of relatively high-grade mineralisation in the Four Mile East deposit shows that uranium is predominantly hosted by uraninite whereas at Beverley the major ore mineral is coffinite. Oxidation-reduction processes were undoubtedly important in uranium deposition at both deposits, with evidence for the role of organic matter and reduced Fe^{2+} (ilmenite, pyrite) in redox reactions. However, other mineralogical differences support the hypothesis of differing timing and/or fluid chemistries in the Four Mile and Beverley systems. District- to regional-scale redox boundaries have yet to be mapped comprehensively, but their geometry will provide evidence of paleo-fluid flow directions. A new method of mapping redox variations in 3D has demonstrated the likely presence of a north-south trending paleochannel system, and/or redox interface, in the upper Namba Formation to the east of Lake Frome.

Exploration implications – Integration of results of this study supports a model of three potential episodes of basin-hosted uranium systems in the Lake Frome region. The Beverley deposit is proposed to have formed during the latest episode, whereas the Four Mile East deposit may have initially formed during either of the latter two ore-forming episodes.

1. Late Cretaceous-Paleocene uranium mineral system: Post-Eromanga Basin uplift of basement that was deeply weathered during the Mesozoic could have triggered gravitationally-driven flow of uranium-rich groundwaters into permeable units of the Eromanga Basin during the Late Cretaceous or Paleocene. Where suitable reductants were available, uranium mineralisation could have formed in the late Cretaceous or Paleocene. These systems potentially were large due to the effects of up to three episodes of oxidised fluid flow. Sub-basins isolated from present day groundwater flow in the Eromanga Basin may be most prospective for preserved mineralisation.
2. Late Eocene-Oligocene uranium mineral system: Post-Eyre Formation uplift and exhumation of the Mt Painter Inlier may have triggered fluid flow from basement areas (deeply weathered) into the Eyre Formation, utilising south-to-north oriented paleochannels. Fluids would have been confined by aquitards and aquicludes within the Eyre Formation, with mineralisation forming in the late Eocene to early Oligocene (~35-28 Ma). Large systems are possible particularly to the north, due to the opportunity for the Eyre Formation to have experienced at least two episodes of oxidised fluid flow.
3. Pliocene-Pleistocene uranium mineral system: Post-Namba Formation uplift and exhumation of basement rocks in the Lake Frome region occurred since ~5 Ma, producing most of the present day relief in the Northern Flinders Ranges and Mt Painter Inlier. Basement that was deeply weathered in the period ~10-20 Ma would now be available for leaching of uranium and transport into permeable units of the Namba Formation, Eyre Formation or Eromanga Basin. Larger uranium systems may exist to the north, where paleochannels converged or met lake systems.

1. Introduction

Roger G. Skirrow

1.1 PURPOSE OF THE STUDY

Australia holds the world's largest share of uranium resources (983,000 t U, 34%) in the Reasonably Assured Resources category, 'recoverable at <USD$80/kg U' (Geoscience Australia, 2008). These resources are dominated by the Olympic Dam iron-oxide copper-uranium-gold deposit (South Australia) together with significant resources in the Ranger and Jabiluka unconformity-related deposits and Yeelirrie surface-related deposit. Although Australia has several major deposits classified as 'sandstone-hosted', including the Beverley, Four Mile and Honeymoon deposits in the Lake Frome region of South Australia, no giant sandstone-hosted uranium deposits have yet been discovered in Australia, despite the presence of sedimentary basins with apparently favourable characteristics. Thus, in terms of resources, this type of deposit appears to be under-represented in Australia on a global comparative basis. The question arises as to whether there is significant potential in Australia for giant sandstone-hosted uranium deposits similar to those in Kazakhstan (e.g., Jaireth et al., 2008a), and if so what exploration criteria may be useful in basin area selection.

Through the Commonwealth Government's $59m Onshore Energy Security Program (OESP, 2006-11), Geoscience Australia is acquiring pre-competitive data in support of exploration for uranium and other resources. A key part of the OESP is an assessment of the potential for undiscovered uranium deposits, based on re-evaluation of (a) the fundamental processes required to form major uranium deposits, (b) the nature and distribution of uranium mineral resources in Australia, and (c) uranium exploration models and criteria.

The Lake Frome region was selected for study in the OESP because it is arguably Australia's foremost metallogenic province for sandstone-hosted uranium mineralisation and is considered to have high potential for further discoveries. Geoscience Australia's study reported herein has the following objectives.

1) Identify the principal regional- and district-scale controls on the location of known uranium mineralisation in the Lake Frome region, applying a 'mineral systems' approach.
2) Provide a new framework for uranium exploration and future assessments of the potential of basins in the region for undiscovered uranium resources, particularly those of large tonnage.

The Lake Frome study area covers approximately 150 000 km^2 (345 km x 450 km) in north-eastern South Australia (Figure 1.1).

1.2 MINERAL SYSTEMS APPROACH

The mineral systems methodology has been applied by Geoscience Australia in addressing Australia's uranium potential. Building on the framework developed by Wyborn et al. (1994), the mineral systems concept was reconfigured into the 'Five Questions' in the Cooperative Research Centre for Predictive Mineral Discovery (pmd*CRC, Barnicoat, 2007). More recently McCuaig and Beresford (2009) have further adapted the mineral systems approach to exploration targeting. The Five Questions are: (1) What are the geodynamic and pressure-temperature histories of the system? (2) What is the architecture of the system? (3) What are the fluid sources and reservoirs? (4) What are the fluid pathways and drivers of the system? (5) What are the metal transport and depositional mechanisms?

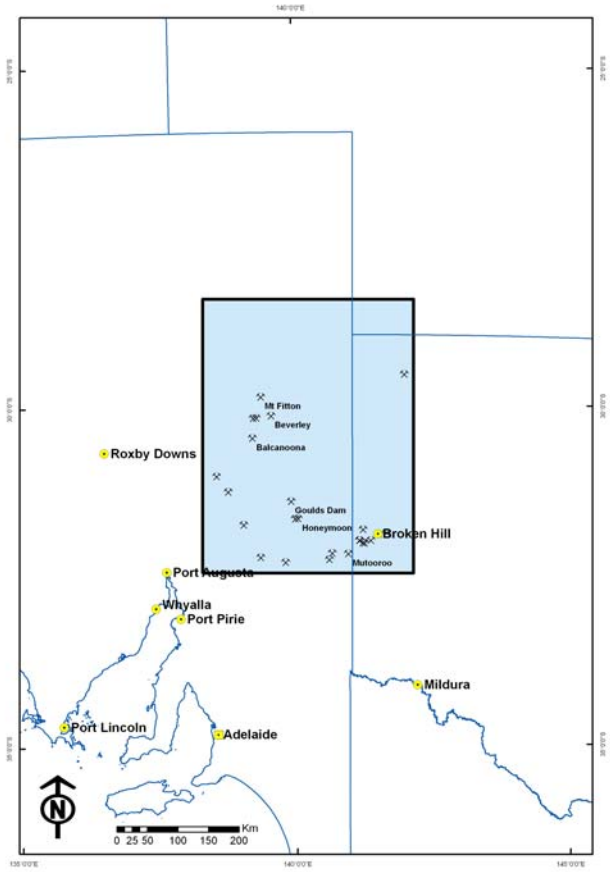

***Figure 1.1**: Location of the Lake Frome region study area. The coordinates of the northwest and southeast corners are 255 000mE, 6 850 000mN; and 600 000mE, 6 400 000mN, respectively (MGA94, Zone 54 coordinates). Crossed-hammer symbols show locations of uranium deposits and occurrences within the study area.*

The essence of all of these proposed schemes is that major ore deposits are the product of crustal- to deposit- to micro-scale geological processes, and require the presence of (a) suitable sources of metals, fluids (aqueous, magmas, etc), ligands (for hydrothermal deposits), sulfur (for sulfide deposits), (b) permeable pathways for transport of metals and for focussing and outflow of fluids, (c) energy source to drive the ore-forming system, and (d) chemical and/or physical gradients where the ore metals are deposited. Suitable sources, permeability architecture, and physico-chemical gradients occur only in specific 'fertile' terranes that have experienced favourable a geodynamic evolution that permits an efficient physical link (permeability architecture) between the sources regions and the ore depositional environments. These relationships are illustrated in Figure 1.2, which introduces the important notion of timing of ore-forming processes. It is self-evident that an effective mineral system demands that sources of ore components and fluids existed during and/or before the period when permeability was created. Similarly, the timing of energy input is crucial and must overlap temporally and spatially with the creation of permeability, otherwise energy is dissipated without major mass transport of ore components. On the other hand, physico-chemical gradients may develop well before the period of through-going permeability creation, for example a lithological contrast across a fault. Permeability is important across all scales from regional to micro. The permeability architecture must allow focussing or 'throttling' of fluid flow (McCuaig and Beresford, 2009) at progressively smaller scales to achieve the generally high fluid/rock ratios inherent in most hydrothermal ore deposits.

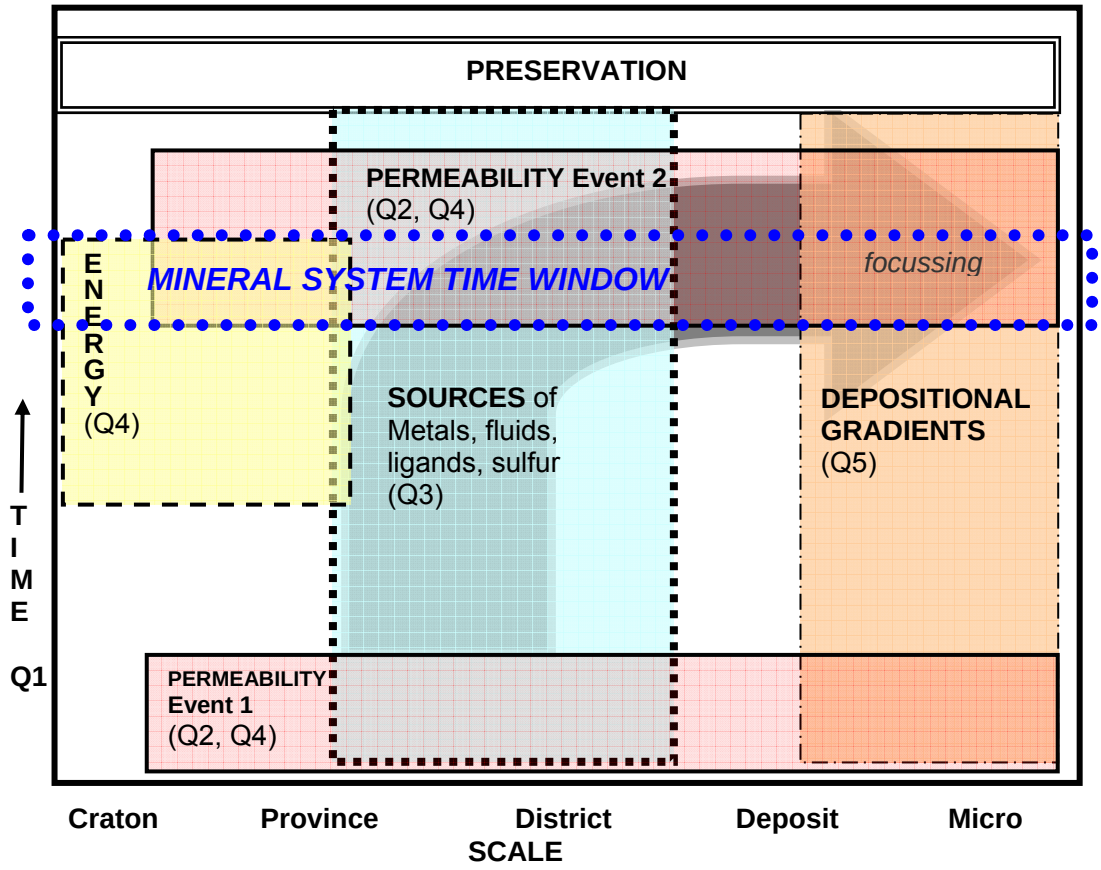

Figure 1.2: *Generalised evolution of a mineral system at varying scales, showing essential components (sources, permeability, energy, depositional gradients) and some of the geological features determining the nature of these essential components. This scheme integrates the Mineral Systems approach of Wyborn et al. (1994)), the Five Questions (Q1-Q5) approach of Walshe et al. (2005) and Barnicoat (2007), and the schema of McCuaig & Beresford (2009), and adds the time dimension and preservation component. Permeability architecture is a product of: tectonic/geodynamic history (Q1), fracture/fault/fold architecture (Q2), lithology, diagenetic evolution; Sources are a product of: geodynamic evolution, tectono-thermal evolution, and lithology; energy is a product of: geodynamic and tectonic evolution; depositional gradients are a product of: lithology, structure, and pressure-temperature-time evolution; preservation is a product of: tectonic evolution, mantle composition, and climate.*

The evolution of a mineral system may be represented as the large arrow, as metals and other ore components are progressively concentrated through time from regional- and district-scale sources into the depositional regime. Whether or not a mineralised zone is preserved at a depth accessible to exploration techniques is strongly dependant on the post-mineralisation geodynamic and tectonic evolution, and on climatic effects, all of which are operative at the full range of scales from craton to micro.

Figure 1.2 shows how Questions 1-5 of the pmd*CRC are important at differing scales and through the temporal evolution of a mineral system. Geodynamic evolution (Question 1) in part determines the character of the sources as well as the permeability architecture and nature of energy sources. Architecture (Question 2) is similar in concept to what is termed *permeability* here, although *permeability* is perhaps more specific to the requirements of a productive mineral system. Through-going permeable pathways for fluids are likely to be a subset of the complete architecture of the mineral system, and it is necessary to identify both the overall architecture and those parts that represent the permeable pathways. Hydrothermal alteration, for example, marks the passage of fluids and identifies permeability in the system. Question 5, fluid sources and reservoirs, is similar to *sources* in Figure 1.2 with the addition of metal, ligand and sulfur sources

here. Fluid flow paths and drivers (Question 4) combines aspects of the *energy* and *permeability* components in Figure 1.2. Finally, metal transport and depositional processes (Question 5) partly corresponds to *depositional gradients* here, although the transport aspects of Question 5 are embedded within the *source* component in our scheme. This is because a requirement of a productive mineral system is the presence of fluids of appropriate composition enabling transport of metals.

1.3 APPLICATION OF MINERAL SYSTEMS APPROACH TO URANIUM IN THE LAKE FROME REGION

The diverse range of uranium deposit types in Australia and globally may be grouped into families of uranium mineral systems that share particular ore-forming processes and that involve three fundamentally different fluid sources (Fig. 1.3, Skirrow et al., 2009).

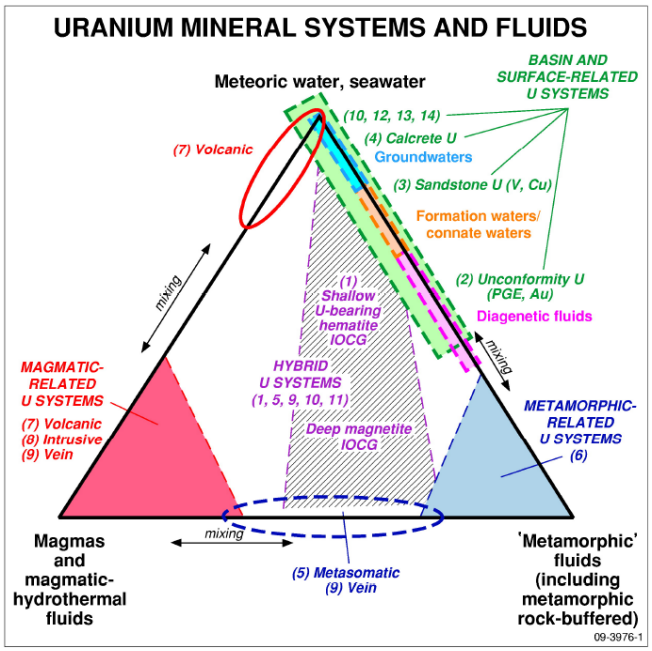

Figure 1.3: *Scheme of three families of uranium mineralising systems, and three end-member fluid types. For reference, numbered deposit types are from the IAEA Red Book, in order of economic importance in Australia. Source: Skirrow et al. (2009).*

The principal known uranium deposits in the Lake Frome region (Beverley, Honeymoon, Four Mile, Oban, Goulds Dam; Fig. 1.5) are conventionally placed within the 'sandstone' uranium deposit class, and include variations of the 'paleochannel' or 'basal channel' style (Beverley, Honeymoon) and perhaps 'roll-front' style (Four Mile). In a broader context, these 'sandstone' uranium deposits can be viewed as members of the family of basin- and surface-related uranium mineral systems (Figs 1.3, 1.4). Meteoric waters, groundwaters and formation waters are the principal fluids involved in uranium ore formation in the shallow parts of basins, and result in a continuum of deposit styles depending upon local basin lithology, structure and available reductants to remove uranium from the oxidised ore fluids.

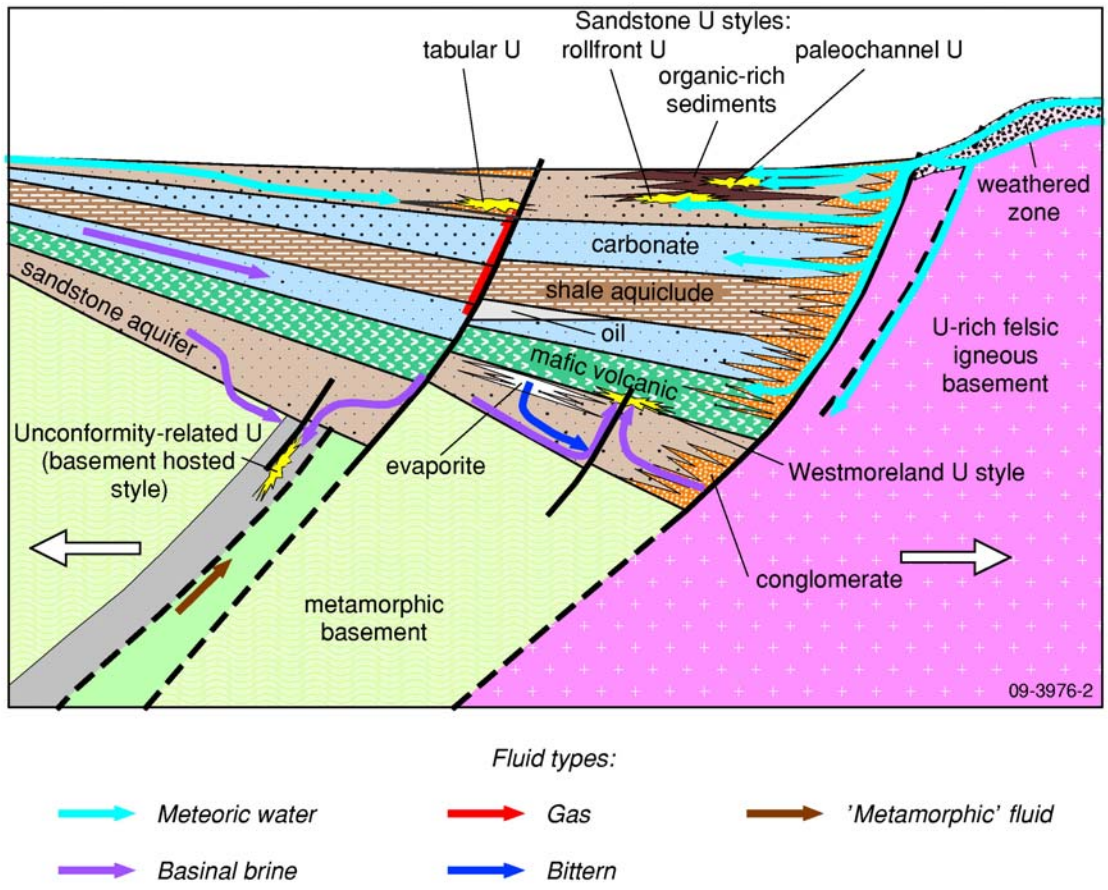

Figure 1.4: *Basin- and surface-related uranium mineral systems, during the extensional stage of basin development. A range of uranium depositional sites and deposit styles are represented in this basin-scale diagrammatic section. Source: Skirrow et al. (2009).*

To apply the mineral systems approach to uranium in the Lake Frome region we first present a 'straw man' model of basin-related uranium mineral systems in Figure 1.6, using the template of Figure 1.2. This 'straw man' is based on published deposit and regional geological data. Implicit in this diagram is the concept of multiple working hypotheses for the formation of uranium mineralisation in the Lake Frome region. For example, multiple possible energy sources are included for completeness. The study aims to identify and map the geological 'proxies' (i.e., observable geological features) for each of the mineral system components: sources, permeability architecture, energy, and depositional gradients.

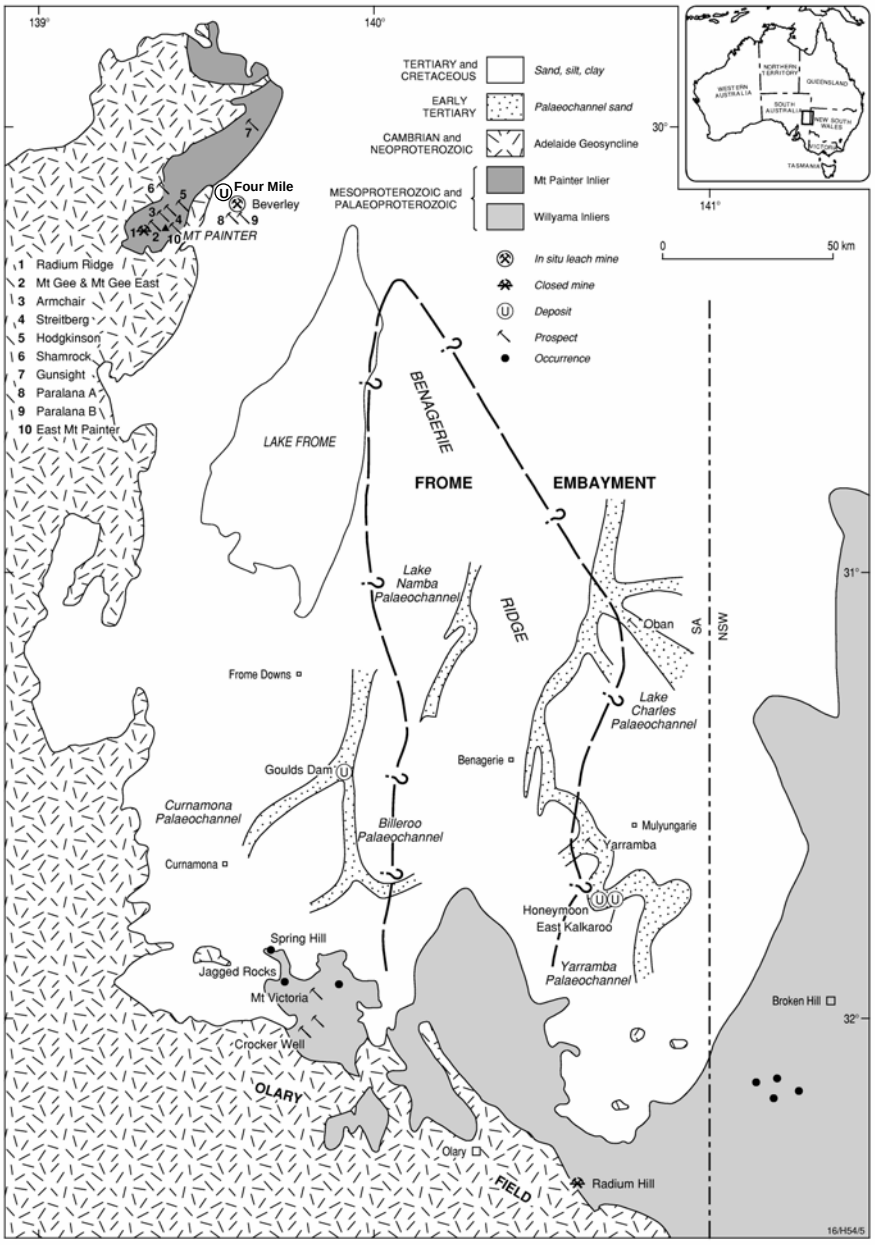

Figure 1.5: *Locations of uranium deposits, known paleochannels, geological domains and uranium deposits and occurrences in the Lake Frome region (modified after Curtis et al., 1990).*

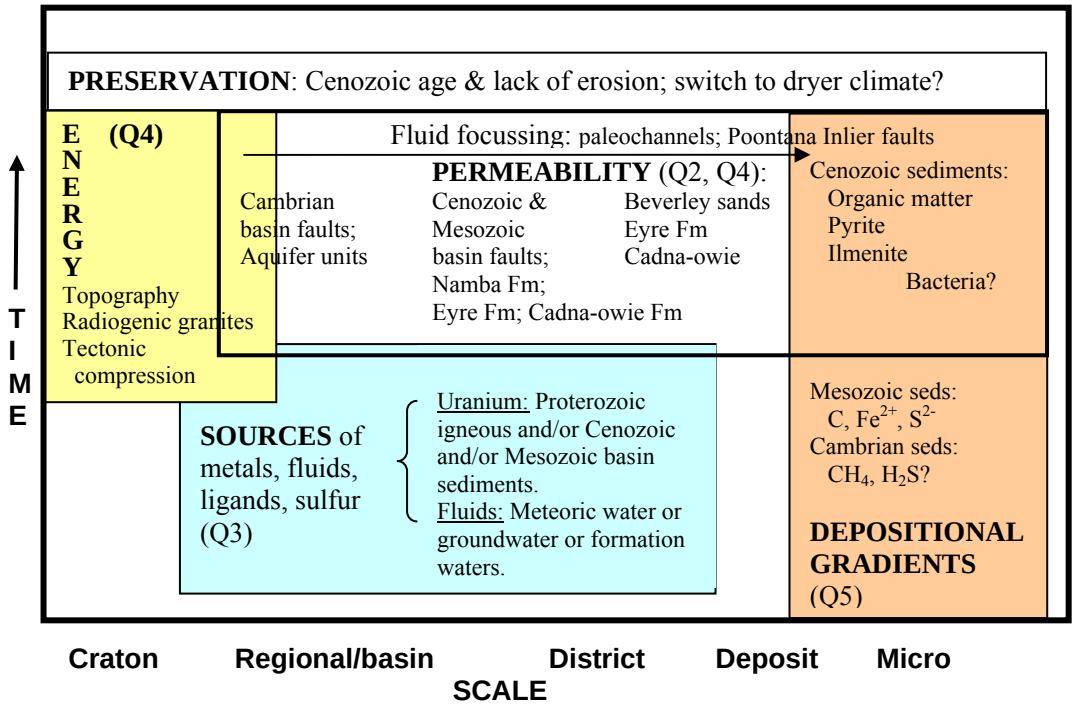

Figure 1.6: *Mineral system model for basin-hosted uranium mineralisation in the Lake Frome region.*

A published deposit model for uranium mineralisation in the Beverley – Four Mile area is shown in Figure 1.7. This site-specific model is based on the conventional generic model for sandstone-hosted roll-front type deposits, shown in Figure 1.8, which also shows the potential role of mobile reductants sourced from oil or gas reservoirs. Figure 1.6 differs in that it allows for multiple ore-forming scenarios, for example involving a range of depositional gradients or uranium sources. By identifying and mapping the mineral system components without bias towards any particular model we aim to generate new 'search spaces' for uranium exploration in the region.

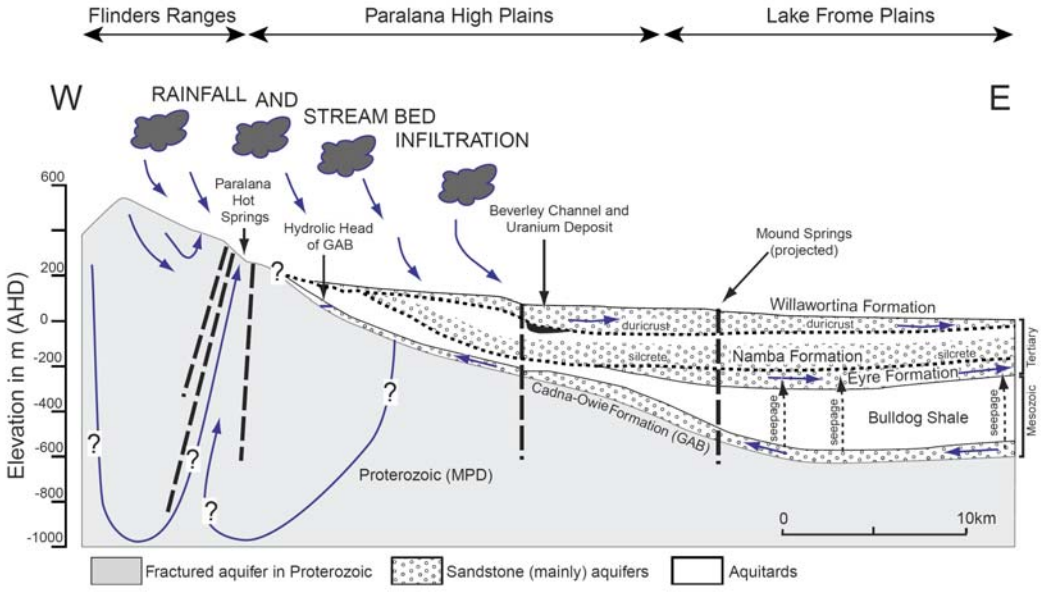

Figure 1.7: *Schematic cross section of the Mt Painter Inlier - Lake Frome area, from Brugger et al. (2005).*

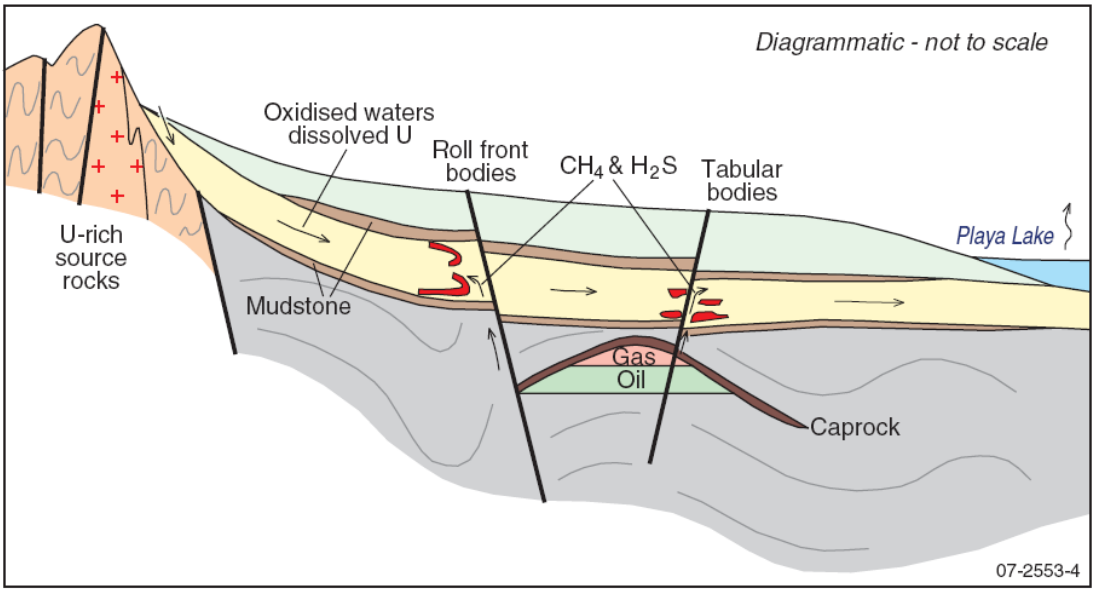

Figure 1.8: *Diagrammatic section of sandstone (yellow unit) hosted uranium system, showing process of infiltration of oxidised U-bearing groundwaters and formation of roll-front and tabular styles of uranium deposits. The potential role of mobile reductants is also shown. Source: Jaireth et al. (2008a).*

1.4 REPORT STRUCTURE

This report is structured around the mineral system components illustrated in Figures 1.2 and 1.5. Following this Introduction, Chapter 2 addresses aspects of the uranium *source* by describing the lithostratigraphy of Proterozoic basement and Cambrian, Mesozoic and Cenozoic basin sediments.

Chapter 3 describes the *permeability* architecture and evolution in terms of regional structural evolution including neotectonics, and geometry of aquifer units in the Lake Frome region. Based on compilations of existing public-domain data including seismic data, these 3D datasets (viewable as 3D pdf files) highlight the geometry of basin-controlling faults of different ages. Aspects of the *energy* driver component of the mineral system are also discussed in this chapter because a key driver of fluid flow was topography, which is largely a product of tectonic processes and climate.

Depositional gradients at district to deposit scales are described in Chapter 4. A new method of mapping and visualising geology and mineralogy in 3D is introduced, with application to mapping variations in oxidation-reduction potential within basin sequences (chemical architecture).

In Chapter 5 we describe uranium deposits of the Lake Frome region based on a review of published information. These descriptions focus on the deposit-scale geology including aspects of the *permeability architecture* and *depositional gradients* at this scale.

Detailed new petrographic descriptions for the Four Mile deposit are presented in Chapter 6. This work addresses the *depositional gradients* at deposit- to micro-scale, and identifies some of the key mineralogical characteristics representing the processes of uranium ore deposition.

In Chapters 2-6 a range of sources, permeable pathways, energy drivers, and depositional gradients are described for uranium mineral systems of the Lake Frome region. It follows that differing combinations of these geological components will result in a range of hypothetical scenarios of uranium ore formation, each with possibly different implications for exploration. The scenario published by Brugger et al. (2005) is just one of several that can be tested for the Lake Frome region. Chapter 7 presents the results of numerical modelling of regional- and district-

scale fluid flow to test the scenario of Brugger et al. (2005) as well as other geological scenarios. A prime aim of this work is to identify the relative importance of parameters such as permeability for differing regional geometric scenarios, rather than to attempt to model in detail the formation of particular deposits. The results help to clarify which characteristics of the basin are most favourable for sandstone-hosted uranium mineralisation.

Finally, Chapter 8 synthesises the key results of the study, and presents exploration criteria to assist in reducing the risk in discovery of the next large uranium deposit in the Lake Frome region.

2. Uranium sources: lithology and stratigraphy

Allison Britt, Roger Skirrow, Simon van der Wielen

2.1 LITHOSTRATIGRAPHY OF THE PROTEROZOIC BASEMENT

Cambrian to Cenozoic basins of the Lake Frome region overlie Proterozoic basement of unusually uranium-rich character. These basins are bounded to the south by Paleoproterozoic metasedimentary and metaigneous rocks of the Willyama Supergroup, deposited up to ~1640 Ma and metamorphosed during the Olarian Orogeny at ~1600 Ma. This sequence forms a major part of the Curnamona Province. Whereas the metasedimentary strata of the Willyama Supergroup are not unusually endowed with uranium, several granitoid suites emplaced between ~1730 and ~1580 Ma have elevated uranium contents. These include alkaline I-type granitoid rocks in the Crockers Well area that are associated with a number of small uranium deposits and occurrences. These granitoids intruded metamorphic rocks of the Willyama Supergroup at ~1580 Ma (Ludwig and Cooper, 1984) and have isotopic compositions suggesting involvement of possibly anomalous, metasomatised, mantle (Rutherford et al., 2007). The Radium Hill uranium-radium deposit in the southern Curnamona Province (McKay and Miezitis, 2001) also appears to be associated with syn- or post-orogenic intrusive rocks.

The north-south Benagerie Ridge occupies the central part of the Curnamona Province and is entirely concealed by Cambrian and younger sedimentary basins. The geology is poorly understood but is known to include the early Mesoproterozoic Benagerie Volcanics, a flat lying sequence of unmetamorphosed dominantly felsic volcanic rocks compositionally similar to the Gawler Range Volcanics in the Gawler Craton to the west. A number of small but significant iron oxide copper-gold (IOCG) deposits are known from the Benagerie Ridge and southern Curnamona Province, including the Portia and Kalkaroo deposits. The North Portia deposit contains uraninite (Teale and Fanning, 2000), whereas deposits further south appear to be less uraniferous (Williams and Skirrow, 2000).

The Mt Painter and Mt Babbage Inliers situated along the northeastern margin of the Curnamona Province comprise early Mesoproterozoic metasedimentary and metaigneous rocks with a complex tectonic history. The effects of the Cambro-Ordovician Delamerian Orogeny were locally intense, with granite intrusion and metamorphism up to amphibolite facies.

The Mt Painter and Babbage Inliers include granites with some of the highest uranium contents of any igneous rocks in Australia. For example, the early Mesoproterozoic Yerila Granite in the Babbage Inlier contains an average of 116 ppm uranium (Neumann et al., 2000). Numerous uranium prospects are present in the Mt Painter Inlier, containing uraninite, torbernite, autunite and other uranium minerals (Drexel and Major, 1990; McKay and Miezitis, 2001). At the Mt Gee prospect breccia-hosted uranium mineralisation with anomalous REE contents and rare molybdenite occurs in the hematite-chlorite-rich matrix between granitic clasts. The breccias are unmetamorphosed, and may have formed in the Late Ordovician to Silurian (Drexel and Major, 1990; McKay and Miezitis, 2001; Elburg et al., 2003), or Permo-Carboniferous (Idnurm and Heinrich, 1993).

The Mt Painter and Babbage Inliers and southern Curnamona Province represent highly uraniferous crust, in the form of both magmatic and hydrothermal enrichments. These are potentially excellent sources of uranium for basin-related uranium mineral systems, whether directly via leaching or indirectly via erosion of uranium-rich detritus into flanking basins. However, the relative importance of the various potential sources depends partly upon the mineralogy of the uranium-bearing phases and the chemical stability of these minerals (see Skirrow et al., 2009, and references therein). Minerals that are relatively soluble in oxidised fluids, such as uraninite, offer a good source, whereas refractory uranium-bearing phases such as brannerite (e.g., Crocker Well), davidite (e.g., Mt Victoria) or zircon are unlikely to represent a viable source unless the minerals are metamict (Cuney and Kyser, 2008) or partially weathered.

The abundance of magmatic-hydrothermal and related 'primary' uranium mineralisation in the Mt Painter Inlier and southern Curnamona Province may be one key factor in determining the fertility of the Frome region for 'secondary' basin-related uranium systems.

2.2 LITHOSTRATIGRAPHY OF PHANEROZOIC BASINS

Parts of the Cambrian Arrowie Basin (Fig. 2.1) are preserved beneath younger basins in the Lake Frome region and crop out in the northern Flinders Ranges. The Paleozoic strata are unconformably overlain by Mesozoic units of the very extensive Eromanga Basin, which locally onlaps onto Proterozoic basement. The lobe of the Eromanga Basin extending southwards into the Lake Frome region is known as the Frome Embayment.

The Mesozoic units are overlain by Cenozoic sediments of the Lake Eyre Basin. The Callabonna Sub-basin constitutes that part of the Lake Eyre Basin bounded to the west by the Flinders Ranges and Mt Painter Inlier, to the south by the outcropping Curnamona Province, and to the east by the Barrier Ranges.

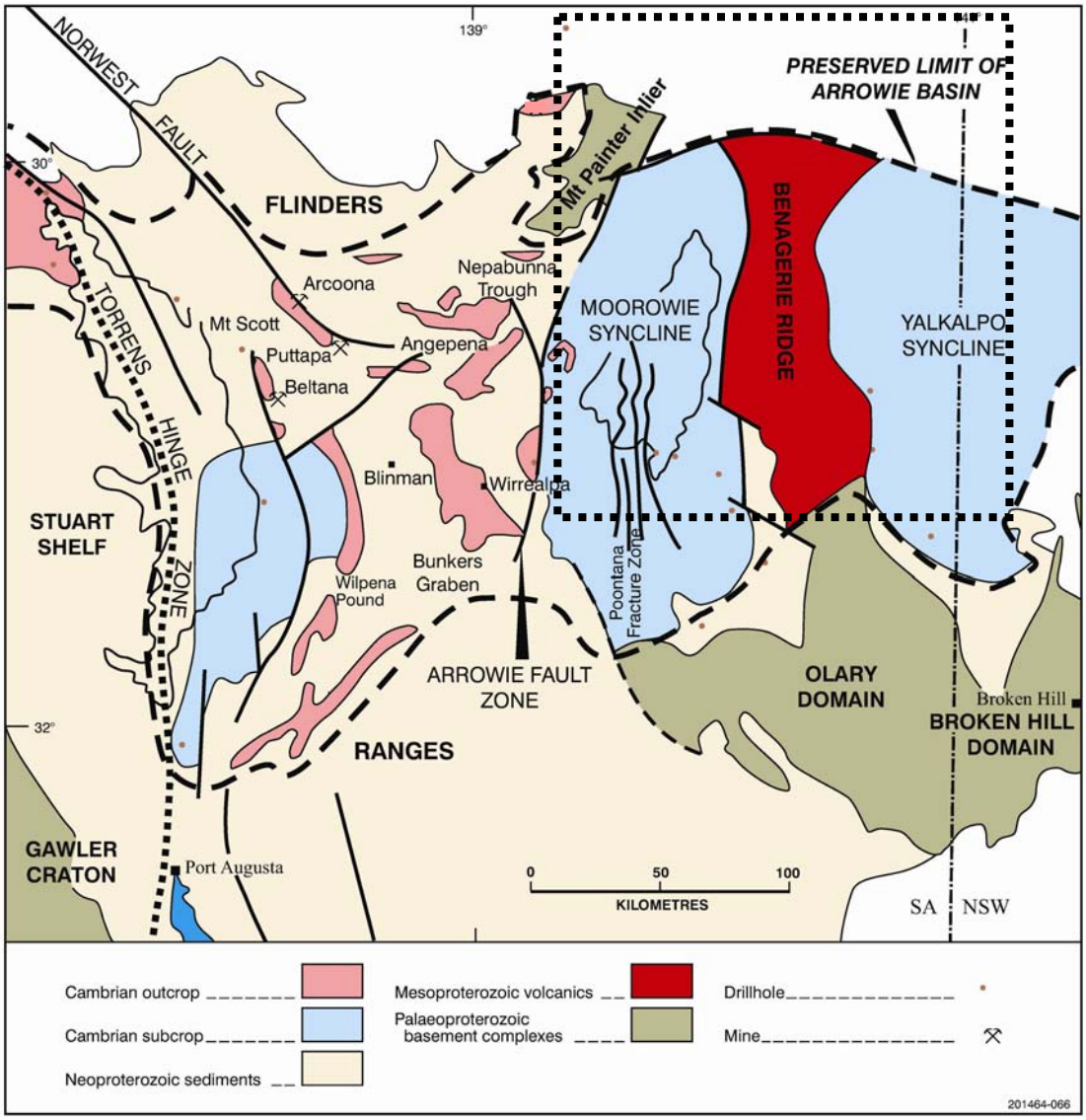

Figure 2.1: *Distribution of Cambrian rocks of the Arrowie Basin in relation to Proterozoic domains in South Australia and western New South Wales. The Olary and Broken Hill Domains form the southern part of the Curnamona Province. The outline of Lake Frome is shown within the area of the Moorowie 'Syncline' or sub-basin. Source: Gravestock and Cowley (1995).*

2.2.1 Paleozoic – Arrowie Basin

In the study area the Arrowie Basin is represented by the Moorowie and Yalkalpo 'Synclines' or sub-basins which contain thick unfolded strata to the west and east, respectively, of the Benagerie Ridge (Gravestock and Cowley, 1995, Figs. 2.1, 2.2). The Arrowie Basin is comprised of shallow marine sedimentary siliciclastic and carbonate deposits. The succession has been subdivided into three sequences: Є1, a carbonate dominated sequence that progrades into evaporite facies at the top the sequence; Є2, a redbed and carbonate sequence, and Є3, a thick package of red sandstones that coarsen up-sequence (Drexel, et al., 1993). Between sequences Є1 and Є2 minor episodic tectonic and volcanic activity occurred.

Petroleum exploration in the Moorowie sub-basin delineated a number of 'shows' but no significant discoveries have been made.

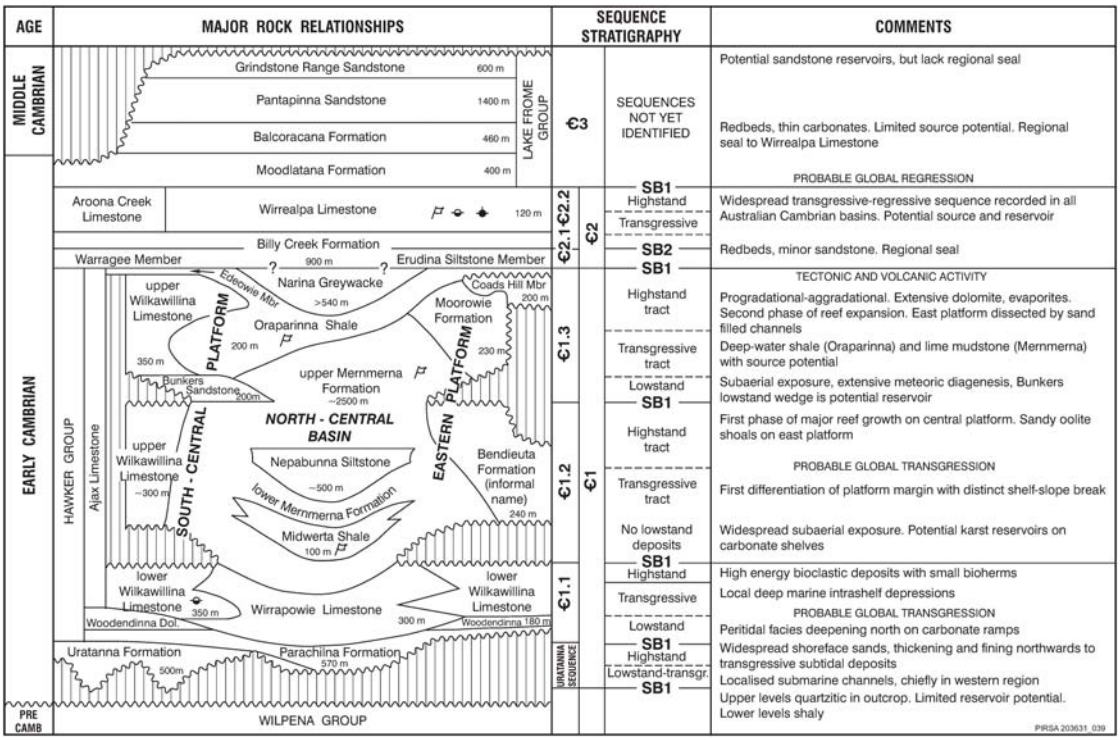

Figure 2.2: *Stratigraphic relationship diagram for the Arrowie Basin showing the correlation between lithologies and sequences. Source: Gravestock and Cowley (1995).*

2.2.2 Mesozoic – Eromanga Basin

The Eromanga Basin is an intracratonic sag basin covering some million square kilometres of east-central Australia (Fig. 2.3). A detailed stratigraphic framework for the Eromanga and adjacent basins was constructed by Gravestock et al. (1986), Krieg (1995) and Radke et al. (2000), among others. The Eromanga Basin has been subdivided into three main stratigraphic sequences: a lower non-marine sequence (early Jurassic to earliest Cretaceous), a middle marine sequence (early Cretaceous) and an upper non-marine sequence (late Cretaceous).

The lower non-marine sequence consists of medium-grained sands deposited in a braided fluvial environment, followed by fine-grained lacustrine sands, silts and shales. Volcaniclastic material is more abundant in the lower non-marine succession to the north and east of the Frome Embayment,

possibly sourced from volcanism in the east (Krieg, et al. 1995). The middle marine sequence comprises basal sands, of which the Cadna-owie Formation occurs in the Frome Embayment, prograding into deeper water shales and muds. Felsic volcanic detritus from the U-rich Gawler Range Volcanics also occurs in the Mt Anna Sandstone, equivalent to the Cadna-owie Formation, along the southwestern margin of the basin (west of Lake Torrens). Of the shales and muds, the Cretaceous Bulldog Shale is the uppermost of the Eromanga Basin units present in the study area. It is described by Ellis (1976) as monotonous blue-grey silty clay. The upper non-marine sequence, the Winton Formation, does not occur in the Frome Embayment. It comprises a thousand-metre thick package of sediments (sandstones, shales and siltstones) that was deposited in a low-energy fluvial to lacustrine environment. Detrital feldspars and ferromagnesian minerals are thought to have been sourced from active volcanoes in eastern Australia (Krieg et al., 1995).

The Great Artesian Basin (GAB) is synonymous with the Eromanga Basin, although the aquifer units are not coincident with the sedimentary limits. The main artesian aquifer comprises a number of formations below and including the Cadna-owie Formation, whereas the upper confined aquifer occurs within the upper non-marine sequence (Krieg et al., 1995). Artesian waters from the GAB debouch onto the surface at a number of mound springs in the Lake Frome region.

Organic matter is abundant in several units of the Eromanga Basin, including the Bulldog Shale in the Frome Embayment. Coal seams are present in the lower and upper non-marine successions (e.g., Birkhead Formation, Winton Formation). In the Moomba region to the north, oil and gas have been recovered from almost all of the lower non-marine units. While much of these hydrocarbons are believed to have migrated upwards from the Cooper Basin, some units in the lower marine Eromanga Basin contain abundant organic matter and are oil mature (Krieg et al., 1995). It is unclear whether Mesozoic rocks in the Frome Embayment experienced the migration of hydrocarbons derived either from within the Eromanga Basin or from the underlying Cambrian strata.

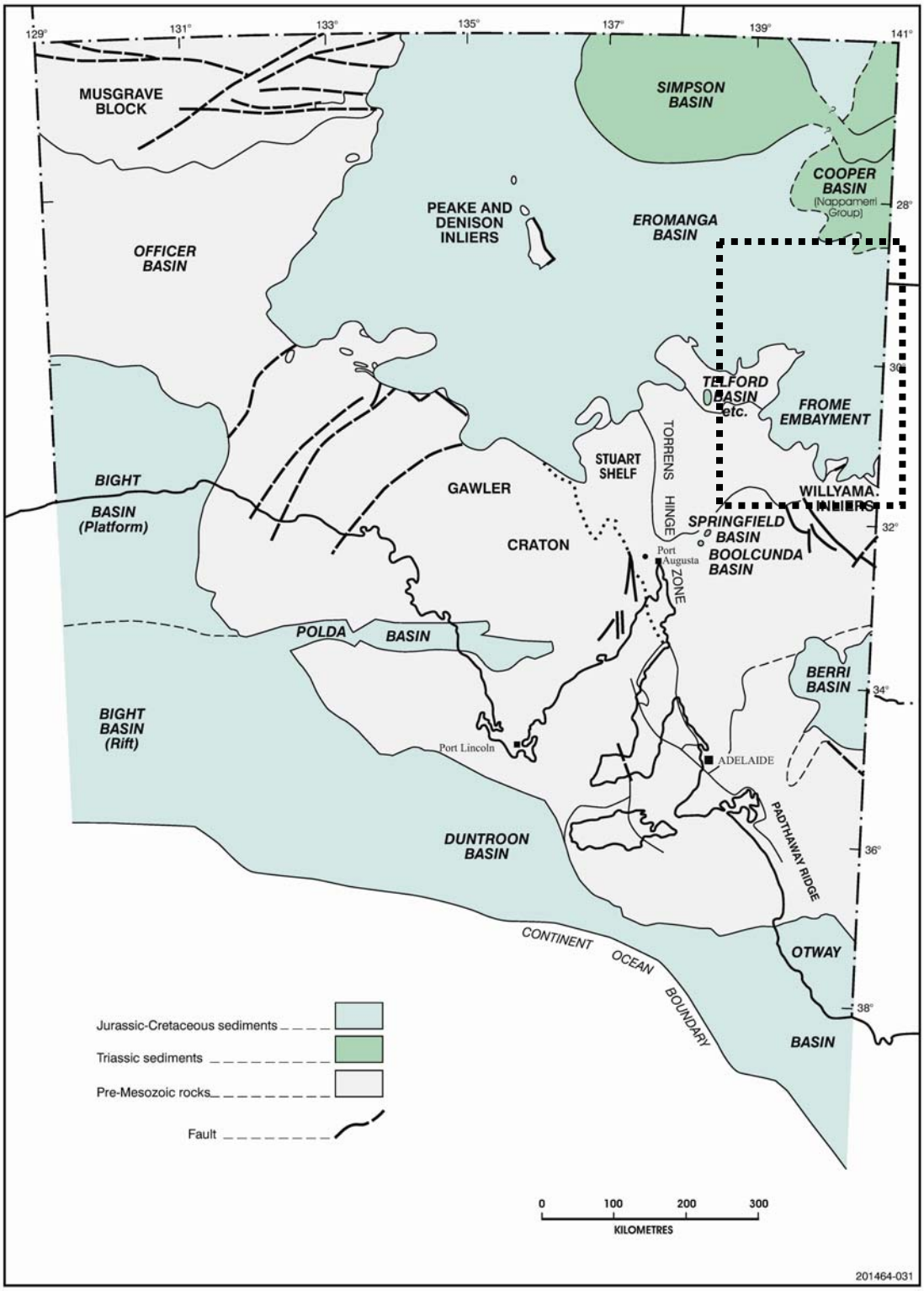

Figure 2.3: *Extents of Cooper and Eromanga Basins in South Australia. Source:Krieg (1995).*

2.2.3 Cenozoic – Lake Eyre Basin

The Lake Eyre Basin was created by tectonic subsidence commencing in the late Paleocene with episodic fluvial and lacustrine sedimentation occurring in the basin until the present day (Callen et al., 1995). The Eyre Formation is the basal unit of the Lake Eyre Basin and unconformably overlies the Eromanga Basin. Sedimentation spanned the latest Paleocene to the Middle Eocene. The Eyre Formation comprises pyritic, carbonaceous mature sand of varying grain size ranging

from silt to gravel with small cobbles in places, and was deposited by braided streams (Alley and Benbow, 1995). In the Callabonna Sub-basin, the Eyre Formation incorporates the Murnpeowie Formation, which contains clay, lignite and basal gravels.

A network of paleochannels filled by Eyre Formation sediments is recognised in the Lake Frome region, incising the underlying Cretaceous units of the Eromanga Basin or directly into Proterozoic basement in places. These paleochannels are important as hosts to many of the uranium deposits in the region, including the Honeymoon, Oban and Goulds Dam deposits (Curtis et al., 1990). In the southern part of the Callabonna Sub-basin the paleochannels have a general northerly trend and indicate sediment transport from south to north. Although the Eyre Formation hosts the Four Mile deposit (Alliance Resources, 2009, www.allianceresources.com.au) it is not clear whether a paleochannel is present in this area.

There is little evidence for further sedimentation in the Lake Eyre Basin until the late Oligocene when widespread gentle folding and uplift rejuvenated the Birdsville Track Ridge some 200 km to the north of the Callabonna Sub-basin. This activity split the Lake Eyre Basin into the Tirari and Callabonna Sub-basins and revived sedimentation which continued to the Pliocene. The new sediments comprise the Namba Formation which disconformably overlies the Eyre Formation. The Namba Formation is equivalent to the Etadunna Formation and this name is commonly used in the historical drill hole logs from the Lake Frome region, though the Etadunna Formation is now restricted to the Tirari Sub-basin.

The Namba Formation sediments are described by Alley and Benbow (1995) as grey, green and white clays, fine-grained sand and carbonate, and minor conglomerate. The formation was deposited in a fluvial lacustrine environment with meandering streams and billabongs. Relief in the region is believed to have been low during deposition of the Namba Formation. The Namba Formation averages 90m thickness, thinning over the Benagerie Ridge and thickening up to 170m towards the Barrier and Flinders Ranges. However, in detail some areas show the opposite thickening trends, for example in the EL5/6 area to the east of Lake Frome (see Chapter 4 and Fig. 4.3). Drill hole logs from the Lake Frome region typically record unconsolidated, very fine- to fine-grained angular sands, black carbonaceous clay, green and grey clays, dolomitic mud and, in places, lignite. At the Beverley deposit the Namba Formation comprises three members: a lower interval known as the Alpha Mudstone which contains plant fragments and carbonised wood; the overlying Beverley Sands (grey silt with sandstone lenses) that host uranium mineralisation, and the overlying Beverley Clay (Curtis et al., 1990). Sinuous sand-filled depressions in the upper surface of the Alpha Mudstone host much of the uranium mineralisation, and are interpreted to represent parts of a broadly north-trending paleochannel system (McConachy et al., 2006).

2.2.4 Quaternary

Quaternary processes have created the present-day fans, claypans, playas, dunes and ephemeral streams of the Callabonna Sub-basin. The oldest Quaternary unit, the Willawortina Formation, formed as piedmont fans around the Flinders and Olary Ranges, with sedimentation commencing in the late Cenozoic and continuing until the Plio-Pleistocene. The Willawortina Formation comprises fine and coarse facies (Callen et al., 1995). The fine facies is an upwards fining, cyclical sequence of sandy mud and silty dolomite, with distal fan, mudflow and playa-lacustrine complexes represented by outcrops of green clay and thick, calcareous paleosols (Callen et al., 1995). The coarse facies, represented in drill holes around the Beverley uranium deposit, comprises braided fans of coarse, framework-supported gravels as well as poorly sorted, matrix-supported debris flows (Callen et al., 1995).

The Coomb Spring and Millyera Formations were deposited from the mid to late Pleistocene (Callen and Benbow, 1995). The beach deposits of the Coomb Spring Formation occur around Lake Frome and consist of white to yellow, often coarse-grained, well-sorted sand (Callen and Benbow, 1995). Present-day topographic contours suggest that it was deposited when lake levels were higher and Lakes Frome and Eyre were possibly joined (Callen and Benbow, 1995). These

Coomb Spring Formation intertongues with the flood-plain and lacustrine deposits of the Millyera Formation, which consists of greenish clay, thin algal limestone and fine-grained white to greenish sand (Callen and Benbow, 1995).

Late Pleistocene sedimentation also resulted in the deposition of the Eurinilla Formation, found in the northern Callabonna Sub-basin and near Lake Frome. It also intertongues with the Millyera Formation and was party deposited in paleochannels formed within the Willawortina Formation (Callen and Benbow, 1995). The Eurinilla Formation consists of bright red-brown to yellow-brown sand and gravel of intermittent streams and their overbank deposits (Callen and Benbow, 1995).

The youngest unit in the Callabonna Sub-basin is the late Pleistocene to Holocene Coonarbine Formation, consisting of aeolian sands of red-coated, frosted quartz grains, yellow to orange grains, clay pellets and gypsum flakes with aeolian cross-bedding (Callen and Benbow, 1995). The sands form a striking pattern of longitudinal dunes, with wind-eroded claypans aligned obliquely. The dunes are typically up to 15m high (Callen and Benbow, 1995) and trend northwards in the northern part of the study area. With Lake Frome as an axis, their orientation progressively rotates to an east-north-easterly trend in the southern part of the sub-basin (Randell, 1973; Callen and Benbow, 1995). Older dunes contain calcareous paleosols and a greater proportion of clay compared to the younger phases of dune formation (Callen and Benbow, 1995). Large transverse dunes also formed along the downwind margins of playas and claypans and on the bed of Lake Frome. Gypsum dunes are built upon clay dunes indicating deflation of the lake floor clays followed by exposure and deflation of the groundwater gypsum horizon (Callen and Benbow, 1995).

Table 2.1: *Quaternary units in the Callabonna Sub-basin. After Callen and Benbow (1995).*

Formation	Age	Maximum Thickness (m)	Depositional Environment
Coonarbine Formation	Pleistocene-Holocene	50	Dunefield
Eurinilla Formation	Late Pleistocene	10	Alluvial
Coomb Spring Formation	Mid-Late Pleistocene	8	Lacustrine Shoreline
Millyera Formation	Mid-Late Pleistocene	9	Playa-lacustrine
Willawortina Formation	Plio-Pleistocene	100	Alluvial and lacustrine

3. 3D architecture and permeability

Simon van der Wielen, Allison Britt, Roger Skirrow

3.1 INTRODUCTION

Faults and permeable sedimentary units comprise the fundamental permeability architecture for uranium and other basin-related mineral systems in the region. This architecture is important in focussing fluids at scales ranging from crustal to basin to deposit. The structural and basin architecture is a product ultimately of the geodynamic and tectonothermal evolution, aspects of which are described in the first section below. The 3D structural architecture is then documented, based on previous work and on newly compiled 3D datasets such as seismic transects. A series of figures of the architecture are presented as 3D pdf files. Finally, the 3D geometry of Cenozoic units including the Eyre and Namba formations is presented for a case study area to the northeast of Lake Frome. These units represent some of the key permeability components in uranium mineral systems in the region.

The chemical architecture and mapping methodology is presented in Chapter 4.

3.2 TECTONIC AND THERMAL EVOLUTION

Uranium mineral systems of the Lake Frome region occur within a part of the Australian continental crust that appears to be unusually enriched in heat-producing elements including uranium. The South Australian Heat Flow Anomaly extends over a broad region between the Mt Painter Inlier in the east and the eastern Gawler Craton in the west, and includes the Flinders Ranges (Neumann et al., 2000). A significant proportion of the heat production is sourced from upper crustal felsic igneous rocks with elevated uranium, thorium and potassium contents (Neumann et al., 2000). McLaren et al. (2002) contended that a major thermal contribution during the Delamerian Orogeny in the Mt Painter region originated from this anomalous high-heat-producing crust and that intense deformation was guided by zones of thermally weakened crust. The region then experienced the effects of the Alice Springs Orogeny in the period ~310-260 Ma, accompanied by exhumation and cooling (Mitchell et al., 2002). Similarly, Célérier et al. (2005) proposed that the present-day topography of the Flinders Ranges including the Mt Painter Inlier can be explained by Paleogene to Cenozoic inversion and faulting focussed on zones of thermally weakened crust. Apatite fission track dating indicates significant exhumation (1.5-2.0 km) and cooling commencing as early as the Paleocene (~65 Ma) or late Cretaceous (Mitchell et al., 2002). However, heating above ~100°C appears to have persisted along the Paralana Fault until ~20-25 Ma, possibly as a result of hydrothermal fluid circulation that largely switched off after this time (Foster et al., 1994; Mitchell et al., 2002). Other studies suggest that much of the present day relief in the Mt Painter Inlier could have been generated since ~4 Ma (Quigley et al., 2007). Increasing strain during the Neogene may be a result of plate boundary forcing as Australian plate commenced its rapid northwards drift (Célérier et al., 2005; Sandiford et al., 2005).

The theme of repeated uplift and deformation occurring in parts of the South Australia Heat Flow Anomaly is potentially important in the development of basin-related uranium mineral systems. First, uplifted uranium-rich basement may have provided both a plentiful source of uranium for leaching by surficial waters as well as the topographic driver for fluid flow into adjacent basins. Second, erosion may have provided uranium-rich detritus to basins flanking the uplands, which are potentially a secondary source of uranium. Third, one of the modes of intraplate compressive deformation proposed for the Flinders Ranges (long-wavelength elastic deformation) resulted in topographic lows bordering the ranges to the east and west, now occupied by Lake Frome and Lake Torrens (Célérier et al., 2005). During wetter climatic periods such lake systems may have accumulated abundant organic matter, which is potentially effective as a reductant to precipitate uranium from oxidised waters (see also Chapter 4).

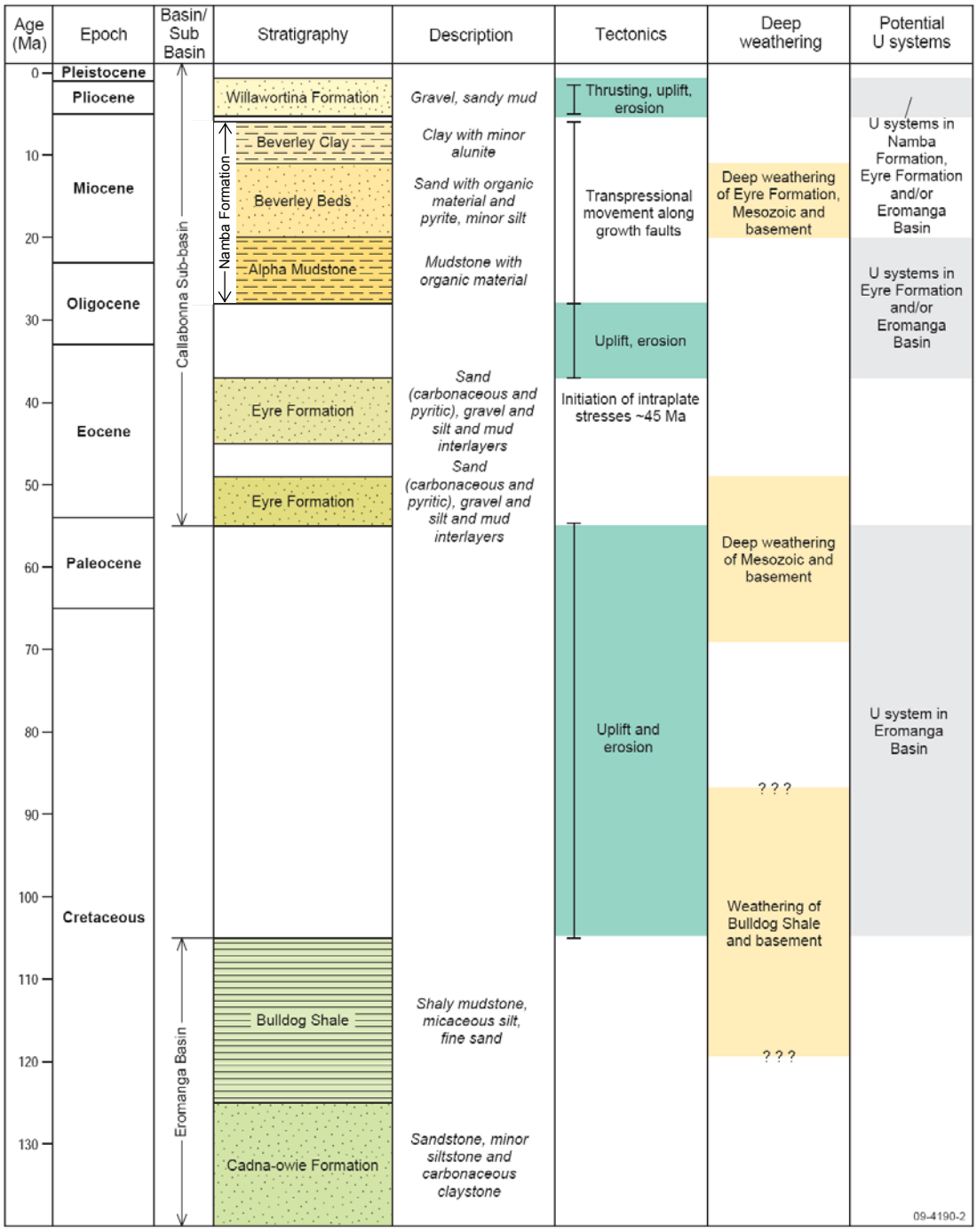

Figure 3.1: *Summary of Late Mesozoic and Cenozoic events in the Lake Frome region, including lithostratigraphy, tectonic evolution, deep weathering episodes, and possible timing of hypothetical uranium mineral systems. See text for sources of data and discussion.*

The timing of deformation and uplift is critical for generation of a productive uranium mineral system. Uplift in the late Cretaceous and Paleocene potentially may have been effective in driving fluid flow in the Mesozoic aquifers of the Eromanga Basin. Increasing intraplate stress and topography generation in the Eocene conceivably would have provided the potential energy for fluid flow through the Eyre Formation which was being deposited during this period, and through older aquifers. The commencement of the latest major period of uplift around 6-10 Ma possibly

drove fluids through the permeable units of the previously deposited Namba Formation. Finally, the current topographic head is the potential energy source for fluid flow through the Willawortina Formation and potentially also into underlying aquifers such as the Namba and Eyre Formations. Thus the interplay of climatic and tectonic evolution may influence the region's potential for large uranium mineral systems. These mineral system scenarios are explored in more detail in Chapter 5 (section 5.4), Chapter 7 and Chapter 8.

3.3 STRUCTURAL ARCHITECTURE AND BASIN FILL GEOMETRY

3.3.1 Data compilation for 3D geological map construction

The Lake Frome region has been a focus for uranium exploration since the late 1960s (Curtis et al., 1990), and extensive historical exploration data exists in various analogue and digital forms. Through the compilation and modelling of seismic, lithological, hydrological and drill log data with modern computing software it is possible to provide new insights into the three-dimensional structure and chemical architecture of this important uranium province.

To better understand the fault and lithological architecture within the study area a 3D model was constructed using gOcad software. The following datasets were integrated into the Frome 3D map:

- The 9 second AusDEM v2 (Geoscience Australia, 2002) with 270 m and 90 m pixel resolution, respectively. As both DEMs are national datasets they were converted from geographic coordinates (latitude and longitude, Geocentric Datum of Australia 1994) to eastings and northings (MGA94, zone 54). The DEMs were clipped to cover the project area. Due to limitations in computer resources, only the 9 second AusDEM was converted into a gOcad 3D surface.
- A portion of the new 1:1,000,000 scale surface geology of Australia (Raymond, 2009) was extracted for the study area and imported into gOcad as curves (Fig. 3.2).
- Seismic data were obtained from PIRSA as 'segy' format and imported into gOcad (Appendix 2 and Fig. 3.2).
- Drill hole data for the study area were compiled from public domain databases held by the South Australia, New South Wales and Queensland geological survey agencies (Fig. 3.2).
- Cultural and physiographic datasets, such as roads (GEOMET 2391), railways (GEOMET 2390), population centres (Gazetteer database, Geoscience Australia, 2005), landuse (GEOMET 3415), drainage (Lawford, et al., 2007), state boundaries (GEOMET 2383) and physiography (GEOMET 2383) were compiled.
- Deposit and mineral occurrence information came from two Geoscience Australia databases: OZMIN mineral deposits database (Ewers et al., 2002) and the MINLOC database.

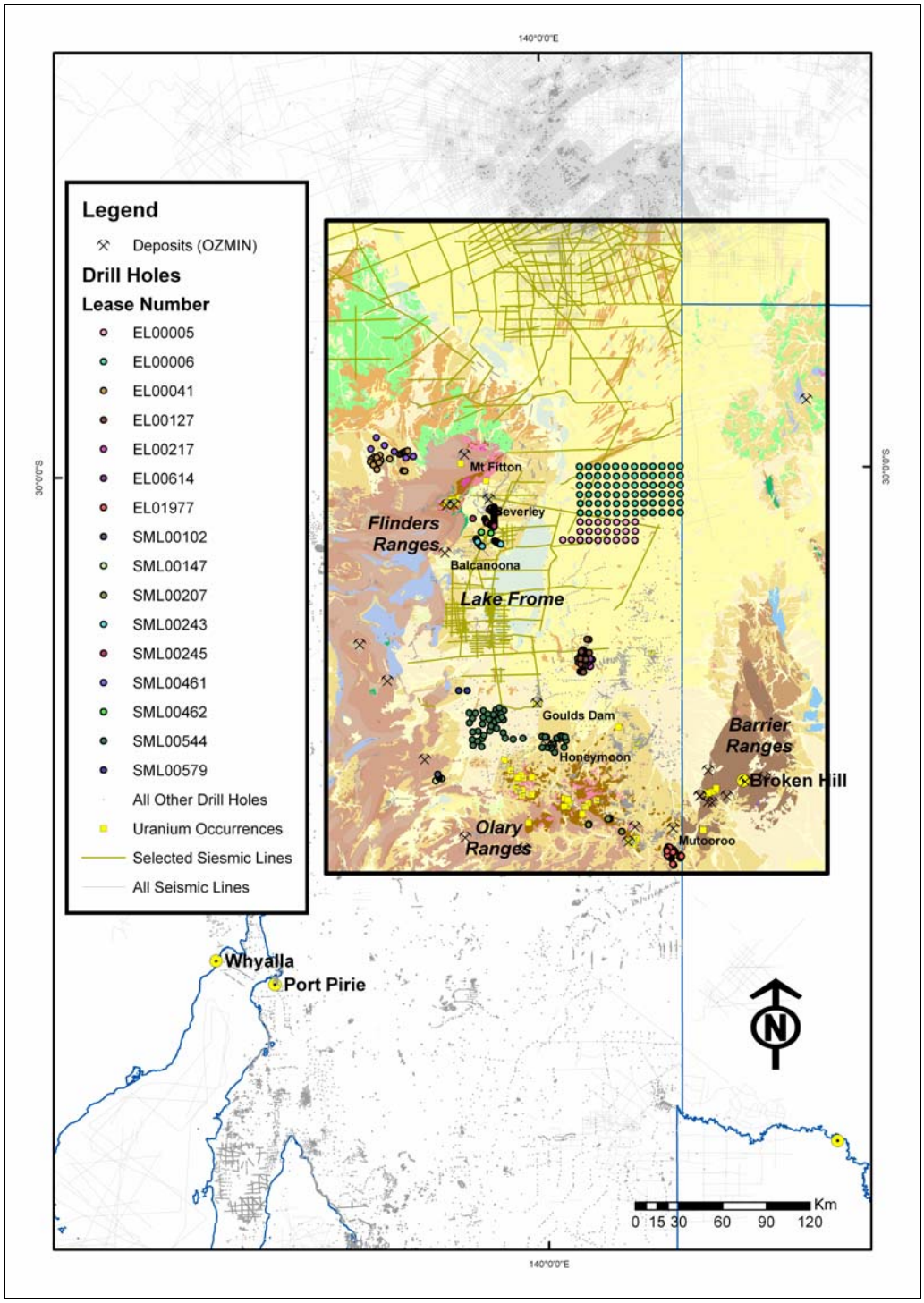

Figure 3.2: *Map showing the surface geology (Raymond, 2009), location of uranium occurrences, mineral deposits (OZMIN database), drilling and seismic lines within the 3D map boundary. The small varicoloured circles are the drill holes for which redox information has been determined (see Chapter 4). Surface geology colours as follows: red, pink and brown tones represent Proterozoic units, blue tones are Paleozoic units, green and tan tones are Mesozoic units, and pale yellow tones represent Cenozoic units.*

Components of the 3D model have been embedded into the electronic version of this document as a series of 3D pdf images (Fig. 3.3 – Arrowie Basin seismic; Fig. 3.4 – Southern margin of the Cooper Basin; Fig. 3.5 – Curnamona Province seismic; Fig. 3.6 – Eromanga Basin seismic and Fig. 3.7 – Drillholes, surface geology, DEM, mineral deposits, radiometrics).

Workflow and metadata for the 3D map are available on request from the authors.

Figure 3.3 (see over): *3D PDF of seismic lines over the Arrowie Basin. In the electronic version of this document, click on the model to activate interactive viewing. Hold down the left mouse button and move the mouse to rotate. Hold down the right mouse button and move the mouse to zoom in and out. Hold down both left and right mouse buttons and move the mouse to pan. Individual objects can be turned on and off by using the model tree (the model tree objects are summarised in Table 3.1). Lighting and surface rendering can be modified using icon buttons that appear at the top the model.*

Table 31: **Model tree objects for Figure 3.3.**

Model Object	Description
Seismic_Arrowie/Frome_Seismic_A_66-MP	Seismic line 66-MP
Seismic_Arrowie/Frome_Seismic_A_70-CFA	Seismic line 70-CFA
Seismic_Arrowie/Frome_Seismic_A_70-CFB	Seismic line 70-CFB
Seismic_Arrowie/Frome_Seismic_A_70-CFC	Seismic line 70-CFC
Seismic_Arrowie/Frome_Seismic_A_70-CFD	Seismic line 70-CFD
Seismic_Arrowie/Frome_Seismic_A_70-CFE	Seismic line 70-CFE
Seismic_Arrowie/Frome_Seismic_A_70-CFF	Seismic line 70-CFF
Seismic_Arrowie/Frome_Seismic_A_70-CFH	Seismic line 70-CFH
Seismic_Arrowie/Frome_Seismic_A_70-CFJ	Seismic line 70-CFJ
Seismic_Arrowie/Frome_Seismic_A_70-CFL1	Seismic line 0-CFL1
Seismic_Arrowie/Frome_Seismic_A_70-CFL2	Seismic line 0-CFL2
Seismic_Arrowie/Frome_Seismic_A_70-CFM	Seismic line 70-CFM
Seismic_Arrowie/Frome_Seismic_A_70-CFN	Seismic line 70-CFN
Seismic_Arrowie/Frome_Seismic_A_70-CFO	Seismic line 70-CFO
Seismic_Arrowie/Frome_Seismic_A_70-CFP	Seismic line 70-CFP
Seismic_Arrowie/Frome_Seismic_A_70-CFQ	Seismic line 70-CFQ
Seismic_Arrowie/Frome_Seismic_A_70-CFR	Seismic line 70-CFR
Seismic_Arrowie/Frome_Seismic_A_70-CFS	Seismic line 70-CFS
Seismic_Arrowie/Frome_Seismic_A_70-CFT	Seismic line 70-CFT
Seismic_Arrowie/Frome_Seismic_A_75-JCQ	Seismic line 75-JCQ
Seismic_Arrowie/Frome_Seismic_A_70-CFK	Seismic line 70-CFK
Seismic_Arrowie/Frome_Seismic_A_75-JCR	Seismic line 75-JCR
Seismic_Arrowie/Frome_Seismic_A_81-CFF	Seismic line 81-CFF
Seismic_Arrowie/Frome_Seismic_A_81-QLC	Seismic line 81-QLC
Seismic_Arrowie/Frome_Seismic_A_81-QLD	Seismic line 81-QLD
Seismic_Arrowie/Frome_Seismic_A_81-QLE	Seismic line 81-QLE
Seismic_Arrowie/Frome_Seismic_A_81-QLF	Seismic line 81-QLF
Seismic_Arrowie/Frome_Seismic_A_81-QLG	Seismic line 81-QLG
Seismic_Arrowie/Frome_Seismic_A_81-QLH	Seismic line 81-QLH
Seismic_Arrowie/Frome_Seismic_A_82-QNP	Seismic line 82-QNP
Seismic_Arrowie/Frome_Seismic_A_82-QNQ	Seismic line 82-QNQ
Seismic_Arrowie/Frome_Seismic_A_82-QNR	Seismic line 82-QNR
Seismic_Arrowie/Frome_Seismic_A_82-QNS	Seismic line 82-QNS
Seismic_Arrowie/Frome_Seismic_A_82-QNT	Seismic line 82-QNT
Seismic_Arrowie/Frome_Seismic_A_82-QNW	Seismic line 82-QNW
Seismic_Arrowie/Frome_Seismic_A_82-QNX	Seismic line 82-QNX
Seismic_Arrowie/Frome_Seismic_A_82-QNY	Seismic line 82-QNY
Seismic_Arrowie/Frome_Seismic_A_82-QNZ	Seismic line 82-QNZ

Model Object	Description
Seismic_Arrowie/Frome_Seismic_A_82-QRN	Seismic line 82-QRN
Seismic_Arrowie/Frome_Seismic_A_82-QRP	Seismic line 82-QRP
Seismic_Arrowie/Frome_Seismic_A_82-QRQ	Seismic line 82-QRQ
Seismic_Arrowie/Frome_Seismic_A_82-QRR	Seismic line 82-QRR
Seismic_Arrowie/Frome_Seismic_A_84-SPG	Seismic line 84-SPG
Seismic_Arrowie/Frome_Seismic_A_84-SPH	Seismic line 84-SPH
Seismic_Arrowie/Frome_Seismic_A_84-SPJ	Seismic line 84-SPJ
Seismic_Arrowie/Frome_Seismic_A_84-SPK	Seismic line 84-SPK
Seismic_Arrowie/Frome_Seismic_A_84-SPL	Seismic line 84-SPL
Seismic_Arrowie/Frome_Seismic_A_84-SPM	Seismic line 84-SPM
Seismic_Arrowie/Frome_Seismic_A_84-SPN	Seismic line 84-SPN
Seismic_Arrowie/Frome_Seismic_A_84-SPP	Seismic line 84-SPP
Seismic_Arrowie/Frome_Seismic_A_84-SPQ	Seismic line 84-SPQ
Seismic_Arrowie/Frome_Seismic_A_84-SPR	Seismic line 84-SPR
Seismic_Arrowie/Frome_Seismic_A_84-SPS	Seismic line 84-SPS
Seismic_Arrowie/Frome_Seismic_A_84-SPT	Seismic line 84-SPT
Seismic_Arrowie/Frome_Seismic_A_84-SPW	Seismic line 84-SPW
Seismic_Arrowie/Frome_Seismic_A_84-SPX	Seismic line 84-SPX
Seismic_Arrowie/Frome_Seismic_A_84-SPY	Seismic line 84-SPY
Seismic_Arrowie/Frome_Seismic_A_84-TJG	Seismic line 84-TJG
Seismic_Arrowie/Frome_Seismic_A_84-TJK	Seismic line 84-TJK
Seismic_Arrowie/Frome_Seismic_A_84-TNX	Seismic line 84-TNX
Frome_Boundary	Boundary Surface
Topography	Topography Image draped onto the DEM Surface

Figure 3.3

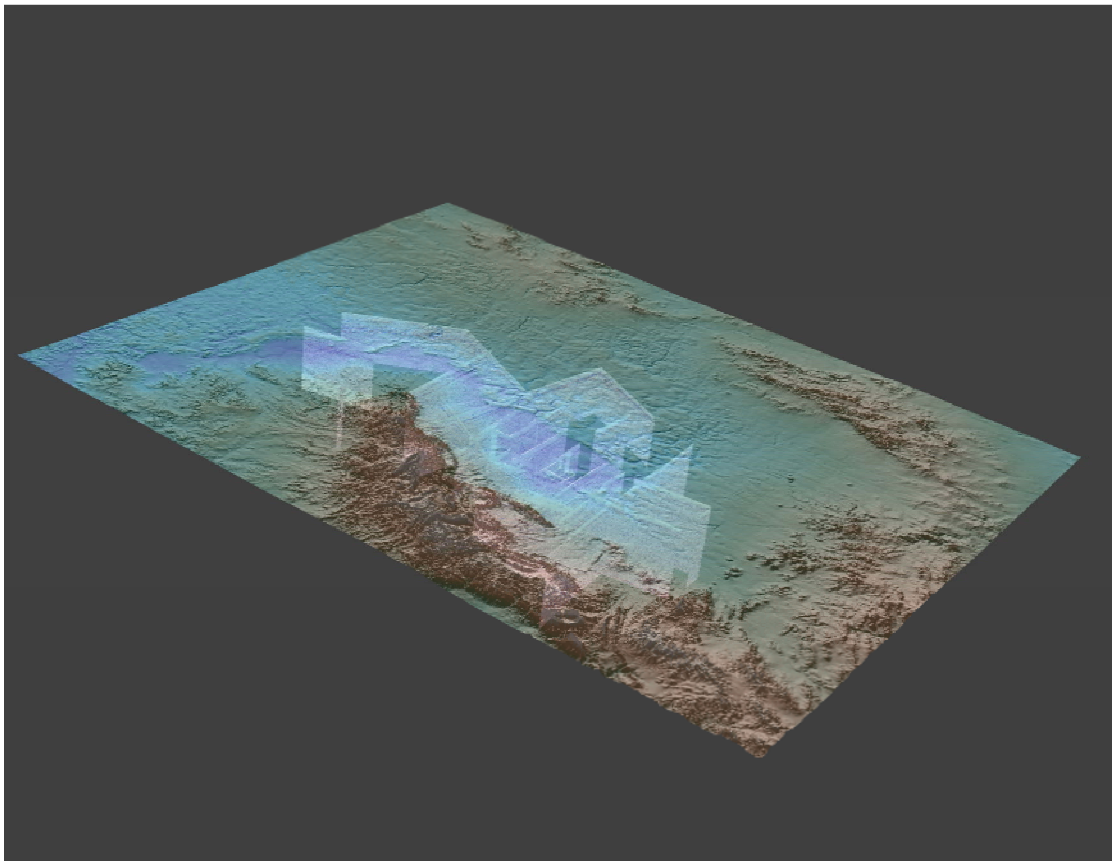

Figure 3.4 *(see over): 3D PDF of seismic lines over the Eromanga Basin. In the electronic version of this document, click on the model to activate interactive viewing. Hold down the left mouse button and move the mouse to rotate. Hold down the right mouse button and move the mouse to zoom in and out. Hold down both left and right mouse buttons and move the mouse to pan. Individual objects can be turned on and off by using the model tree (the model tree objects are summarised in Table 3.2). Lighting and surface rendering can be modified using icon buttons that appear at the top the model.*

Table 3.2: Model tree objects for Figure 3.4.

Model Object	Description
Frome_Boundary	Boundary surface
Topography	Topography image draped onto the DEM surface
Seismic_Eromanga_Frome/Frome_Seismic_E_84-TZW	Seismic line 84-TZW
Seismic_Eromanga_Frome/Frome_Seismic_E_82-RBH	Seismic line 82-RBH
Seismic_Eromanga_Frome/Frome_Seismic_E_84-XAA	Seismic line 84-XAA
Seismic_Eromanga_Frome/Frome_Seismic_E_91ER-01	Seismic line 91ER-01
Seismic_Eromanga_Frome/Frome_Seismic_E_A85-MA04	Seismic line A85-MA04
Seismic_Eromanga_Frome/Frome_Seismic_E_A85-MA05	Seismic line A85-MA05
Seismic_Eromanga_Frome/Frome_Seismic_E_A85-MA06	Seismic line A85-MA06
Seismic_Eromanga_Frome/Frome_Seismic_E_A85-MA07	Seismic line A85-MA07
Deposits and Mineral Occurrences/Frome_OZMIN	Location of mineral deposits
Deposits and Mineral Occurrences/Frome_Mineral_Occurrence_Diamonds	Location of diamond occurrences
Deposits and Mineral Occurrences/Frome_Mineral_Occurrence_Gold	Location of gold occurrences
Deposits and Mineral Occurrences/Frome_Mineral_Occurrence_Iron	Location of iron occurrences
Deposits and Mineral Occurrences/Frome_Mineral_Occurrence_Lead	Location of lead occurrences
Deposits and Mineral Occurrences/Frome_Mineral_Occurrence_Manganese	Location of manganese occurrences
Deposits and Mineral Occurrences/Frome_Mineral_Occurrence_MineralSands	Location of mineral sand occurrences
Deposits and Mineral Occurrences/Frome_Mineral_Occurrence_Nickel	Location of nickel occurrences
Deposits and Mineral Occurrences/Frome_Mineral_Occurrence_PlatinumGroupElements	Location of PGE occurrences
Deposits and Mineral Occurrences/Frome_Mineral_Occurrence_Silver	Location of silver occurrences
Deposits and Mineral Occurrences/Frome_Mineral_Occurrence_Tantalum	Location of tantalum occurrences
Deposits and Mineral Occurrences/Frome_Mineral_Occurrence_Tin	Location of tin occurrences
Deposits and Mineral Occurrences/Frome_Mineral_Occurrence_Tungsten	Location of tungsten occurrences
Deposits and Mineral Occurrences/Frome_Mineral_Occurrence_Uranium	Location of uranium occurrences
Deposits and Mineral Occurrences/Frome_Mineral_Occurrence_Zinc	Location of zinc occurrences
Deposits and Mineral Occurrences/Frome_Mineral_Occurrence_Diamonds	Location of diamond occurrences
Frome_Surface_Geology_Clip_Drape	1:1,000,000 surface geology curves
Frome_Seismic_Lines_Clip_Drape	Location of seismic lines
Geophysics_EM/Frome_Geophysics_EM-Lines	Proposed location of EM lines
Geophysics_EM/Frome_Geophysics_EM-Outline	Proposed location of GA's EM survey

Figure 3.4

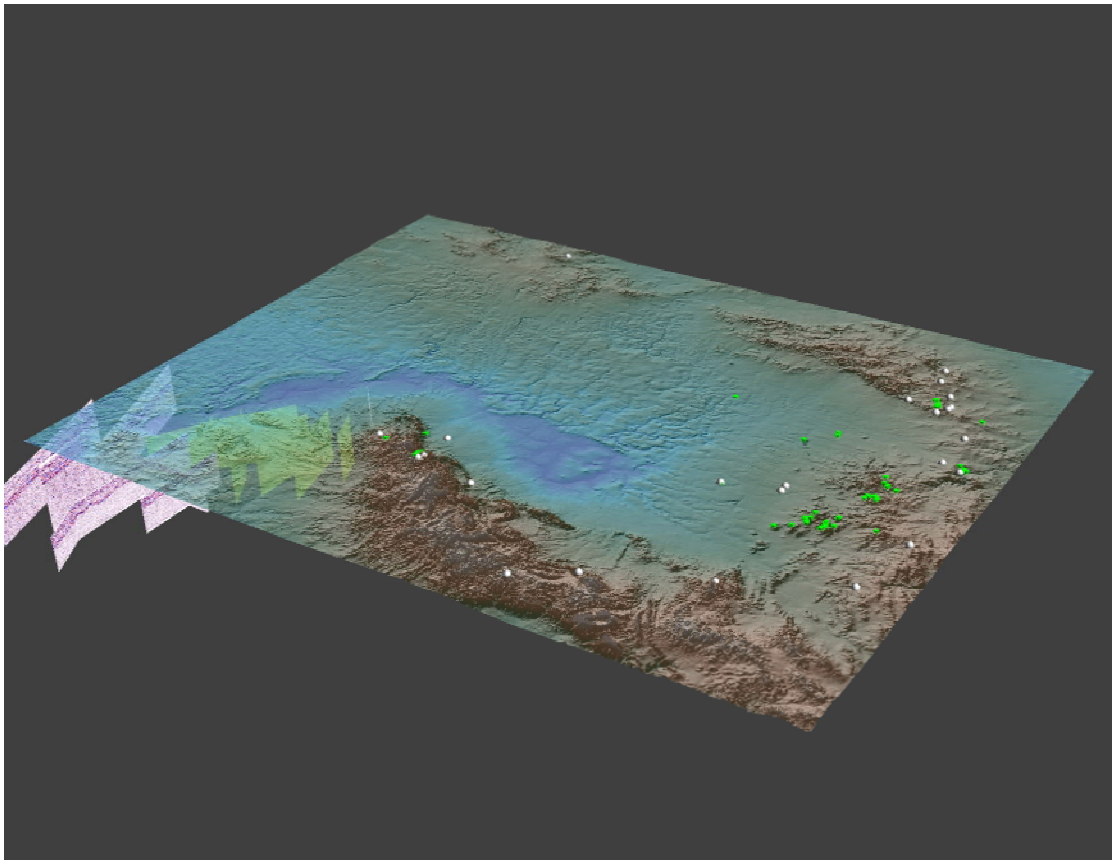

Figure 3.5 (see over): *3D PDF of seismic lines over the Cooper Basin. In the electronic version of this document, click on the model to activate interactive viewing. Hold down the left mouse button and move the mouse to rotate. Hold down the right mouse button and move the mouse to zoom in and out. Hold down both left and right mouse buttons and move the mouse to pan. Individual objects can be turned on and off by using the model tree (the model tree objects are summarised in Table 3.3). Lighting and surface rendering can be modified using icon buttons that appear at the top the model.*

Table 3.3: Model tree objects for Figure 3.5.

Model Object	Description
Seismic_Cooper/Frome_Seismic_C_75-JCF	Seismic line 75-JCF
Seismic_Cooper/Frome_Seismic_C_76-JFY	Seismic line 76-JFY
Seismic_Cooper/Frome_Seismic_C_76-JGD	Seismic line 76-JGD
Seismic_Cooper/Frome_Seismic_C_76-JGE	Seismic line 76-JGE
Seismic_Cooper/Frome_Seismic_C_77-JLH	Seismic line 77-JLH
Seismic_Cooper/Frome_Seismic_C_79-JSM	Seismic line 79-JSM
Seismic_Cooper/Frome_Seismic_C_79-JSN	Seismic line 79-JSN
Seismic_Cooper/Frome_Seismic_C_79-JSS	Seismic line 79-JSS
Seismic_Cooper/Frome_Seismic_C_82-LQG	Seismic line 82-LQG
Seismic_Cooper/Frome_Seismic_C_82-LQS	Seismic line 82-LQS
Seismic_Cooper/Frome_Seismic_C_82-LQT	Seismic line 82-LQT
Seismic_Cooper/Frome_Seismic_C_82-MBZ	Seismic line 82-MBZ
Seismic_Cooper/Frome_Seismic_C_82-MCE	Seismic line 82-MCE
Seismic_Cooper/Frome_Seismic_C_82-MCHR	Seismic line 82-MCHR
Seismic_Cooper/Frome_Seismic_C_82-MCM	Seismic line 82-MCM
Seismic_Cooper/Frome_Seismic_C_82-MCN	Seismic line 82-MCN
Seismic_Cooper/Frome_Seismic_C_82-MCP	Seismic line 82-MCP
Seismic_Cooper/Frome_Seismic_C_82-MCY	Seismic line 82-MCY
Seismic_Cooper/Frome_Seismic_C_82-MDT	Seismic line 82-MDT
Seismic_Cooper/Frome_Seismic_C_82-MFB	Seismic line 82-MFB
Seismic_Cooper/Frome_Seismic_C_83-LYZ	Seismic line 83-LYZ
Seismic_Cooper/Frome_Seismic_C_83-NAP	Seismic line 83-NAP
Seismic_Cooper/Frome_Seismic_C_83-NBF	Seismic line 83-NBF
Seismic_Cooper/Frome_Seismic_C_83-NBS	Seismic line 83-NBS
Seismic_Cooper/Frome_Seismic_C_84-SDZ	Seismic line 84-SDZ
Seismic_Cooper/Frome_Seismic_C_84-SHX	Seismic line 84-SHX
Seismic_Cooper/Frome_Seismic_C_84-SJC	Seismic line 84-SJC
Seismic_Cooper/Frome_Seismic_C_84-SJH	Seismic line 84-SJH
Seismic_Cooper/Frome_Seismic_C_84-SJJ	Seismic line 84-SJJ
Seismic_Cooper/Frome_Seismic_C_84-SJKR	Seismic line 84-SJKR
Seismic_Cooper/Frome_Seismic_C_84-SWX	Seismic line 84-SWX
Seismic_Cooper/Frome_Seismic_C_84-SWY	Seismic line 84-SWY
Seismic_Cooper/Frome_Seismic_C_84-SWZ	Seismic line 84-SWZ
Seismic_Cooper/Frome_Seismic_C_85-XKM	Seismic line 85-XKM
Seismic_Cooper/Frome_Seismic_C_85-XKP	Seismic line 85-XKP
Seismic_Cooper/Frome_Seismic_C_85-XKW	Seismic line 85-XKW
Seismic_Cooper/Frome_Seismic_C_85-XKX	Seismic line 85-XKX
Seismic_Cooper/Frome_Seismic_C_85-XKY	Seismic line 85-XKY
Seismic_Cooper/Frome_Seismic_C_85-XKZ	Seismic line 85-XKZ
Seismic_Cooper/Frome_Seismic_C_85-XLA	Seismic line 85-XLA
Seismic_Cooper/Frome_Seismic_C_85-XWJ	Seismic line 85-XWJ
Seismic_Cooper/Frome_Seismic_C_85-XWM	Seismic line 85-XWM
Seismic_Cooper/Frome_Seismic_C_85-XWP	Seismic line 85-XWP
Seismic_Cooper/Frome_Seismic_C_85-XZZ	Seismic line 85-XZZ
Model Object	**Description**
Seismic_Cooper/Frome_Seismic_C_85-YAN	Seismic line 85-YAN

Seismic_Cooper/Frome_Seismic_C_85-YAR	Seismic line 85-YAR
Seismic_Cooper/Frome_Seismic_C_85-YBD	Seismic line 85-YBD
Seismic_Cooper/Frome_Seismic_C_85-YBE	Seismic line 85-YBE
Seismic_Cooper/Frome_Seismic_C_87-ASN	Seismic line 87-ASN
Seismic_Cooper/Frome_Seismic_C_87-AXG	Seismic line 87-AXG
Seismic_Cooper/Frome_Seismic_C_87-BDGR	Seismic line 87-BDGR
Seismic_Cooper/Frome_Seismic_C_93-EKD	Seismic line 93-EKD
Seismic_Cooper/Frome_Seismic_C_93-EKK	Seismic line 93-EKK
Seismic_Cooper/Frome_Seismic_C_94-ETG	Seismic line 94-ETG
Seismic_Cooper/Frome_Seismic_C_94-EYT	Seismic line 94-EYT
Seismic_Cooper/Frome_Seismic_C_94-FGL	Seismic line 94-FGL
Seismic_Cooper/Frome_Seismic_C_94-FGP	Seismic line 94-FGP
Seismic_Cooper/Frome_Seismic_C_95-FXB	Seismic line 95-FXB
Seismic_Cooper/Frome_Seismic_C_95-FXC	Seismic line 95-FXC
Seismic_Cooper/Frome_Seismic_C_95-FXD	Seismic line 95-FXD
Seismic_Cooper/Frome_Seismic_C_95-FXE	Seismic line 95-FXE
Seismic_Cooper/Frome_Seismic_C_95-GFA	Seismic line 95-GFA
Seismic_Cooper/Frome_Seismic_C_95-GFC	Seismic line 95-GFC
Frome_Boundary	Boundary Surface
Topography	Topographic image draped onto the DEM surface

Figure 3.5

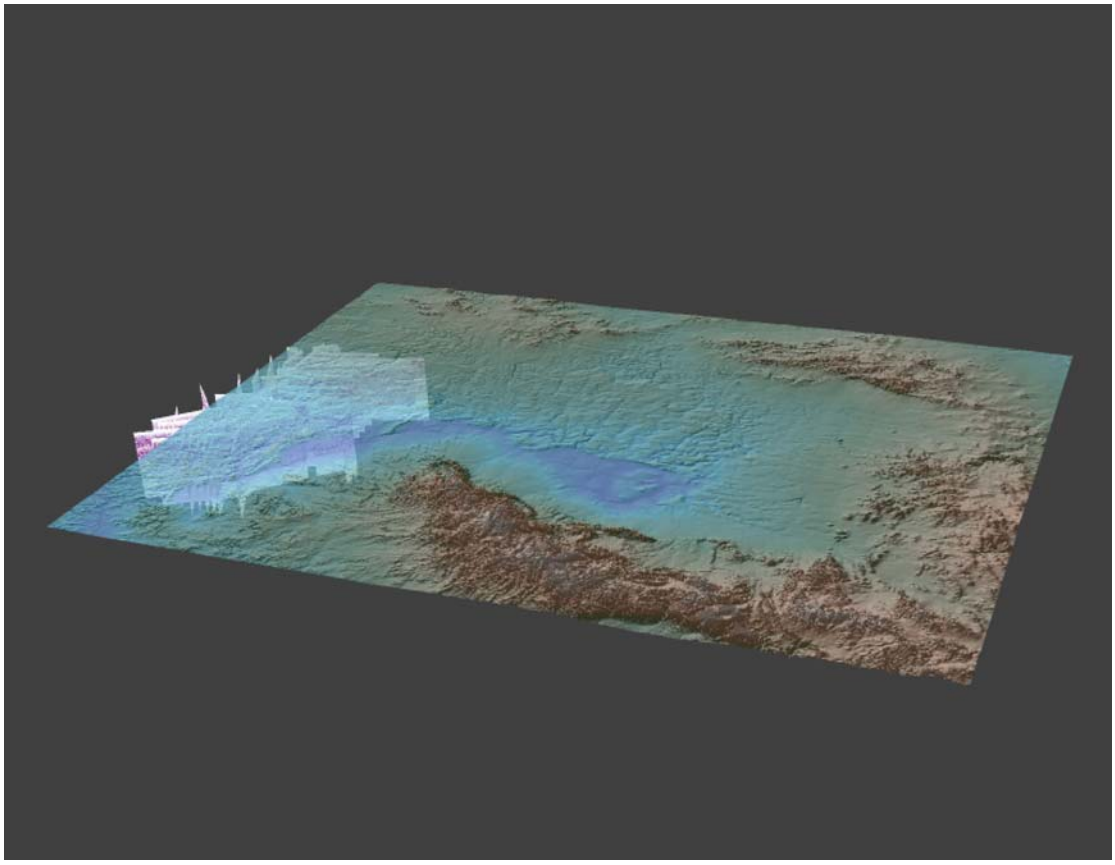

Figure 3.6 (see over): *3D PDF of seismic lines over the Curnomona Craton. In the electronic version of this document, click on the model to activate interactive viewing. Hold down the left mouse button and move the mouse to rotate. Hold down the right mouse button and move the mouse to zoom in and out. Hold down both left and right mouse buttons and move the mouse to pan. Individual objects can be turned on and off by using the model tree (the model tree objects are summarised in Table 3.4). Lighting and surface rendering can be modified using icon buttons that appear at the top the model.*

Table 3.4: Model tree objects for Figure 3.6.

Model Object	Description
Frome_Boundary	Boundary Surface
Topography	Topography Image draped onto the DEM Surface
Seismic_Curnamona/Frome_Seismic_CC_96AGSBH1A	Seismic line 96AGSBH1A
Seismic_Curnamona/Frome_Seismic_CC_03GACU1	Seismic line 03GACU1
Seismic_Curnamona/Frome_Seismic_CC_Blank_08GA-C01	Blank surface showing the position of seismic line 08GA-C01
Deposits and Mineral Occurrences/Frome_OZMIN	Location of mineral deposits
Deposits and Mineral Occurrences/ Frome_Mineral_Occurrence_Diamonds	Location of diamond occurrences
Deposits and Mineral Occurrences/ Frome_Mineral_Occurrence_Gold	Location of gold occurrences
Deposits and Mineral Occurrences/ Frome_Mineral_Occurrence_Iron	Location of iron occurrences
Deposits and Mineral Occurrences/ Frome_Mineral_Occurrence_Lead	Location of lead occurrences
Deposits and Mineral Occurrences/ Frome_Mineral_Occurrence_Manganese	Location of manganese occurrences
Deposits and Mineral Occurrences/ Frome_Mineral_Occurrence_MineralSands	Location of mineral sands occurrences
Deposits and Mineral Occurrences/ Frome_Mineral_Occurrence_Nickel	Location of nickel occurrences
Deposits and Mineral Occurrences/ Frome_Mineral_Occurrence_PlatinumGroupMetals	Location of PGEs occurrences
Deposits and Mineral Occurrences/ Frome_Mineral_Occurrence_Silver	Location of silver occurrences
Deposits and Mineral Occurrences/ Frome_Mineral_Occurrence_Tantalum	Location of tantalum occurrences
Deposits and Mineral Occurrences/ Frome_Mineral_Occurrence_Tin	Location of tin occurrences
Deposits and Mineral Occurrences/ Frome_Mineral_Occurrence_Tungsten	Location of tungsten occurrences
Deposits and Mineral Occurrences/ Frome_Mineral_Occurrence_Uranium	Location of uranium occurrences
Deposits and Mineral Occurrences/ Frome_Mineral_Occurrence_Zinc	Location of zinc occurrences
Frome_Surface_Geology_Clip_Drape	1:1,000,000 surface geology curves
Frome_Siesmic_Lines_Clip_Drape	Location of seimic lines
Geophysics_EM/Frome_Geophysics_EM-Lines	Proposed location of EM lines
Geophysics_EM/Frome_Geophysics_EM-Outline	Proposed location GA's EM survey in the Lake Frome region

Figure 3.6

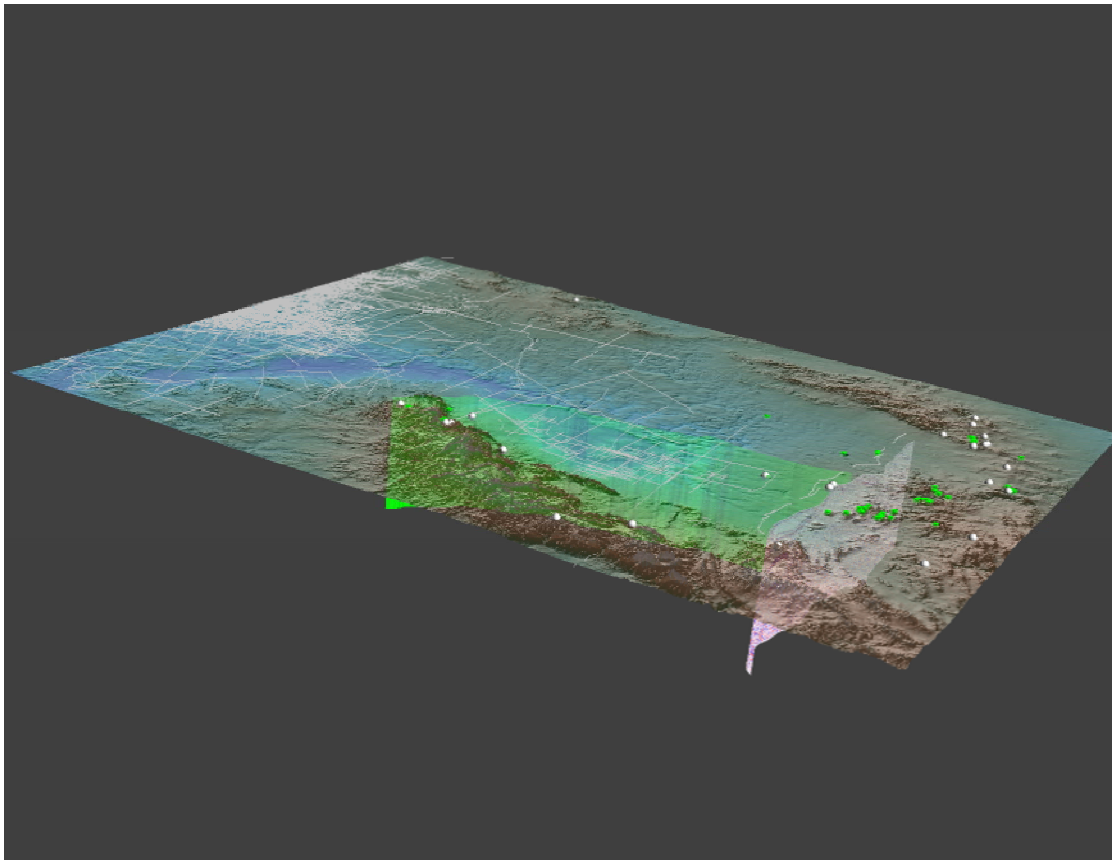

Figure 3.7 (see over): *3D PDF of drill holes, surface geology, digital elevation model, radiometrics and mineral deposits in the study area. In the electronic version of this document, click on the model to activate interactive viewing. Hold down the left mouse button and move the mouse to rotate. Hold down the right mouse button and move the mouse to zoom in and out. Hold down both left and right mouse buttons and move the mouse to pan. Individual objects can be turned on and off by using the model tree (the model tree objects are summarised in the Table 3.5). Lighting and surface rendering can be modified using icon buttons that appear at the top the model.*

Table 3.5: Model tree objects for Figure 3.7.

Model Object	Description
Frome_Boundary	Boundary Surface
Topography	Topography Image draped onto the DEM Surface
Deposits and Mineral Occurrences/Frome_OZMIN	Location of mineral deposits
Deposits and Mineral Occurrences/ Frome_Mineral_Occurrence_Diamonds	Location of diamond occurrences
Deposits and Mineral Occurrences/ Frome_Mineral_Occurrence_Gold	Location of gold occurrences
Deposits and Mineral Occurrences/ Frome_Mineral_Occurrence_Iron	Location of iron occurrences
Deposits and Mineral Occurrences/ Frome_Mineral_Occurrence_Lead	Location of lead occurrences
Deposits and Mineral Occurrences/ Frome_Mineral_Occurrence_Manganese	Location of manganese occurrences
Deposits and Mineral Occurrences/ Frome_Mineral_Occurrence_MineralSands	Location of mineral sands occurrences
Deposits and Mineral Occurrences/ Frome_Mineral_Occurrence_Nickel	Location of nickel occurrences
Deposits and Mineral Occurrences/ Frome_Mineral_Occurrence_PlatinumGroupMetals	Location of PGEs occurrences
Deposits and Mineral Occurrences/ Frome_Mineral_Occurrence_Silver	Location of silver occurrences
Deposits and Mineral Occurrences/ Frome_Mineral_Occurrence_Tantalum	Location of tantalum occurrences
Deposits and Mineral Occurrences/ Frome_Mineral_Occurrence_Tin	Location of tin occurrences
Deposits and Mineral Occurrences/ Frome_Mineral_Occurrence_Tungsten	Location of tungsten occurrences
Deposits and Mineral Occurrences/ Frome_Mineral_Occurrence_Uranium	Location of uranium occurrences
Deposits and Mineral Occurrences/ Frome_Mineral_Occurrence_Zinc	Location of zinc occurrences
Frome_Surface_Geology_Clip_Drape	1:1,000,000 surface geology curves
Frome_Seismic_Lines_Clip_Drape	Location of seismic lines
Frome_Seismic_A_84-SPG_Interp_MODELLING	Seismic line interpretation for line 84-SPG
Frome_Seismic_Blank	Proposed location GA's EM survey in the Lake Frome region
Geophysics_EM/Frome_Geophysics_EM-Lines	Proposed location of EM lines
Geophysics_EM/Frome_Geophysics_EM-Outline	Proposed location GA's EM survey in the Lake Frome region
Radiometrics/Radiometrics_K	Integrated potassium band radiometrics and DEM image draped onto DEM surface
Radiometrics/Radiometrics_Th	Integrated thorium band radiometrics and DEM image draped onto DEM surface
Radiometrics/Radiometrics_U	Integrated uranium band radiometrics and DEM image draped onto DEM surface
Drilling/Drilling_Minerals_NSW/ Frome_Drilling_Minerals_NSW_path	Well paths for New South Wales mineral exploration drill holes
Drilling/Drilling_Minerals_NSW/ Frome_Drilling_Minerals_NSW_derrick	Collar location for New South Wales mineral exploration drill holes
Drilling/Drilling_Petroleum_NSW/ Frome_Drilling_Petroleum_NSW_path	Well paths for New South Wales petroleum drill holes
Model Object	**Description**

Drilling/Drilling_Petroleum_NSW/ Frome_Drilling_Petroleum_NSW_derrick	Collar location for New South Wales petroleum drill holes
Drilling/Drilling_Petroleum_QLD/ Frome_Drilling_Petroleum_Qld_derrick	Collar location for Queensland petroleum drill holes
Drilling/Drilling_Petroleum_QLD/ Frome_Drilling_Petroleum_Qld_path	Well paths for Queensland petroleum drill holes
Drilling/Drilling_Minerals_SA/ Frome_Drilling_Minerals_SA_derrick	Collar location for South Australian mineral exploration drill holes
Drilling/Drilling_Minerals_SA/ Frome_Drilling_Minerals_SA_path	Well paths for South Australian mineral exploration drill holes
Drilling/Drilling_Minerals_SA/ Frome_Drilling_Minerals_SA_Markers	Stratigraphic markers for South Australian mineral exploration drill holes
Drilling/Drilling_Petroleum_SA/ Frome_Drilling_Petroleum_SA_derrick	Collar location for South Australian petroleum drill holes
Drilling/Drilling_Petroleum_SA/ Frome_Drilling_Petroleum_SA_path	Well paths for South Australian petroleum drill holes
Drilling/Drilling_Petroleum_SA/ Frome_Drilling_Petroleum_SA_Markers	Stratigraphic markers for South Australian petroleum drill holes

Figure 3.7

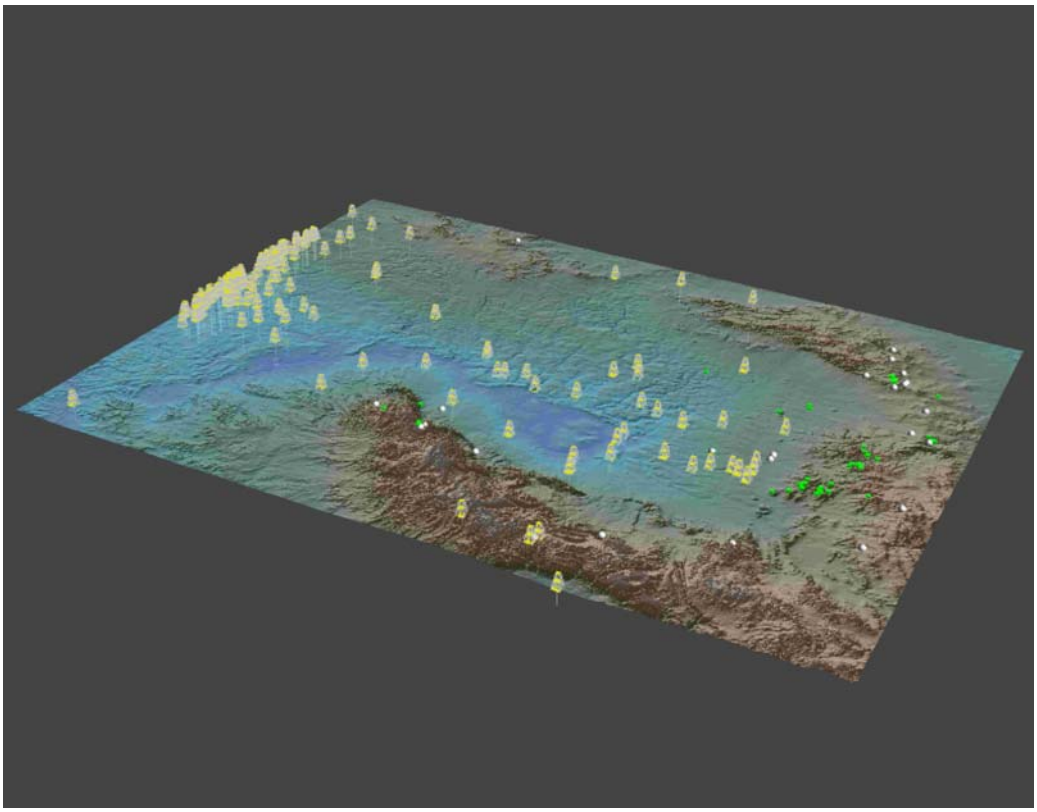

3.4 RESULTS

3.4.1 3D structure

The gross structural architecture of the Lake Frome region was largely established during the Paleoproterozoic to Mesoproterozoic basin-forming and orogenic events, followed by Neoproterozoic rifting. The Delamerian Orogeny variably affected the study area with intense deformation and metamorphism recorded in the southern Curnamona Province (Broken Hill region) and Mt Painter Inlier. The architecture of the pre-Delamerian Cambrian Arrowie Basin in the study area was controlled by broadly north-south trending basin margin and intra-basin faults including the Poontana Fracture Zone and faults at the margins of the northerly trending Benagerie Ridge (Figs. 3.7, 3.8). This basement ridge bisects the basin into the Moorowie and Yalkalpo sub-basins. The north-south trending fault sets appear to have been reactivated repeatedly since the early Paleozoic, controlling younger sedimentation even as recently as the Quaternary.

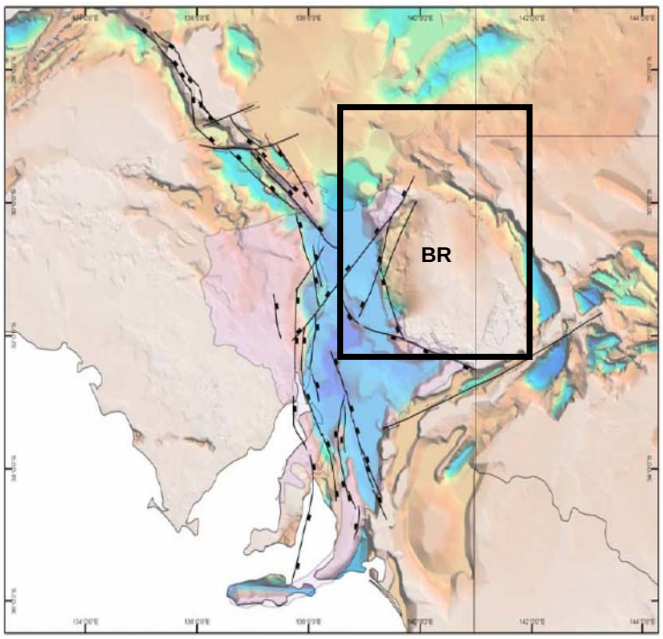

Figure 3.7: *OZ SEEBASE™ image of depth to pre-Neoproterozoic basement for part of southern Australia including the study area (rectangle), showing faults active during a stage (780-735 Ma) of the Neoproterozoic rifting event. Blue tones represent greater depth to pre-Neoproterozoic basement than pink tones. The Benagerie Ridge (BR) and flanking Moorowie and Yalkalpo sub-basins are visible in the image. Source: FrOG Tech (2006).*

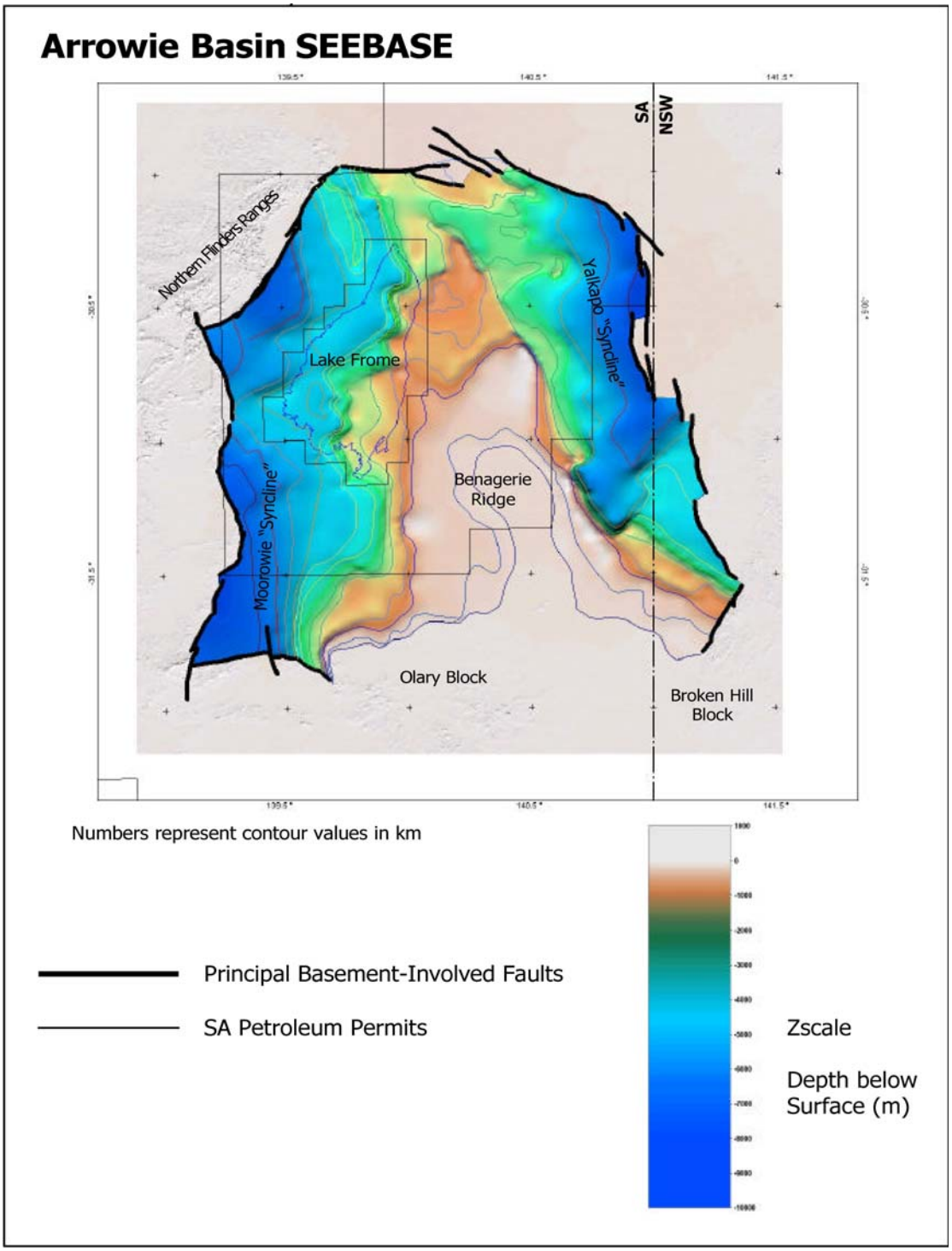

Figure 3.8: *Eastern Arrowie SEEBASE™ image of depth to pre-Paleozoic basement for the Lake Frome region, with principal faults active during Arrowie Basin formation. Blue tones represent greater depth to pre-Paleozoic basement than reddish tones. The Benagerie Ridge and flanking sub-basins (Moorowie and Yalkalpo 'synclines') of the Arrowie Basin are labelled. Source: Teasdale et al. (2001).*

In the Moorowie sub-basin up to 2300 m of Cambrian strata occur in the north-south striking half graben. Based on seismic data a series of north-south and northeast trending faults appear to control thickness variations in the Cambrian sequences, and hence these are interpreted to be syn-depositional Cambrian structures. One of these north-south trending faults identified in the seismic data is an east dipping normal fault with a half-graben in the hangingwall. There also appears to be some later inversion on the fault surface (Fig. 3.3, seismic line 84-SPG) that probably occurred during the Delamerian Orogeny with minor reactivation during recent times.

Previous mapping of surface geology in the study area (e.g., compiled in the 1:1m map of Raymond, 2009) identified several exposed faults within the Mesozoic and Cenozoic sedimentary units (Sandiford, 2008, in Heathgate Resources, 2009). Seismic data show that the locations of mound springs near the eastern shore of Lake Frome are controlled by deep-seated long-lived faults that transect Cenozoic, Mesozoic and Paleozoic strata (Fig. 3.9). A surface expression of this fault system is evident in the SRTM 90m DEM where it controls the lake shore and adjacent playa lakes as well as truncating a series of low ridges. Figure 3.8 and the 3D map (Fig. 3.3) show the Benagerie Ridge forming a basement high draped by Mesozoic and Cenozoic sediments.

Sandiford (2008, in Heathgate Resources, 2009) identified a series of faults in the vicinity of the Beverley and Four Mile uranium deposits which have been mapped in 3D (Figures 3.5, 3.6, 3.10, 3.11). The Wooltana Range Front Fault is a west dipping thrust fault that outcrops along the Wooltana Range. In the north the Wooltana Range Front Fault is concealed by the Paralana alluvial fan where it has been mapped as the Wooltana Fault by Sandiford (2008, in Heathgate Resources, 2009). The Wooltana Fault terminates against, or is offset from, the Poontana-Parabarana Fault system.

The Poontana-Parabarana Fault system has largely been identified in drilling through variations in thickness of Cenozoic units on either side of the fault and from seismic data for two lines (84-SPJ and 84-SPG) that image the fault. As with the Wooltana faults; the Poontana-Parabarana Fault system has been interpreted as a west-dipping thrust fault.

The Paralana Fault is a shallow west-dipping thrust fault that has directly controlled the deposition of the Paralana alluvial fan and the position of the Paralana Hot Springs. The Paralana Fault system is a deep-seated, long-lived structural zone it has been active since the Neoproterozoic when it controlled the deposition of the Adelaidean sediments (Preiss, 1987).

The Four Mile fault is a splay off the main Paralana Fault, located along the range front near the Four Mile West uranium deposit. Two other fault segments, the Adams Fault and Buxton Fault (Fig. 3.5), as well as the Four Mile Fault are all west-dipping thrusts. The kinematics are clearly evident in several exposures along the range front, where Neoproterozoic sedimentary rocks have been thrust over Cainozoic sediments (see Localities 11 and 13, Appendix 1).

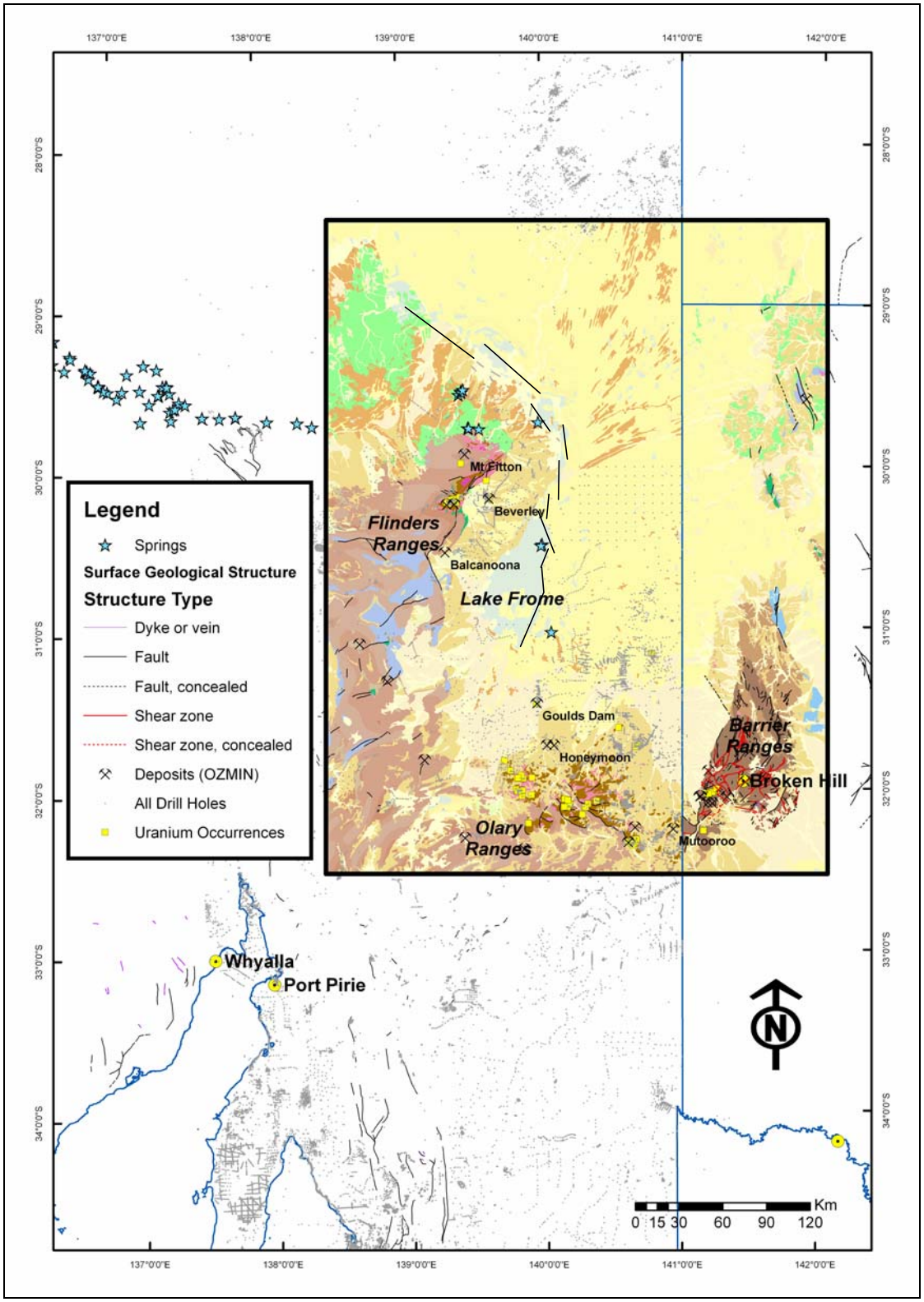

Figure 3.9: *Surface geology showing the location of mound springs and Lake Frome in relation to faults. Surface geology colours as follows: red, pink and brown tones represent Proterozoic units, blue tones are Paleozoic units, green and tan tones are Mesozoic units, and pale yellow tones represent Cenozoic units (from Raymond, 2009). Faults along eastern shore of Lake Frome and to the north of the lake are interpreted from the SRTM 90m DEM.*

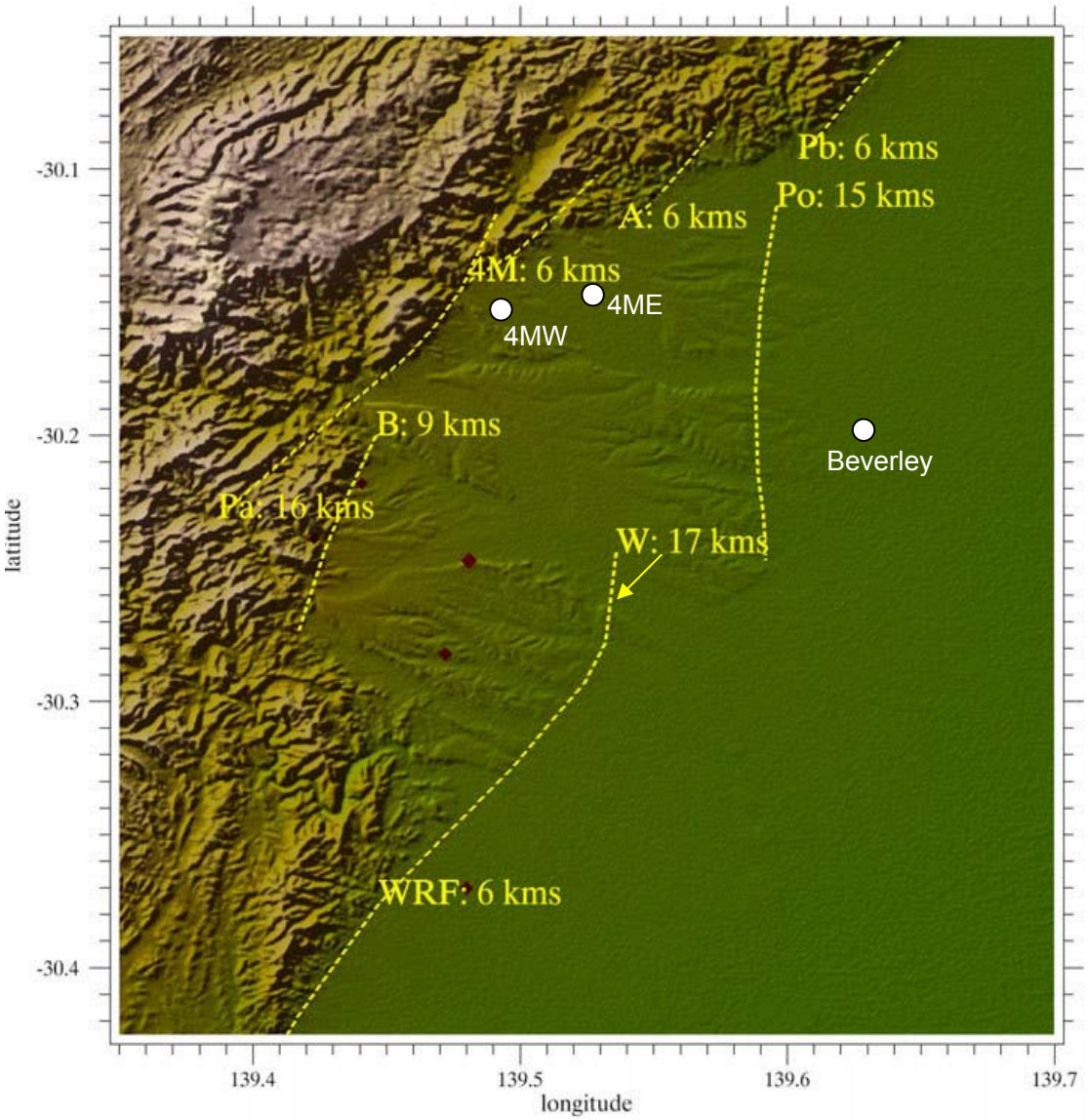

Figure 3.10: *Digital elevation model of the Four Mile – Beverley area, showing fault traces and lengths. 4M – Four Mile Fault, A – Adams Fault, B – Buxton Fault, Pa – Paralana Fault, Pb – Parabarana Fault, Po – Poontana Fault, W – Wooltana Fault, WRF – Wooltana Range Front Fault. The locations of the Four Mile East (4ME) and Four Mile West (4MW) uranium mineralised zones, and the Beverley deposit, are labelled. Lower elevations shown in green tones, higher elevations in pinkish tones. Source: Sandiford (2008, in Heathgate Resources, 2009).*

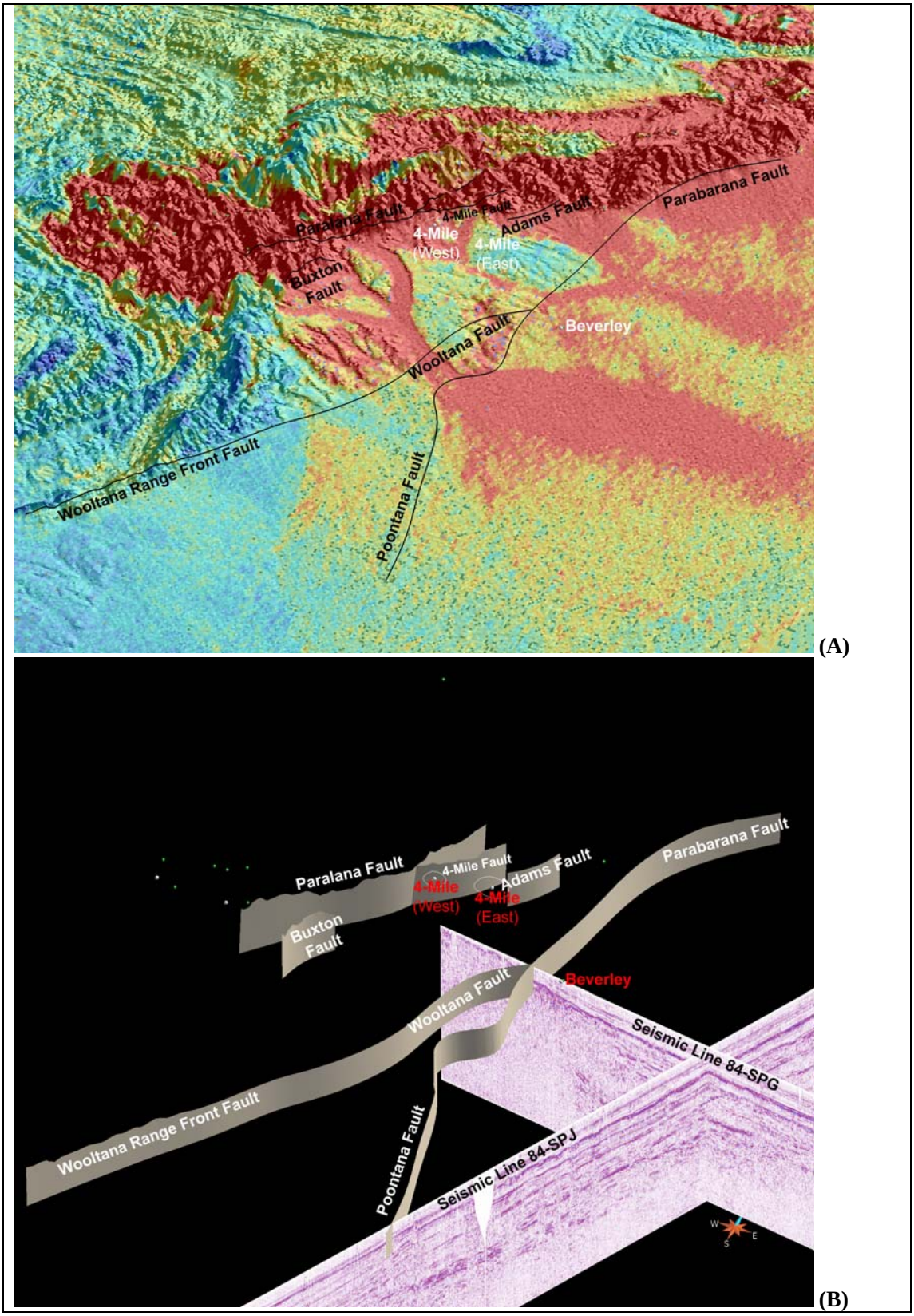

Figure 3.11: *Screen captures of the 3D map showing faults in the vicinity of the Beverley and Four Mile uranium deposits, at ten times vertical exaggeration, looking north-northwest. (A) Uranium band radiometrics draped onto the DEM, and surface trace of the faults. Red tones represent higher U-band responses, blue tones are lower U-band responses. (B) 3D fault surfaces and seismic lines.*

4. Uranium depositional gradients and chemical architecture

Simon van der Wielen, Allison Britt

4.1 INTRODUCTION

A new method has been developed for 3D mapping of key attributes of mineral systems relevant to the uranium potential of sedimentary basins. This method has been applied in the Lake Frome region to map (a) the 3D geometry of selected stratigraphic units, and (b) variations in the oxidation-reduction state of the rocks (redox). The 'chemical architecture' of redox variations is fundamentally important in basin-related uranium systems as it may represent the signature of the flow of oxidised uranium-bearing fluids within the basin (e.g., Cuney and Kyser, 2008), and can potentially provide exploration vectors towards mineralisation. In terms of the uranium mineral system, the chemical architecture constitutes parts of both the *depositional gradient* and fluid pathway or *permeability architecture* components of the system, and is important at district to deposit scales (Fig. 1.2).

The method was initially applied to the Eromanga Basin (van der Wielen et al., 2009) and then adapted for the Lake Frome region, as described below.

4.2 METHOD FOR MAPPING AND MODELLING THE GEOLOGICAL AND CHEMICAL ARCHITECTURE

A large PIRSA dataset, covering the south Australian portion of the Eromanga Basin, comprises various historical drilling data including location, stratigraphy, lithology and some 153,700 drill log descriptions. Geological descriptions of rock/sediment colour and mineralogy have been used as proxies for the oxidation-reduction state of the basin sedimentary fill. To this end, we developed a list of words (Table 4.1) that were used to filter the drill log entries. The filter words were chosen to discriminate between lithological intervals representing oxidised conditions (e.g., the description contained words such as ferruginous, limonite, red, or laterite) from those representing reduced conditions (e.g., lignite, pyrite, green, blue, black, chlorite).

Many of the filter words were shortened so as to capture multiple versions of the word. For example, filtering for "ferr" captured "ferruginous", "ferruginization", "ferruginisation", "ferruginized", "ferruginised", "ferric", "ferro" and "ferricrete". Similarly, "iron" captured "iron stained", "iron staining", "iron oxide" and "ironstone".

Once the filter word had been run against the data set, any occurrences of that word were flagged. False positive results were then eliminated. For example, the word "limonite" would be flagged by the program as an oxidised entry, whereas the log entry may read "no more limonite". Thus, we ran a second filter against the flagged occurrences using the words "no, non, none, not, un" and then manually checked and removed any false positives.

The use of abbreviations presented a significant challenge. The following example is an entry from Drill Hole 229023, 94 to 105 m:

> **Ple gy-br wkly ox vfg mx slty-chty AB wth com fg bk bi+-mt spots & bi vnlts. Vmnr VQ as abv. Tr-vmnr Ma fract fil-vnlt, 1 spk in ox qz vn fragt. Com mnr gy ox-wthd py & tr cp or tarn Py?**

Thus we filtered for as many "shorthand" variants of the filter words as practical. Hematite, for example, was commonly shortened to "hm", "hem", "he" and "ht", and chlorite to "chl", "cl", "cht" or "ct".

Table 4.1: List of redox filter words

Oxidised Words			
Red	Ferruginous	Manganese	Gypsum
Pink	Ferric	Mn	Blown
Maroon	Laterite	Iron	Dune
Orange	Lateritic	Fe	Duricrust
Yellow	Limonite	FeO	Ferricrete
Saffron	Hematite	Fe_2O_3	
Purple	Goethite	Oxide	
Ochre	Martite	FeOx	
Mustard	Maghemite		
Mottled	Specularite		
Reduced Words			
Green	Pyrite	Glauconite	Lignite
Blue	Mundic	Chlorite	Coal
Black	Chalcopyrite	Biotite	Organic
Olive	Chalcocite	Garnet	Carbonaceous
Khaki	Marcasite	Olivine	Graphite
Dark Grey	Galena	Peridotite	Bitumen
Fresh	Sphalerite	Actinolite	Creosote
Gley	Pyrrhotite	Pyroxene	Petrol
	Magnetite	Amphibole	Kerosene
	Sulfur, Sulphur	Hornblende	Hydrocarbons
	Sulfides, Sulphides		H_2S
			Odour

A third issue was the use of the term “as above” or similar. This was addressed by flagging all instances of the words “as above”, “a. a”, “a.a”, “ditto”, “a/a” and “as for”, and where the entry had its own flag from the filter list, we assigned the same flag.

After the filtering process, a value was assigned to each drill log entry. Where only oxidised words had been flagged, the value given was “1”. Where only reduced words had been flagged, the value was “-1”. If both oxidised and reduced words were detected, then the value assigned was “0”. If the filtering process did not flag the entry, then “-99999” was assigned. Thus, each interval for each drillhole in the dataset was assigned a numeric value and these values, along with location coordinates, depths and hole angles were entered into the gOcad modelling program.

Figure 4.1 shows an example of a drill hole log with changes in redox characteristics over narrow intervals within the Namba Formation.

Drill hole C8, EL 6.

Logged by J. Wright, Union Corp (Australia) Pty Ltd, 5 May 1973.

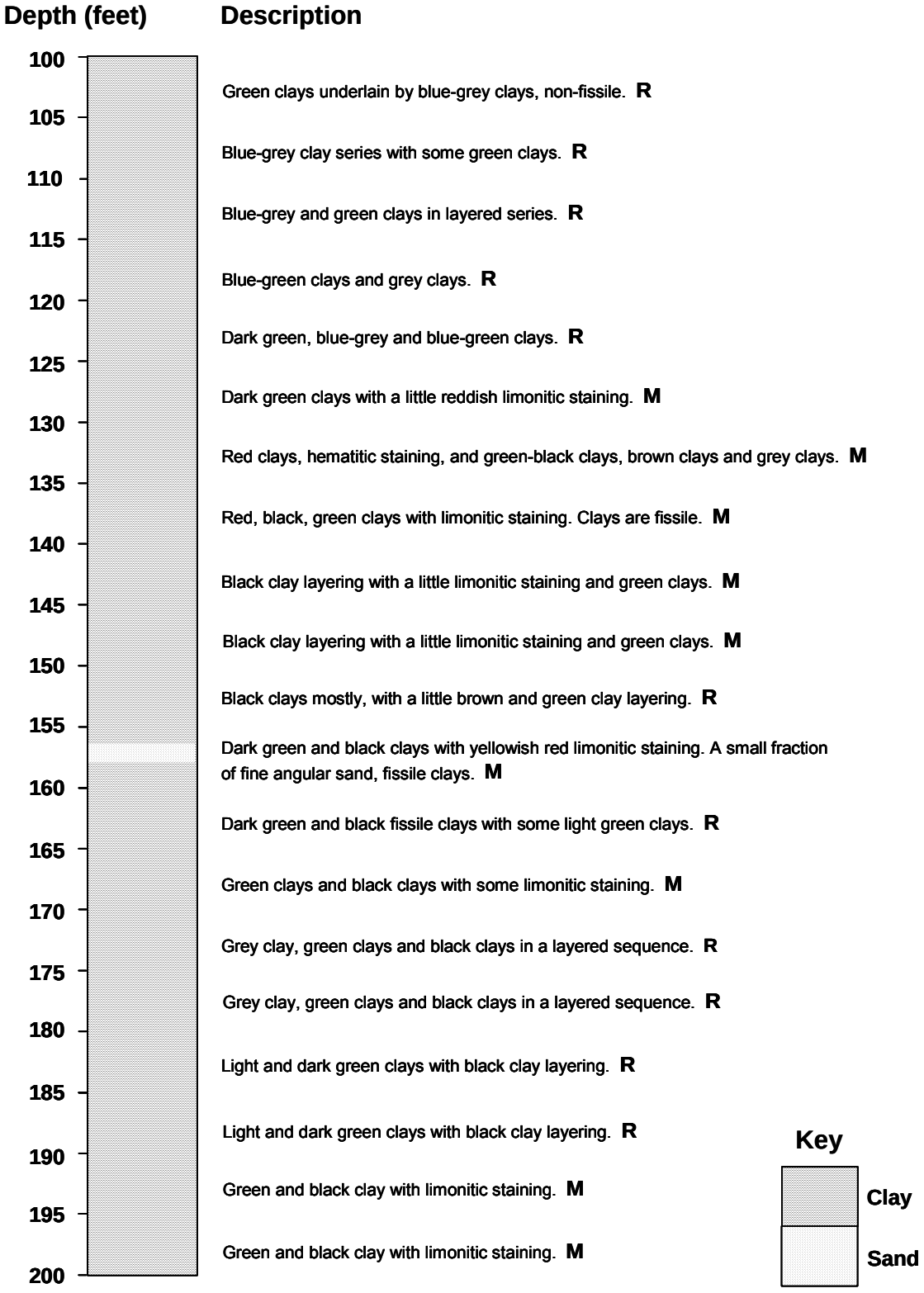

Figure 4.1: *Drill log of Hole C8 from EL 6 showing variability in the redox characteristics of the Namba Formation between 100 and 200 feet depth. R = reduced, M = mixed (reduced and oxidised characteristics).*

4.2.1 Datasets for the Lake Frome region

Despite the size of the PIRSA dataset, the gOcad results based on available digital data records showed that there was very sparse redox information for the Lake Frome region. Analogue (hard copy) records, however, provided valuable additional information and were manually searched and assigned redox values.

The PIRSA drill hole dataset for the Lake Frome region, while not exhaustive, was extensive and recorded the hole locations, elevations, depths and the report number in which the original drill hole information was recorded. Only some of the historical reports are available in digital form (Table 4.2, Fig. 4.2), from which pertinent data were extracted.

As the drill log entries were not digital, redox values were derived by manually recording the depth values, converting to metres where necessary, and assigning a value based on the list of filter words developed earlier for the Eromanga Basin (van der Wielen et al., 2009). Over 12,000 new data points in 441 drill holes were recorded for the Lake Frome region. These values were then entered into gOcad to create a three-dimensional map.

Table 4.2: *Reports used to map redox values in the Lake Frome region.*

Number	Year	Company	# Drill holes	# data points
SML 102	1966 to 1967	Cominco Exploration Pty Ltd	22	342
SML 147	1967	Cominco Exploration Pty Ltd	3	43
SML 207	1968 to 1970	Australian Gold and Uranium Pty Ltd	27	177
SML 243	1968 to 1970	Petromin NL	17	231
SML 245	1968 to 1970	Petromin NL	40	478
SML 461	1970 to 1971	Central Pacific Minerals NL	6	44
SML 462	1970 to 1970	Petromin NL	4	83
SML 544	1971 to 1973	Pacminex Pty Ltd and Esso Australia Ltd	49	825
SML 579	1971	Petrocarb Exploration NL	2	23
EL 5	1972 to 1973	Union Corp. (Australia) Pty Ltd	23	2209
EL 6	1972 to 1973	Union Corp. (Australia) Pty Ltd	72	6631
EL 41	1973	Nissho-Iwai Co. (Aust.) Pty Ltd	21	198
EL 127	1974 to 1975	Tricentrol Australia Ltd	27	147
EL 217	1975 to 1981	Mines Administration Pty Ltd and Teton Exploration Drilling Company Pty Ltd	20	218
EL 614	1975 to 1981	Mines Administration Pty Ltd and Teton Exploration Drilling Company Pty Ltd	22	203
EL 1977	1994 to 1996	North Mining Ltd	84	255

* SML= Special Mining Lease; EL=Exploration Licence

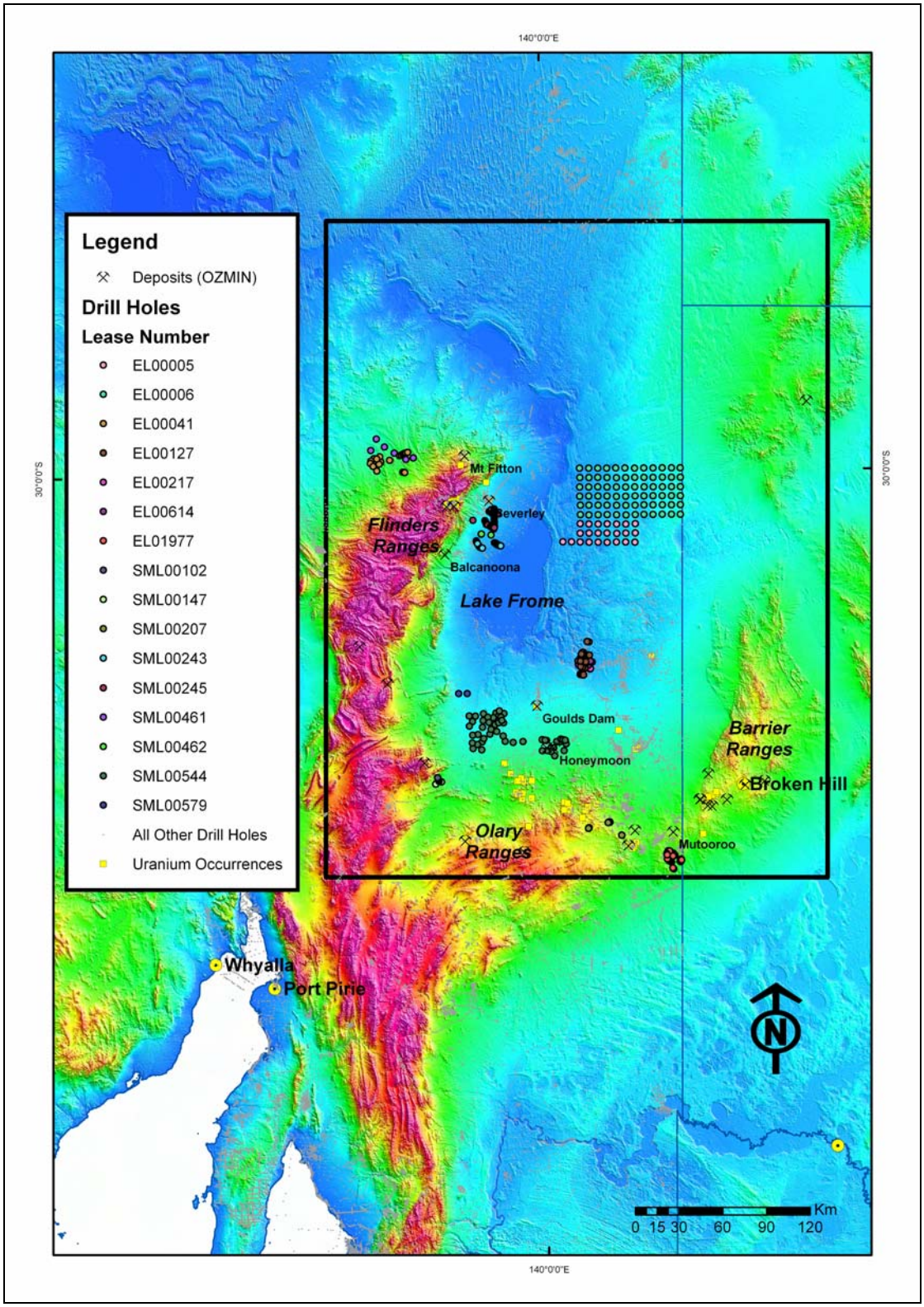

Figure 4.2: *Locations of drill holes used in the study of chemical architecture in the Lake Frome region, with digital elevation model (magenta, red – high elevation, blue – low elevation).*

In addition, we used the gOcad program to create a voxet – a solid 3D model – of Exploration Licences (ELs) 5 and 6. These adjacent ELs are situated east of the Beverley and Four Mile uranium deposits (Fig. 4.2). The drill holes were logged in some detail by the same geologists on the same campaign with the resulting data being of high quality. Discrete Smooth Interpolation (Mallet, 1992) was used to produce a 3D grid of redox.

4.3 VOXET LITHOLOGY MODEL OF EL5 AND 6

The voxet model (Fig. 4.3) shows the upper surface of the Cretaceous Bulldog Shale dipping to the west. It is unconformably overlain by the Cenozoic Eyre Formation which ranges in thickness from 30 to 80 m. The upper surface of the Eyre Formation has greater relief than the other unit surfaces and, like the Cretaceous surface, it dips to the west. There appears to be a thickening of the Eyre Formation sediments midway across the model to form a north-south trending ridge. To the west of this ridge the surface dips more steeply westwards. The surface of the Eyre Formation forms a disconformable contact with the overlying Namba Formation. The upper surface of the Namba Formation dips more gently to the west. It is the thickest unit in the voxet model, ranging up to 120 m thickness at the western edge of the voxet. The uppermost Quaternary unit is rarely more than 20 m thick. Its upper surface also dips gently westward and has little relief, even with exaggerated vertical scale.

The gentle westerly dips of the Cretaceous, Eyre and Namba surfaces in the area of EL5/6 to the east of Lake Frome are opposite to dips of these surfaces in the Beverley area (e.g., Curtis et al., 1990, and Fig. 1.7). This may indicate a basinal structure of Cenozoic units, which is supported by seismic data for the region (see Fig. 7.2, and further discussion of significance in section 8.1.3).

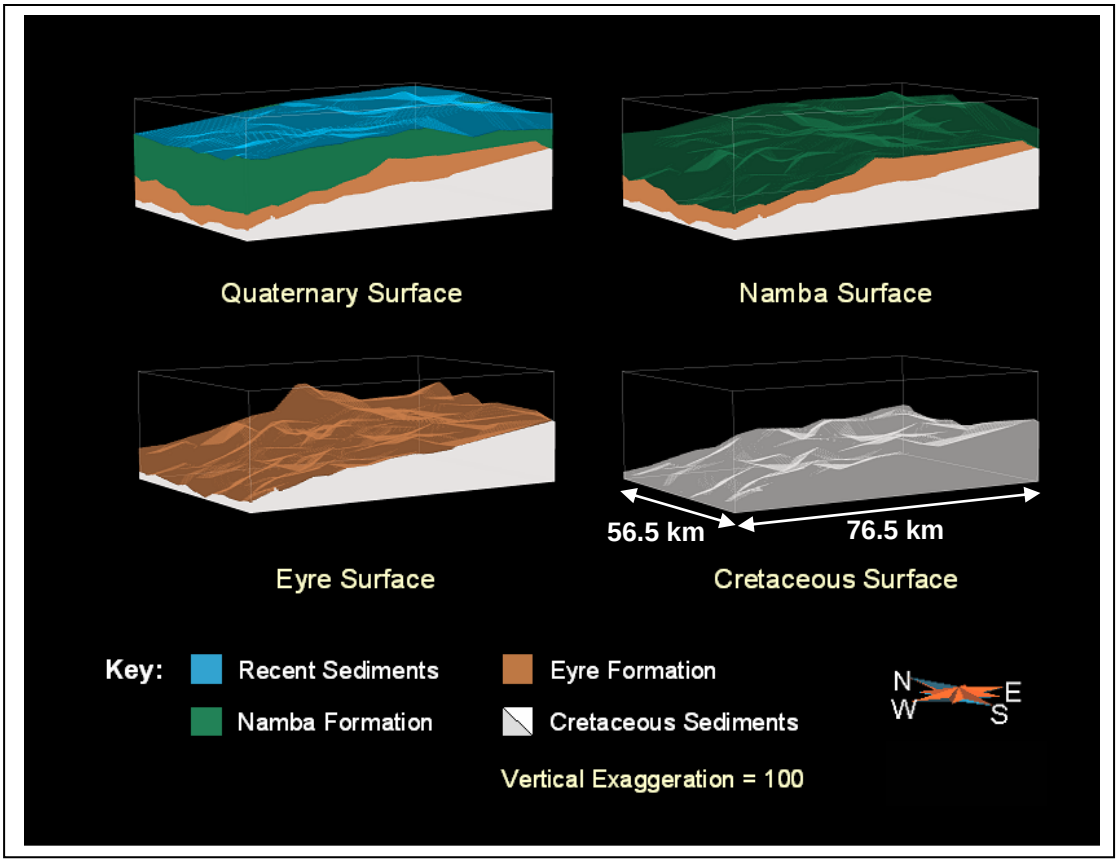

Figure 4.3: *Voxet model of lithology and topography in the EL 5/6 area, east of Lake Frome.*

4.4 3D CHEMICAL ARCHITECTURE

4.4.1 Redox Patterns in the Lake Frome region

The 3D map of the Lake Frome region (Fig. 4.4) shows the scattered nature of the data with the most striking feature being the variability in the redox pattern between areas. Some areas, such as

Special Mining Lease (SML) 245, just south of the Beverley deposit, appear to be grossly oxidised whereas other areas, such as EL 5/6 and SML 544 (southwest of Goulds Dam and west of Honeymoon) show much greater variability in redox state. The general pattern, however, shows oxidation close to surface, underlain by a zone of mixed oxidised and reduced rocks, and a generally reduced zone at depth.

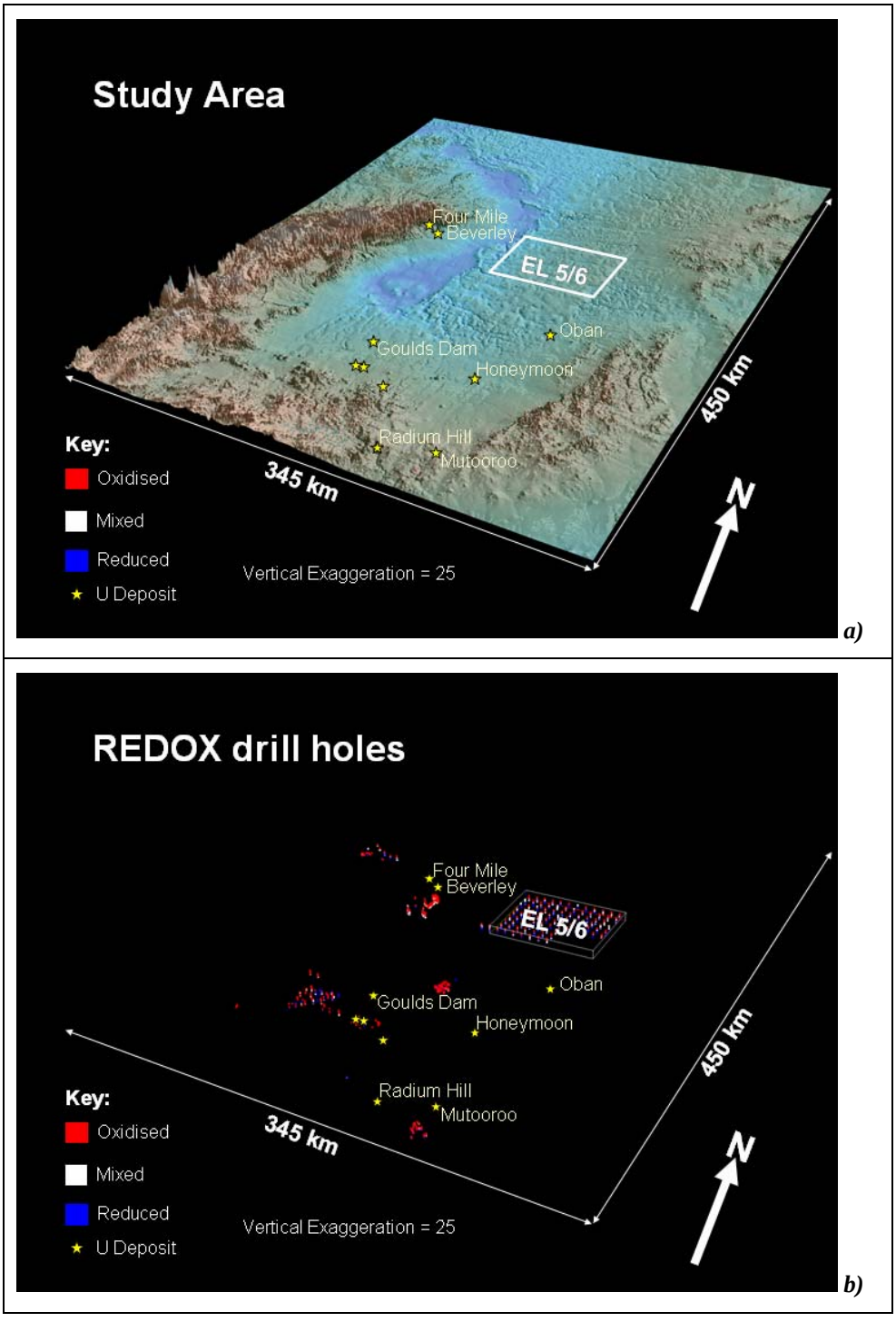

Figure 4.4: *3D map of the Lake Frome region showing (a) the study area, (b) redox characteristics of selected drill holes.*

4.4.2 Voxet Model of EL 5 and 6, north-eastern Lake Frome region

The gross pattern of shallow oxidised and deeper reduced zones observed regionally in Figure 4.4 appears also to hold for the EL5-6 area. However, as shown in Figure 4.5, there are important vertical and lateral redox variations within this area that are potentially important for uranium mobilisation and deposition. It is also clear that there is considerable vertical variability in redox over narrow intervals of a few metres to 10s of metres (Fig. 4.5).

The model shows that the westerly dipping upper surface of the Cretaceous Bulldog Shale is mostly reduced with localised areas of oxidised and mixed redox. The largest oxidised zones occur in the upslope areas with smaller zones down slope. The areas of mixed redox show a similar pattern.

The redox pattern on the upper surface of the Cenozoic Eyre Formation shows that this surface is also mostly reduced with localized mixed redox and oxidised zones. The oxidised areas mostly occupy the roughly north-south trending ridge in the centre of the EL5-6 area, with others occurring upslope to the east and partway down the westerly slope. The areas of mixed redox have a more random distribution.

The upper surface of the gently west-dipping Cenozoic Namba Formation shows the greatest variability in redox values. Roughly half the area is oxidised, a third is of mixed redox and the remainder reduced. The most striking feature of the voxet model is the sinuous broadly north-south trending channel-like pattern of the reduced values, coloured blue in Figure 4.6. It is possible these features represent parts of a paleochannel system within the upper Namba Formation, with reduced material occupying parts of the channel.

The Quaternary upper surface dips gently to the west and is almost uniformly oxidised with some scattered areas of mixed redox and reduced values.

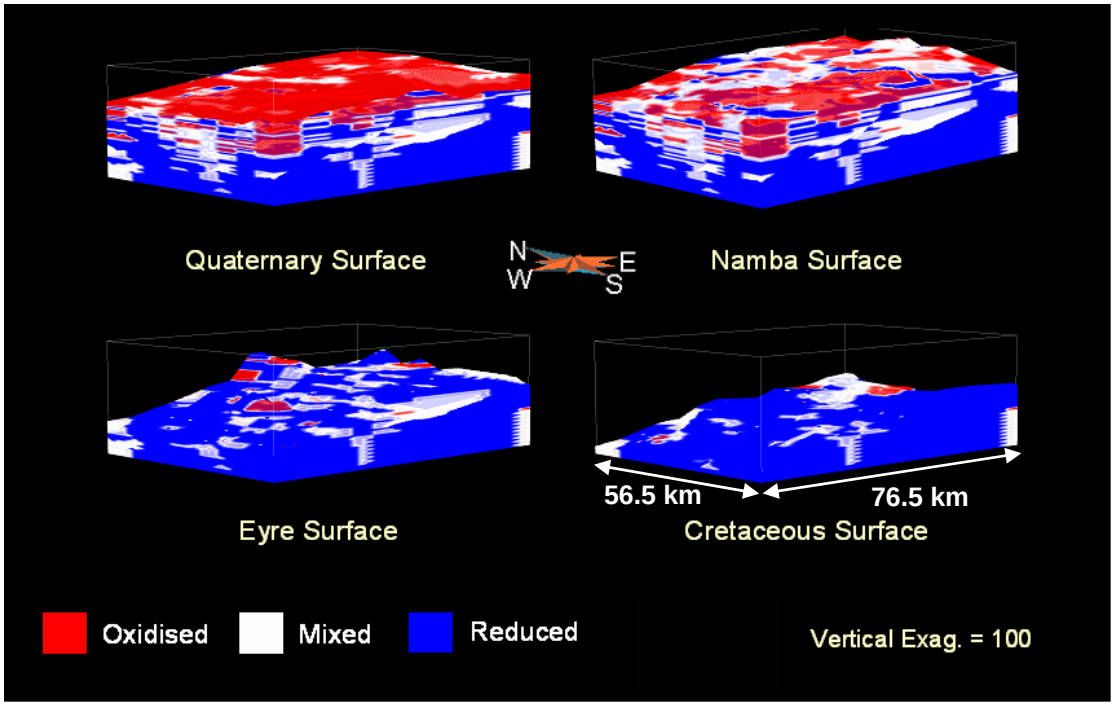

Figure 4.5: *Voxet model of redox and topography of each lithological surface in the EL 5/6 area.*

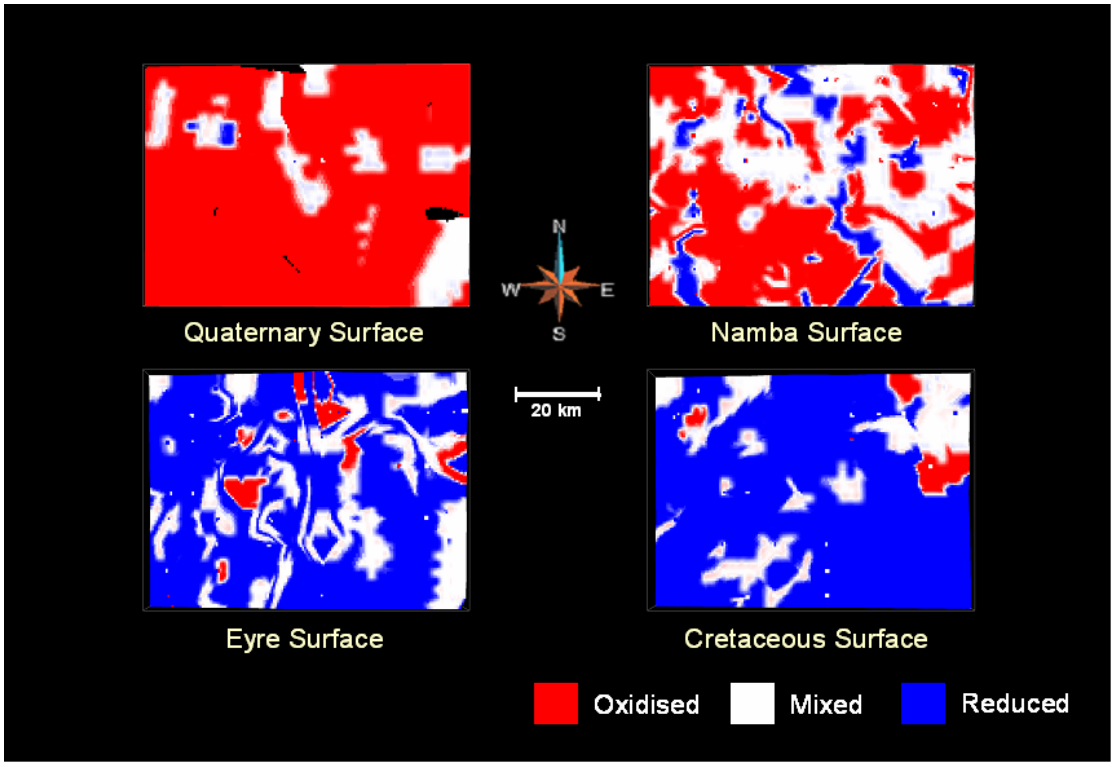

Figure 4.6: *Plan view of the voxet model showing the redox patterns on each lithological surface in the EL 5/6 area.*

4.4.3 Distribution patterns of selected materials in ELs 5 and 6

In order to better understand the causes of the redox patterns, and relationships between redox, lithology and permeability, information on the occurrence of particular minerals, rock types and sediment grain size sand was extracted from the drill logs. The spatial distribution of carbonaceous material, lignite, pyrite, hematite and limonite was mapped in 3D, along with data on the occurrence of gravel, pebbles and carbonate. Two-dimensional plan projections of the results are shown in Figures 4.7 and 4.8. Results for the Namba Formation are shown in Figure 4.7. At top left of the figure, the redox patterns define a semi-continous zone of reduced materials (blue) trending broadly north-south in the central-eastern part of the area, resembling a paleochannel. However, the distributions of the selected redox-sensitive materials in Figure 4.7 (carbonaceous material, lignite, pyrite, hematite and limonite) only partly match the location of the possible paleochannel. One possible reason for this apparent lack of spatial correlation is that not all materials and criteria listed in Table 4.1 are shown in Figures 4.7 and 4.8. For example, the colour criteria in Table 4.1 are not illustrated in Figure 4.7. Carbonaceous material occurs in the southern part of the inferred paleochannel, whereas limonite appears to negatively correlate with the location of some of the reduced zones. The distribution of sand versus gravel potentially may correlate with the presence of paleochannels, but this is not evident in the data. Silt and clay (not shown in Fig. 4.7) are the dominant constituents of the Namba Formation, whereas sand is sporadic and gravel and pebbles are uncommon.

Results for the Eyre Formation show a correlation between the redox pattern and the occurrence of carbonaceous material (Fig. 4.8). Pyrite and lignite are less widespread but contribute to the broad extent of reduced zones in the Eyre Formation. Restricted oxidised zones correlate partly with the presence of hematite and limonite. Sand is ubiquitous within this formation and gravel and pebbles are also common. Carbonate materials are mostly restricted to the south-west corner of the area.

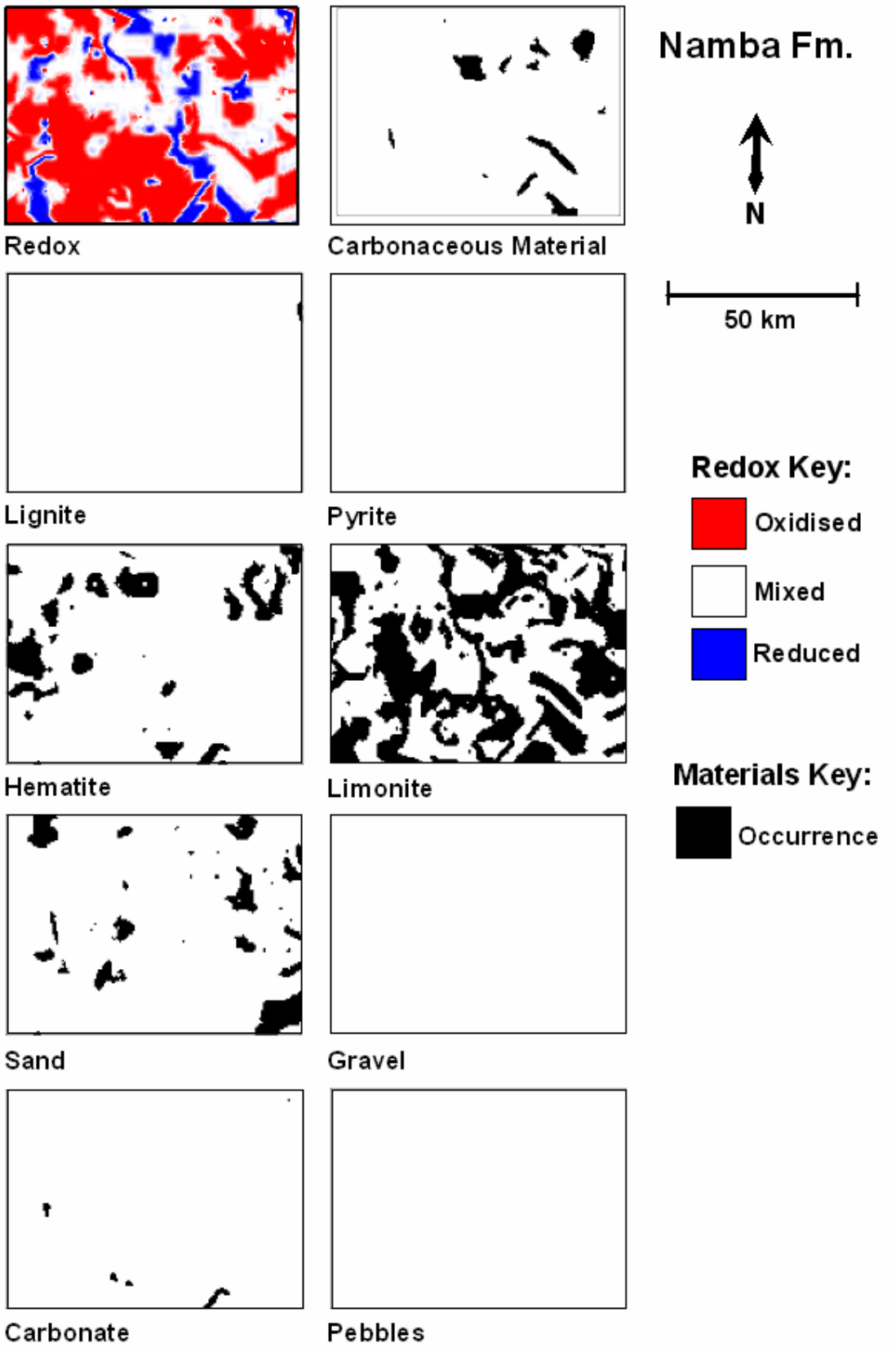

Figure 4.7: *Plans of the occurrence of selected materials in the Namba Formation and comparison with the redox pattern at the upper surface of the formation, EL 5/6.*

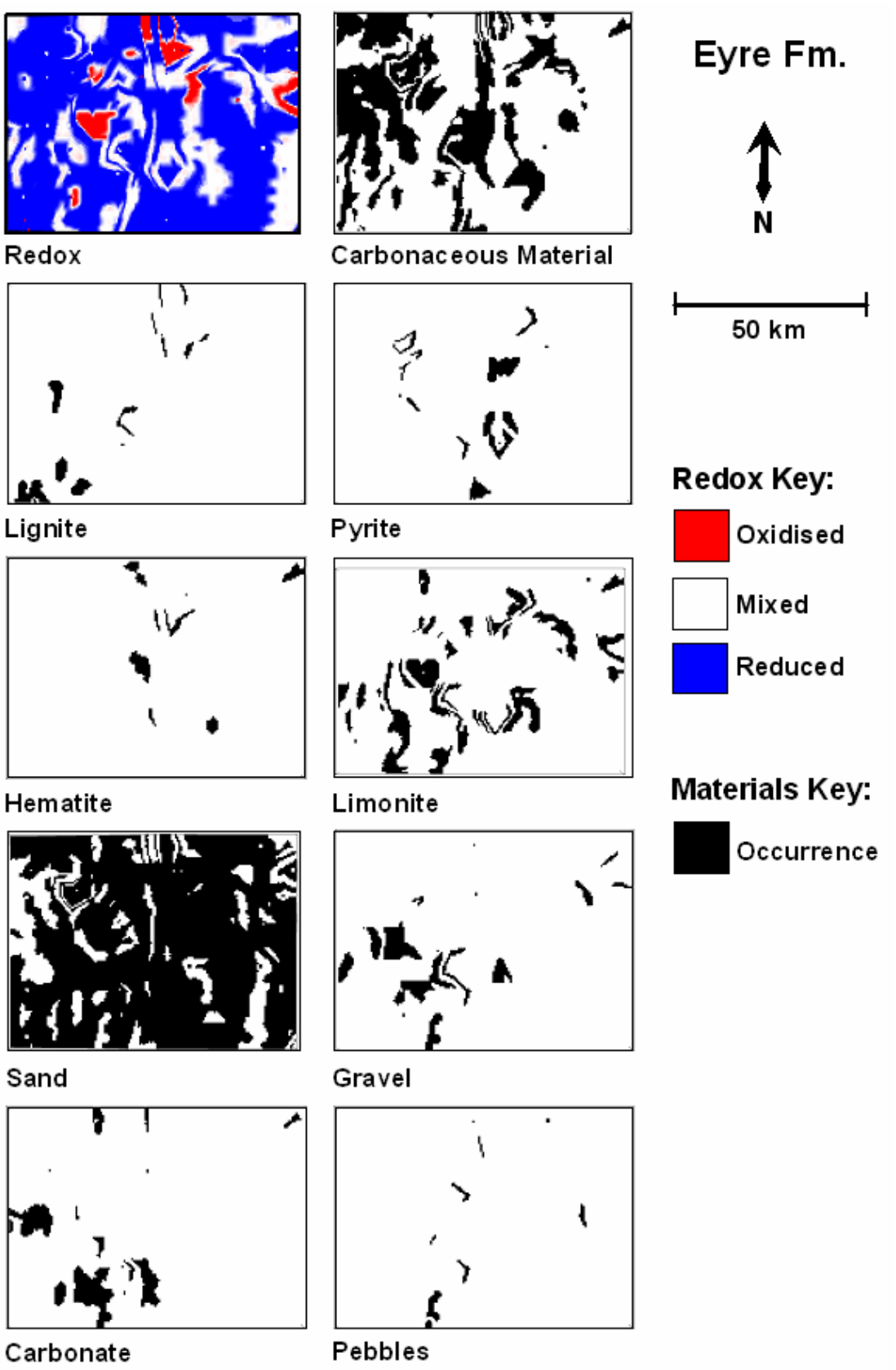

Figure 4.8: *Plans of the occurrence of selected materials in the Eyre Formation and comparison with the redox pattern at the upper surface of the formation, EL 5/6.*

4.5 DISCUSSION

4.5.1 Reliability of the 3D chemical maps

Uncertainties in the spatial distribution of redox characteristics shown in the voxet model arise from the following sources.

- Quality of original observations and descriptions in drill hole logs;
- Efficiency in the filtering methodology in accurately assigning redox values;
- Data spacing, determined by the drill hole spacing;
- Accuracy in the gridding algorithms used in the gOcad program in spatially representing the redox variation.

The broad patterns of oxidation and reduction shown in the 3D models are considered to reflect real variations in redox characteristics of basin sediments and rocks (e.g., shallower oxidised and deeper reduced zones). However, in detail the results should be used with caution in targeting uranium mineralisation because of the inherent uncertainties listed above. Areas with close drill hole spacing clearly will yield results with greater reliability than areas of widely spaced drilling.

4.5.2 Sediments and redox

Vertical sections of the voxet model such as the examples shown in Figure 4.9 show that significant changes of redox state occur at some stratigraphic and lithological boundaries. In particular the results show that the Eyre Formation is significantly more oxidised than the underlying Bulldog Shale in the EL 5-6 area, and the Namba Formation is overall more oxidised than the Eyre Formation. The Namba Formation exhibits the greatest internal variation.

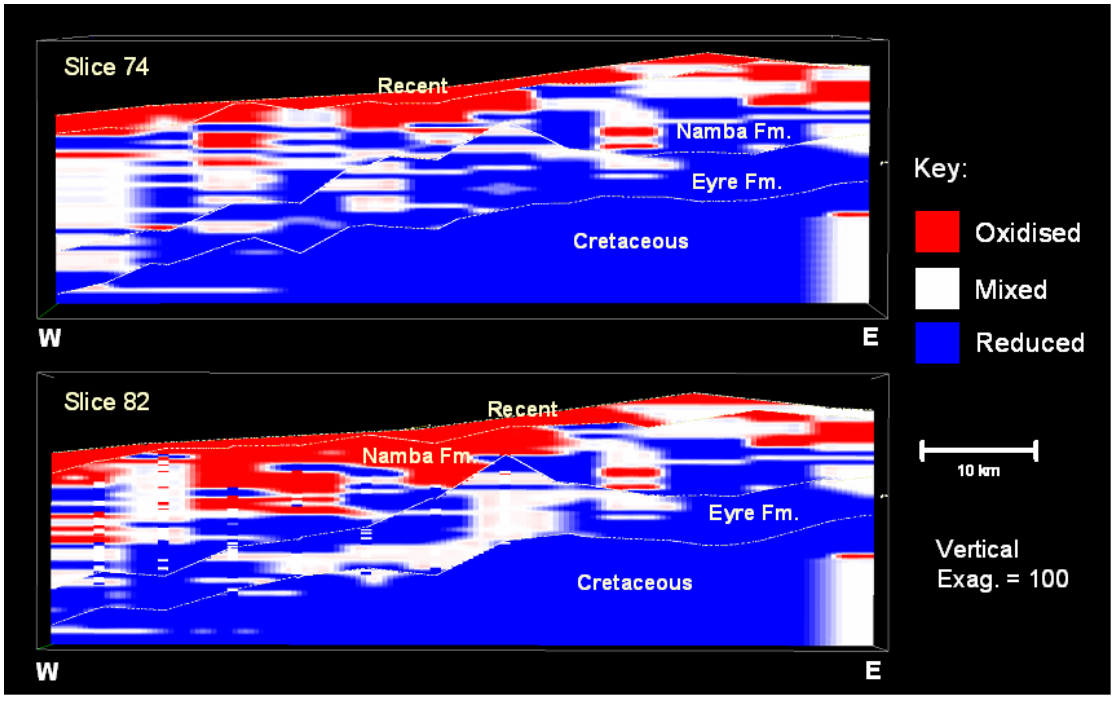

Figure 4.9: *Examples of the redox pattern in vertical sections through the EL 5/6 voxet model.*

Also evident in comparing Figures 4.5, 4.6 and 4.9 are the complex 3-dimensional shapes of oxidised and reduced zones within each stratigraphic formation. Perhaps some of the most significant features for uranium mineral systems are the deeper zones of oxidation within the Eyre

and Namba Formations. In the Eyre Formation zones of 'mixed' redox within reduced rocks appear to form elongate north-south domains mainly along and down-slope (westwards) from the medial ridge that is apparent in the upper surface of the Eyre Formation. Given the current westerly dip of the Eyre Formation it is plausible that these zones represent oxidation fronts produced by oxidised waters moving down-dip from east to west within the Eyre Formation. This geometry implies that any uranium mineralisation in the Eyre Formation in the EL 5-6 area that was deposited along interfaces between oxidised and reduced rock would occur in north-south oriented zones, mainly in the central-western half of the area. Alternatively, the north-south oriented zones may reflect fluid movement along north-south oriented paleochannels within the Eyre Formation. Indeed, paleochannels that involved broadly south to north sediment transport are well known in the Eyre Formation further south (e.g., Yarramba and Lake Namba Paleochannels). The distributions of sand, gravel and pebbles intersected in drill holes (Fig. 4.8) do not discriminate between these alternative scenarios, suggesting that closer spaced drilling and/or other methods of defining paleochannels would be required to further test the 3D model presented herein

Deeper zones of oxidation within the Namba Formation, like those in the Eyre Formation, also appear to be best developed to the west of the ridge in the upper surface of the Eyre Formation. One explanation is that the thicker parts of the Namba Formation to the west of this ridge represent a broad northerly trending paleochannel that also carried oxidised groundwaters. However, in detail the complex geometry of the interfaces between oxidised and reduced domains within the Namba Formation makes interpretation of potential uranium depositional sites difficult in the EL 5-6 area. It is interesting to note a small zone of oxidation in the Namba Formation to the east of the ridge in the upper surface of the Eyre Formation. This may also represent oxidised fluid flow in a subsidiary paleochannel, although its orientation is unknown.

In the uppermost Namba Formation, above the small oxidised zone noted above, a zone of reduced rocks forms a sinuous north-south channel-like geometry. This feature, noted earlier (Figs. 4.6, 4.7) and enlarged in Figure 4.10, apparently aligns with the orientation of known paleochannels in the underlying Eyre Formation (Fig. 4.11). There is, however, no obvious correlation with the drillhole distributions of sands, gravels and pebbles shown in Figure 4.7.

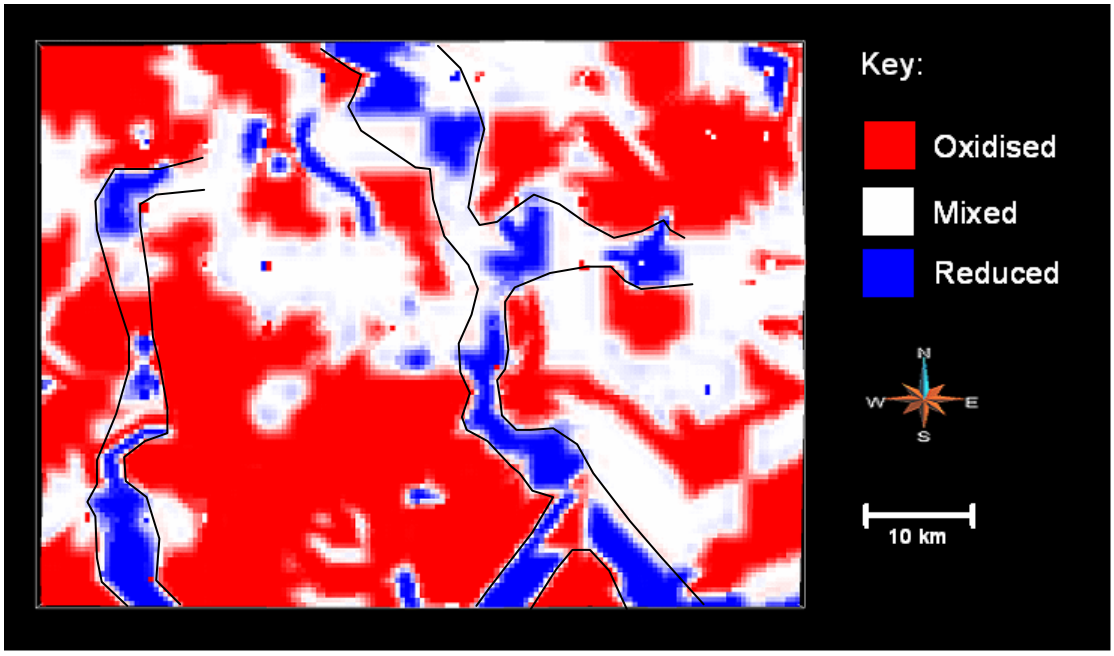

Figure 4.10: *Plan of the Namba surface showing the redox pattern in EL 5/6. The reduced areas have the appearance of paleochannels. The interpreted extent of reduced material is outlined.*

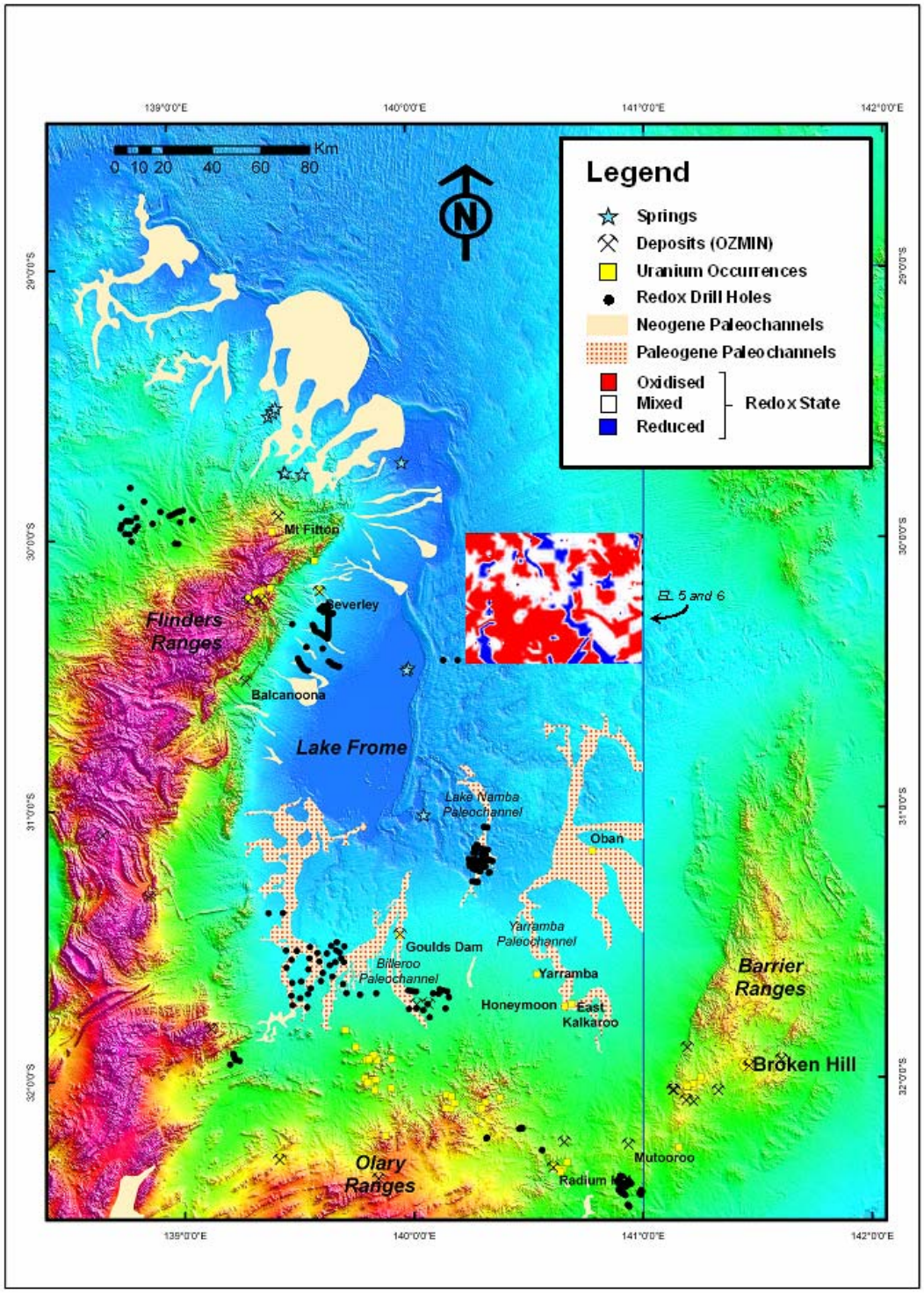

Figure 4.11: *Known distribution of paleochannels and paleovalleys in the Lake Frome region (after Hou et al., 2007), and the redox pattern (from voxet model) on the upper surface of the Namba Formation in the EL 5 and 6 area.*

Union Corporation geologists in the 1970s recognised paleochannel stratigraphy in the drill holes of ELs 5-6 but the four-mile grid spacing of drilling prevented mapping of the possible channels (Randell, 1973). Their preferred model invoked a deltaic environment with westward paleo-flow towards a larger ancestral Lake Frome (in which the Namba carbonates and dolomitic ooze in the south-western corner of the tenements were deposited).

It is notable that the possible eastern paleochannel in the upper parts of the Namba Formation correlates well with the position and orientation of the Yarramba Paleochannel in the underlying Eyre Formation to the south. One interpretation is that a general northwards direction of sediment transport was via paleochannels was extant during both the deposition of the Eyre Formation and Namba Formation. Similar northerly transport of sediment in the Beverley paleochannel seems probable, based on branching geometry of the channel (see Chapter 5). However, it cannot be assumed that groundwater flow during uranium mineralising events followed the same directions as the channels because of possible neotectonic modifications to paleodips in the region.

5. Uranium deposits of the Lake Frome region

Subhash Jaireth

Post-Paleozoic basins of the Lake Frome region host four known uranium deposits and many occurrences and prospects including the recently discovered Beverley North (Pepegoona) prospect (Heathgate Resources, announcement September 2009). The Honeymoon and Oban deposits in the southern part of the region and Four Mile deposit in the northwest are hosted by organic-rich sands of the Paleogene Eyre Formation, whereas Beverley is hosted by organic-rich permeable sand lenses (Beverley Sands) of the Neogene Namba Formation. Beverley is the only uranium deposit known to be hosted by the Namba Formation. Most deposits in the southern part of the Lake Frome region are located within mapped fluviatile paleochannels in the Eyre Formation (such as Yarramba, Lake Namba, Billeroo paleochannels, Fig. 4.11). Paleochannels in the Beverley and Four Mile area have been poorly defined, although available data suggest that at least the Beverley deposit is associated with a paleochannel in the Namba Formation (McConachy et al., 2006).

Both the Four Mile and Beverley deposits are located within 20 kms of uranium-rich rocks outcropping in the Mount Painter Inlier, whereas the Honeymoon and Oban deposits in the south occur within 50 km of uranium-rich Proterozoic basement of the Curnamona Province.

5.1 BEVERLEY URANIUM DEPOSIT

The Beverley uranium deposit is located ~15 km east of the outcropping Mount Painter Inlier. It was the first sandstone uranium deposit to be discovered in the area, and contains a total resource (production + remaining resource) of ~6 million tonnes of ore at an average grade of 0.23 % U_3O_8 which is equivalent of 16 300 tonnes of U_3O_8 (Geoscience Australia, 2009). Since 2000 it has been mined by the *in-situ* leaching technique. Summary descriptions of the Beverley deposit have been published by Brunt (2005), McConachy et al. (2006), Wülser (2005), Marsland-Smith (2005), Curtis et al. (1990), Haynes (1975), and by Heathgate Resources in various on-line reports. Wülser (2009) recently completed a doctoral thesis on the Beverley deposit. The following descriptions are based on these publications.

5.1.1 Host rocks

Uranium mineralisation occurs in the Beverley Clay, Beverley Sands and Alpha Mudstone units of the Namba Formation (late Oligocene to Miocene), although the bulk of mineralisation is located in the lower part of the Beverley Sands close to the contact with the Alpha Mudstone (Brunt, 2005; McConachy et al., 2006). Mineralised sands are thus sealed from above and below by relatively impermeable clays units. Provenance studies indicate that both the Beverley Sands and Beverley Clays were derived from the reworking of Early Cretaceous glacio-lacustrine sediments (Wülser, 2009).

The Namba Formation is overlain by unconsolidated sands, gravels and clays of the Willwortina Formation (Pliocene to Quaternary) which is sourced from the Mount Painter Inlier. Within the mine area the ore-bearing Namba Formation is unconformably underlain by the Cretaceous Bulldog Shale (early Aptian to mid Albian) which in turn overlies a fine-grained sandy sequence of the Cadna-owie Formation (mid-Neocomian to early Aptian). The sediments of Cadna-owie Formation and the equivalent Parabarana Sandstone were deposited in fluviatile conditions.

Sands of the Eyre Formation which underlies the ore-bearing Namba Formation is intersected in drill holes outside the Beverley deposit. They are composed dominantly of carbonaceous and

pyritic sands, intercalated with clays and gravels interpreted to be deposited in braided river channels (Wülser, 2009).

5.1.2 Geometry of paleochannels

Mineralisation at Beverley is interpreted to be hosted by sands which infill Miocene paleochannels incised into the underlying lacustrine Alpha Mudstone (Fig. 5.1, Haynes, 1975; Curtis et al., 1990). The paleochannel and the associated NE trending half graben is controlled by the Paralana-Wertaloona fault system (Curtis et al., 1990). According to Curtis et al. (1990) an oxidation interface with anomalous uranium is traceable within the Namba Formation along a NE trending zone measuring 25 x 15 km. Interpretation by Heathgate Resources shows a system of branching paleochannels (Fig 5.1). Three-dimensional modelling of the underlying Alpha Mudstone surface based on drilling reveals several paleo-highs and lows with the depressions interpreted as channels (McConachy et al., 2006). The N-S drainage system is complicated by several cross-cutting structures (McConachy et al., 2006). The shape and orientation of paleochannels are important factors which determine possible provenance of infill-sediments, fluid-flow direction at the time of mineralisation and distribution of in-situ organic reductants in the sediments. In Figure 4.1 the arrows show the directions of present day groundwater flow. However, the geometry of paleochannel branching suggests that sediment transport was originally from the south.

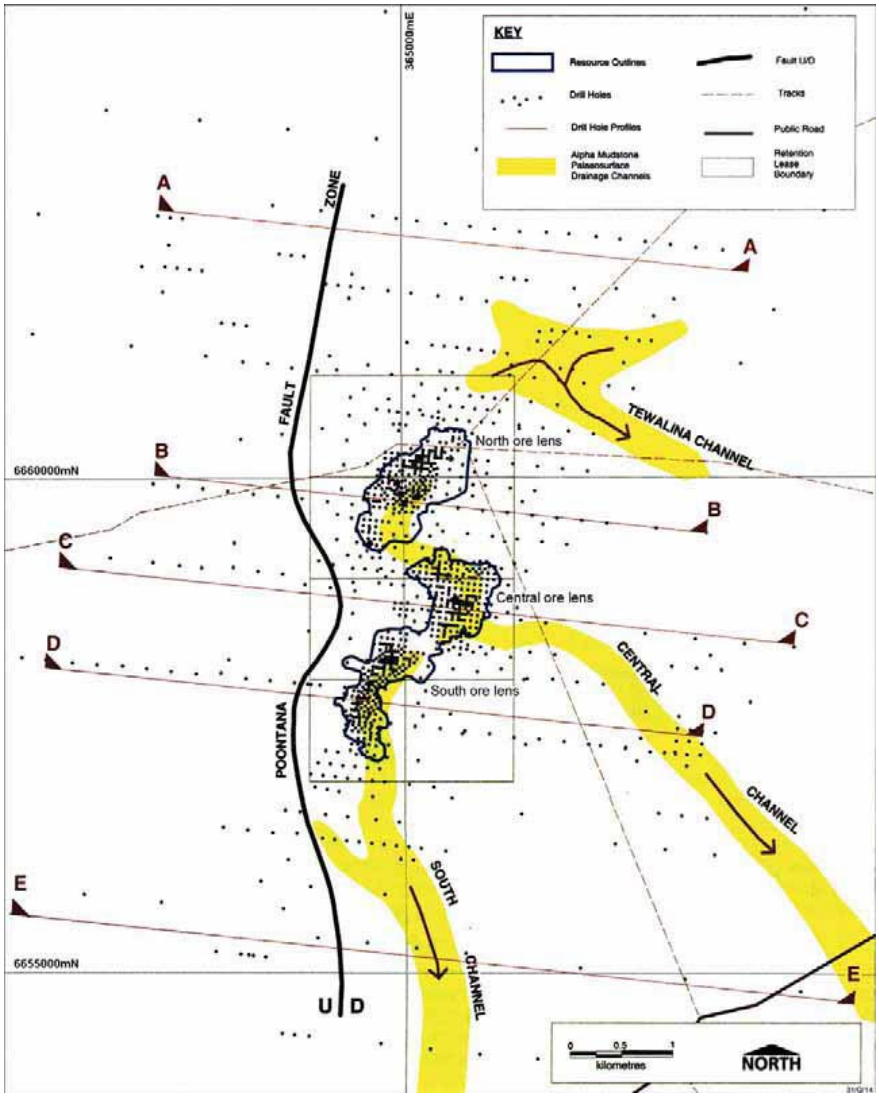

Figure 5.1: *Map of Beverley uranium deposit (resources outlined) and inferred paleochannels (yellow) within the Namba Formation. Source: Heathgate Resources 1998).*

5.1.3 *In-situ* reductants

The Beverley Sands are generally poor in organic material. The dominantly quartzose sands are fine to medium grained and contain laminae and beds of sandy clay, silt and clay and only sparse fragments of organic material. The Alpha Mudstone, however, is rich in organic material represented by plant fragments and large pieces of carbonised wood. In general organic carbon in grey sands ranges from 0.05% to 0.5% increasing up to 2% in a few samples (Heathgate Resources, 1998).

5.1.4 Beverley mineralisation

Uranium mineralisation at the Beverley deposit occurs in predominantly tabular and lenticular zones, mainly at the contact with the organic rich Alpha Mudstone (Fig. 5.2, Brunt, 2005). The combined thickness of ore zones varies typically from 20 to 30 m. The principal uranium mineral is coffinite which fills voids and forms coatings on quartz grains (McConachy et al., 2006). Minor uraninite has been reported but requires confirmation. The uncemented grey sand in the ore zone also contains pyrite, marcasite, feldspars, clays (kaolinite and montmorillonite), gypsum and alunite. Alunite and gypsum may be associated with later oxidation which also produced carnotite (Wülser, 2009).

The ores contains traces of Th, Rb, Sr, Cu, Zn, Mo, V, Se and As, which are typical for sandstone uranium systems (Heathgate Resources, 1998).

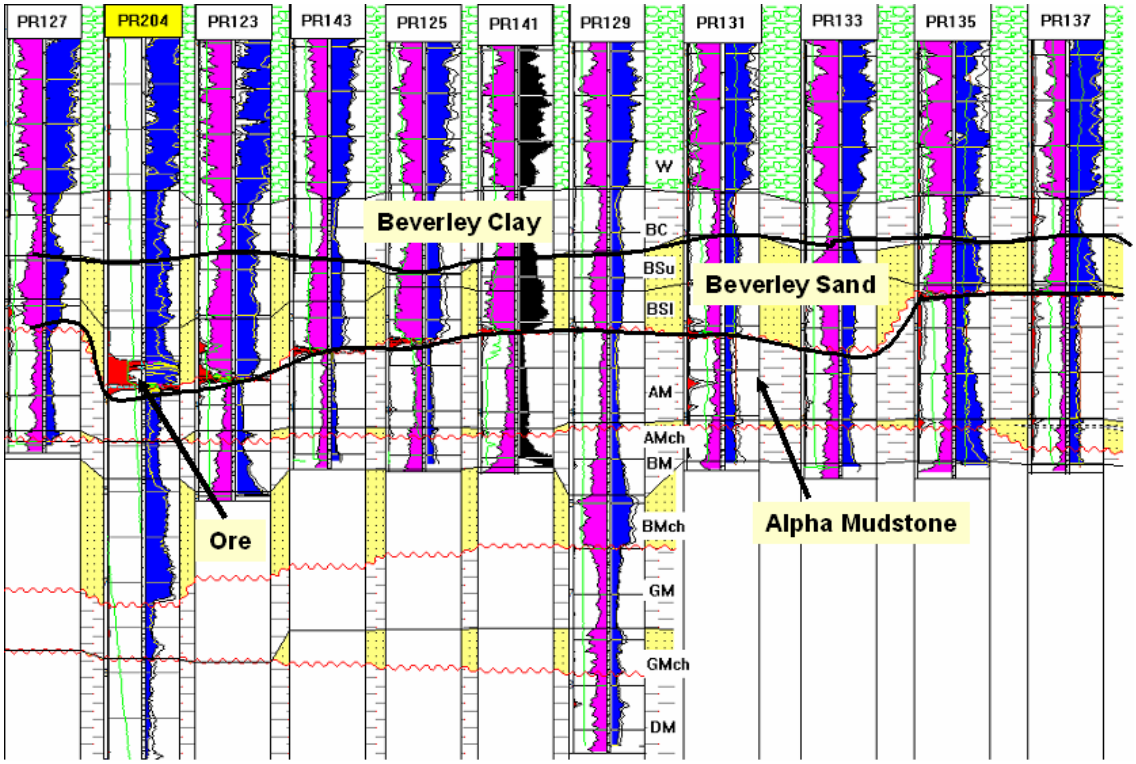

Figure 5.2: *North-south cross section showing uranium mineralisation (red) in the Beverley Sand, Namba Formation (modified after Brunt, 2005). Note that mineralisation is located generally at or near the contact with Alpha Mudstone.*

5.2 Four Mile deposit

The Four Mile deposit was discovered in 2005 and is located 8 km NW of the Beverley deposit. Mineralisation is located in two separate zones: Four Mile West (15 000 tonnes of U3O8 at 0.37% U3O8, Geoscience Australia, 2009) and Four Mile East (14400 tonnes of U3O8 at 0.314% U3O8, Geoscience Australia, 2009).

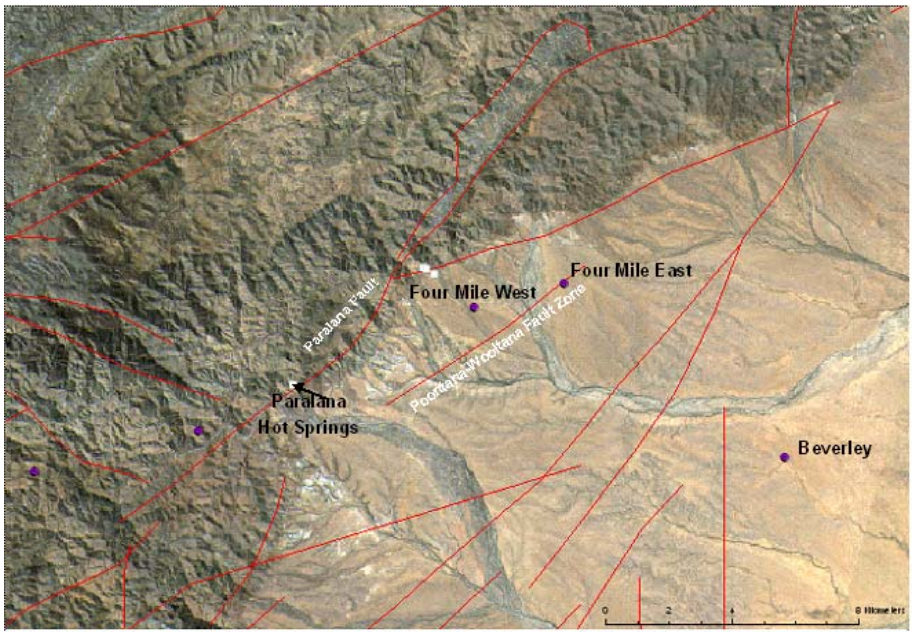

Figure 5.3: *DTM image showing location of the Beverley and Four Mile deposits. Four Mile East and Four Mile West are located in the Four Mile Embayment formed by the Paralana Fault in the west and Poontana-Wooltana Fault in the east. Faults (red lines) from SEEBASE (FrOG Tech, 2005).*

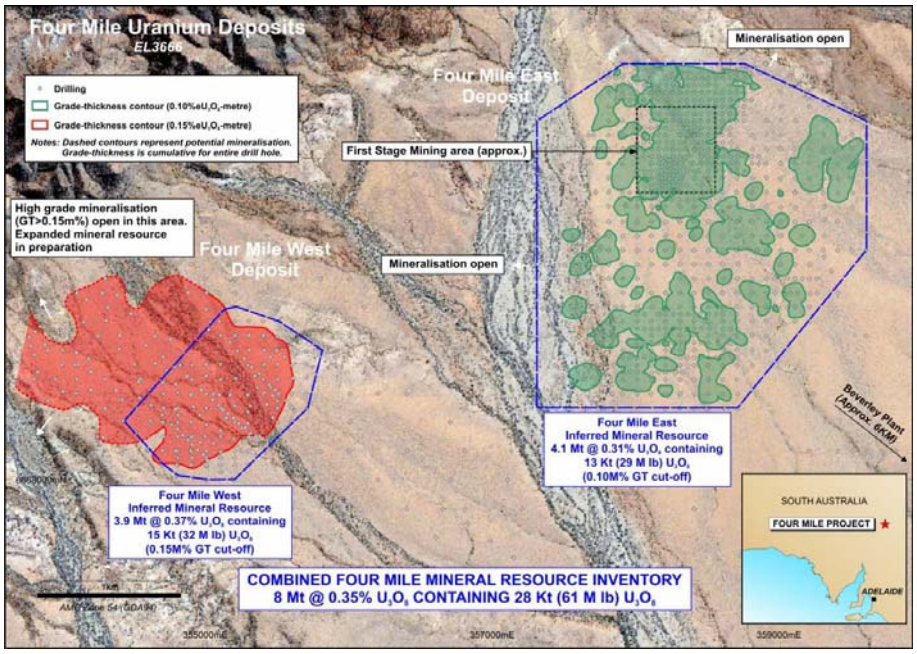

Figure 5.4: *Map showing location of uranium mineralisation at Four Mile East and Four Mile West deposits (Alliance Resources, 2009).*

5.2.1 Host rocks

According to Quasar Resources and Alliance Resources mineralisation at the Four Mile deposit is hosted by fluviatile sands of the Upper Eyre Formation within an area defined as the Four Mile Embayment (Figs. 5.3, 5.4). The NE trending embayment is confined to a structural zone between the Paralana Fault in the west and the Poontana and Wooltana Fault zone in the east. The eastern margin of the embayment represents a horst-like structure (Poontana Inlier). It is possible that the Four Mile Embayment itself represents a Paleogene paleochannel trending NE.

The Eyre Formation at the Four Mile deposit is generally composed of mature sands that are richer in carbonaceous material and pyrite than the Beverley Sands. The sands of the Eyre Formation are interlayered with fine grained silt and coarse grained gravels. The sediments were deposited in a braided river environment. Within the Eyre Formation mineralisation tends to be localised towards the lower contact with a diamictite unit (Alliance Resources, 2009). The diamictite overlies fractured basement rocks (possibly Proterozoic rocks of the Mt Painter Inlier).

The Eyre Formation sands are capped by silcrete (<5 m thick) which is overlain by a sand and shale sequence of the Namba Formation (~100 to 150 m thick).

5.2.2 Four Mile mineralisation

Mineralisation is located in the northeast trending Four Mile Embayment which deepens to the northeast. The west and east zones at Four Mile are less than 2 km from the outcropping Mt Painter Inlier. The highest grades reported for the Four Mile West zone include 3.1m @ 2.2% pU_3O_8, and the highest grade-thickness intercept is 9.5m @ 1.57% U_3O_8 (Alliance Resources, 2009). Grades of up to 1.69% pU_3O_8 have been reported by Alliance Resources for the Four Mile East zone. Interpretations of mineralisation distribution based on drill hole data at Four Mile West show two separate roll-front style mineralised zones closing to the southeast (Alliance Resources, 2009).

As described in detail in Chapter 5, uraninite is the dominant ore mineral in the Four Mile East zone, based on samples studied to date. Pyrite is common and occurs in four textural types, of which the earliest in the paragenetic sequence was replaced by uraninite. Abundant kaolinite and a variety of REE- and U-bearing phosphate minerals are present in the Four Mile East ore zone. Detrital ilmenite was replaced by rutile and other secondary titanium minerals.

5.3 HONEYMOON URANIUM DEPOSIT

The Honeymoon deposit (discovered in 1972) is located in the buried Yarrramba Paleochannel in the southern part of the Lake Frome region (Fig. 4.11). It contains a resource of 2 880 tonnes of U_3O_8 with an average grade of 0.20% U_3O_8 (Geoscience Australia, 2009). The Honeymoon deposit recently was approved for mining by the in-situ leaching method. The Yarramba Paleochannel also hosts the nearby East Kalkaroo and Yarramba uranium prospects (Skidmore, 2005).

5.3.1 Host rocks

The Yarramba Paleochannel incises into Mesoproterozoic basement rocks of the Willyama Supergroup, including uranium-rich granitoids. The Eyre Formation sediments filling the channel comprise an upward fining succession of interbedded sand, silt and clay. The average width of the channel is ~3 km reaching a maximum of 6 km east of Honeymoon (Southern Cross Resources, 2000). The sequence is overlain by a thick succession (~75 m) of lacustrine sediments of the Namba Formation (Fig. 5.5, Skidmore, 2005).

Mineralisation is predominantly localised in the basal aquifer of the Eyre Formation that directly overlies altered basement. The lower sandy aquifer in the Eyre Formation is locally pyrite-rich (average 2.6%, estimated on the basis of sulfur analysis by Bampton et al. (2001), and averaging 7% as cited in Southern Cross Resources (2000)) and contains an average 0.3% carbonaceous matter. The organic material is in the form of lignite and fragments of plant and woody material (Bampton et al., 2001; Skidmore, 2005). The clast-supported sand is interlayered with gravel units. The upper parts of the basal sands are enriched in carbonaceous material which includes coarse lignitic wood fragments. Clayey intervals dominate both middle and upper parts of the Eyre Formation in the Honeymoon area.

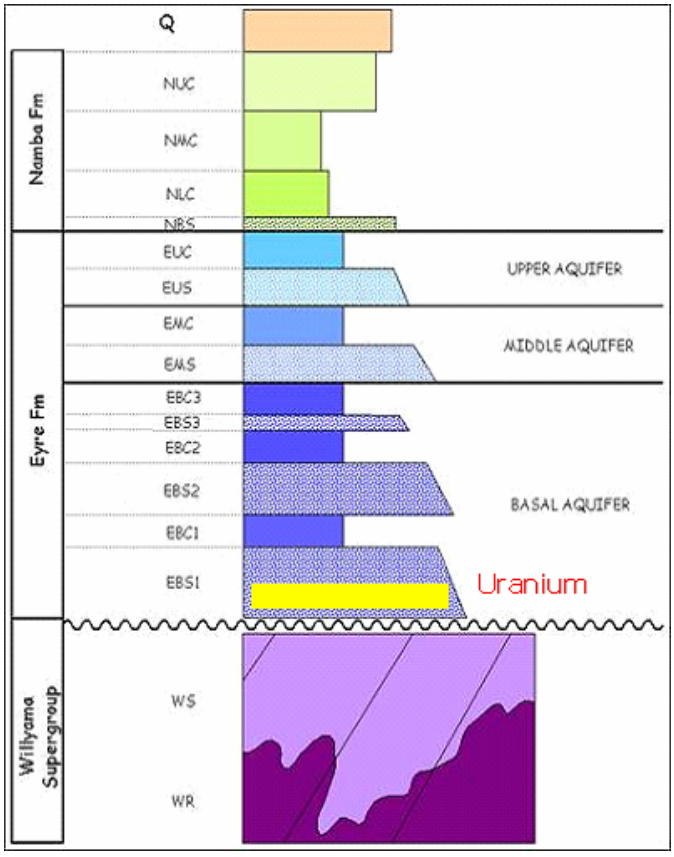

Figure 5.5: *General stratigraphy at Honeymoon deposit. Uranium mineralisation is predominantly located in the lowermost sandy aquifer in the Eyre Formation (Skidmore, 2005).*

5.3.2 Geometry of Yarramba Paleochannel

According to Skidmore (2005), the geometry of ~115 km long Yarramba Paleochannel is strongly controlled by the stratigraphy and structure of underlying basement. The orientation of the northwest- to north-trending paleochannel system is interpreted to have been controlled by faults active during deposition of the Eyre Formation (Skidmore, 2005). Mineralisation at Honeymoon is located at a major bend in the paleochannel where it traverses a basement ridge evident in gravity data (Fig. 5.6). Graphitic metapelitic rocks in the basement ridge may have been more resistant to weathering and erosion than adjacent metaevaporite-bearing rocks of the Bimba Formation. The Yarramba prospect (north of Honeymoon) occupies a similar position on a bend (see Fig 6.2 in Report by Southern Cross Resources (2000)). An important feature of the main channel is the presence of branches and tributaries. Some of these tributaries have catchments covering basement with uranium-rich felsic rocks. For example, a drill hole in the upstream part of a tributary close to the Honeymoon deposit intersected syenogranite containing up to 75 ppm uranium (Skidmore, 2005).

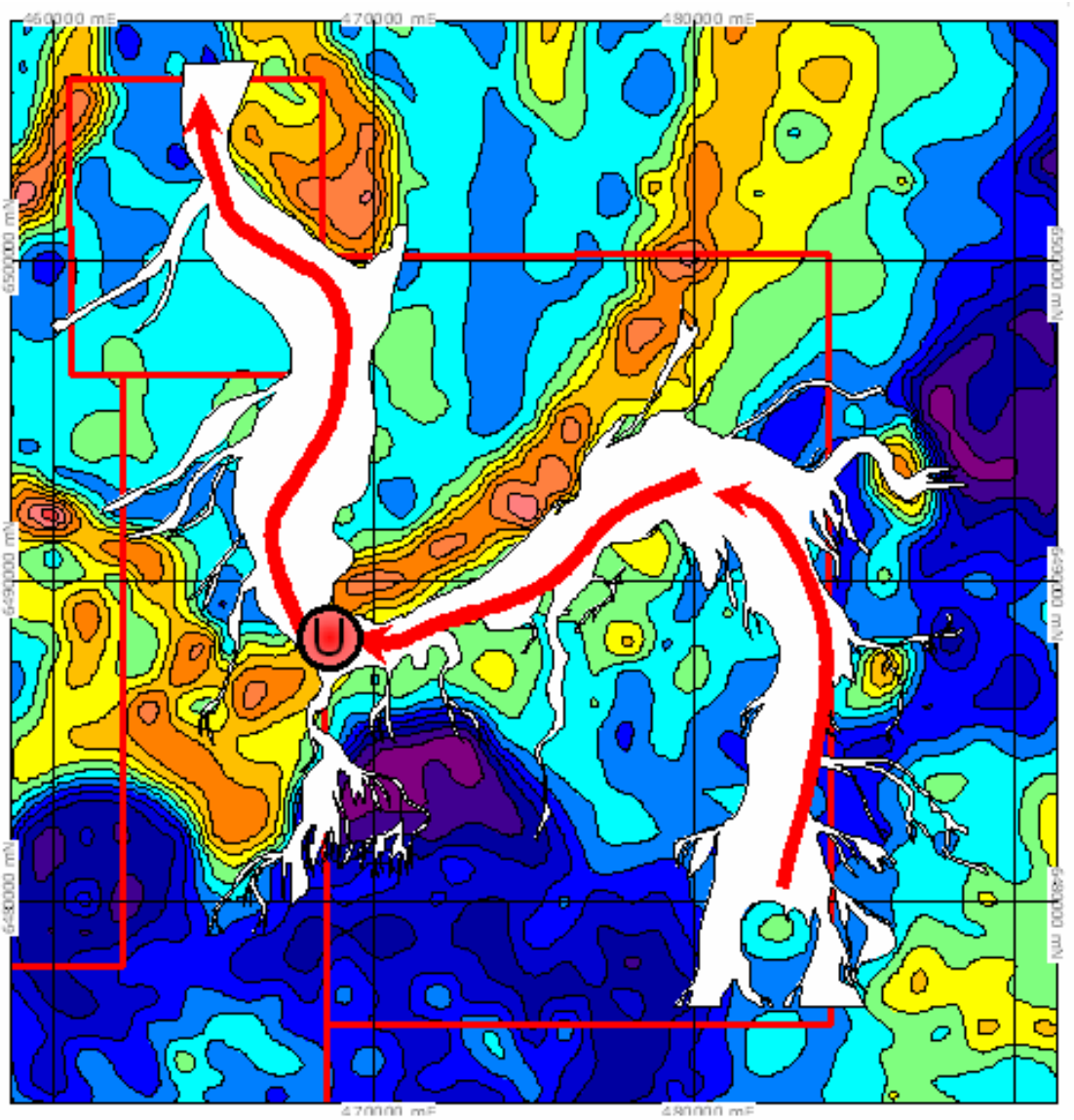

Figure 5.6: *Bends in the main Yarramba paleochannel (white with red arrow). Note several tributaries draining in to the main channel. Honeymoon deposit is located at the bend (circled symbol U). Paleochannel is plotted over gravity (0.5 mgal residual gravity contours). NE trending gravity high coincides with the ridge. Honeymoon deposit is located at the faulted breach in the ridge. N-trending tributary south of Honeymoon and draining in to the main channel crosses uranium-rich granites (roughly coinciding with purple areas on the gravity). Source: Skidmore (2005).*

5.3.3 Honeymoon mineralisation, and oxidation-reduction patterns

Tabular ore zones occur at a depth of 110 m below surface and average 4.3 m in thickness (Fig. 5.7). The mineralisation is in the form of microscopic coffinite closely associated with humic and pyritic material (McKay and Miezitis, 2001; Skidmore, 2005).

Much of the paleochannel infill sediments appear to have been oxidised with only local occurrences of reduced sands. A roll-front type geometry of the oxidation-reduction interface has not been observed at Honeymoon. The influx of oxidised waters in the aquifer is still active causing selective dissolution and removal of uranium.

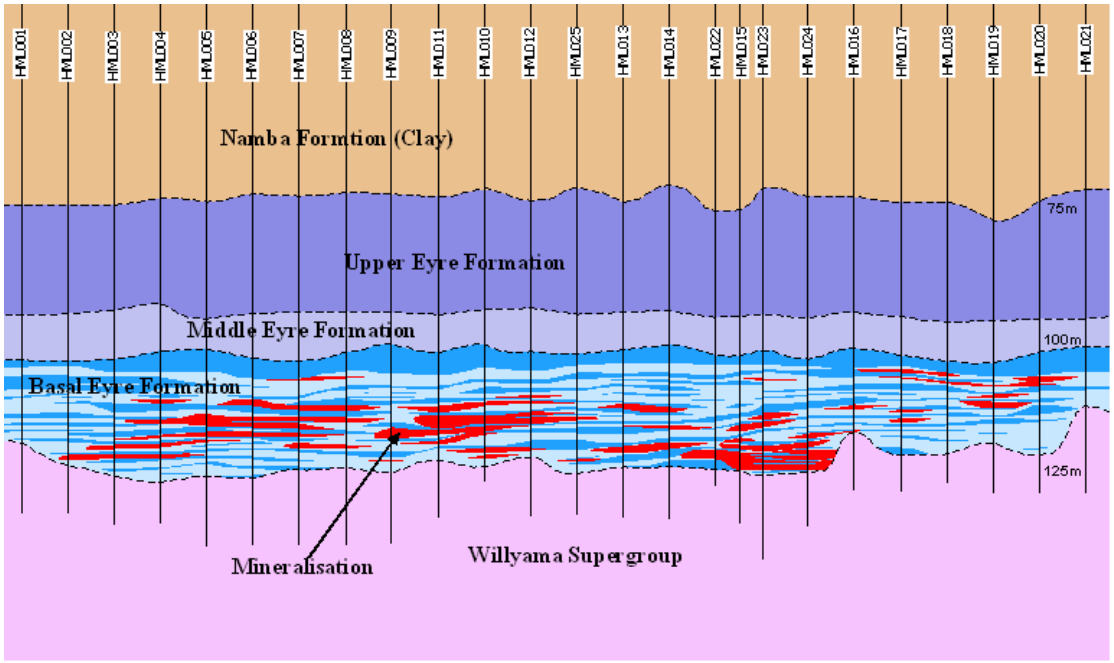

Figure 5.7: *Cross section showing uranium mineralisation at the Honeymoon deposit. Tabular zones are located in the basal sandy unit of the Eyre Formation. Locally, mineralisation occupies depressions in the paleo-relief at the base of the Eyre Formation. Vertical exaggeration 5 times. Source: Skidmore (2005).*

5.3.4 Factors controlling uranium ore deposition at Honeymoon

The ore zones at the Honeymoon deposit are located at a prominent bend in the Yarramba paleochannel. As mentioned above the location of this bend is the result of a combination of factors which may include the structure and composition of the bed rock and the presence of a fault zone cutting relatively dense bedrock strata. At this stage it is not clear if the ore zone's location is related to changes in the relative permeability of sands in a fining-upward sequence of point bars, or due to selective concentration of detrital organic material in the sediments. Fine-grained overbank sediments that cap the sandy sequence are typically rich in organic material (Miall, 1992). Migration of channels commonly leads to abandoned channels which are filled with silt and clay with abundant plant material (LeBlanc, 1972).

Studies on the distribution of organic matter in low-energy meandering streams show that the presence of abundant woody debris at bends enhances the content of organic matter in bed material (Daniels, 2006). Thus the location of ore zones at the bends of paleochannels can be explained by increased concentration of organic reductant in the sediments at the bends. The change in fluid flow rates at bends can also facilitate effective interaction between the fluid and the organic reductant.

An additional factor in localising mineralisation at the Honeymoon deposits may be the close proximity of uranium-rich granitoids in the basement. A north trending tributary of the Yarramba Paleochannel drains an area of buried granitoid with uranium contents of ~ 75 ppm. Thus a combination of two factors, the presence of beds enriched in organic material and an hydrological connection with uranium-rich source near the bend, may explain the position of ore in the Yarramba Paleochannel.

5.4 TIMING OF URANIUM MINERALISATION: HYPOTHESES

5.4.1 Maximum ages of mineralisation

The depositional ages of host rocks provide maximum ages of mineralisation. The Four Mile East zone and Honeymoon deposit are hosted by the Eyre Formation. Sediments of the Eyre Formation were deposited in two separate episodes (late Paleocene to late Eocene, i.e. ~55 to 49 Ma; and early middle Eocene to middle Eocene, i.e., ~45 to 37 Ma) interrupted by a period of non-deposition and possibly erosion (Fig. 3.1). Sedimentation of the Eyre Formation was terminated by a period of uplift and erosion (Middle Eocene to Late Oligocene, i.e. ~37 to 28 Ma).

Mineralisation at the Beverley deposit is hosted by the Beverley Sands in the Namba Formation. Palynological studies indicate that the age of the Namba Formation is between ~ 24 Ma and 4-6 Ma (Martin, 1990, in Wülser, 2009, page 38).

In most sandstone uranium systems the sandstone aquifers hosting mineralisation are hydrologically constrained between aquitards or aquicludes, and it is thought that mineralisation forms after the deposition of the upper aquiclude/aquitard (Dahlkamp, 1993). In the Lake Frome region the Eyre Formation contains an alternating series of interlayed aquifer (sand, silt) and aquitard (shale) units (e.g., Fig. 5.5). Hence, the maximum age of uranium mineralisation hosted by the Eyre Formation is that of the shaley/clay intervals overlying mineralisation in this Formation. These are potentially as old as ~55 Ma. Alternatively, thick regionally distributed aquitards/aquicludes in the hangingwall of mineralisation may have been an important control on timing of mineralisation. The Alpha Mudstone or Beverley Clay (Namba Formation) both could have functioned as regional seals. In this case, uranium mineralisation in the Eyre Formation would have post-dated deposition of the Alpha Mudstone (late Oligocene to early Miocene, i.e. ~28 to 20 Ma) or the Beverley Clay (late Miocene, ~10-6 Ma).

Similarly, the Beverley Clay may have been a regional seal during formation of the Beverley deposit. In this case, mineralisation at Beverley would have formed after ~6 Ma.

In summary, based on depositional ages of host rocks and aquitards/aquicludes, the maximum ages of mineralisation hosted by the Eyre Formation and Beverley Sands are ~55 Ma and ~6 Ma, respectively.

5.4.2 Mineralisation timing constraints from uplift and cooling history

The periods of uplift and erosion could be significant for the generation of sandstone uranium systems by creating highland topography in the region. Uplift of basement potentially can trigger gravity-driven shallow-level groundwater flow into aquifer units surrounding the basement uplift, a concept supported by our numerical modelling (Chapter 7). These conditions also may be favourable for the leaching of uranium from uranium-rich source rocks in the basement. Thus, an understanding of uplift and cooling history may provide constraints on the timing of mineralisation.

As noted in section 3.2 and illustrated in Figure 3.1, thermochronological and other studies have revealed three major episodes of regional cooling and corresponding uplift since the late Mesozoic in the Lake Frome region and Mt Painter Inlier in particular (Foster et al., 1994; Mitchell et al., 2002; Célérier et al., 2005; Quigley et al., 2007). Some of this uplift has occurred on the Paralana Fault Zone, located at the eastern margin of the Mount Painter Inlier. The fault system was initiated in the Mesoproterozoic and has been repeatedly reactivated. Early in the development of Neoproterozoic rifting it was active as an extensional or transtensional fault, and may have been reactivated as a steep reverse fault in the Cenozoic and/or Quaternary (Preiss, 1995), commencing in the early Paleocene or even in the late Cretaceous (Mitchell et al., 2002). Observations of tilted gravel deposits suggest that major uplift of the northern Flinders Ranges occurred during the Late Pliocene or Early Pleistocene (Foster et al., 1994). Using cosmogenic ^{10}Be erosion-rate estimates

Quigley et al. (2007) suggested that current rugged topographic relief in the northern Flinders Ranges could have formed in the past 4 million years. Seismic activity in the area indicates that the Paralana Fault is still active with reverse movement (Sprigg, 1984).

If three major episodes of uplift and exhumation occurred since the late Mesozoic, as appears likely from available evidence, then we may infer that there is potential for three periods of fluid flow from uplifted regions into the surrounding basins. Each of these fluid flow episodes may have resulted in uranium mineralisation (Fig. 3.1), although this hypothesis remains to be tested. The Beverley deposit is interpreted to have formed during the third episode (i.e., since ~6 Ma), whereas deposits hosted by the Eyre Formation (e.g., Four Mile, Honeymoon) may have formed either in the second (late Eocene – early Oligocene) or third episodes of uplift and fluid flow. No significant uranium mineralisation has been described in the literature within Mesozoic sediments in the region. Our synthesis of available data suggests there is potential for fluid flow driven by late Cretaceous uplift in the region and hence the possibility of late Mesozoic – Paleocene uranium mineralisation. However, the presence or absence of other components of a fertile mineral system (Fig. 1.2) will determine whether any such mineralisation is of economic significance.

Present day groundwater flow in the Beverley Sands, in conjunction with evidence for disequilibrium of radioactive parent and daughter isotopes (Wülser, 2009), suggests that mineralisation at Beverley may be still in the process of formation, or at least re-mobilisation. Similarly, flowing groundwaters in the Yarramba Paleochannel may be actively forming or redistributing uranium mineralisation in the Honeymoon deposit.

6. Four Mile uranium deposit: mineralogy

Anthony Schofield, Mäité Le Gleuher, Andrew Cross, Subhash Jaireth

6.1 INTRODUCTION

The Four Mile U deposit, including the Four Mile East and West zones, is hosted within the late Paleocene to middle Eocene Eyre Formation (Heathgate Resources, 2009). The Eyre Formation consists of carbonaceous sand, with minor clay lenses and abundant organic material (Callen, 1990). Although this deposit represents the most significant recent U discovery in Australia, no published mineralogical and petrological information exists. This chapter will discuss preliminary results from a petrographic investigation of material from the Four Mile East zone, and will briefly compare these with observations from the Beverley uranium deposit. It is intended to provide a framework for future geochronological studies by placing the U-hosting mineralogy into its textural and paragenetic context.

6.2 SAMPLES AND ANALYTICAL PROCEDURES

The samples used in this investigation were obtained with permission from the Australian Nuclear Science and Technology Organisation (ANSTO). Twenty-eight samples were collected from the Four Mile East zone, spanning both mineralised and non-mineralised zones. The samples are taken from drill holes AKC026 (1 sample), AKC028 (1 sample), AKC029 (20 samples). AKC030 (2 samples), AKC032 (1 sample) and AKC035 (1 sample). Five polished scanning electron microscope (SEM) mounts prepared by ANSTO were obtained from the Beverley deposit for analysis.

Optical and scanning electron microscopy (SEM), and electron microprobe analysis was undertaken on the samples. Electron microprobe analysis was performed using a Cameca SX100 instrument at the Research School of Earth Sciences, Australian National University. SEM examination of the sample thin sections was made using a Cambridge S360 instrument fitted with a Tracor Northern energy dispersive X-ray analyser (EDXA) and a Zeiss UltraPlus analytical field emission SEM (FESEM) fitted with an INCA Energy 450 EDXA, both located at the Research School of Biological Sciences, Australian National University. A JEOL 6490LV SEM fitted with a JEOL JED-200 EDXA located at Geoscience Australia was used for further observations.

X-ray diffraction analyses of 21 crushed and unoriented bulk samples were recorded with a Siemens D500 diffractometer operating at 40 mA and 40 kV using Cu Kα radiation, with a counting time of 2 seconds per 0.02º 2θ. Twenty two bulk samples from inside and outside the ore zone were selected for XRD analysis. Four extra subsamples consisting of macroscopically different material in a uranium-rich sample from AKC029 were also analysed.

6.3 MINERALOGY

6.3.1 Detrital phases

On XRD patterns, the signal is dominated by quartz and kaolinite. Angular to subrounded detrital quartz grains up to 0.5 mm constitute the most abundant mineral across all of the samples. Some quartz grains display embayed boundaries, suggesting that a degree of quartz dissolution has occurred. Quartz dissolution is much more intense in regions of high organic content. No quartz precipitation was observed however. Minor sericitised, subrounded detrital feldspars of up to 250 μm comprise the other framework mineral observed in the samples. Other detrital minerals

observed as an accessory phase are chalcopyrite, zircon, xenotime, monazite, muscovite and ilmenite. It is also likely that some detrital apatite is also present.

Detrital ilmenite contains about 3% MgO and traces of Mn, and is mostly altered to a Ti-rich product and pyrite to a variable extent (Fig. 6.1). The cryptocrystalline and porous Ti-rich (>70% TiO_2) alteration product, or leucoxene, consists of Ti-oxides (brookite or anatase) associated with unaltered ilmenite remnants. The Ti-rich alteration product is depleted in Mg and enriched in V and U, which are not present in the original ilmenite (Fig. 6.1). This suggests precipitation of a U-V mineral in the pore spaces of leucoxene, or the adsorption of these elements onto the surface of anatase. Iron released during the alteration of the ilmenite grains to Ti-oxides is incorporated into pyrite, which replaced the ilmenite along the rims and fissures of the grain, indicating that the alteration took place under reducing conditions (Weibel and Friis, 2007). The alteration rim (A) around the pyrite is enriched in S and V, and Mg was leached away from the alteration site.

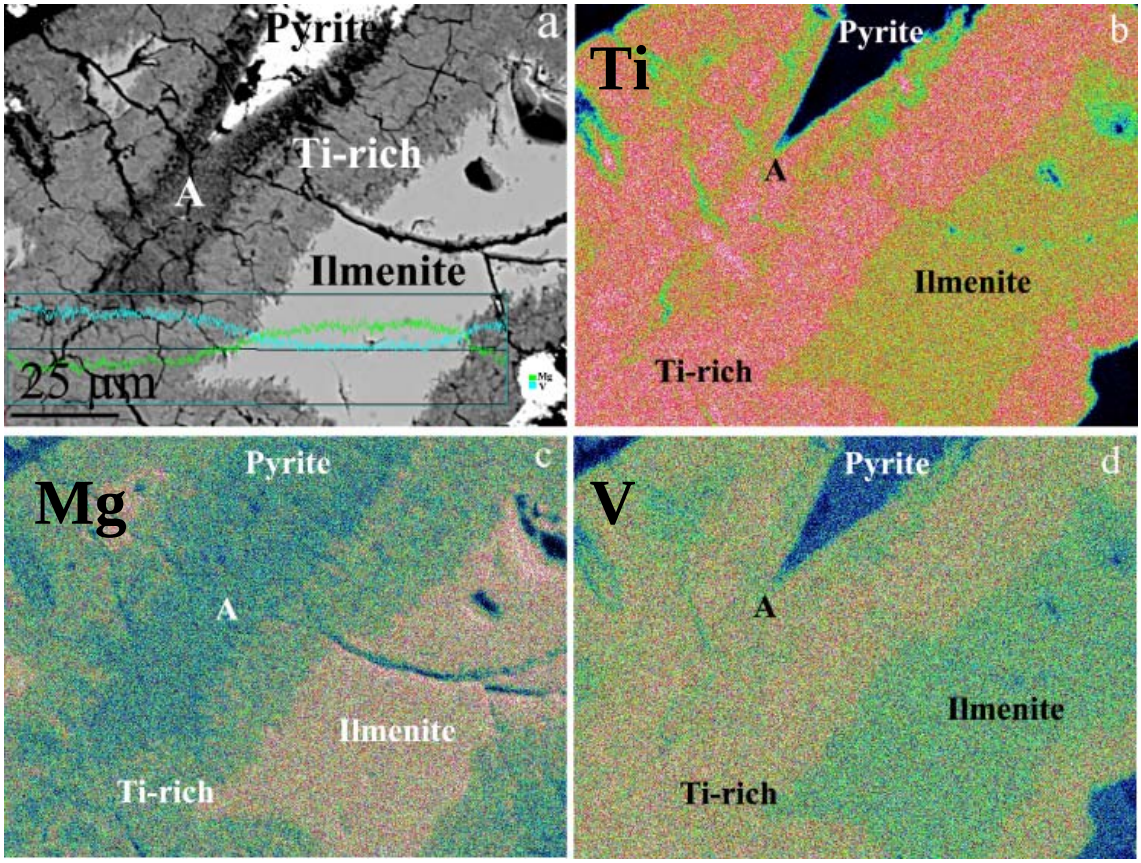

***Figure 6.1**: (a) SEM micrograph (secondary electron image) of an ilmenite grain partially replaced by pyrite and leucoxene (Ti-rich). (b), (c) and (d): Ti, Mg and V distribution maps, respectively, of the same area as (a), determined by SEM. Ilmenite and leucoxene can be distinguished by their antithetic V and Mg distribution: Mg is released during ilmenite alteration and is not retained in the leucoxene alteration products which are enriched in V and U. A = alteration rim.*

Kaolinite is the dominant mineral found in the clay matrix. It is interpreted to be of generally detrital origin, and occurs as platy crystals. Illite is also interpreted to be present in the matrix, given the presence of K in energy dispersive spectra (EDS). Much of the matrix is organic-rich. Typically, this gives the samples a brown stained appearance in plane transmitted light, which obscures much information. Small (1-2 µm) pyrite crystals are also prominent in the matrix, and this will be discussed further below.

The content of organic material is high in mineralised samples, resulting in a dark grey to black appearance in hand sample. Most of the organic matter is represented by finely disseminated material in the matrix, but larger clasts of organic material are distributed unevenly throughout the samples. In organic-rich parts of samples, mineral grain size is typically finer, and quartz dissolution is more intense. U-bearing minerals are rare amongst organic clasts, and are of a very fine grain size where they occur.

6.3.2 Post-depositional phases

A wide range of sulfide, oxide, silicate and phosphate minerals were precipitated within the Eyre Formation host rocks after sedimentation. The occurrence of secondary pyrite, phosphate and uranium-bearing phases is described below.

6.3.2.1 Pyrite

Pyrite is a common post-depositional mineral in the Four Mile samples, and is evident on XRD scans. Four types of pyrite are recognised in the sample (Fig. 6.2). The earliest phase of pyrite growth is represented by framboidal pyrite aggregates. These are most likely bacterial in origin, and formed during or shortly after the deposition of the original sediment. A second phase of pyrite crystallisation is represented by euhedral pyrite growth, commonly occurring as cement. This is commonly seen to overprint the earlier framboidal pyrite, indicating a later place in the paragenetic sequence. They are generally terminated with a perfect crystal face, suggesting that the cement grew in open space between grains. These cements are generally (although not universally) associated with euhedral marcasite. The relationship between pyrite and marcasite is difficult to determine, although it appears that, in general, marcasite occurs as a core to pyrite. Thus, there is a transition in FeS_2 mineralogy with time. A third phase of pyrite is evident as overgrowth rims on the euhedral pyrite. The fourth type of pyrite occurs as tiny euhedral crystals in the clay matrix. It is not possible to distinguish a chronology between the pyrite in the matrix and the large authigenic pyrite and rims, and the matrix pyrite may have formed contemporaneously or independently of either.

There is a strong association between the authigenic pyrite and ilmenite/Ti-oxide, with authigenic pyrite frequently observed to nucleate around detrital grains of Ti-oxides, and sometimes replace them. Pyrite is also intimately associated in places with phosphate and uraninite (see below).

6.3.2.2 Phosphate minerals

Two main types of phosphates have been identified:

1. Hydrated LREE-rich phosphates (rhabdophane and ningyoite); and
2. Aluminous hydroxy phosphates.

Hydrated LREE-rich phosphates Phosphates of the rhabdophane group have been detected in 11 samples. Minerals of this group have the general formula of XPO4.nH2O where X can be REE, Y, Ca, Pb, Th and U (Jones et al., 1996). Two types of these rare earths phosphates have been distinguished by their chemical compositions, XRD spectra and habits. The most common is a La-Ce-Ba rhabdophane, which forms micrometric, diffuse, cloudy aggregates scattered amongst the matrix in both the organic-rich and mineralised segments (Figs. 6.3 and 6.4). A second type of hydrated LREE phosphate occurs as pseudomorphs of a detrital mineral, possibly apatite. It has been identified as ningyoite, a U-Ca-Ce-La-Nd hydrated phosphate (Figs. 6.5, 6.6 and 6.7).

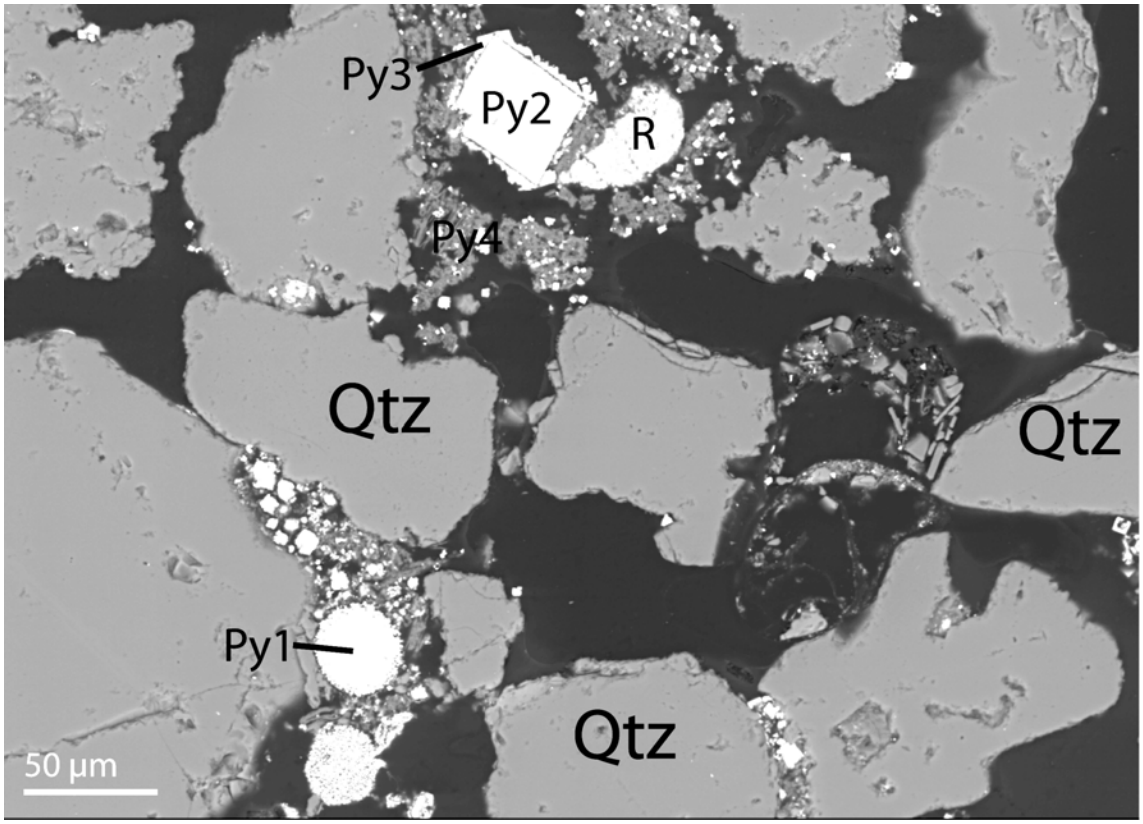

***Figure 6.2**: SEM micrograph (backscattered electron image) showing the four types of pyrite encountered in samples from Four Mile East. Note that several quartz grains appear to have embayed boundaries. Py1 = early framboidal pyrite, Py2 = euhedral pyrite, Py3 = pyrite overgrowth rims, Py4 = euhedral pyrite in matrix, Qtz = quartz, R = rutile.*

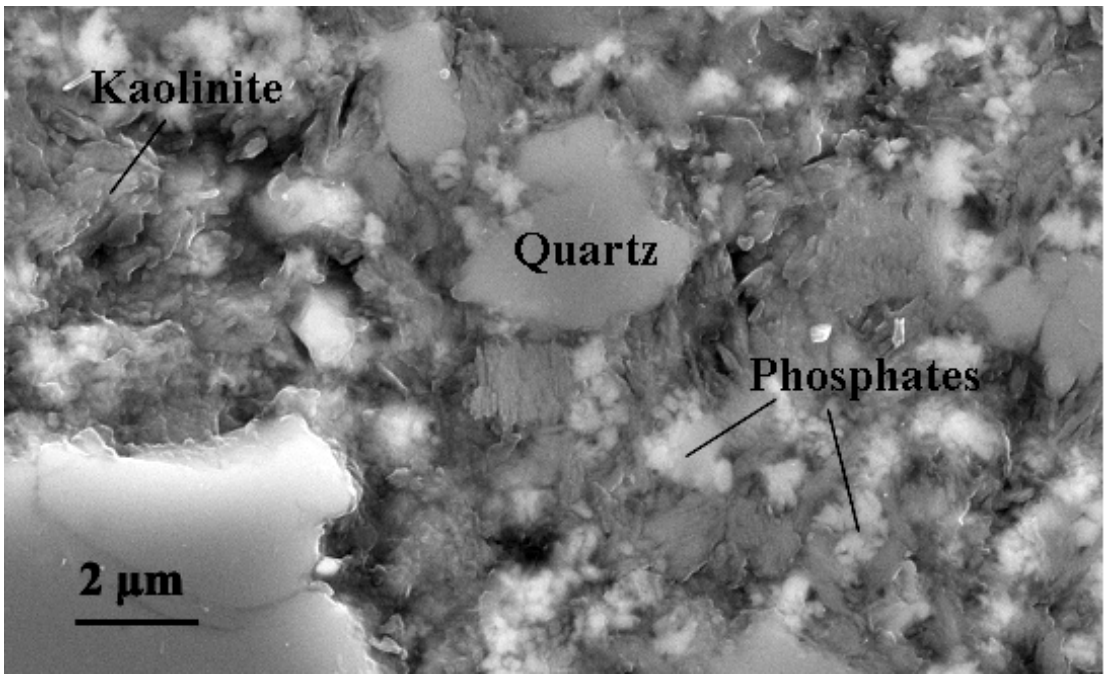

***Figure 6.3**: FESEM micrograph (secondary electron image) showing phosphate minerals in the organic-rich material. Aggregates of submicrometric rhabdophane crystals (phosphates) are scattered in a matrix of corroded micrometric quartz grains and randomly oriented kaolinite plates.*

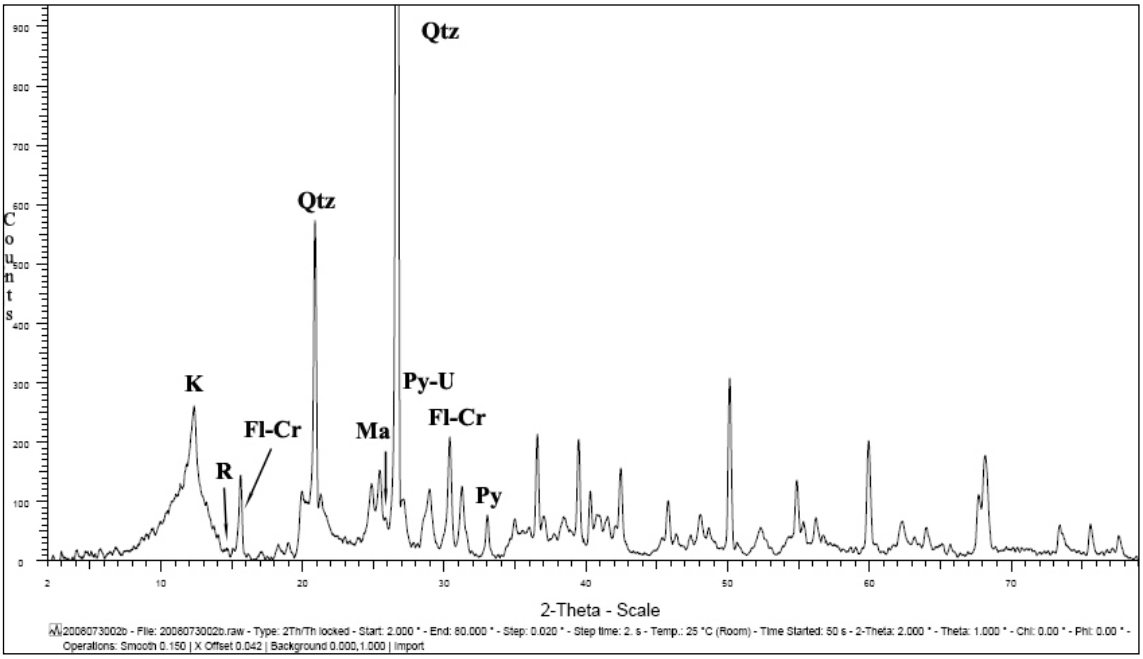

***Figure 6.4**: XRD diffraction pattern of the organic-rich material. Fl-Cr = florencite-crandallite, K = kaolinite, Ma = marcasite, Qtz = quartz, Py = pyrite, Py-U = pyrite + uraninite, R = rhabdophane.*

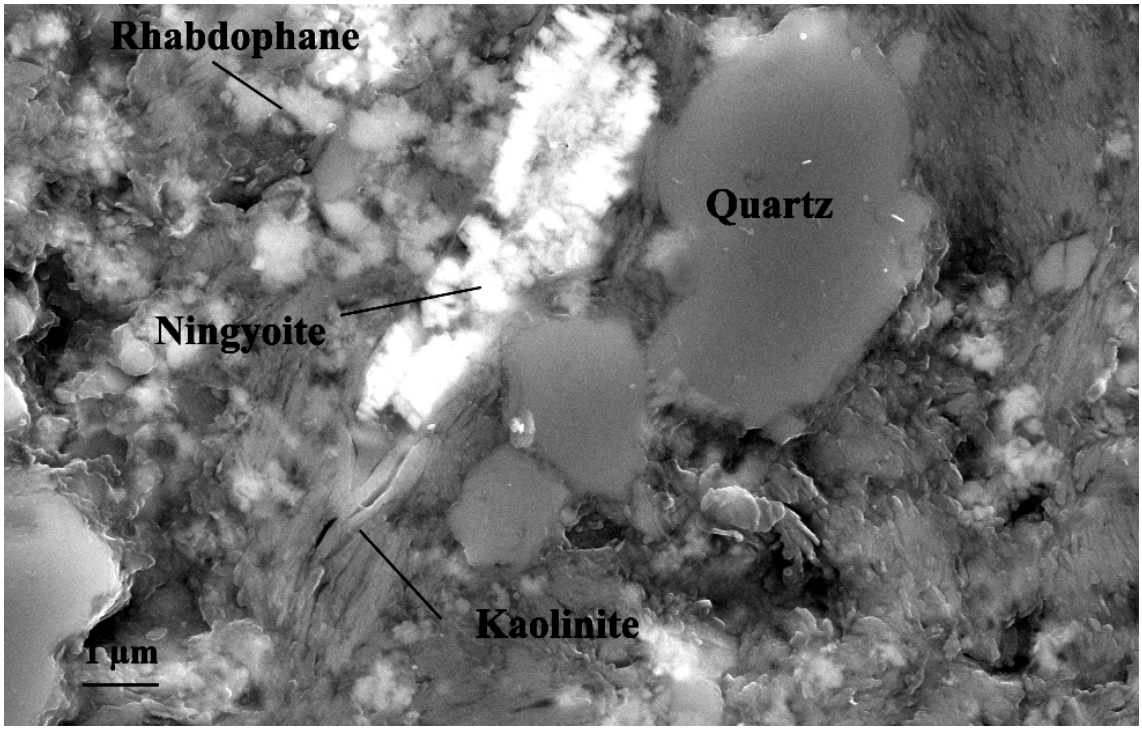

***Figure 6.5**: FESEM micrograph (secondary electron image) showing radiating ningyoite crystals replacing an elongate precursor grain (apatite?) grain, and scattered rhabdophane crystal aggregates.*

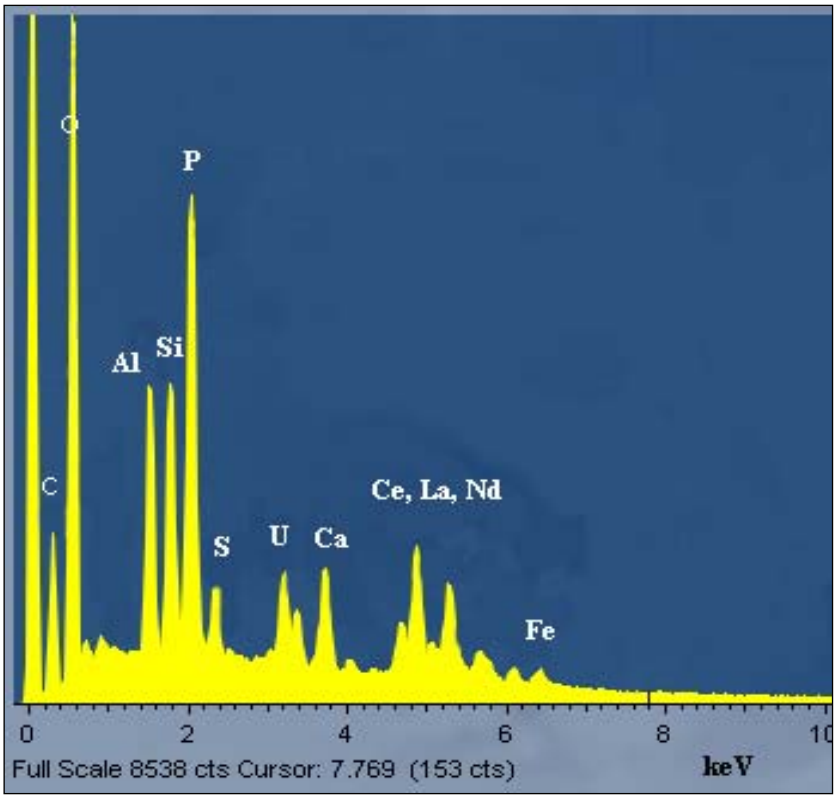

***Figure 6.6**: EDAX spectrum collected from ningyoite pseudomorphing apatite(?) and the surrounding kaolinitic matrix, in organic-rich material.*

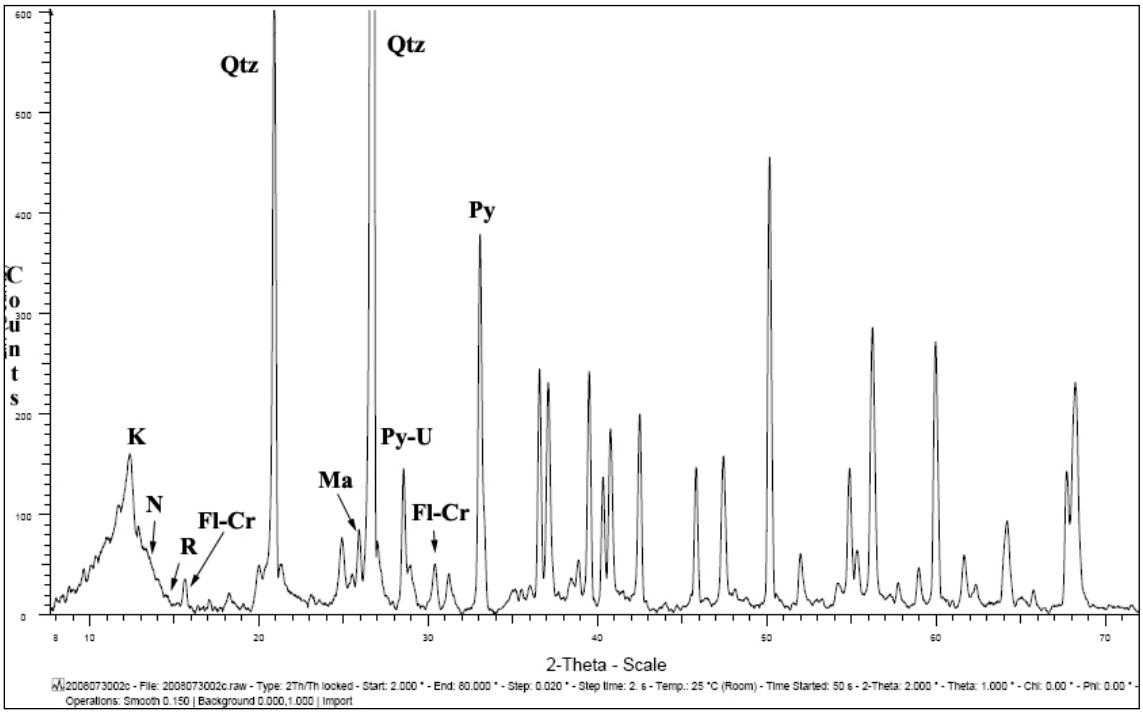

***Figure 6.7**: XRD diffraction pattern of uraninite-rich material showing the presence of pyrite associated with marcasite, uraninite and phosphates. Phosphates are less abundant than in the organic-rich material. Fl-Cr = florencite-crandallite, K = kaolinite, Ma = marcasite, N = ningyoite, Qtz = quartz, Py = pyrite, Py-U = pyrite + uraninite, R = rhabdophane.*

Aluminous hydroxy phosphates Aluminous hydroxy phosphates of the crandallite group are present in four of the analysed samples. The general formula of the minerals of this group is AB3(XO4)2(OH)6.H (Schwab et al., 1990). The XRD and EDAX data indicate that it is a phosphate of the florencite-crandallite series containing LREE, Ba and Ca. The A position is filled by Ce, La, Ba and Ca, the B position by Al or Fe and X by P or S. Figure 6.8 shows the phosphates forming along cleavages in kaolinite (also evident in XRD spectra, see Fig. 6.7). The nearby uraninite also forming along kaolinite cleavages does not contain LREE or Ba.

6.3.2.3 Other secondary minerals

Sphalerite was observed in minor quantities in one sample. Titanium-oxides (most likely low-temperature forms, possibly anatase or lucoxene) may be considered a secondary phase, as they are commonly seen to replace detrital ilmenite.

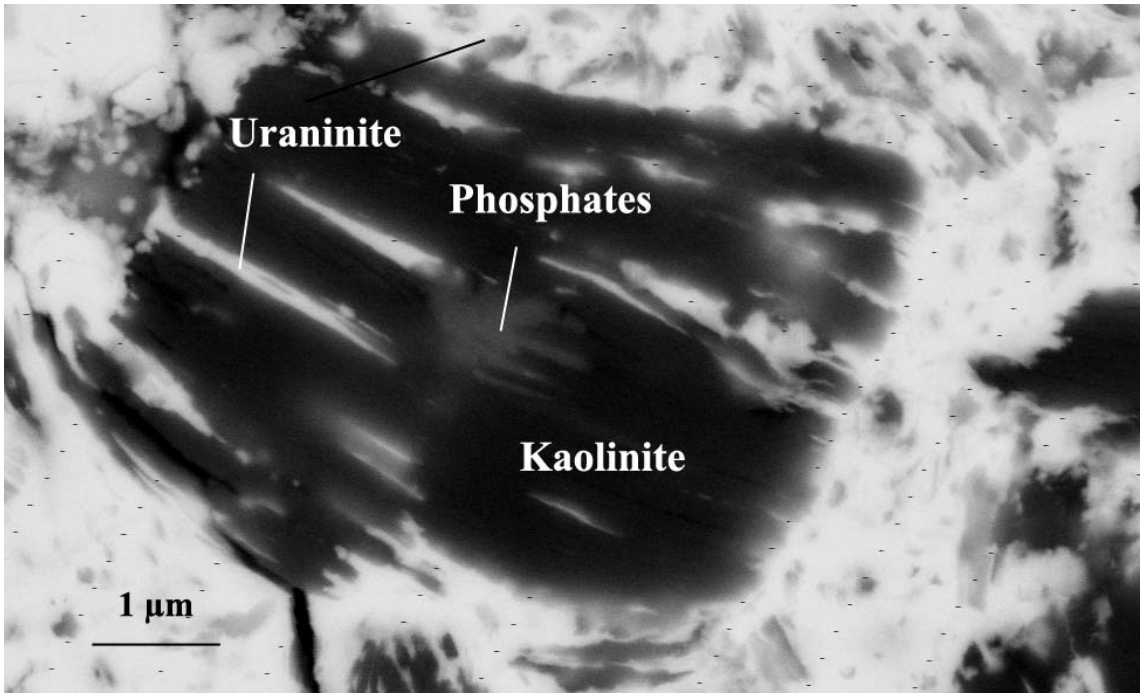

***Figure 6.8**: FESEM micrograph (backscattered electron image) showing kaolinite with uraninite and a La-Ce-Ba-Ca aluminous hydroxy phosphate forming along cleavages.*

6.3.3 Uranium-hosting mineralogy

6.3.3.1 Uraninite

Uraninite is the dominant U-hosting mineral in all Four Mile East samples. Electron microprobe analysis of uraninite grains contain up to 68 wt. % U. The rare earth elements including La, Ce, Nd, Sm, Gd, and Dy, which substitute for U^{4+} in the uraninite crystal structure (Janeczek and Ewing, 1992), are present at concentrations of up to 3.6 wt. %. Of the REE, Dy is particularly abundant, constituting up to 2.1 wt. % of the uraninite. By comparison, Ca, which also substitutes for U^{4+}, is relatively low (average of 1.3 wt. %). Arsenic and S reach concentrations of 1.3 wt. % and 1.5 wt. %, respectively.

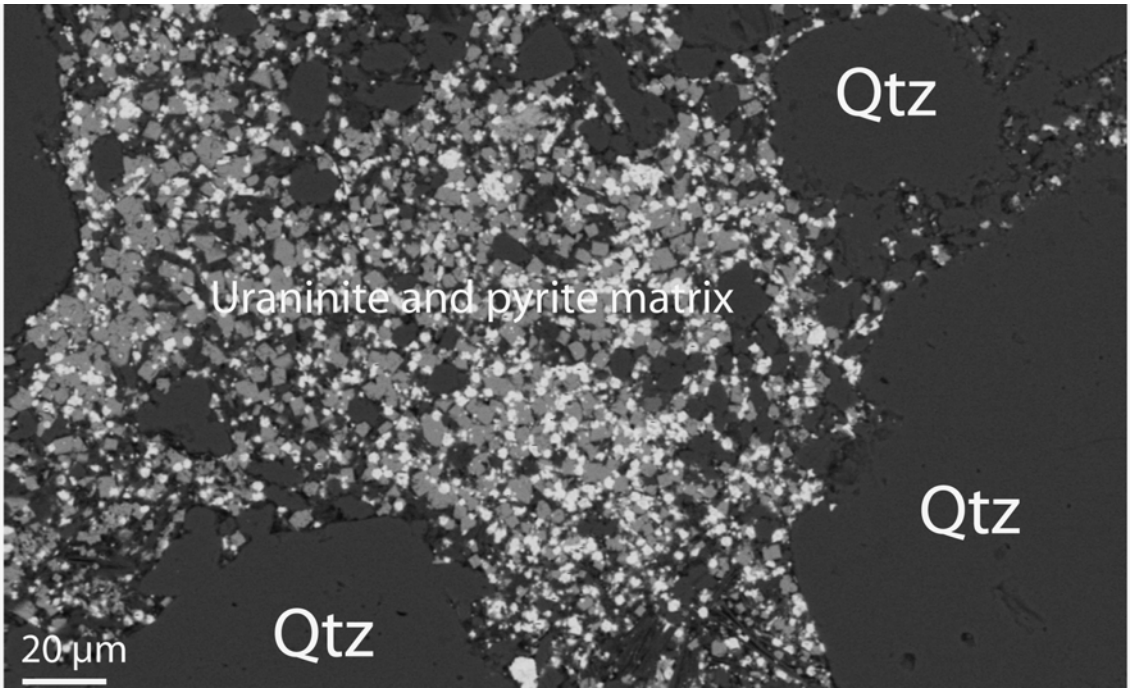

***Figure 6.9**: FESEM micrograph (backscattered electron image) showing the common occurrence of uraninite at the Four Mile East deposit. Note that uraninite and pyrite are intimately associated in the matrix. Qtz = quartz.*

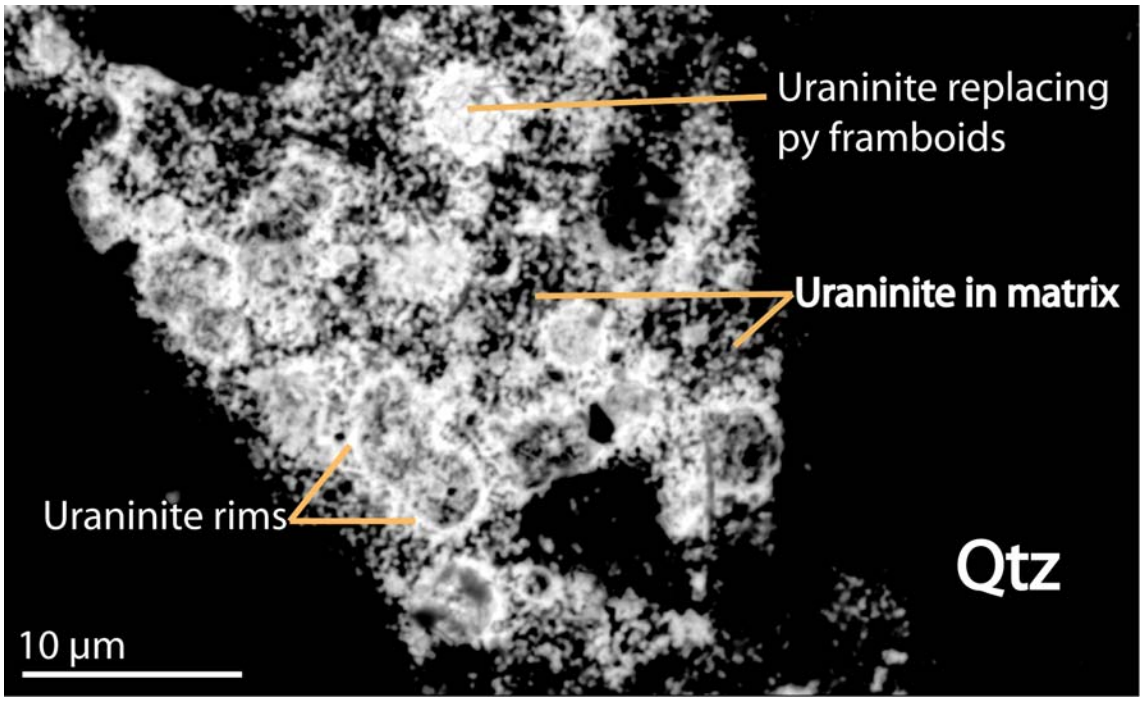

***Figure 6.10**: SEM micrograph (backscattered electron image) showing uraninite replacing early framboidal pyrite. Py = pyrite, Qtz = quartz.*

Individual grains of uraninite observed in the Four Mile samples are small, reaching a maximum of ~30 µm (although typically <10 µm). The overwhelmingly small grainsize renders optical recognition of uraninite difficult, and SEM use is necessary. It is common for small uraninite grains to coalesce to form micro-domains very rich in uraninite. Uraninite mostly occurs in the matrix, and between quartz grains (Fig. 6.9). It is commonly intimately intergrown with pyrite, and more rarely with phosphate minerals. In places, uraninite pseudomrophs early framboidal pyrite. Where this is the case, EDS analysis shows traces of remnant Fe and S. Colloform uraninite rims are also observed on many of the pyrite framboids (Fig. 6.10).

Similarly to pyrite, uraninite in places shows an affinity for Ti-oxide minerals, and is interpreted to have replaced the oxides some instances (Fig. 6.11). Uraninite also is interpreted to have replaced kaolinite (Fig. 6.8). The paragenetic relationship between uraninite and secondary pyrite growth is uncertain. In some cases, euhedral pyrite growth appears to post-date the replacement of early framboidal pyrite by uraninite (Fig. 6.12). However, in other cases, tiny inclusions of uraninite are observed within pyrite crystals. Inclusions of U minerals (probably uraninite) are also observed as inclusions in sphalerite nodules.

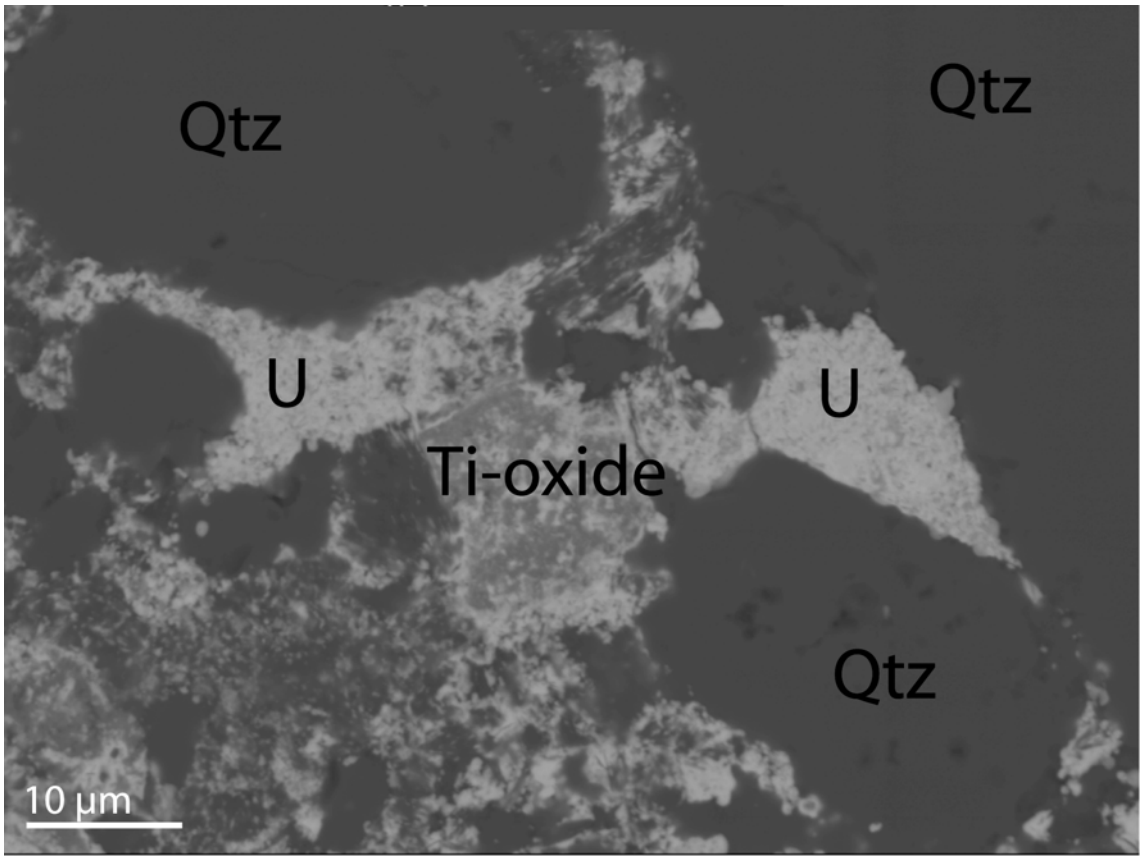

Figure 6.11: *SEM micrograph (backscattered electron image) showing uraninite interstitial to detrital quartz grains. Uraninite is also intergrown with rutile. U = uraninite, Q = quartz.*

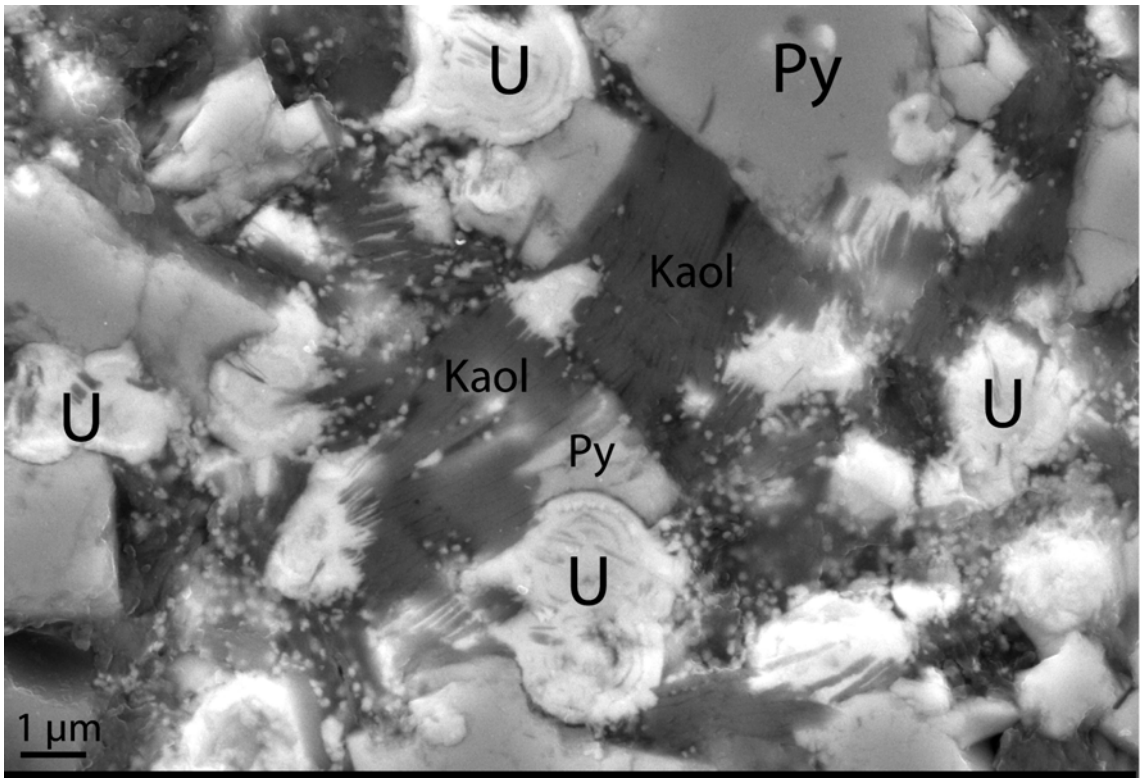

Figure 6.12: *FESEM micrograph (secondary electron image) showing the relationship between early concentrically zoned framboidal pyrite (replaced by uraninite), euhedral pyrite, uraninite and kaolinite. Note that uraninite pseudomorphs of framboidal pyrite appear to be overgrown by the euhedral pyrite, which also includes some uraninite. U = uraninite, Kaol = kaolinite, Py = pyrite.*

6.3.3.2 Other uranium minerals

Despite the high grade of mineralisation, other U minerals are rare in the Four Mile East deposit. A rare U-V mineral was detected. It is probable that this mineral is carnotite ($K(UO_2)_2Si_2O_7.6H_2O$). Another minor U-bearing phase containing S was also observed. A precise identification is not possible at this stage, although uranopilite ($((UO_2)6[(OH)10SO_4].12H_2O$) is a potential candidate. Alternatively this mineral may represent the replacement of pyrite by uraninite, with remnant S remaining in the crystal structure, although no Fe is present. Coffinite may also be present in minor quantities, although this is inconclusive.

6.3.3.3 Uranium-bearing phosphates

The hydrated LREE-rich phosphates (rhabdophane and ningyoite) contain significant U, with ningyoite containing more U than rhabdophane. Ningyoite has been observed only in the U-mineralised samples. Thus there appears to be a positive correlation between the presence of U-rich phosphates and uraninite. Further work is required to confirm this observation.

6.4 COMPARISON WITH THE BEVERLEY URANIUM DEPOSIT

The Beverley uranium mine is situated approximately 8 km from the Four Mile deposit. Despite their proximity, there are important mineralogical differences, the most significant of which is the U-hosting mineralogy. In contrast to the uraninite-dominant assemblage at Four Mile, uranium at the Beverley deposit is hosted almost entirely by coffinite ($U(SiO_4)_{1-x}(OH)_{4x}$) with only very minor uraninite reported. The coffinite is present as fine disseminations amongst the clay-rich matrix. In some cases, coffinite mineralisation is preferentially concentrated around grains of detrital ilmenite (Fig. 6.13).

Further differences between the Four Mile and Beverley deposits are evident in the minor mineral assemblage. The samples studied from Beverley contain malachite, arsenopyrite and probable sphalerite. In addition, unidentified Fe-Ni-Cr and Cu-Zn minerals were also observed. Barite is present as inclusions in quartz grains at Beverley. Pyrite is not as prevalent at Beverley compared with Four Mile, and no phosphate minerals were observed.

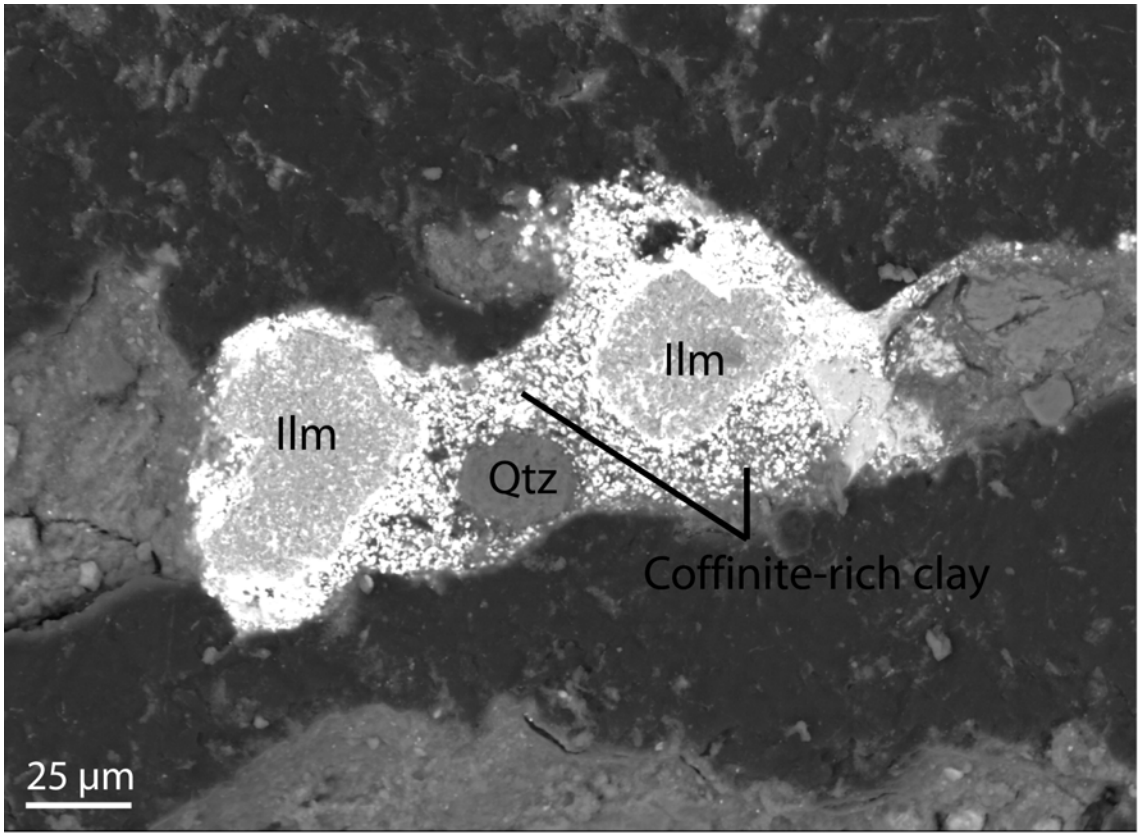

***Figure 6.13**: SEM micrograph (backscattered electron image) of a typical occurrence of coffinite at the Beverley deposit. Ilm = ilmenite, Qtz = quartz.*

6.5 DISCUSSION

The paragenetic context of uranium mineralisation at the Four Mile East deposit has yet to be established in detail. Secondary processes affecting the unconsolidated to weakly consolidated sediments of the host Eyre Formation may include early diagenesis, weathering, and low-temperature hydrothermal alteration. In this reconnaissance study it has not been possible to distinguish the effects of these possible secondary processes.

Nevertheless, a working hypothesis for the paragenetic sequence has been developed (Fig. 6.14). The major detrital phases are quartz, feldspar, and ilmenite. The timing of very fine kaolinite interstitial to framework grains appears to be early in the paragenetic sequence, as it is replaced by uraninite and phosphate minerals. Kaolinite may have been detrital or washed in, partially filling interstices.

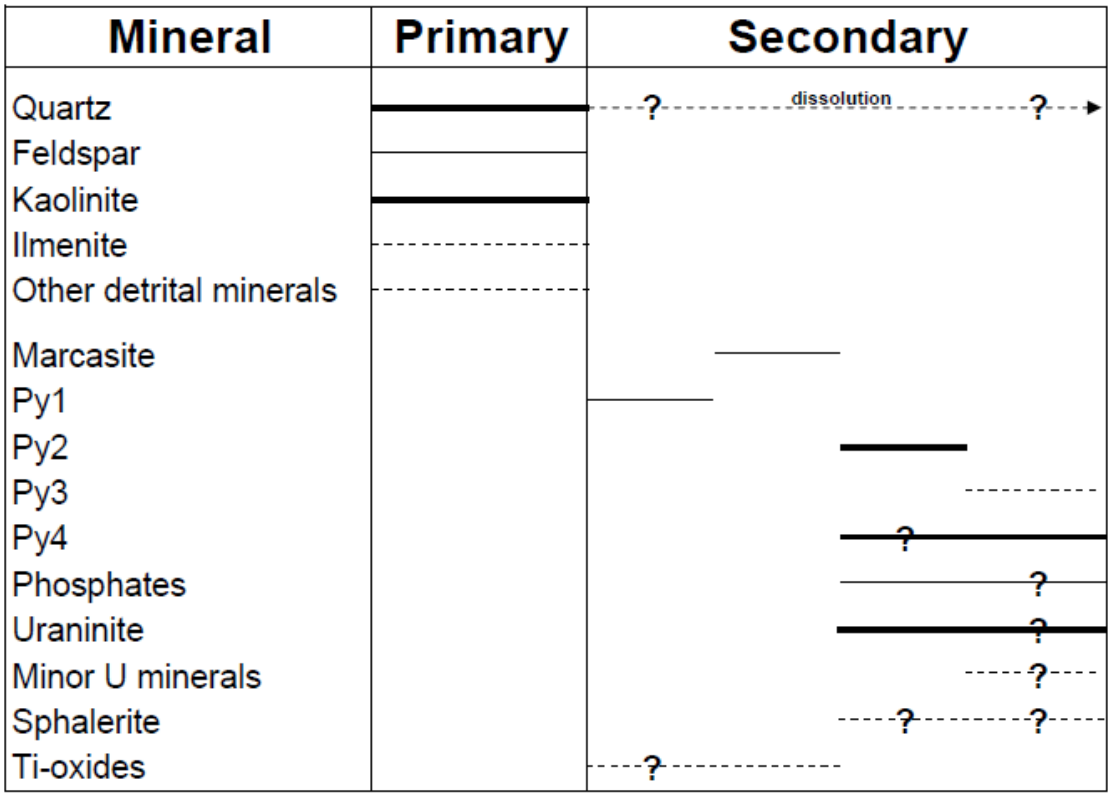

Figure 6.14: *Provisional paragenetic sequence for the Four Mile East deposit, based on reconnaissance petrography. Heavy lines – abundant; thin lines – minor; dashed lines – trace amounts.*

Our observations indicate that uraninite replaced and possibly overgrew early framboidal pyrite (Py1) of presumably bacterial origin. Uraninite also appears to have replaced some kaolinite along its cleavages, in association with phosphate minerals. Whereas euhedral pyrite (Py2) in the matrix of the sediment appears to have overgrown uraninite pseudomorphs of framboidal pyrite (Fig. 6.11), other Py2 hosts small inclusions of uraninite. This suggests either that (a) there were two separate phases of uraninite growth, or (b) that uraninite and Py2 were broadly coeval, and that only some Py2 included U minerals. For simplicity, scenario (b) is favoured. The timing of very fine overgrowths of Py3 on Py2 euhedra relative to extremely fine Py4 in the matrix is unclear.

Detrital grains of ilmenite with low U contents are replaced by U-V-rich Ti-oxide alteration products (brookite and/or anatase). Whereas the V may have been sourced from the ilmenite, the elevated levels of U in the Ti-oxide alteration products suggest that the alteration of ilmenite occurred in the presence of a U-bearing fluid.

Textures of relict detrital quartz suggest that quartz was corroded, particularly where the organic matter content is higher, although the timing of this process is unclear. Quartz dissolution, as well as the apparent lack of significant amounts of the U-silicate coffinite, and replacement of kaolinite by uraninite and phosphate minerals, together point to the presence of silica-undersaturated fluids, at least locally. This would appear to contrast with the Beverley deposit where coffinite is common, there is little evidence for quartz dissolution in the few samples studied, and silcrete occurs only a few metres or tens of metres above ore zones.

The intimate association of uraninite with REE phosphate minerals, both replacing kaolinite, together with the high P content of uraninite as shown by electron microprobe data, suggest that

U, P and REE may have been precipitated simultaneously from the ore fluid(s). This is supported by the high U contents of some of the phosphate minerals. The PO_4^{3-} ligand is highly effective in transporting U^{6+} at a range of temperatures and pH values provided that the fluids are relatively oxidised (see Cuney and Kyser, 2008 and references therein). Thus, P-rich fluids potentially may transport U^{6+} at relatively high concentrations, although other ligands such as carbonate ions and hydroxyl ions also may be important (see reviews by Cuney and Kyser, 2008; Skirrow et al., 2009). Deposition may have occurred via reduction, for example through reaction with reduced carbon or iron already present in the sediment, or in mobile form (e.g. aqueous or gaseous CH_4, H_2S). Alternatively, the formation of phosphate minerals may destabilise U in the fluid. The source of P in the fluids is unknown, but may have been either local organic matter, apatite in the sediments, or from distal sources carried by groundwaters or hydrothermal fluids. On the other hand the source of the REE is unlikely to be the immediate host sediments of the Namba Formation, which are typically composed of quartz, feldspar, kaolinite, and minor heavy minerals. The presence of REE-rich minerals would appear to demand REE transport from sources beyond the immediate host sequence, such as the REE-rich igneous rocks of the Willyama Supergroup and/or Mt Painter Inlier.

The ubiquitous presence of high levels of organic matter in mineralised samples of the Eyre Formation is most likely the primary control on U deposition in the Four Mile East deposit. Reduced Fe minerals, such as pyrite and ilmenite, are also probable sites of uranium reduction and deposition. It is interesting to note that the REE-rich rhabdophane contains Ba, an element normally transported only in reduced fluids. The possibility of fluid mixing between oxidised U-rich waters and a reduced fluid warrants further investigation as a U-depositional mechanism at the Four Mile deposit. This process has potential to result in high grades of uranium mineralisation, perhaps higher than simply through fluid-rock reaction.

6.6 CONCLUSIONS

Based on reconnaissance studies of a limited number of samples, uranium mineralisation at the Four Mile East deposit is overwhelmingly composed of uraninite. This is in contrast to the nearby Beverley uranium deposit, where coffinite is the dominant uranium phase. A precise paragenetic sequence is difficult to constrain for the fine grained secondary minerals including uraninite. However, it is inferred that uraninite formed contemporaneously with a second phase of pyrite (Py2) and REE phosphate minerals. Other uranium minerals present in the Four Mile deposit (carnotite and uranopilite) are oxidised uranium minerals, and probably represent a later stage of uranium remobilisation.

Although the Four Mile deposit is high grade, the composition of uraninite is unusual. In particular, high Fe and Ti contents are anomalous, and may be related to the association between Ti-oxides and uraninite. The uraninite also contains elevated levels of P and REE including Dy.

These observations will assist in future geochronological studies. In particular, the differences between Beverley and Four Mile are curious given the proximity of the two deposits and previous assumptions of similar origin.

7. Numerical modelling of regional fluid systems and uranium mineralisation

Evgeniy N. Bastrakov, Subhash Jaireth

7.1 INTRODUCTION

To test geological scenarios for the formation of basin-related uranium systems within the Lake Frome region, we have undertaken integrated numerical modelling of fluid flow, heat, and mass transport. To this end we used the Desktop Modelling Toolkit (DMT) and the PmdPyRT code developed by the Computational Geoscience group at CSIRO Exploration and Mining Division (Cleverley et al., 2006; Cleverley, 2008).

7.2 OBJECTIVES AND METHODOLOGY

7.2.1 Objectives of the study

This chapter presents the results of numerical modelling of regional- and district-scale fluid flow for a number of possible geological scenarios of uranium mineral systems in the Lake Frome region, based on data in the public domain. The primary objective of this work is to evaluate several scenarios for the origin of uranium mineralisation by modelling the fluid flow regimes that operate in simplified 2D models of the geology representing differing basin architectures. This was complimented by auxiliary geochemical modelling calculations, reported below. The numerical modelling can test hypotheses about the key parameters of the mineral system and their appropriate values: permeability architecture (e.g., role of faults and sediment permeability), energy drivers (e.g., role of topography and radiogenic heat), and depositional gradients (e.g., role of reductants). This information, when combined with other results in this study, can be used to test particular models of ore formation, and allows predictions of the geological settings favourable for undiscovered uranium mineralisation in the region.

7.2.2 Geological constraints

The Beverley, Four Mile East and Four Mile West uranium deposits contain more than 75% of known uranium resources in the Lake Frome region and the local geology of the deposits is relatively well understood from drilling and seismic studies. Thus, we focussed our attention on a geological cross-section within the immediate vicinity of the Beverley and Four Mile deposits (Figs. 7.1, 7.2).

Heathgate Resources (1998) and Brugger et al. (2005) counted 5 aquifer systems within the area of interest (Figure 7.3): (1) fractured Proterozoic granitic and metamorphic rocks of the Mt Painter Inlier (MPI); (2) Cretaceous sandstones of the Cadna-owie Formation; (3) Cenozoic sands of the Eyre Formation; (4) Cenozoic sands, clays, and silts of the Namba Formation; and (5) Cenozoic and Quaternary conglomerates and sands of Willawortina Formation. Within the Frome Embayment, the Cadna-owie Formation serves as a discharge area for the Great Artesian Basin (GAB). Water discharges from the GAB aquifer system through diffuse upwards leakage and from point mound springs (Radke et al., 2000).

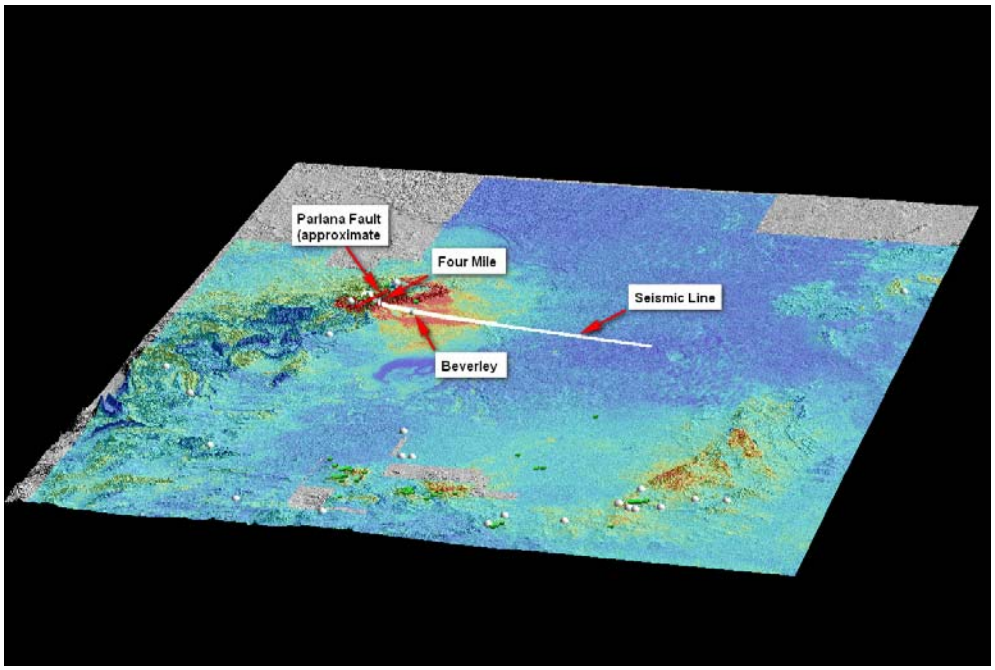

Figure 7.1: *Lake Frome region with the position of the seismic line used to create the 2D geological model for fluid flow modelling, superimposed on the digital elevation model of the Lake Frome area (grey), with a coloured drape of radiometrics (uranium channel). The Paralana Fault and the Four Mile and Beverley deposits are shown for reference. Silver circles and green squares depict the position of uranium and other mineral occurrences, respectively. Vertical scale exaggeration 10 times. The length of the east-west seismic line is 130 km.*

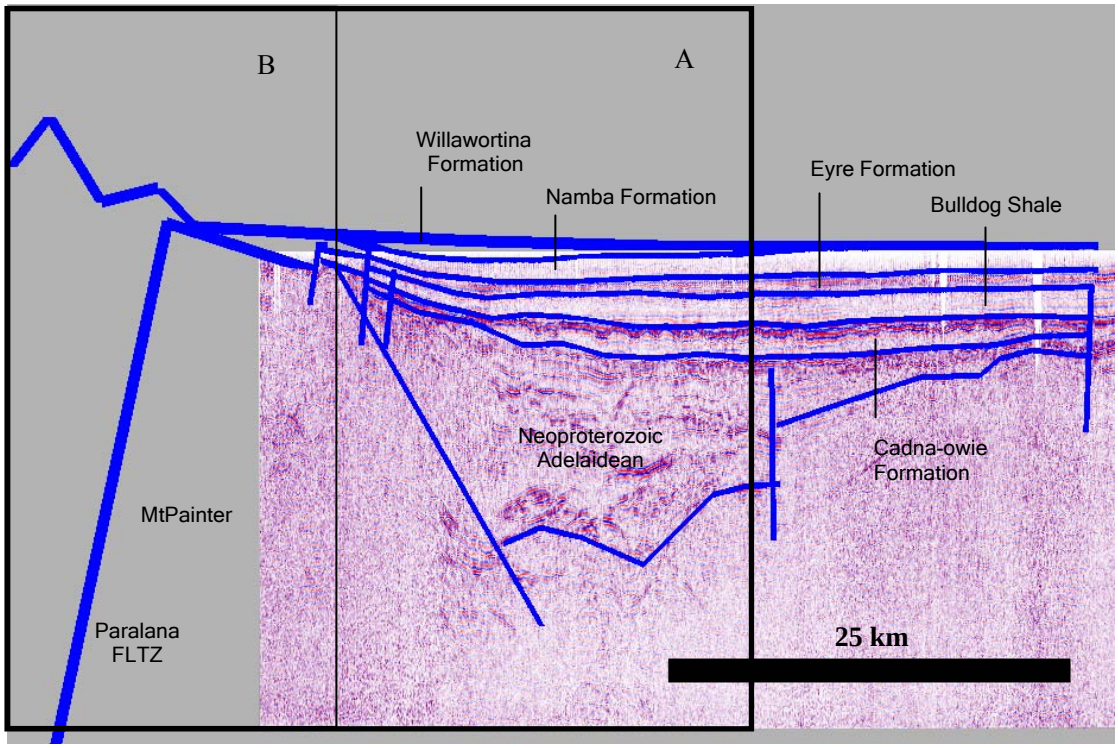

Figure 7.2: *Seismic data for the western part of the line shown in Figure 7.1, with preliminary geological interpretation (blue linework). A – area for fluid flow modelling; B – part of the model shown in Figures 7.4 to 7.8. Vertical scale exaggeration 10 times.*

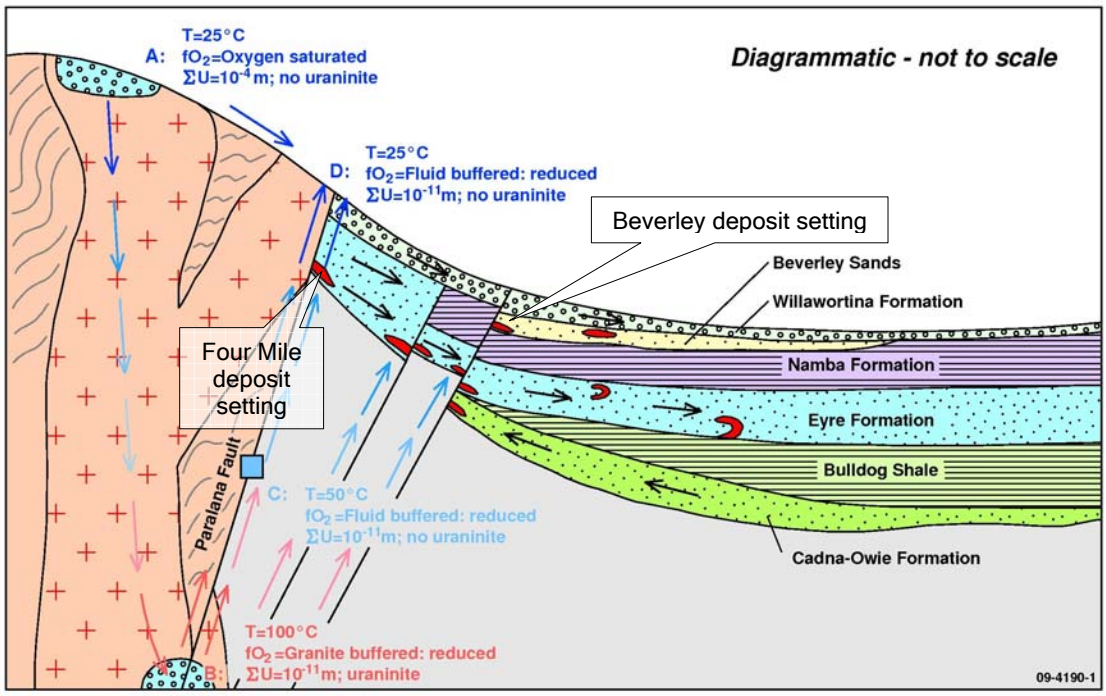

Figure 7.3: *Schematic diagram of the conceptual geological model used for geochemical modelling of the Paralana Hot Springs and sandstone-hosted uranium mineralisation in the Beverley – Four Mile district. The blue to red arrows show the heating and cooling cycle of fluid related to the Paralana Hot Springs; the black arrows show the fluid flow in the present-day aquifers; the red zones show hypothetical zones of uranium mineralisation. Modified after Brugger et al. (2005) and Heathgate Resources (1998; 2009). The schematic settings of the Four Mile and Beverley deposits are indicated.*

Geological constraints important for understanding the results of modelling are:

1. The Beverley and Four Mile East deposits are hosted by sands of Paleogene and Neogene ages, respectively.

2. The Beverley orebody is hosted by fluvial sands and shales of the Namba Formation. Most of the mineralisation is confined to the Beverley Sands which are underlain and overlain by the Alpha Mudstone and Beverley Clay, respectively.

3. At Four Mile East mineralisation is hosted by fluvial sands of the Eyre Formation.

4. As Beverley and Four Mile East deposits are hosted by sands of different ages, mineralisation at the two deposits has either resulted from one late Miocene event (corresponding to the maximum age of Beverley mineralisation) or two separate events (for example, late Paleogene for Four Mile East and late Miocene for Beverley, although other timing scenarios are possible – see Chapter 5).

5. Provenance studies on sands hosting Beverley mineralisation show that the sands were derived from the reworking of Early Cretaceous glacial or glacio-lacustrine sediments (possibly in proximity to Mount Painter Inlier) originally sourced from Eastern Australia (Sprigg, 1986; Wülser et al., 2005).

6. The Paralana Fault system was initiated in the Mesoproterozoic but underwent periodic reactivation, the latest of which was as young as ~4 to 5 Ma (Preiss, 1995; Quigley et al., 2007). The present-day relief is thought to have resulted from this latest tectonic activity.

The principle aim of the fluid-flow and chemical modelling was to test hypotheses of uranium mobilisation, transport and deposition based on the well-known 2D model suggested by Heathgate Resources (1998) and discussed further by Brugger et al. (2005), Jaireth et al. (2008b) and others (Figure 7.3). The latter implies removal of uranium from the Mt Painter source rocks and its transport into reduced Paleogene and Neogene sands.

Previous numerical modelling work includes (a) hydrogeological modelling of present-day fluid flow in the Lake Frome region, undertaken as part of the approval process for mining operations at Four Mile East (Jeuken, 2008) and (b) reactive-transport modelling for a highly simplified paleo-uranium system (Fisher et al., 2008). In the current study we have placed special emphasis on the role played by basin-basement architecture (such as role of faults and paleorelief). Importantly, our models attempt to simulate past rather than current geological scenarios for the formation of uranium mineralisation. We have selected a period in the Miocene at ~6 Ma, that is permissive of contemporaneous formation of uranium mineralisation within the Eyre and Namba formations (see Chapter 5 and Fig. 3.1 for details). The present-day grownd water flow pattern in the Great Artesian Basin was initiated only after ~2 to 5 Ma (Radke et al., 2000; Bethke and Johnson, 2008).

Specifically, we aimed to test two hydrogeological regimes created by two scenarios of basin-basement architecture controlled by tectonic activity on the Paralana Fault system:

1. Pre-Paralana Fault architecture, with relatively subdued relief in the Mount Painter area;

2. Post-Paralana Fault architecture, with relatively high relief in the Mount Painter area.

Thus, the main objectives of modelling are as follows.

- Investigate the feasibility of the widely publicized model of easterly fluid flow from the Mt Painter Inlier into the Cenozoic basins, suggested by Heathgate Resources (1998, Fig. 7.3).

- Examine the effect of variations of parameters such as permeability, topographic head, fault architecture, and weathering of basement areas, for each of the two architectures as these affect the potential sites of uranium mineralisation in the basins.

From a geological point of view, the numerical modelling has the following limitations:

- The models discussed below examine the fluid flow only in two-dimensional space. For example, our models do not account for the components of the fluid flow oblique or normal to the model section (*e.g.*, they cannot account for fluid flow along north-south trending paleochannels).

- The models deal only with saturated fluid flow (i.e., no vadose zone is present in the models).

- The modelled section does not take into account second-order lithological and permeability contrasts within a lithological rock sequence/aquifer. For example, the Namba Formation is an alternating sequence of multiple sand and shaly packages. The same is true for the Eyre Formation.

The modelling software permits integration of fluid flow, heat, mass transport and, optionally, chemical reaction processes in reactive-transport models. We have chosen to use non-reactive tracers to track the paths of chemical components rather than integrating chemistry and fluid flow,

partly due to computational limitations in running large reactive-transport models. However, to better understand some of the chemical processes, a separate chemical modelling exercise was undertaken (see Geochemical Modelling, below).

7.2.3 Building simplified 2D geological models for fluid flow modelling

7.2.3.1 Geometrical models

The modelling is based on a simplified geological cross-section interpreted from the seismic survey data close to the mineralised area (Fig. 7.2). Details of the lithostratigraphy and architecture are presented in Chapters 2 and 3, and uranium deposit descriptions are given in Chapter 5.

The model section consists of 7 stratigraphic units (Figure 7.4) and up to 3 basement faults propagating into the overlying Mesozoic and Cenozoic units: the Paralana Fault system and the western and eastern faults that define the horst structure within the Proterozoic basement and the overlying basin. The complex Paralana Fault system was simplified in the model as a single fault zone, and hereafter is termed the Paralana Fault.

The interpreted boundaries of the geologic units were imported from GoCad into the Gmsh software, a three-dimensional finite-element mesh generator program (Geuzaine and Remacle, 2009), and further manually edited to simplify the initial geometrical model and create its variations. The simplified models were subsequently meshed into unstructured triangular finite elements. Unstructured triangular meshes allow realistic representation of geological features with arbitrary shapes, including narrow wedges of geological units (Cleverley et al., 2006).

Initial model runs have demonstrated that most of the fluid flow occurred within the ~2 x 40 km block (Fig. 7.2). Thus, to speed up the calculations and focus the research effort on the area relevant to mineralisation the geometrical model was constrained to this area containing approximately 50,000 mesh elements. Depending on the particular purpose of the model variation, this basic cross-section was modified further (Figs 7.4 to 7.9).

7.2.3.2 Physical properties

The assigned permeabilities for each rock unit are explicitly shown in Figures 7.4A to 7.9A in log units. Generally, we have assumed that the Mt Painter Inlier block represents the most impermeable rock unit compared to other lithologies in the modelled section, and we have assumed a single permeability value for the entire MPI. The exception is the group of models for which we specified a layer of weathered and fractured granite above the fresh coherent rock (Figs. 7.8, 7.9), with the fractured layer having a permeability two orders of magnitude higher than the coherent rock. According to Domenico and Swartz (1998) and Freeze and Cherry (1979), permeabilities of fractured igneous and metamorphic units (directly proportional to hydraulic conductivities) can be up to four to five magnitudes higher than their unfractured counterparts.

In most of the models we have presumed that permeabilities of the fault zones were two to three orders of magnitude higher than permeabilities of the immediate host units, with the exception of a special case presented in Figure 7.9. The Cadna-owie, Eyre, and Willawortina Formations are considered to be largely sand units; thus, their permeabilities are two orders of magnitude higher than the Bulldog Shale and the Namba Formation. To compensate for the current inability of the PmdPyRT code to handle unsaturated fluid flow, and to speed up calculations, permeability of the Willawortina Formation was artificially suppressed relative to the permeabilities of the Cadna-owie and Eyre Formations (Figures 7.4 to 7.9).

We have not considered changes in permeabilities and porosities that might have resulted from the reaction between fluids and rocks (cf. Cleverley, 2008).

7.2.3.3 Boundary conditions and model variations

The model was uniformly saturated with fluid, with uninterruptible fluid supply at the top of the model. The top of the model was fixed at atmospheric pressure (~1 MPa) and 25°C. The initial pressure-temperature conditions were based on hydrostatic pressures and a geothermal gradient of 60°/km (drillhole Paralana 1B recorded 109°C at ~1,807 m; Petratherm, 2007). The base of the model was maintained at constant temperature, determined by the initial geothermal gradient. No additional heat flow was specified at the base or sides of the model. For the MPI we have specified a radiogenic heat production of 0.00308×10^{-6} W/kg (Neumann, pers. comm., 2008), but this heat production has not noticeably perturbed the average geothermal gradient for the initial temperature conditions. The sides of the model were open, and the base of the model was closed with respect to fluid flow.

The main set of models was run without fluid overpressure within the Cadna-owie Formation (Figs. 7.4 to 7.8). However, it is well known that groundwaters in the Cadna-owie Formation are currently overpressured, as evident from the presence of active mound springs in the region and artesian water in aquifers of the GAB (e.g., Radke et al., 2000). To illustrate the impact of this phenomenon on the overall structure of the fluid flow model within Pliocene-Pleistocene epochs, a separate model was created with fluid overpressure (Fig. 7.9) within the Cadna-owie Formation, accounting for the westward fluid flow at ~1 m y^{-1}.

Routine models were run without reactive-transport but with an added tracer (a non-reactive component dissolved in hydrothermal fluids) to investigate the hydrodynamics of the system in response to changes in geometrical (the topography and structure) and permeability parameters. In the case of "single-domain" MPI models, the tracer was initially distributed exclusively within the coherent MPI rocks on both sides of the Paralana Fault (Figs. 7.4D to 7.7D); within the "layered-domain" models, the tracer was introduced exclusively within the weathered layer (Figs. 7.7D, 7.8D). In both cases, the initial concentration of tracer within the fluid was specified at the 10 mol kg^{-1} level. The geochemical rationale behind this approach was to trace the fluids from the rocks that are the assumed sources of uranium (granitic rocks, and oxidized granitic rocks, respectively).

7.2.4 Representation of results – fluid flow modelling

To summarise output results from the numerous modelling runs and to facilitate visual comparison, we present results as follows (Figs. 7.4 to 7.9). Table 7.1 summarises the variables changed throughout the presented model set. For each model under discussion, we show plots with distribution of (a) permeabilities, (b) temperatures, (c) instantaneous Darcy fluxes, and (d) distribution of the tracer. Additionally, plots (a), (b), and (d) show fluid flowlines, but plot (c) shows the instantaneous Darcy fluxes and vectors to clearly identify the regions where the most fluid flow occurs. All the plots are compiled for the same time slice (or close time slices for different models, around 10,000 years). The notional locations of the Four Mile East and Beverley deposits are shown in Fig. 7.3.

Table 7.1: Values of permeabilities and fluid fluxes changed throughout the presented fluid-flow model set.

Figure (model)		7.4	7.5	7.6	7.7	7.8	7.9
Permeability (m^2)	Paralana Fault	1.E-13	1.E-13	1.E-12	n/a	1.E-13	1.E-13
	Eastern Fault	1.E-13	1.E-13	1.E-13	1.E-16 to 1.E-13	1.E-13	1.E-13
	Western Fault	1.E-13	1.E-13	1.E-13	1.E-16 to 1.E-13	1.E-13	1.E-13
	[1]Willawortina Formation	1.E-15	1.E-15	1.E-15	1.E-15	1.E-15	1.E-15
	Namba Formation	1.E-16	1.E-16	1.E-16	1.E-16	1.E-16	1.E-16
	Eyre Formation	1.E-13	1.E-13	1.E-13	1.E-14	1.E-13	1.E-13
	Bulldog Shale	1.E-17	1.E-17	1.E-17	1.E-17	1.E-17	1.E-17
	Cadna-owie Formation	1.E-13	1.E-13	1.E-13	1.E-13	1.E-13	1.E-13
	Neoproterozoic Adelaidean	1.E-16	1.E-16	1.E-16	1.E-16	1.E-16	1.E-16
	Mt Painter (weathered)	n/a	n/a	n/a	n/a	1.E-15	1.E-15
	Mt Painter	1.E-17	1.E-16	1.E-16	1.E-17	1.E-16	
[2]Imposed fluid flux ($m\ y^{-1}$)							1

[1]Permeability of the Willawortina Formation artificially suppressed to compensate for the current inability of the PmdPyRT code to handle unsaturated fluid flow.
[2]Westward fluid flow within the Cadna-owie Formation.

7.3 RESULTS AND DISCUSSION – FLUID FLOW MODELLING

7.3.1 Fluid flow scenarios in the Beverley – Four Mile district

Fisher et al. (2008) pioneered the reactive transport modeling of the formation of the sandstone-hosted uranium mineralisation inspired by the Frome Embayment scenario. Initially they used a generic geological model with a 2D cross-section cutting across a broad, 8-km wide, paleochannel hosted by basin rocks of similar permeabilities. Once more, the fluid flow within the model was topographically driven to the east, away from U-enriched granites of the MPI. The palaeochannel, hosted by oxidized basin rocks, served as a "local" reduction trap for uraniniferous fluids. Although Fisher et al. (2008) proceeded to more "realistic" layered geometries at the expense of detailed structure in the paleochannel, their initial approach emphasized the potential importance of local chemical heterogeneities within otherwise hydraulically homogeneous rocks. Nevertheless, their 2D approach suffered from the assumption of fluid flow across, rather than along, paleochannels.

The results of both Fisher et al. (2008) and the current study show that the relative permeabilities of the rock units are the fundamental control on fluid flow and fluid fluxes. Potential energy represented by topography drives fluid flow in the models in both studies.

In our study, despite somewhat different patterns of the fluid flow depicted in Figures 7.3 to 7.8, most of the fluid flow occurs within the Eyre Formation. Overall, the eastward paleo fluid-flow pattern reproduced in the models within Cenozoic sediments is similar to the one suggested by Heathgate Resources (1998) and Brugger et al. (2005) (e.g., Figure 7.3). However, our results

suggest that the Beverley and Four Mile deposits were unlikely to have formed along the same fluid flow pathway, as discussed below.

The present-day groundwater flow in the proposed Four Mile East mining zone was modeled by Jeuken (2008). His conceptual model was similar to the model depicted in Figure 7.3, though Jeuken (2008) used a pseudo-3D modeling approach using a multi-layer 2D geometry. According to the results of his modelling, the groundwater is expected to flow to the north-east, through the hydraulic constriction across the Poontana Fault Zone and then to the east into the Lake Frome area (Figures 7.8 and 7.9 in Jeuken, 2008). The recharge to the Eyre Formation is mostly from infiltration to the southwest of the Four Mile deposit where the Eyre Formation crops out. Jeuken (2008) concluded that the conceptual model is hydraulically feasible, and can be further calibrated using realistic aquifer properties and boundary conditions that are supported by real data.

In our models, most of the fluid recharge occurs within the Eyre Formation, both for pre-, and post-Paralana Fault groups of models (for example, cf. Figs 7.4 and 7.7). This raises the question of the source of uranium, as most of the fluid flow bypasses the MPI (mostly, "runs off"). In part, this problem was considered separately in a group of models where we imposed a layer of Mt Painter rocks with permeabilities higher than the permeabilities of the Eyre Formation.

For the tested range of scenarios, the exposed top of the Paralana Fault (if characterised by permeabilities equal to, or higher than the permeability of the Eyre Formation) acts simultaneously as a zone of major recharge of a surficial fluid component, and minor discharge of deeply circulated fluids into permeable units below the surface. The fluids discharged at the top of the Paralana Fault could have penetrated to significant depths and could have been heated to temperatures from 50 to 200°C (Figs. 7.4 to 7.6, and 7.8, 7.9). The geochemical modelling calculations of Brugger et al. (2005) and Jaireth et al. (2008b) imply contributions of relatively "reduced" and "oxidized" fluids with different uranium-bearing capacities. In particular, the fluids re-equilibrated with the Mt Painter rocks at elevated temperatures will have limited capacity to transport significant uranium. In any case, the fluid fluxes associated with the discharge from the the Paralana Fault are 1-2 orders of magnitude less than fluid fluxes associated with the surficial fluids recharging within the Eyre Formation.

Given the limitations imposed by the boundary conditions of the tested models (namely, the top of the models is open to fluid flux but is set to a fixed temperature), we cannot model the discharge of the *heated* Paralana Spring waters onto the surface of the model. However, the model does demonstrate heat transport along the Paralana Fault when we specify slightly elevated permeabilities of rocks within the Mt Painter Domain (e.g., the change from 10^{-17} to 10^{-16} m^2, Figs 7.4 to 7.6).

In the case of "single-domain" MPI models (where the tracer was initially distributed exclusively within the coherent MPI rocks), the tracer is quickly leached from the MPI block, starting from the top western part of the model (e.g., Fig. 7.4) (note that the striping in tracer plots in Figs. 7.4, 7.6 and 7.7 is a plotting artefact). Analysis of the intermediate calculation results (i.e., within 0 to 10,000 years) shows that the tracer is partially removed through a minor discharge zone within the Eyre Formation, but also propagates to the east within the Eyre Formation (still visible in Fig. 7.6). The tracer exhibits similar behaviour in all the models, with most of the tracer washed out from the depicted parts of the Paleogene and Neogene units by 10,000 years. Within the "layered-domain" models, the tracer displays similar behaviour as well, with Figs. 7.8 and 7.9 also demonstrating propagation of the tracer from the top MPI layer deep into the Paralana Fault Zone.

The simple fluid flow pattern observed in virtually all models (namely, the eastward flow within the Eyre Formation and, the Cadna-owie Formation in non-overpressured models) has very straightforward implications for the genetic models for the Four Mile and Beverley deposits. The

fluids with surficial signature (Figs. 7.8 and 7.9) (initially saturated with atmospheric oxygen) can have only one major reduction front that cannot be duplicated down a flow line (cf. Fisher et al., 2008; Jaireth et al., 2008). Thus, we cannot attribute the formation of the Four Mile and Beverley deposits to the same geological process within a simple 2D hydrological system.

However, within the model of a simple eastward fluid flow, even the formation of the Four Mile East deposit is, in fact, problematical. All our examined models suggest that most of the fluid flow is sourced from the surface of and focussed within a spatially restricted part of the Eyre Formation, within a polygon of approximate size 2 000 x 150 x 200 metres (Figs. 7.4C to 7.9C). This observation creates two problems for the formation of Four Mile East – the uranium source, and the depositional mechanism.

7.3.2 Uranium mass balance calculations – Four Mile East deposit

As noted above, in all of the scenarios modelled here, the fluids responsible for the formation of Four Mile East are very largely sourced by recharge into the Eyre Formation outcrop and not by subsurface flow through uraniferous basement. If a portion of the Eyre Formation itself is the uranium source, the relative volumes (and areas) of the source rocks required to produce the Four Mile East type mineralisation can be estimated as follows.

For a tabular ore body, the amount of the contained uranium (m_U), can be calculated as follows:

$$m_U = C_{ore} * \rho_{ore} * (S_{ore} * D_{ore})$$

and for the source area,

$$m_U = C_{source} * \rho_{source} * (S_{source} * D_{source}),$$

where C is concentration of uranium, ρ is rock density, S is the area of an appropriate rock domain, and (S*D) is the rock volume. Assuming that densities of the source rock and the uranium ores are approximately the same, and adopting U concentrations of 5,000 ppm and 15 ppm in ores and the source region, respectively, for a two-dimensional model we have

$$S_{source} = S_{ore} * (C_{ore} / C_{source}) = S_{ore} * (5{,}000/15) \sim S_{ore} * 333.$$

Based on the Four Mile East deposit, we assume the size of a tabular ore body to be 750 to 2 500 m^2 (Wülser, 2009). The area of the Eyre Formation characterised by maximal fluid fluxes (Figs. 7.4C to 7.9C) is calculated as ~350 000 m^2, yielding a S_{source} to S_{ore} ratio of 140 to 470. This is a similar value to that estimated earlier, but this estimate is based on 100% efficient leaching of uranium from the source rocks as well as perfectly efficient (100%) deposition which are clearly overestimates. Furthermore, examination of the Figures 7.4C to 7.9C reveals essentially uniform fluid flow, without focussing that would allow some depositional process (presumably reduction) to cause uranium concentration in a small ore body. These calculations strongly suggest there is no adequate source or depositional mechanism for the formation of a roll-front style uranium system directly adjacent to the MPI within a west to east fluid-flow system as envisaged in the conceptual models discussed earlier in this chapter.

The following options are possible to explain the location of the Four Mile East deposit:

(a) The Four Mile East system formed in the current context, with fluid flow parallel to the MPI range front (including the scenarios where fluid flow could have been focussed into south-north oriented paleochannels);
(b) The geological setting was different when the mineral system was active – for example the Eyre Formation may have been more extensive and the MPI topography subdued or absent. However, the scenario modelled in Figure 7.7 shows that under such circumstances fluid fluxes were 1 to 2 orders of magnitude lower than in other scenarios.

(c) In combination with (a) or (b), fluid focussing occurred due to locally enhanced permeabilities (due to coarser sediments or small-scale, permeable faults) and the reductant was mobile, and uranium deposition was due to structural or other local control on the pathways of mobile reductants. This could have allowed locally greater fluid fluxes and more efficient deposition to occur.

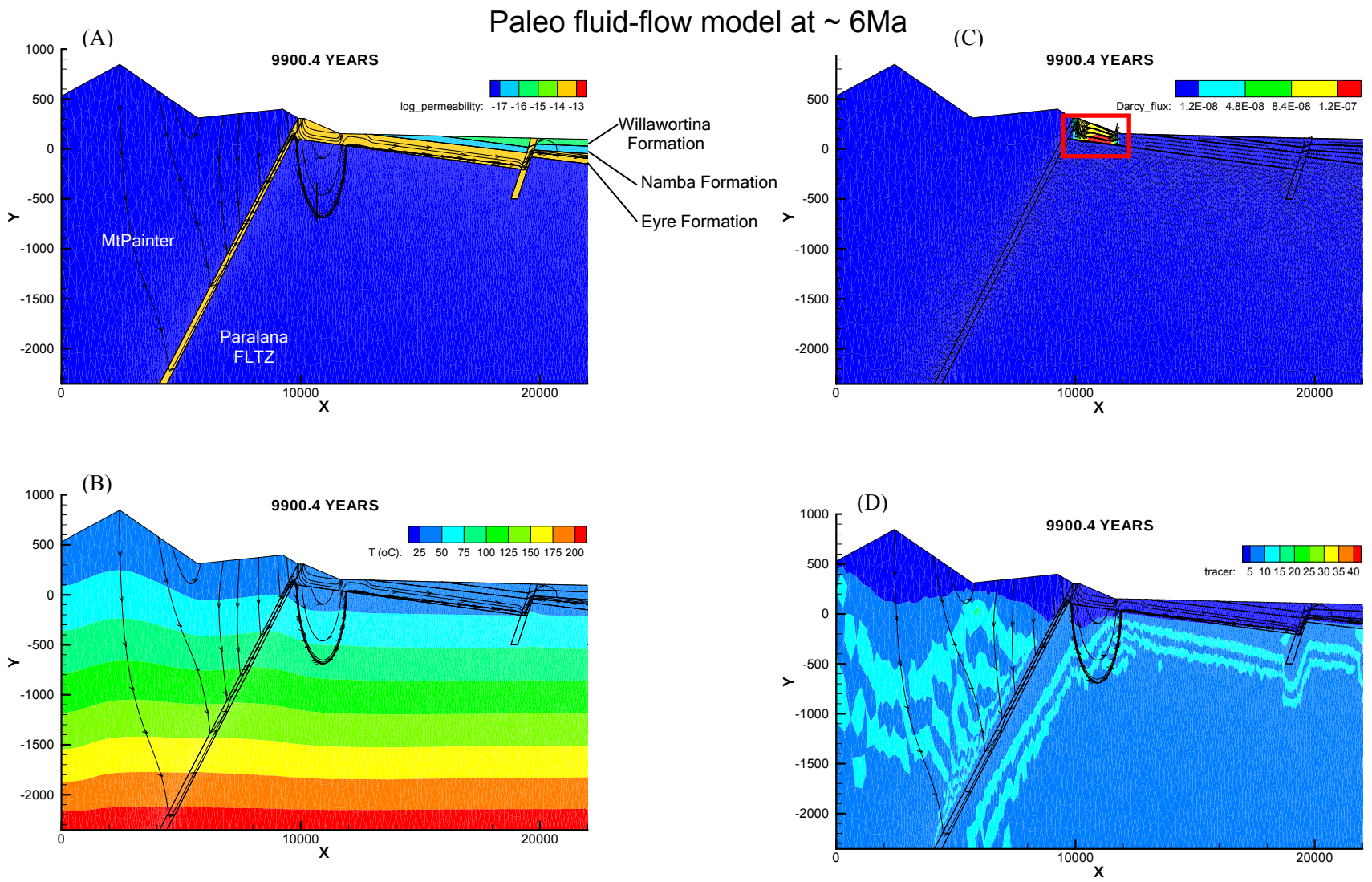

Figure 7.4: *Paleo fluid-flow Post-Paralana Fault reference model. A – distribution of the assigned permeabilities; B – distribution of temperature; C – Darcy fluxes and vectors; D – distribution of the tracer. A, B, and D show fluid flow lines. The red box in (C) outlines the area of the maximal fluid flow that is pertinent for all the subsequent figures. The model does not represent the present-day hydrogeological regime in areas proximal to the Four Mile and Beverley deposits.*

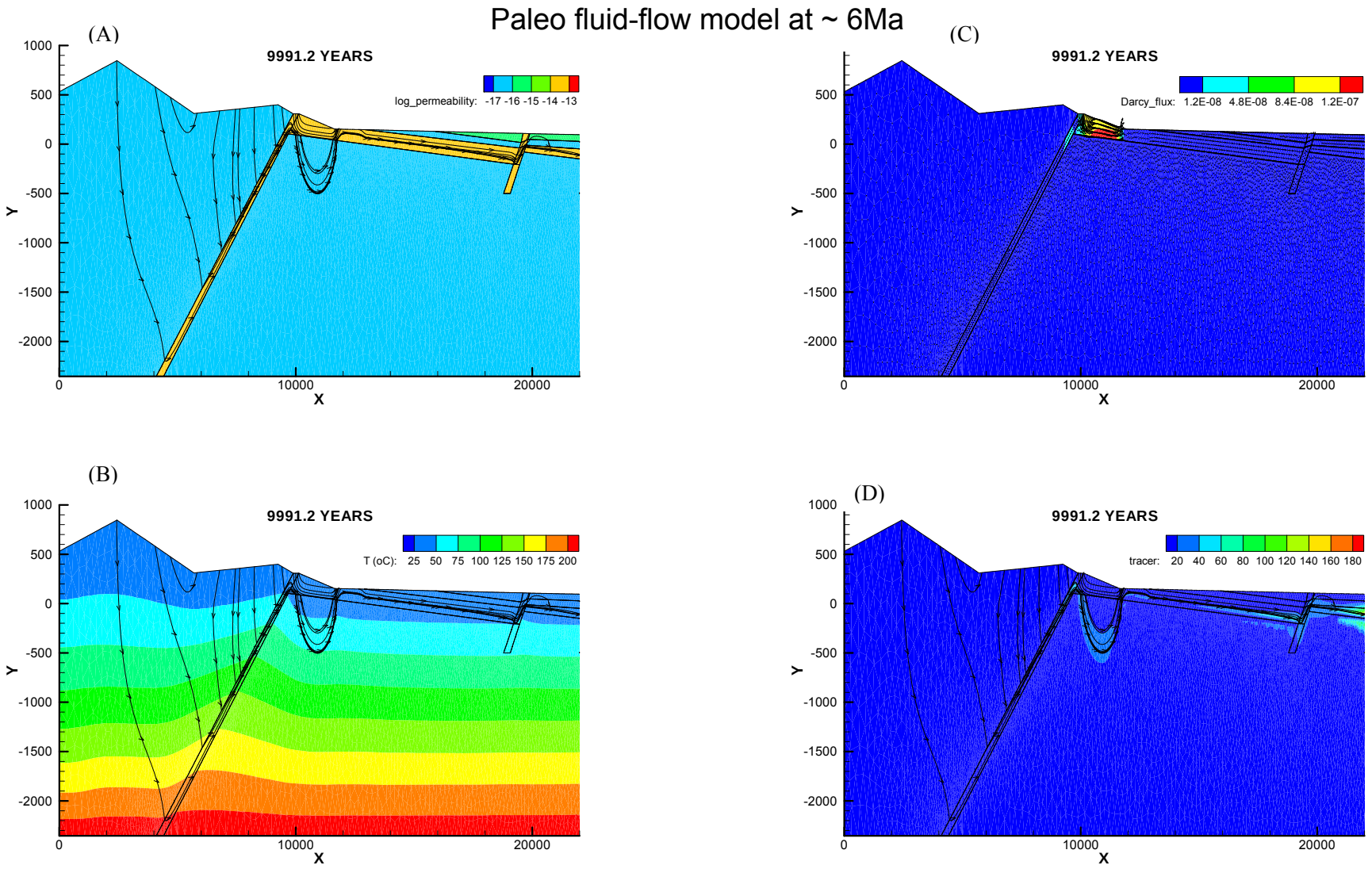

Figure 7.5: *Paleo fluid-flow Post-Paralana Fault model with enhanced permeabilities of the Mt Painter Inlier. A – distribution of the assigned permeabilities; B – distribution of temperature; C – Darcy fluxes and vectors; D – distribution of the tracer. A, B, and D show fluid flow lines. Note the elevated heat transport along the Paralana Fault zone (B) and different tracer results (D) compared to the reference model (Figure 7.4). The model does not represent the present-day hydrogeological regime in areas proximal to the Four Mile and Beverley deposits.*

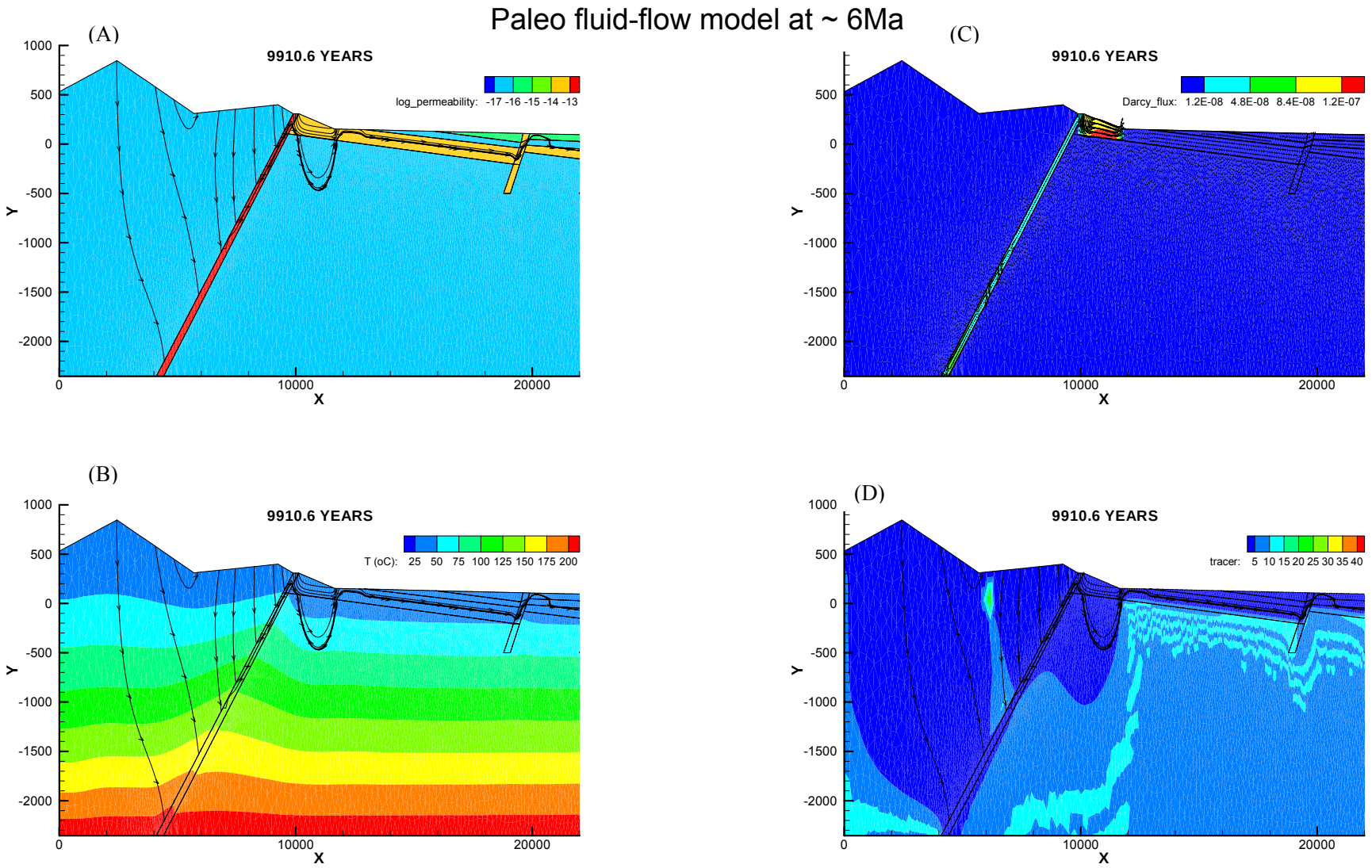

Figure 7.6: *Paleo fluid-flow Post-Paralana Fault model with enhanced permeabilities of the Mt Painter Inlier and Paralana Fault zone. A – Distribution of the assigned permeabilities; B – distribution of temperature; C – Darcy fluxes and vectors; D – distribution of the tracer. A, B, and D show fluid flowlines. Note virtually no difference with Figure 7.5 in terms of temperature distribution. The model does not represent the present-day hydrogeological regime in areas proximal to the Four Mile and Beverley deposits.*

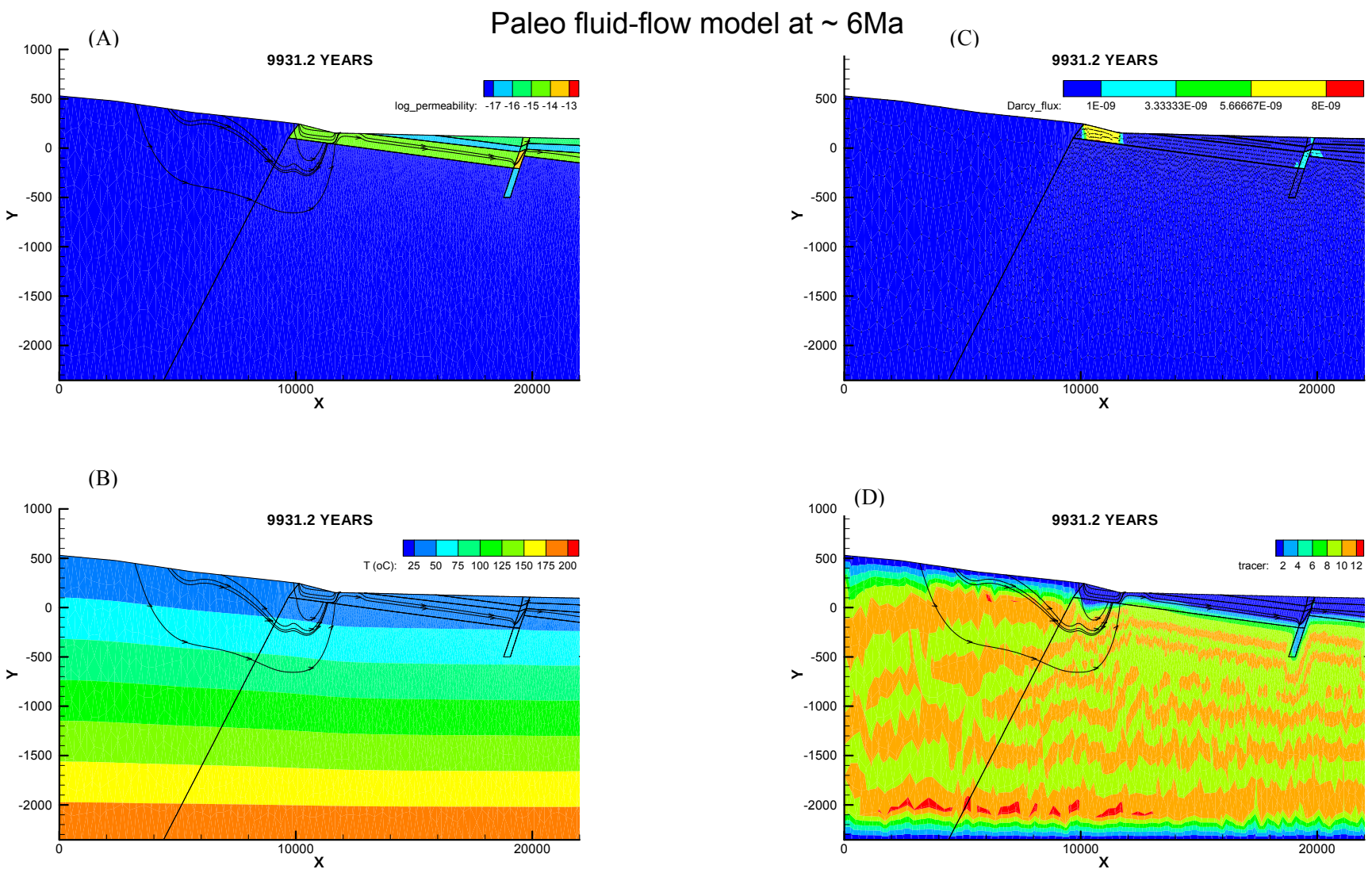

Figure 7.7: *Paleo fluid-flow for pre-Paralana Fault model, with relatively low relief in the Mt Painter Inlier. A – distribution of the assigned permeabilities; B – distribution of temperature; C – Darcy fluxes and vectors; D – distribution of the tracer. A, B, and D show fluid flow lines. The model does not represent present-day hydrogeological regime in areas proximal to Four Mile and Beverley deposits.*

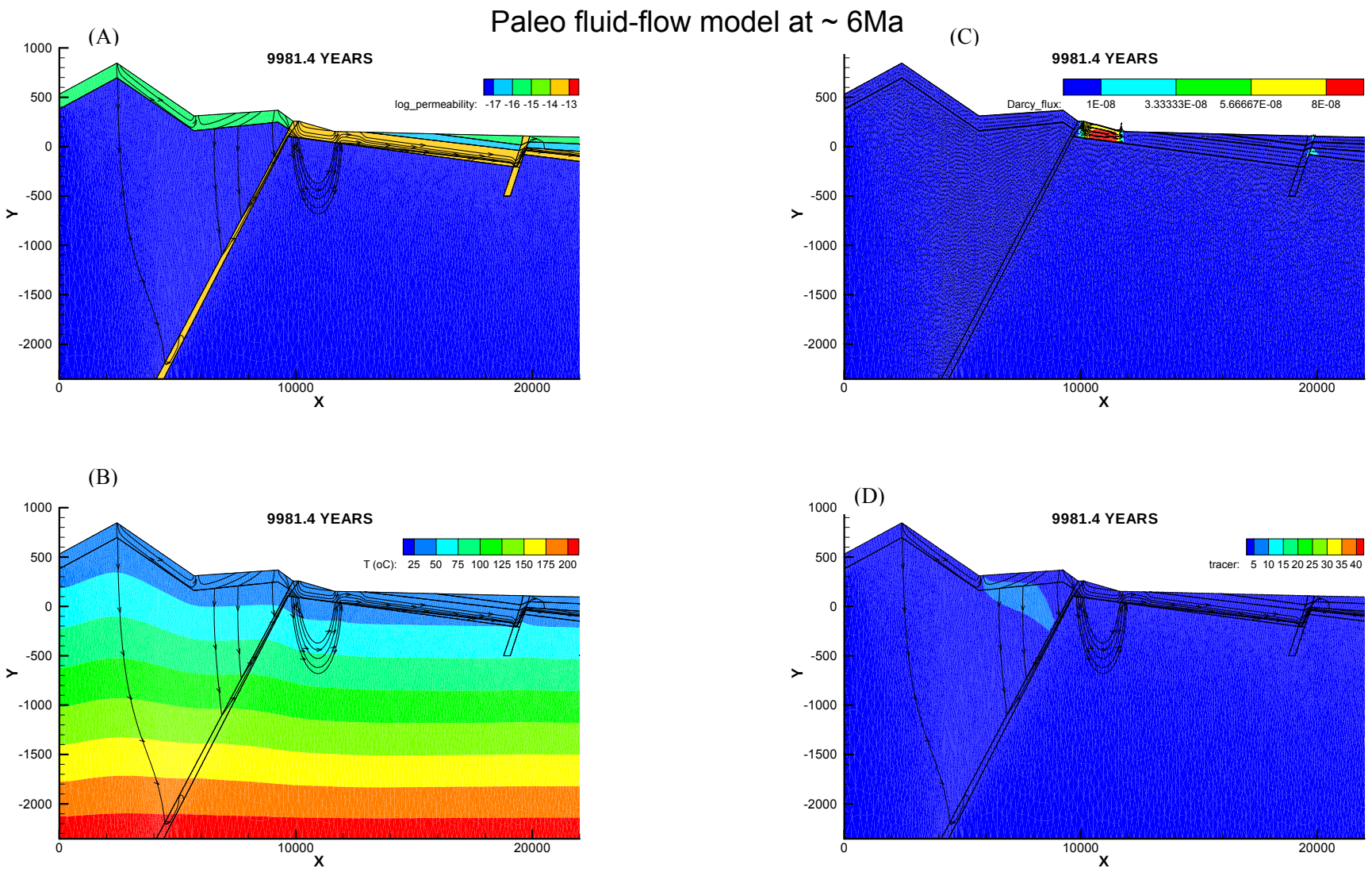

Figure 7.8: *Paleo fluid-flow Post-Paralana Fault model with a layer of weathered and fractured granite as part of the Mt Painter Inlier. A – distribution of the assigned permeabilities; B – distribution of temperature; C – Darcy fluxes and vectors; D – distribution of the tracer. A, B, and D show fluid flow lines. Compared to the models above, the tracer is introduced within the fractured/weathered sub-domain of the Mt Painter Inlier rocks only. The model does not represent the present-day hydrogeological regime in areas proximal to the Four Mile and Beverley deposits.*

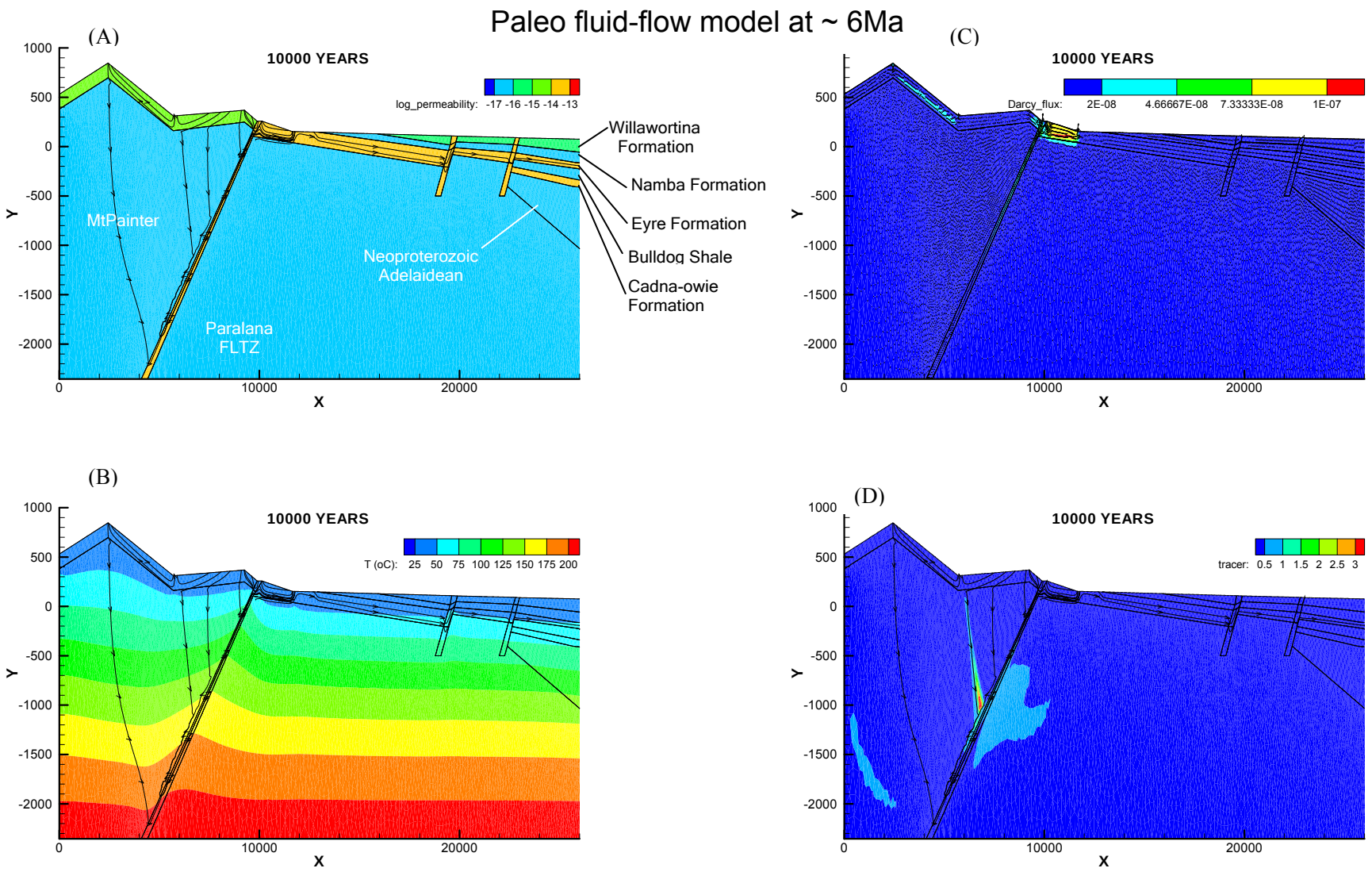

Figure 7.9: *Paleo fluid-flow Post-Paralana Fault model with overpressure superimposed within the Cadna-owie Formation. A – distribution of the assigned permeabilities; B – distribution of temperature; C – Darcy fluxes and vectors; D – distribution of the tracer. A, B, and D show fluid flow lines. The model does not represent the present-day hydrogeological regime in areas proximal to the Four Mile and Beverley deposits.*

7.4 GEOCHEMICAL MODELLING OF FROME URANIUM SYSTEMS

To test the chemical implications of predicted fluid-flow patterns for uranium solubility, transport and deposition, a set of auxiliary geochemical modelling calculations have been undertaken. These calculations allow the prediction of uranium solubility in equilibrium with different rock types, as well as changes in uranium solubility due to fluid-rock reactions at different temperatures and pressures relevant to uranium systems of the Lake Frome region.

7.4.1 Methodology and model setup

The geochemical model used for runs with equilibrium-dynamic and reactive-transport modelling components was created using the HCh software for geochemical modelling (Shvarov and Bastrakov, 1999). To focus on the most important controls on uranium mobilisation, transport, and deposition, we have simplified the composition of the rock units. It is assumed that all the rock types are represented essentially either by granites or arkose sedimentary rocks, and are composed of quartz, K-feldspar, albite, muscovite, chlorite, biotite, and hematite/magnetite (Table 7.2). Parts of the system are modelled to contain uraninite (the MPI) or elemental carbon as a reductant (the Eyre Formation).

The initial chemistry oof the rocks was defined by volume fractions of minerals, and fluids as moles of the dissolved components. A simple Na-K-Ca-Mg-Cl-S solution with ~12 ppm of dissolved salts was used as a starting composition for surface waters (Table 7.3).

Table 7.2: Rock compositions used in the calculations

Minerals (weight %)	**Granite**	**Sandstone**
Quartz	32	80
K-feldspar	35	8
Plagioclase	9	2
Muscovite	7	3
Biotite as annite	15	0
Epidote	0.6	0
Chlorite as chamosite	0.6	0
Kaolinite	0	6
Calcite	0	0.4
Carbon as graphite	0	0.5
Ilmenite	0.5	0
Magnetite	0.9	0
Apatite	0.5	0
Fluorite	0.6	0
Pyrite	0.02	0.1
Uraninite	0.006	0

Granite composition based on the composition of Mount Neil Granite Porphyry (Coats and Blissett, 1971). Sandstone composition corresponds to the composition of a sandstone (except for carbon) in Kazakhstan (Fyodorov, 1999).

Table 7.3: Composition of fluid/water used in the calculations

Component (ppm)	Surface water	Paralana Hot Springs
Na^{+}	4	272
K^{+}	0.2	23
Ca^{2+}	0.4	42
Mg^{2+}	0.4	15
Cl^{-}	6	310
Total dissolved sulfur	1.3	136
U (ppb)	0	0.07

Surface water composition derived from the rainwater analysis at Verdum station, South Australia (Blackburn and McLeod, 1983). The composition of Paralana Hot Springs water is from Brugger et al. (2005).

7.4.2 Granite-water interaction (modelling Paralana Hot Springs)

Interaction of oxygen-saturated surface water with uranium-bearing granite is modelled to explore the possibility of uranium leaching from granites of the Mt Painter Inlier. Recent studies of the geochemistry of the Paralana Hot Springs show that these surface-derived waters were deeply circulated within the granite-bearing basement of the Mount Painter Inlier and moved up along more permeable fault zones such as the Paralana Fault (Brugger et al., 2005; this study). The uranium content of the Paralana Hot Springs is low (0.07ppb, Table 7.3) compared with some of the groundwaters in the district (Brugger et al., 2005). In this section we seek to explain this geochemistry through geochemical modelling, and to determine the implications for uranium mineralising systems.

First, a simple model is constructed for granite-water interaction simulating downflow of surface (meteoric) waters into granite. The surface water is saturated with oxygen and carbon dioxide at their respective partial atmospheric pressures ($\log fO_2 = -1$ and $\log fCO_2 = -3.5$) and is assumed to be of low salinity (11 ppm of total salts, NaCl, KCl, $CaCl_2$, $MgCl_2$) with 0.5 ppm of dissolved sulfur (Table 7.3). In the modelling, this 25ºC water is then equilibrated with a rock similar in composition to the Mount Neil Granite in the Mount Painter Inlier (Table 7.2, Coats and Blissett, 1971) at a 1:1 weight ratio. Initial concentration of uranium in the granite is set at 50 ppm in the model. The results show that the oxygen saturated water at 25°C dissolves all the available uranium, and all Fe^{+2}-bearing silicates and oxides are converted to hematite. To model the downward flow of this fluid into the granite and accompanying heating of the fluid due to the geothermal gradient, the fluid resulting from the initial reaction with granite reacts at equilibrium with the fresh granite at increasing temperature up to 100°C. The results show that the fluid which was oxidised at 25°C and uranium rich is immediately reduced by the granite, and the uranium concentration in the fluid drops significantly (from 100 ppm to less than $1x10^{-9}$ ppm; Fig. 7.10). Thus the fluid moving downward through the fresh granite cannot dissolve geologically significant concentrations of uranium. Only at very high fluid rock ratios (of >1000) will the fluid in equilibrium with the granite be sufficiently oxidised to carry significant concentrations of uranium. However, to attain such high fluid/rock ratios, the fresh granite would be required to have unrealistically high permeability. Nevertheless, extremely high permeabilities may be possible in some weathered zones and/or in breccia zones.

Second, the chemical changes during upflow of the fluid in the circulation system are modelled. The properties of this fluid are initially set to be the same as those derived from the final interaction of down-flowing water with granite at 100°C, modelled above. Upflow is modelled by cooling the fluid to 25°C at rock-buffered conditions (in equilibrium with the granite, see Fig. 7.3). As the initial concentration of uranium in the fluid is very low ($<1x10^{-9}$ ppm), the cooling and rising fluid neither deposits geologically significant uranium nor transports to the surface much dissolved uranium (Fig. 7.11). Even if the upflowing fluids did not equilibrate with granite or did not cool to 25°C, the

results for uranium transport and deposition are essentially the same. The model thus explains why waters in the Paralana Hot Springs contain such low levels of uranium.

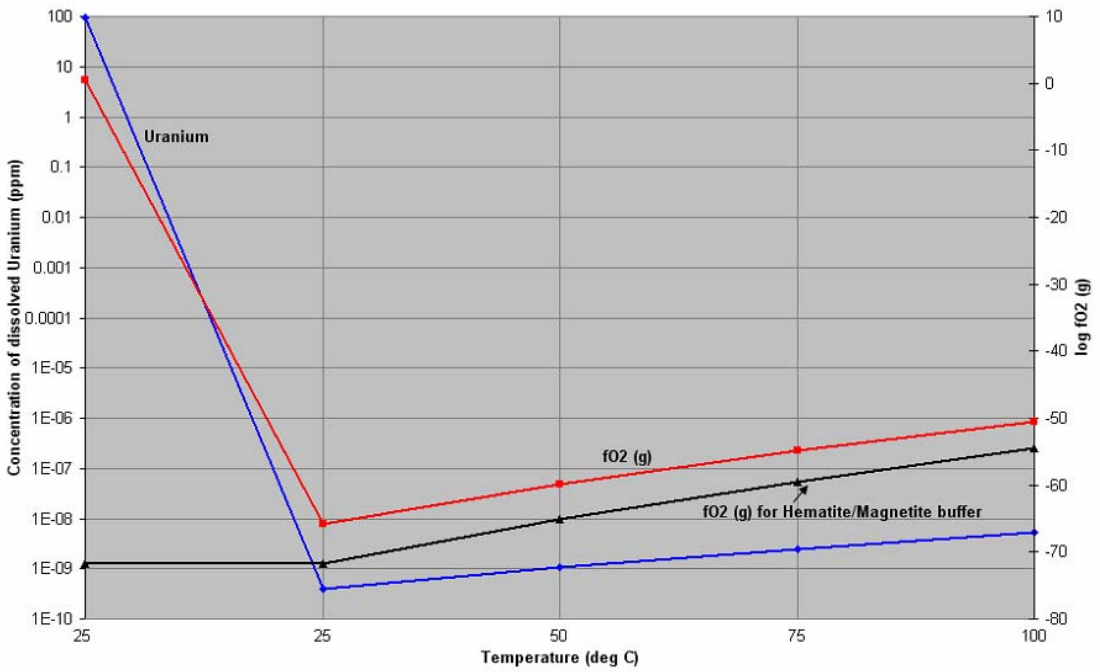

Figure 7.10: *Simulation of surface water downflow into granite at 25-100ºC, showing changes in the concentration of dissolved uranium (blue line) and in the oxidation state of the fluid (red line; initially saturated with oxygen). The calculations are for equilibrium with a uranium-bearing granite similar to the Mount Neil Granite.*

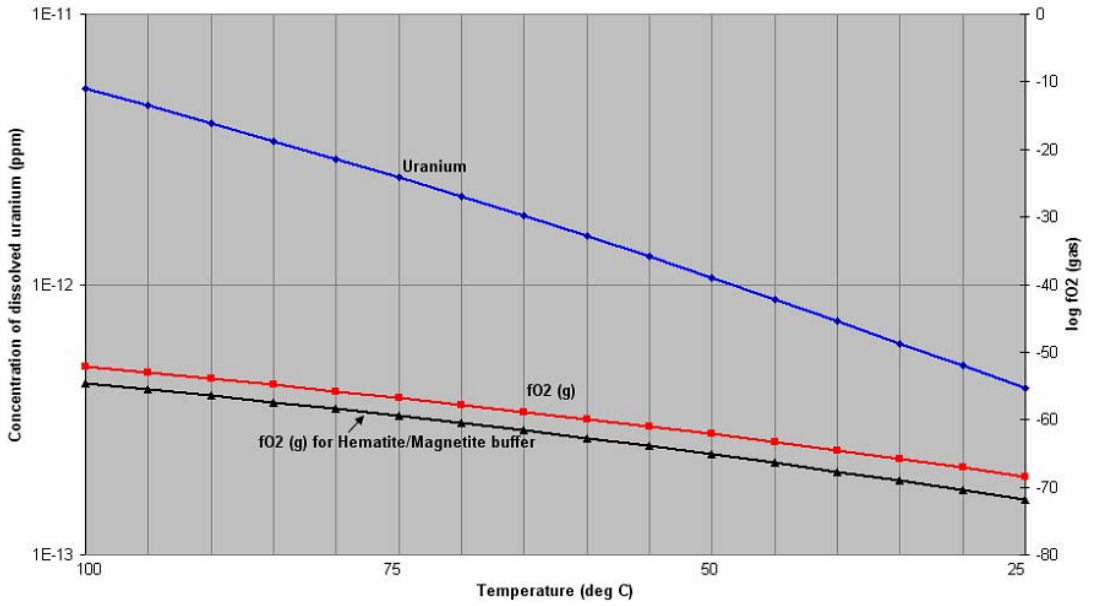

Figure 7.11: *Simulation of fluid upflow along the Paralana Fault zone at 100-25ºC, showing changes in the concentration of dissolved uranium (blue line) and in the oxidation state of the fluid (red line). The calculations assume equilibrium with and rock buffering by a uranium-bearing granite similar to the Mount Neil Granite.*

7.4.3 Modelling granite-water-sandstone interaction (formation of sandstone-hosted uranium mineralisation)

Geochemical constraints on the formation of sandstone uranium deposits are well known with oxidation-reduction reactions playing a major role in the transport and deposition of uranium. In this model the starting composition of fluid is the same as that used above in modelling of granite-water interaction, i.e., low-salinity surface water saturated with atmospheric oxygen and CO_2 is equilibrated with a uranium-bearing granite similar in composition to the Mount Neil Granite (Tables 7.2, 7.3) at a 1:1 weigh ratio. This reaction produces fluids containing up to 100 ppm of dissolved uranium.

In this model, the uranium-rich fluid is reacted with fresh sandstone containing pyrite and graphite (to model the effect of reductants). The initial composition of the sandstone is mineralogically similar to that of sandy aquifer units in the Namba Formation or Eyre Formation.

To explore the effect of increasing fluid/rock ratio on transport and deposition of uranium, 1 kg of sandstone in the model is reacted with successive batches (each batch is 50 kg) of uranium-bearing oxidised fluid. Changes in the concentration of dissolved uranium in the fluid and of uranium oxides deposited in the sandstone are shown in Figures 7.12 and 7.13, respectively. The figures also show the changes in the oxidation state of the fluid.

As the first batch of fluid reacts with graphite-bearing sandstone dissolved uranium is quantitively precipitated to form uranium oxides, and the uranium concentration in the fluid decreases from ~100 ppm to less than $1x10^{-9}$ ppm (Fig. 7.12). The pattern continues until the fluid/rock ratio reaches ~2000 when the uranium concentration in the fluid begins to increase. At fluid/rock ratios of less than ~2000, deposition of uranium from successive batches of fluids can form a model ore zone containing up to ~11 weight percent uranium oxides (Fig. 7.13). Further inflow of oxidised fluid in the sandstone begins to oxidise the sandstone, and uranium oxides deposited earlier begin dissolving. Above fluid/rock ratios of ~ 3500 all uraninite is dissolved. At each step reduction of the fluid produces methane which at higher fluid/rock ratios is oxidised to form carbonates. As expected pyrite is oxidised to hematite.

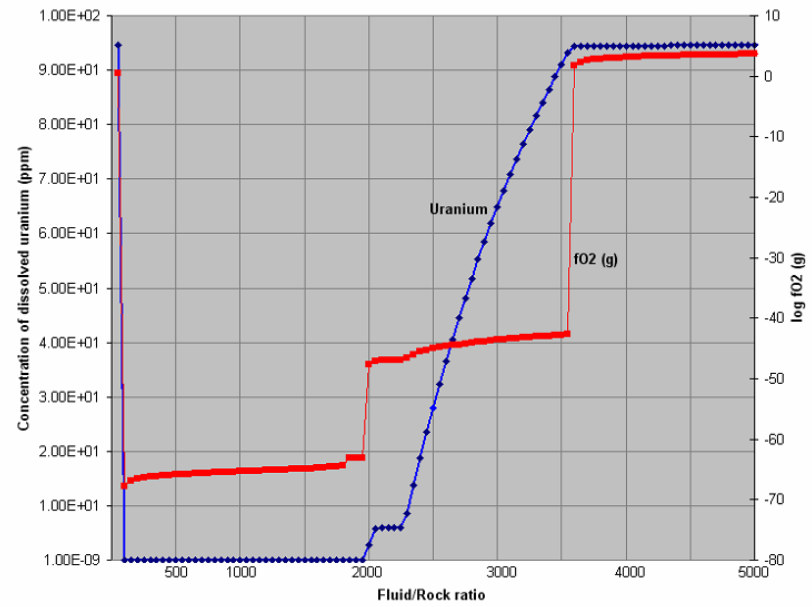

Figure 7.12: *Simulation of interaction of oxygen-saturated, uranium-rich fluid with graphite bearing sandstone (at 25°C). Uranium concentration in the fluid dramatically decreases as it reacts with initially reduced sandstone. Introduction of successive batches of the oxygenated input fluid through the same sandstone volume causes complete oxidation of the sandstone at a fluid/rock ratio of ~3500, at which the uranium concentration in the fluid reverts to the original value.*

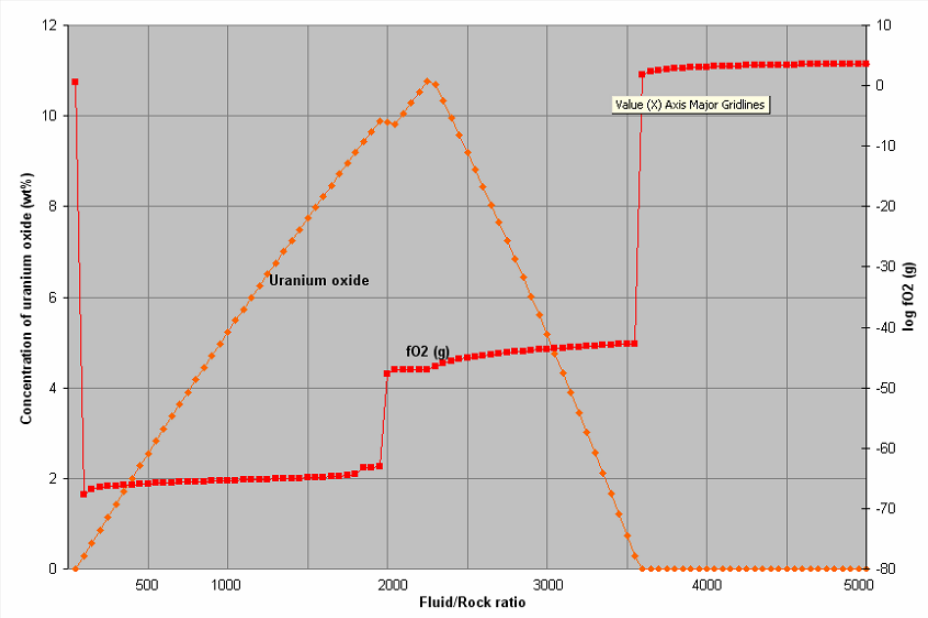

Figure 7.13: *Simulated interaction of oxygen-saturated, uranium-rich fluid with graphite bearing sandstone (at 25°C). Uranium oxides commence precipitating upon initial reaction of fluid with sandstone. Passage of successive batches of the fluid throught the same volume of sandstone causes increase precipitation of uranium oxides, reaching a maximum of ~11 weight percent. At a fluid/rock ratio of ~2500 the uranium oxides begin to dissolve and disappear at a fluid/rock ratio of ~3500. Preservation of ore zone thus requires isolation from subsequent batches of oxygen-saturated fluid. The 'peak' in uranium oxide deposition may represent a 'roll-front' style uranium ore zone, with deposition of uranium oxides on the 'downstream' side of the system (to left of 'peak', at lower fluid/rock ratios and more reduced fluid and rock conditions), and leaching on the 'upstream' side of the system (to the right of the 'peak', at higher fluid/rock ratios and more oxidised fluid and rock conditions).*

7.4.4 Summary of geochemical modelling results

Geochemical modelling of a simplified granite-water interaction designed to simulate uranium transport and deposition in the Paralana Hot Spring system shows the following.

- Fluids observed in the Paralana Hot Springs are incapable of transporting geologically significant concentrations of uranium because they are relatively reduced through reaction with fresh granite at depth.
- These relatively reduced fluids may serve as a mobile reductant for uranium precipitation. This will be favoured where the hydrogeological architecture allows mixing of such fluids with oxygen-saturated and uranium-bearing fluids moving through sandstone aquifers such as the Beverley Sands or sandy units of the Eyre Formation. Additionally, the deeply-circulated and relatively hot (~100°C) reduced fluids may react with organic material in the sands and underlying carbonaceous shales, generating gaseous mobile reductants such as methane and H_2S, which in turn can provide either additional reductant or catalyse the reduction reaction initiated by organic material present in the sands.

Geochemical modelling of a simplified sandstone-water interaction designed to simulate uranium transport and deposition in sandstone-hosted systems leads to the following conclusions.

- Under favourable hydrogeological architecture uranium from uranium-rich rocks such as the Mount Neil Granite can be leached into sandstone aquifers. Reduction of these fluids by organic

material (*in situ* or introduced) may result in zones enriched in uranium oxides. However it is important that the ore zone is hydrologically isolated from the later influx of oxidised fluids to ensure preservation of uranium mineralisation.
- Permeability of the sands, fluid-flow rate, and concentration of reductant all will play significant roles in determining the downstream distance of the uranium-rich ore zone within the sands relative to the location of uranium-rich source rocks.

7.5 CONCLUSIONS – NUMERICAL MODELLING

Within the limitations of the two-dimensional fluid flow modelling, and simplified geochemical modelling scenarios, the following conclusions are drawn.

- The overall fluid flow pattern predicted by our numerical models confirms the general concept of gravitationally-driven eastwards fluid flow within Cenozoic rocks, previously suggested by Heathgate Resources (1998), Brugger et al. (2005) and others. However, the results of the numerical simulations suggest that these previous models cannot adequately explain the presence of the Four Mile deposit so close to the present-day Mt Painter Inlier range front.

- The simple fluid flow pattern modelled within the Eyre Formation does not allow formation of more than one oxidation-reduction (roll-type) front along a single fluid flow path. We conclude that the occurrence of the Four Mile East and Beverley uranium deposits cannot be explained by a simple two-dimensional flow-through type model in which both deposits formed along a single fluid flow path. Rather, the numerical modelling highlights the possibility of two differing processes and ages of uranium deposition in the Lake Frome region. On the other hand, at a higher degree of resolution, the Eyre Formation aquifer is heterogeneous and composed of sands capped by shaly sediments. Therefore, it is possible that oxidation-reduction fronts could form in separate sand units at different stratigraphic levels.

- Simple mass-balance estimations, based on the architecture of fluid flow, further highlight the problems of formation of the Four Mile East style of mineralisation. Based on the present day geology, there would appear to be insufficient volume of Eyre Formation to the west or southwest of the Four Mile East deposit for a major ore system to have developed in the manner of typical 'roll-front' style mineralisation. Further work is warranted to examine scenarios of uranium transport and deposition along north-south oriented paleochannels, and also the possible role of fluid mixing in this setting.

- Provided that the Paralana Fault indeed represents a zone of high permeability (i.e., comparable with, or higher than the permeabilities of the Eyre Formation), as might be expected when the fault zone was active, it does not represent an impediment to uranium transport into the Frome Embayment and Callabonna Sub-basin.

- The fluids discharged at the top of the Paralana Fault could have penetrated to significant depths and been heated to temperatures of 50° to 200°C. Geochemical calculations predict these fluids will be relatively reduced via reactions with fresh granites and gneisses and, subsequently, uranium-poor (e.g., Paralana Hot Springs). Mixing of these fluids with uranium-rich groundwaters in aquifers such as the Eyre and/or Namba Formations may potentially form uranium mineralisation.

8. Synthesis, and implications for exploration

Roger G. Skirrow, Subhash Jaireth, Simon van der Wielen, Anthony Schofield

8.1 ESSENTIAL COMPONENTS OF BASIN-RELATED URANIUM MINERAL SYSTEMS OF THE LAKE FROME REGION

8.1.1 Sources of ore constituents and fluids

The source(s) of ore components including uranium in deposits of the Lake Frome region is presently unknown. It has been commonly assumed that the uranium-rich Mt Painter Inlier and Willyama Supergroup have sourced the uranium. Alternatively, sediments of the Frome Embayment and/or Callabonna Sub-basin may have contributed uranium (Wülser et al., 2005). While the presence of uranium-rich Proterozoic rocks is one key factor in the development of a fertile basin-related uranium province, the availability of fluids of appropriate composition to mobilise the uranium is also critical. Moreover, the availability of uranium in source areas is dependant on the mineralogical characteristics of the source.

Uranium bound in crystal structures of minerals such as zircon and monazite in igneous rocks is generally not readily leached. However, metamictisation caused by prolonged radiation damage will result in greater vulnerability of U-bearing minerals to secondary processes of leaching (Cuney and Kyser, 2008). Uranium-rich Proterozoic rocks are therefore a favourable source of uranium.

However, it may be much younger processes in the source regions that have combined to produce a major basin-related uranium province in the Lake Frome region. In particular, we suggest that the timing of deep weathering, climate change, and uplift / exhumation were crucial in the development of uranium mineralisation (Fig. 3.1). Paleomagnetic dating of hematite formation in ultra-deep (>100m) weathered profiles in the Cobar region to the east of the study area and elsewhere in Australia indicate at least three major periods of deep weathering: ~15±5 Ma, ~60±10 Ma, and late Mesozoic (Pillans, 2004; Smith et al., 2009). In the Lake Frome region, Proterozoic basement and upper parts of the Eromanga Basin would have been affected by all three deep weathering events, whereas the Eyre Formation probably experienced only the latest period of deep weathering. All units including the Namba Formation are affected by the current weathering regime, which appears to not penetrate as deeply as particularly the ~15±5 Ma episode. Also of note are the results of paleomagnetic studies of hematitic breccias in the Mt Gee area in the Mt Painter Inlier, which do not record any significant resetting events since the Permo-Carboniferous (Idnurm and Heinrich, 1993).

Smith et al. (2009) note that “iron oxide/oxyhydroxides , including hematite, are important hosts for elements released and dispersed from weathering ore deposits. Periods of humid, deep weathering would have dispersed some elements but fixed others in the iron oxides and oxyhydroxides. Subsequent weathering under drier or arid conditions would have imposed a chemically and physically different weathering regime, with different dispersion processes, predominantly mechanical”. In relation to the Lake Frome region, at least three stages of deep weathering of Proterozoic basement may have released uranium from metamict host minerals (Fig. 3.1). The strong tendency for uranium to be adsorped on the surface of iron oxides and oxyhydroxides (Sherman et al., 2008) means that uranium may have been only locally redistributed within the weathered rocks, depending on fluid chemistry among other parameters.

A critical process in uranium systems development in the region was uplift and exhumation of uranium-rich Proterozoic basement. It is during these periods of exhumation, in three major periods after deposition of each of the Mesozoic Eromanga Basin, Paleocene-Eocene Eyre Formation, and Miocene Namba Formation (Fig. 3.1), that previously deeply weathered basement may have been subject to leaching by oxidised meteoric waters and groundwaters, during climatically favourable periods. In this hypothesis, major quantities of loosely bound (adsorbed) uranium residing within deeply weathered relatively permeable uplifted basement may have been the source of uranium that was chemically transported into sediments of the Eromanga Basin and Callabonna Sub-basin.

The fluids required to mobilise and transport large quantities of uranium in the near-surface parts of sedimentary basins are necessarily highly oxidised, with minimum logfO_2 values several units above the hematite-magnetite buffer (see Skirrow et al., 2009, and references therein). One of the problems in understanding uranium transport and deposition in general is how high oxidation states are maintained during fluid flow through rocks with redox buffering capacity (Skirrow et al., 2009). For example, in section 7.4.2 it is shown that oxygen-saturated rainwater deeply circulated within the uranium-rich granites of the Mt Painter Inlier loses its capacity to transport significant uranium as it is buffered to relatively low oxidation states. The hypothesis of uranium leaching from already deeply weathered basement rocks solves this problem because the weathered rock is oxidised to the extent that oxygen-saturated meteoric waters may pass without being buffered to significantly lower redox state, enabling uranium transport. Nevertheless, to remove adsorbed uranium and prevent further local adsorption of uranium on iron oxides and oxyhydroxides the fluid chemistry must be different to that during the process of adsorption. Uranium adsorption on iron oxides and oxyhydroxides is highly pH-dependant and occurs preferentially at pH values around neutral (Payne and Airey, 2006). Hence, acidic or highly alkaline oxidised groundwaters potentially may de-adsorb uranium and transport it significant distances through the deeply weathered basement rock and into basin sediments. Possible sources of acidity in the Lake Frome region are not clear, but may include: oxidation of sulfide minerals; buffering by clay minerals; humic acid generation in organic-rich environments; and high CO_2 content. Highly alkaline waters may occur in some playa lake environments.

This hypothesis allows some testable predictions to be made.

1. Deeply weathered basement is predicted to contain uranium adsorbed on iron oxides and oxyhydroxides in areas not leached of uranium during mineralising events.
2. A large proportion of the uranium in Proterozoic basement rocks is expected to be hosted by either metamict minerals (zircon, monazite, allanite, etc) or by other readily leacheable uranium minerals such as uraninite (e.g., pre-existing uranium mineralisation).
3. Uplifted and exhumed areas of deeply weathered basement are predicted to have been more extensively leached of uranium than areas uplifted to a lesser extent. Of course mechanical erosion may have removed some or all of the weathered profile (cf. Mt Gee area where there is no evidence of Cenozoic weathering; Idnurm and Heinrich, 1993).
4. Areas of deeply weathered basement that were subsequently leached of adsorbed uranium may exhibit alteration by either acidic or strongly alkaline fluids. This alteration may persist down-stream into mineralised areas. Alteration by acidic fluids will result in destruction of most silicate and carbonate minerals, including even clay minerals (cf. quartz corrosion and replacement of kaolinite by uraninite and phosphate minerals at Four Mile East, Chapter 5).

8.1.2 Energy and timing

The timing of uplift in the hinterland to the Frome Embayment and Callabonna Sub-basin is critical in the evolution of uranium mineral systems, partly because topography provides the potential energy to drive fluids down into basins, and partly for reasons involving effective leaching of source areas, discussed above. The three proposed episodes of uplift and exhumation were potentially the triggers for the formation of major basin-hosted uranium systems (Fig. 3.1). Optimal conditions existed with the coincidence in time and space of this source of energy, the availability of readily leacheable uranium in deeply weathered uplifted basement, and the permeability architecture and depositional gradients (reductants) already present in paleochannels within the Eyre and Namba Formations (Fig. 1.6). The three hypothetical episodes of uranium system development in the Lake Frome region are summarised below.

1. Late Mesozoic-early Cenozoic uranium mineral system: Post-Eromanga Basin uplift of basement that was deeply weathered during the Mesozoic could have potentially triggered gravitationally-driven flow of uranium-rich groundwaters into aquifers of the Eromanga Basin. The apatite fission track results of Mitchell et al. (2002) from the Mt Painter Inlier suggest regional denudation from ~90 Ma until the Paleocene, when deposition of the Eyre Formation commenced. If suitable reductants were available in aquifers of the Eromanga Basin, then uranium mineralisation potentially could have formed in the Late Cretaceous or Paleocene.

2. Eocene-Oligocene post-Eyre Formation uranium mineral system: Cessation of deposition of the Eyre Formation in the Late Eocene (~35 Ma) and development of a disconformity is roughly contemporaneous with the initiation of intraplate stresses due to changes in motion of the Australian plate (Célérier et al., 2005). Uplift and exhumation in the Paleocene was inferred from fission track data from the Mt Painter Inlier (Mitchell et al., 2002), prior to deposition of the Namba Formation. This tectonism and resultant topography may have triggered fluid flow from basement areas (at least twice deeply weathered) into the Eyre Formation, utilising south-to-north oriented paleochannels. In this hypothetical uranium mineral system, fluids would have been confined by aquitards and aquicludes within the Eyre Formation, and mineralisation would have formed in the late Eocene to early Oligocene (~35-28 Ma).

3. Pliocene-Pleistocene post-Namba Formation uranium mineral system: the most recent major period of uplift and exhumation of basement rocks in the Lake Frome region occurred since ~5 Ma, producing most of the present day relief in the Northern Flinders Ranges and Mt Painter Inlier. Basement that was deeply weathered in the period ~10-20 Ma would now be available for leaching of uranium and transport into permeable units of the Namba Formation, Eyre Formation or Eromanga Basin.

8.1.3 Permeability architecture and fluid flow

Fault architecture that developed during the Proterozoic controlled the formation of the Arrowie Basin, including the Moorowie and Yalkalpo sub-basins to the west and east, respectively, of the Proterozoic Benagerie Ridge. North-south trending faults as well as northeast-southwest trending faults imaged in seismic data controlled the architecture of Cambrian half-graben.

Seismic data show that several reactivated Cambrian faults cut upwards through the Mesozoic Eromanga Basin sediments and also cut Cenozoic sediments. Some modern topographic features

such as the eastern shore of Lake Frome and segments of the eastern range front of the Mt Painter Inlier also may be controlled by reactivated Paleozoic faults. The general northwards trend of many of the major Cenozoic paleochannels in the Frome Embayment and Callabonna Sub-basin including those hosting uranium mineralisation at the Honeymoon and Beverley deposits, suggests a fundamental tectonic-topographic control exerted by the early fault architecture. Mound springs in the Lake Frome area (Fig. 3.8) are potentially another manifestation of faults connecting artesian aquifers (Eromanga Basin?) with the present day surface, although the geometry of such faults is unknown.

Subsurface hydrocarbons and seeps of methane have been recorded in the Moorowie sub-basin. Reactivated Paleozoic faults therefore provide potential pathways linking Cambrian hydrocarbon fluids with near-surface environments. It is in such settings that potential may exist for mobile reductants to catalyse the precipitation of uranium carried in oxidised surface-derived waters. This concept has been recently described by Jaireth et al. (2008a). The 3D lithological and fault architecture presented for the Lake Frome region in Chapter 3 provides some of the key spatial data that may be utilised for targeting of this type of basin-related uranium mineralisation.

Evidence from 3D modelling of Cenozoic lithological units to the east of Lake Frome (Fig. 4.3), suggests that the Eyre Formation and Namba Formation dip gently to the west and the Namba Formation thickens to the west (i.e. towards the Benagerie Ridge). On the opposite (western) side of the Benagerie Ridge the Cenozoic units are not well constrained regionally by drilling although they are well constrained near the uranium deposits. Published cross sections from the Beverley area show the Namba Formation thickening eastwards across the Poontana Fault, and both the Eyre and Namba Formations having easterly dip components towards the Benagerie Ridge (McConachy et al., 2006; SKM, 2008). Thus there is evidence for a Cenozoic basin structure or perhaps two sub-basins flanking the Benagerie Ridge. There are important implications for present and paleo-groundwater flow. Based on this current architecture, easterly and westerly components of flow are likely on opposite sides of the Benagerie Ridge. However, major paleochannels in the Eyre Formation appear to trend broadly north-south, and branching relationships indicate sediment transport from south to north. This apparent contradiction may be reconciled if post-Eocene tilting has occurred to the east of Lake Frome. Further work is required to resolve this question, which has important ramifications for uranium exploration. In particular it is recommended that the northerly extensions of known paleochannels in the Eyre Formation are mapped, for example using airborne electromagnetic (AEM) and other methods of delineating paleochannels.

Paleochannels in the Namba Formation are less well defined than those in the Eyre Formation. At the Beverley deposit sinuous depressions in the top of the Beverley Clay are interpreted as parts of a paleochannel system (McConachy et al., 2006). Branching architecture suggests sediment transport from south to north, although current groundwater flow appears to be in the opposite direction (Fig. 5.1, Heathgate Resources, 1998). Chemical architecture studies to the east of Lake Frome also suggest north-south oriented channel-like features in the uppermost Namba Formation (Chapter 4). These interpreted orientations in the Eocene to Miocene contrast with the radial patterns of Pliocene-Pleistocene channels within the overlying Willawortina Formation, centred on the Mt Painter – Mt Babbage inliers (Fig. 4.11). Broadly north-south trending syn-Namba faults in the Beverley area (Poontana Fault) may have controlled the geometry of paleochannels within the Namba Formation, yet the similarity in low-energy Namba Formation lithologies on either side of the Poontana Fault suggest that relief was not great at this time.

The hypothesis of broadly north-south oriented paleochannels of both Eocene and Miocene ages in the Callabonna Sub-basin has significant implications for uranium mineral systems. The permeability architecture established during the Eocene and Miocene, along with the distribution of

potential reductants in the paleochannel sediments such as carbonaceous matter, is likely to be the primary control on the location of major uranium mineralisation. This permeability architecture is predicted to have controlled groundwater flow, even if the waters were sourced in upland areas lateral to the major paleochannel systems, such as the Mt Painter Inlier. Thus, for the Beverley deposit three alternative scenarios are: (a) sediment transport and groundwater carrying uranium flowing from south to north (even though current flow is north to south), (b) sediment transport from south to north; uraniferous groundwater sourced from west (Mt Painter Inlier), but diverted to south-north flow when encountering the paleochannel system, (c) sediment transport and uraniferous groundwaters both sourced from west, or northwest, and transported broadly eastwards or southeastwards. Scenarios (a) and (b) imply significant post-Namba reversal or rotation of dips. Scenario (c) is currently the most widely accepted model for the Beverley deposit.

Tests of these hypotheses are required, the simplest of which is to map zoning patterns of oxidised and reduced rocks around the Beverley deposit. However, if groundwater flow directions have reversed within the paleochannel system, as would be the case if scenarios (a) or (b) are correct, then redox zoning patterns will be complex due to overprinting. Indeed, these two scenarios predict that uranium mineralisation at Beverley may be in the process of being leached in the modern hydrological system, and mobilised in the opposite direction to that during ore formation.

A similar set of scenarios can be constructed for the Four Mile deposits. The implications of scenarios (a) and (b) are that major uranium systems developed with source regions for sediment, groundwaters and uranium to the south or south west of the Callabonna Sub-basin, for example in the Willyama Supergroup and Neoproterozoic sequences. These models of paleochannel architecture, whether in the Eyre Formation or Namba Formation, lead to the simple prediction that greater focussing of fluid flow would have occurred northwards as paleochannels merge. Fluid focussing may have been enhanced near syn-sedimentary faults. Fluid dispersal, on the other hand, would have occurred where paleochannels meet inland paleo-lake systems. Hence the identification of such sedimentalogical settings may mark the limits of large paleochannel-hosted uranium systems.

Numerical modelling of regional fluid flow in two dimensions (Chapter 7) confirms the critical role of permeability in controlling fluid flow and hence uranium mineralisation. In particular, the permeability evolution of faults in the Lake Frome region was probably a determinant on whether scenario (b) above could have occurred, that is, fluid flow eastwards from the Mt Painter Inlier across the Paralana and Poontana Faults and into the Beverley area. Active faulting would have allowed such passage, provided that permeable units of the Eyre and Namba Formations were hydrologically juxtaposed across the faults. Thus, it is predicted from the numerical modelling that uranium-bearing waters sourced from the Mt Painter Inlier could have flowed in the plane of the two dimensional modelling towards the Beverley area, although this would have been constrained to periods of active tectonism. At least two periods of uplift on the Paralana Fault have been inferred in the Cenozoic (Mitchell et al., 2002), and correspond to hypothetical mineral systems 2 and 3 outlined in the section above. Conversely, inactive faults may have acted as aquitards, confining fluid flow to domains between faults. Modelling of fluid flow in the third dimension is crucial in such geological scenarios, and hence in the current 2D study we have not evaluated the significance of flow along the strike of faults such as the Poontana Fault. Clearly this is critical if uranium mineralising fluids utilised paleochannel(s) controlled by north-south faults.

A key outcome of the numerical modelling is that the Four Mile and Beverley uranium deposits probably did not form upstream and downstream, respectively, along the same fluid path within the same hydrological system.

Provided that interconnected permeability existed across faults, the numerical modelling implies that the Eyre Formation not only in the vicinity of the Four Mile deposit but elsewhere in the Lake Frome region is prospective for uranium mineralisation. Thus, stacked orebodies in Eyre Formation and overlying Namba Formation are a possible scenario. The study of 3D chemical architecture indicates the potential for major north-south trending paleochannel systems of Paleogene age extending further northwards into the Frome Embayment and Callabonna Sub-basin than previously recognised.

8.1.4 Depositional gradients for uranium mineralisation

3D modelling of the chemical architecture has revealed important regional variations in the oxidation-reduction characteristics of Cenozoic units. Drill holes to the south of the Beverley deposit intersected sediments with overwhelmingly oxidised character even at deeper levels of >100m in the Namba and Eyre Formations (Fig. 4.4). Similar patterns are observed in drill holes clustered around the Namba Paleochannel. Other areas of drilling show greater variability from oxidised to reduced, with a general pattern of shallow oxidised and deeper reduced lithologies. The voxet model of the area of ELs 5 and 6 (Randell, 1973) east of Lake Frome shows a sinuous zone of reduced rocks near the top of the Namba Formation, trending roughly north-south in the eastern half of the EL5/6 area (Fig. 4.6). Union Corporation interpreted a north-south trending paleo-shoreline of a Cenozoic lake in this area, comprising a string of deltas. Alternatively the sinuous zone of reduced sediments may represent a paleochannel system within the Namba Formation. If so, this could represent a younger and northerly extension of the Yarramba Paleochannel system in the underlying Eyre Formation that hosts the Honeymoon and Oban uranium deposits (Fig. 4.11). Further work is in progress to test the paleochannel and shoreline hypotheses. In either case, the new 3D methodology developed in this study has demonstrated the presence of regional-scale redox interfaces within Cenozoic sediments. 3D mapping of redox interfaces is critical in targeting of uranium mineralisation in basins, and this method offers a cost-effective means of focussing exploration programs.

Public domain data indicate that Four Mile East is hosted by the Eyre Formation whereas Beverley is contained within the Namba Formation. New petrographic observations of the Four Mile East deposit reported in Chapter 5 have revealed significant differences with mineralisation at the Beverley deposit, despite their proximity. Although not yet comprehensive, the work at Four Mile East indicates that uraninite is the dominant ore mineral, in comparison with mainly coffinite at Beverley. This difference potentially is important from a metallurgical standpoint. Moreover, this and other mineralogical differences may indicate substantially different ore-forming chemical conditions that are not easily reconciled if both deposits formed along the same hydrological fluid flow paths. For example, at Four Mile there is textural evidence for quartz and kaolinite dissolution yet at Beverley the silica-bearing coffinite indicates saturation of ore fluids with respect to silica.

The presence of U-bearing and REE-rich phosphate minerals in uraninite-rich samples from Four Mile East is interpreted to indicate that the U-bearing ore fluids were mobilising the REE and phosphorous. Transport of some of the LREE and Eu is redox-sensitive and so the presence of REE phosphates directly associated with uranium mineralisation is an indication of the role of redox processes during alteration and uranium deposition. Possible reductants present in Eyre Formation sediments prior to mineralisation were carbonaceous matter, biogenic (framboidal) pyrite, and ilmenite. Moreover, the possible role of bacteria should not be disregarded, and indeed there are bacteria that thrive by reducing aqueous uranium U^{6+} to solid-phase U^{4+} in the presence of organic

nutrients (Loveley et al., 1991). Oxidation of ilmenite to rutile and anatase and incorporation of U in the Ti oxide alteration minerals (Fig. 5.1) suggests but does not prove that this oxidation accompanied uranium deposition. New pyrite growth with uraninite could be interpreted to indicate that conditions in the ore zone were not overwhelmingly oxidised and that the ore fluids contained significants amounts of sulfur (e.g., as SO_4^{2-}?). The presence of U- and REE-rich phosphate minerals is consistent with transport of uranium by aqueous PO_4^{2-} complexes, which are one of the most stable of uranium species at low temperature conditions over a wide range of pH (see Skirrow et al., 2009 and references therein). Other potential complexes include those of carbonate, oxy-hydroxide. Destablisation of uranium-phosphate complexes, and deposition of uranium, is possible via reduction, or a dramatic change in the activities of aqueous calcium and/or phosphate such as would occur if a phosphate-bearing fluid reacted with a Ca-bearing rock. The replacement of kaolinite along cleavages and apparent co-precipitation of phosphate minerals with uraninite (e.g., Figs. 6.9, 6.13) could indicate ore fluids out of equilibrium with kaolinite. However, changes in fluid pH (e.g., acidification) are not normally sufficient to cause uraninite deposition except at very low pH and high Cl^- or F^- and elevated temperature conditions (see Skirrow et al., 2009).

8.2 PALEOGEOGRAPHIC AND URANIUM MINERAL SYSTEM EVOLUTION

Figure 8.1 synthesises key results of this report as a time-series of schematic cross sections and paleogeographic interpretations of a broad region centred on the Lake Frome study area. The paleogeographic interpretations are redrawn from the Paleogeographic Atlas of Australia (Langford et al., 1995), and annotated with the schematic locations of potential uranium mineralisation. Our results largely support this earlier work, in particular the broadly south-to-north orientation of major paleochannel systems in the Lake Frome region during the Paleogene and Neogene. The cross sections (not to scale) represent a generic profile from a highland area of uranium-rich Proterozoic basement in the southwest or south (e.g., Curnamona Province or Mt Painter Inlier), to a basin setting in the north. The section follows the general trend of uranium transport and deposition in one part of three-dimensional uranium mineral systems. The reader may find Figure 3.1 useful in reading Figure 8.1. Note the predicted episodic evolution of uranium mineral systems, in three periods from the Late Cretaceous-Paleocene to the Pleistocene. During each episode there was a coincidence of mineral system components: driver of fluid flow (topographic uplift driven by far field tectonic processes), source of mobile uranium (e.g., weathered U-rich basement), source of oxidised fluids (meteoric waters), permeable fluid pathways (sandy sediment, faults), and depositional physico-chemical gradients (in-situ or mobile reductants). The intervening periods generally lacked one or more components.

It is emphasised that the three episodes of uranium mineral systems illustrated in Figure 8.1 are hypothetical. We are *predicting* that uranium mineralisation could have occurred within permeable units of the Eromanga Basin, Eyre Formation and Namba Formation during three periods in the Cenozoic. This ‘straw man’ model remains to be tested, for example by dating the uranium mineralising processes and by more detailed mapping of paleochannel systems and redox architecture of the basin sediments. Indeed, ongoing work by Geoscience Australia is currently being undertaken to this end.

Figure 8.1 (over): *Evolution of paleogeography and predicted uranium mineral systems during the Cenozoic, Lake Frome region. Paleogeographic interpretations (panels at left) are redrawn from Langford et al. (1995), and annotated with generalised locations of possible uranium mineralisation (U). The section line A-B corresponds to the cross sections to the right. Schematic cross sections are not to scale. The projected outline of the Cooper Basin is also shown.*

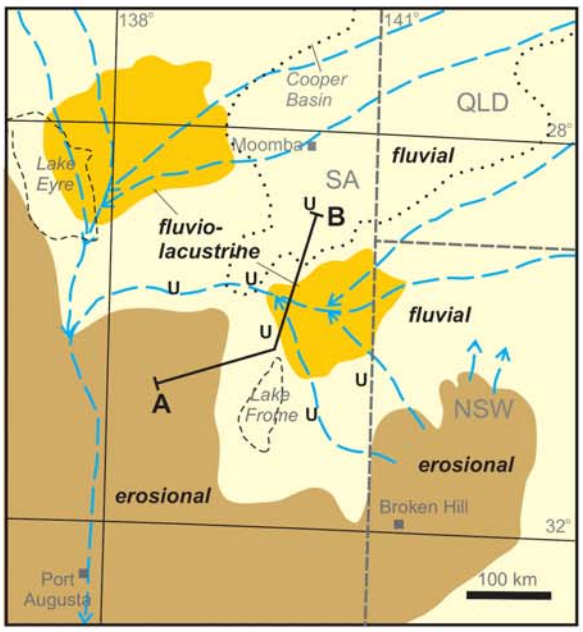

Late Cretaceous, Paleocene and early Eocene (~100 to ~52 Ma; episode 1 U system)

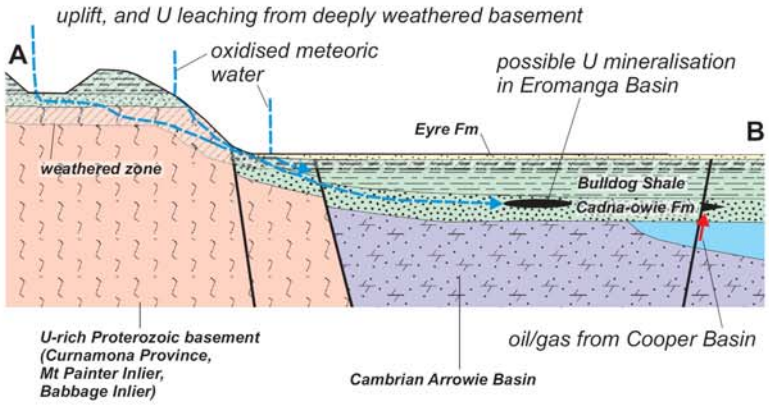

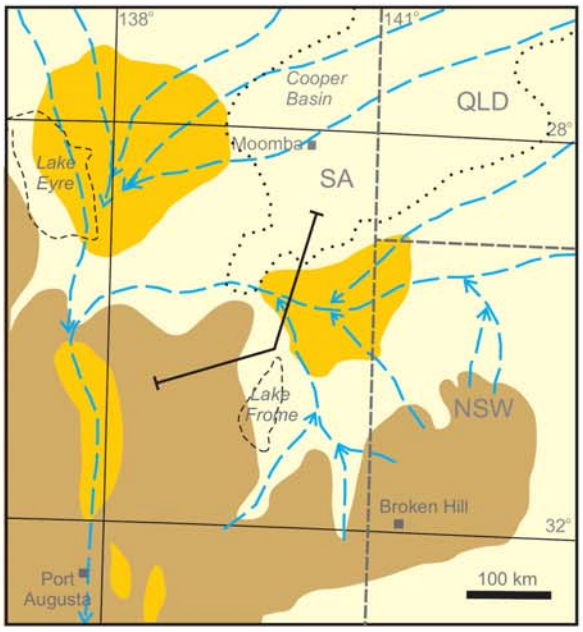

Middle and Late Eocene (~52 to ~37 Ma)

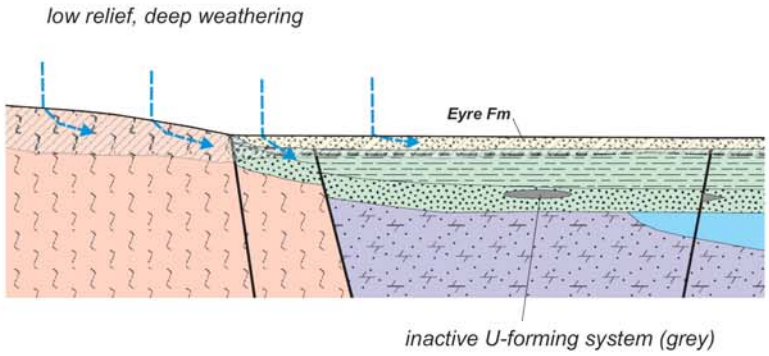

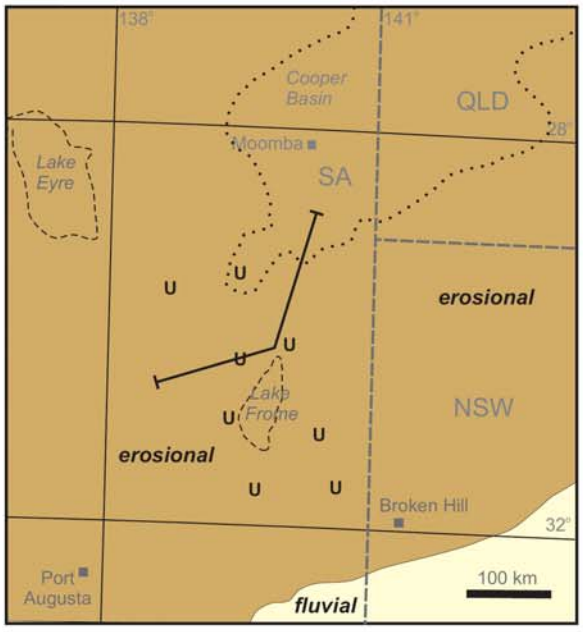

Late Eocene to Early Oligocene (~37 to ~28 Ma; episode 2 U system)

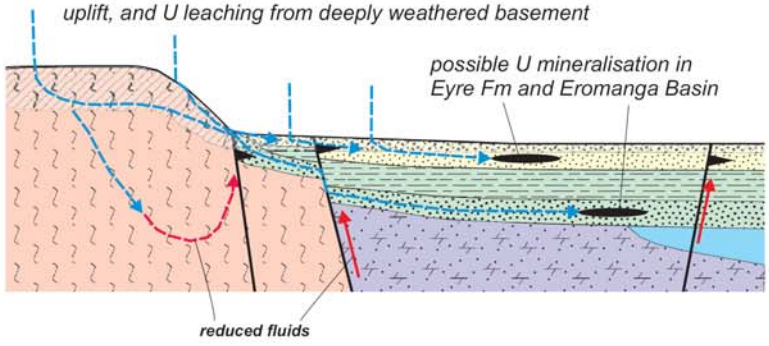

Figure 8.1

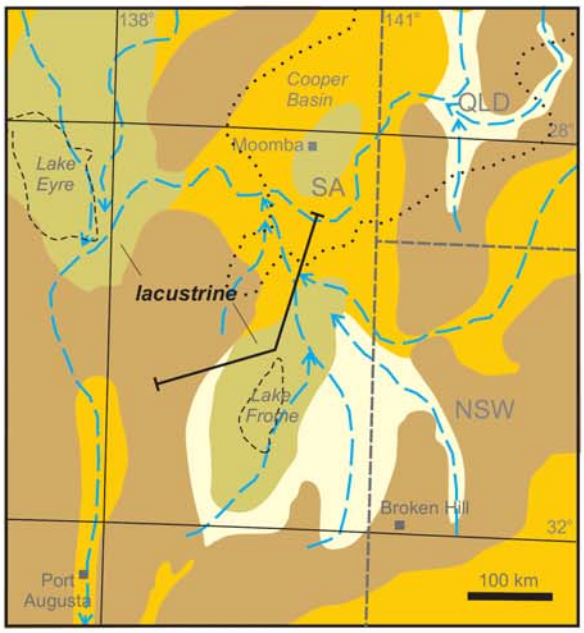

Late Oligocene to Middle Miocene (~28 to ~10 Ma)

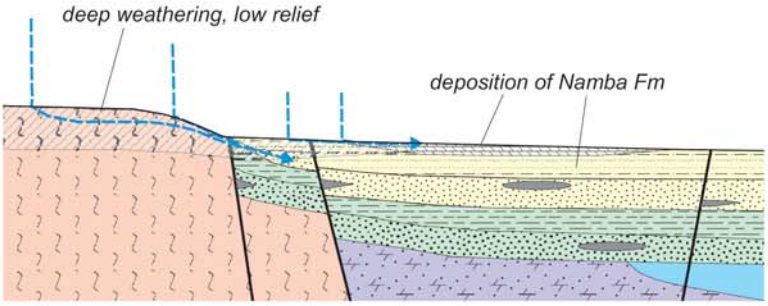

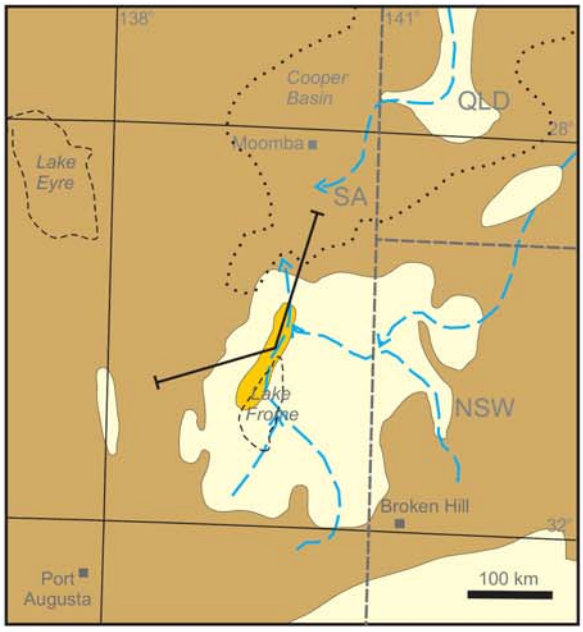

Middle to Late Miocene (~10 to ~5.3 Ma)

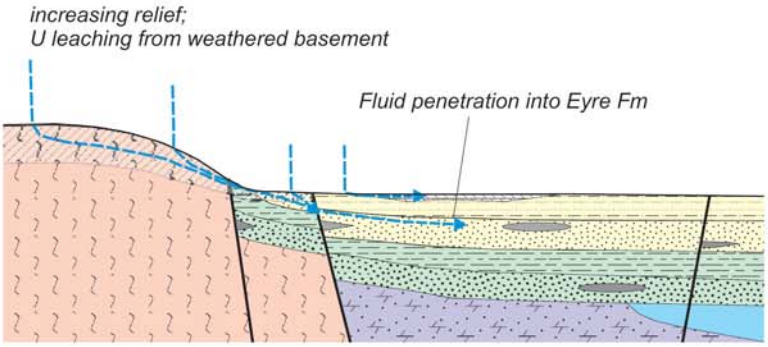

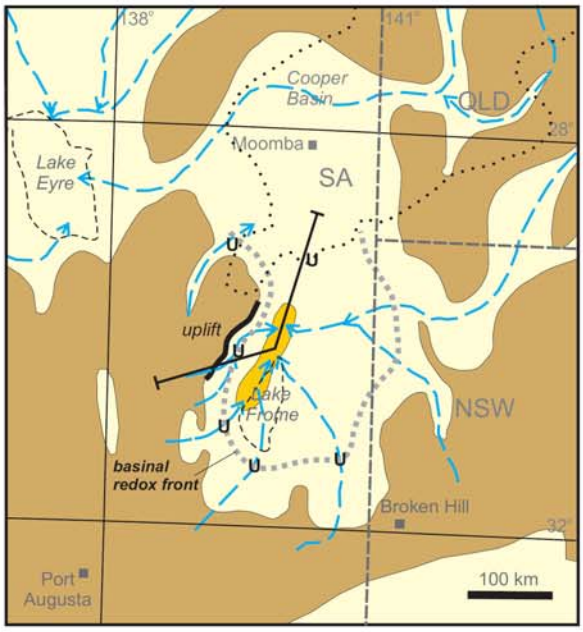

Pliocene and Pleistocene (~5.3 to ~0.01 Ma; episode 3 U system)

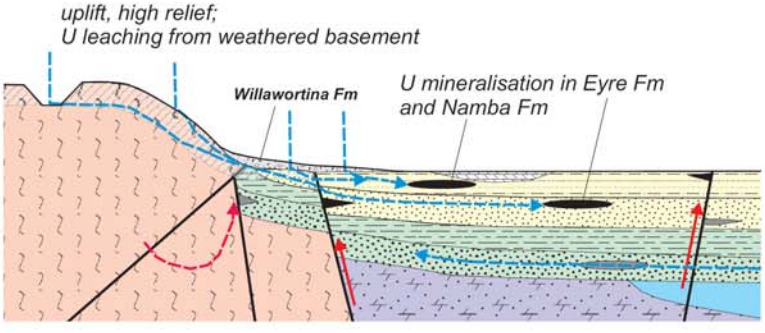

Figure 8.1

8.3 EXPLORATION CRITERIA

Exploration criteria for basin-hosted uranium mineral systems in the Lake Frome region are summarised in Table 8.1. In addition, the hypothesis of three basin-hosted uranium systems in the Lake Frome region (Fig. 8.1) leads to the following implications for exploration.

1. Late Cretaceous-Early Cenozoic uranium mineral system: Post-Eromanga Basin uplift of basement that was deeply weathered during the Mesozoic is predicted to have triggered gravitationally-driven flow of uranium-rich groundwaters into aquifers of the Eromanga Basin. Where suitable reductants were available, uranium mineralisation could have formed in the late Cretaceous or Paleocene. These systems potentially were large due to the effects of up to three episodes of oxidised fluid flow, although recently reversed fluid flow may have destroyed the early uranium mineralisation. Sub-basins isolated from present day groundwater flow in the Eromanga Basin may be most prospective for preserved mineralisation.
2. Late Eocene-Oligocene uranium mineral system: Post-Eyre Formation uplift and exhumation inferred in the Mt Painter Inlier may have triggered fluid flow from basement areas (deeply weathered at least twice) into the Eyre Formation, utilising broadly south-to-north oriented paleochannels. In this uranium mineral system, fluids would have been confined by aquitards and aquicludes within the Eyre Formation, with mineralisation in the late Eocene to early Oligocene (~37-28 Ma). Larger systems than in the Namba Formation are possible particularly to the north, due to the opportunity for the Eyre Formation to have experienced at least two episodes of oxidised fluid flow by this time.
3. Pliocene-Pleistocene uranium mineral system: Post-Namba Formation uplift and exhumation of basement rocks in the Lake Frome region occurred since ~5 Ma, producing most of the present day relief in the Northern Flinders Ranges and Mt Painter Inlier. Basement that was deeply weathered in the period ~10-20 Ma would now be available for leaching of uranium and transport into permeable units of the Namba Formation, Eyre Formation or Eromanga Basin. The larger systems may exist to the north, where paleochannels converged or met paleo-lake systems.

The Beverley deposit formed during the latest system (i.e., since ~5 Ma), whereas the Four Mile East deposit may have formed during either the second or third ore-forming episode (i.e., since ~35 Ma).

During each of these episodes of uranium mineralisation, multiple styles of uranium mineralisation were possible, including tabular styles controlled by sub-horizontal redox boundaries, ‘roll-front’ styles, and structurally controlled styles proximal to faults where mixing of oxidised and reduced fluids may have been important. These styles are illustrated schematically in Figure 8.1.

8.3 RECOMMENDATIONS FOR FURTHER WORK

The following further work is recommended to better constrain and test the hypotheses outlined in this study.

- Provenance studies of sedimentary sequences hosting mineralisation, to test and refine models of sediment transport and paleochannel development.
- Mapping redox interfaces within basin sediments to test whether mineralising fluids flowed from south (or southwest) to north (or northwest) in the Eyre and Namba Formations.

- Improved regional mapping of paleochannel systems, using airborne electromagnetic (AEM) methods, night-time thermal infrared satellite data, and/or other methods.
- Geochronology of uranium mineralising processes including dating of uranium-bearing ore minerals in the major deposits.
- Geochemical character and timing of deep weathering, including the mineralogical sites of uranium and its behaviour during weathering and fluid flow events.
- Further mapping and interpretation of fault architecture and its evolution, using 3D methods.

Table 8.1: Basin-hosted uranium mineral systems of the Lake Frome region: exploration criteria

Mineral sys component	Question[#]	Ingredients	Importance	Mappable/measurable features	Scale
Sources - metals	Q3	Leachable U-enriched source, including one or more of the following: • U-rich felsic rocks rimming and/or underlying the basin. • Lithic fragments of felsic rocks (including volcanic ash) in the sandstone aquifer. • Leachable detrital U-rich minerals (zircon, monazite, allanite, apatite etc) in sandstone • Felsic volcanics in and/or close proximity to the sandstone aquifer • Uranium mineralisation occurrences in hinterland • Deeply weathered U-rich source rocks	Leachable U: essential; U enrichment: highly desirable; deep weathering: highly desirable	U enrichment indicated by γ-ray spectrometric data, geochemical analyses of potential sources; U distribution in source minerals; history of deep weathering and its spatial distribution	Terrane (basin)
Sources - fluids	Q3	Large volumes of highly oxidised (initially air-saturated) fluids, e.g. meteoric water, lake water, requiring sub-aerial conditions and moist climate (at least seasonally)	Essential	Oxidised alteration/weathering/diagenetic assemblages in source areas and pathways; paleoclimate data; sub-aerial sediments	District (camp) and deposit
Sources - ligands		Phosphate, bicarbonate, F or Cl ions	Desirable	Phosphate-, carbonate-, F- or Cl-bearing minerals in source areas or pathways, altered/leached	
Sources – fluids, metals, ligands	Q3	Leached U sources (from fresh or weathered source rock areas), requiring fluids of appropriate composition	Desirable	U depletion zones as indicated by γ-ray spectrometric data, wire-line logs and geochemical analyses; U-leached paleoweathering profiles	District (camp) and terrane (basin)
Permeability and chemical architecture	Q3,Q4	Preservation of high redox state (and low pH?, high ligand activity, etc) of fluids along pathways, requiring subaerial setting of fluid recharge	Essential	Evidence of subaerial setting of fluid recharge; extensive oxidised alteration zones in reduced aquifers; low feldspar content (mature seds); low Ca content?	District (camp)
Permeability and chemical architecture	Q3,Q4	Preservation of low pH?, high ligand activity, etc of fluids along pathways	Essential	Low feldspar content (mature seds); low Ca content; high phosphate mineral content	District (camp)
Permeability and chemical architecture	Q1	Permeable clastic sediments / rocks interstratified with aquitards or aquicludes	Essential	Clastic sediments / rocks with high primary or secondary permeabilities, typically mature sands, silts, sandstones, siltstones in continental fluvial and/or mixed fluvial-shallow marine environments	Terrane (basin)
Permeability and chemical architecture	Q2,Q4	Fluid confinement and focussing geometries within basin	Desirable	Embayment geometry of basin at 10-100km scale; paleochannel systems; constrictions in channels; lateral facies variations in permeability; onlaps of aquifers on aquitards; some fault and fold geometries	District (camp)
Energy driver	Q4, Q1	Topography causing hydraulic head in pre-existing aquifers		Evidence for uplift and exhumation of basin margins or basement and history of events, e.g. v. coarse piedmont clastics, fission track dating, etc	
Energy, Permeability and chemical architecture	Q4, Q2	Gentle slope of aquifers away from basin margin at times of fluid flow, resulting from: • Primary depositional dip • Tilting of sequence due to reactivation of basin margin faults • Change in continental stress fields (e.g. compression or extension) • Basinal subsidence • Doming	Essential	Geometry of basin at times of fluid flow, as determined from field mapping, sedimentary facies, structural measurements, seismic, gravity, MT and AEM data; tectonic history	District (camp)
Depositional gradient	Q1-Q5	Evidence of uranium (and related) mineral system activity	Desirable	Distribution of mineral occurrences (U, Cu, V, Co, Pb-Zn, etc)	Continental to terrane (basin)
Depositional gradient	Q4,Q5	Regional gradation from oxidized (upstream) to reduced conditions (downstream) in aquifers	Essential	Regional-district-deposit scale mapping of redox variations and geochemistry in aquifers; mapping of hydrogeochemical gradients in groundwaters from regional aquifers; AEM may map reduced zones	Terrane (basin) to deposit
Depositional gradient	Q5	Presence of in-situ reductants in aquifers or aquitards, including: • Solid carbonaceous material (e.g. woody material, coal, humic/humate components • Locally derived reduced waters (e.g. with H_2S etc from bacterial activity) • Inorganic reductants (e.g., Fe^{2+}-rich rocks & minerals, sulfides (particularly pyrite) • Bacteria colonies capable of reducing U^{6+}	Essential	Bends in paleochannels may have concentrations of organic matter; some carbonaceous materials may be mappable using EM; drill hole logs from water and exploration drill holes; sedimentary facies analysis	District (camp)
Depositional gradient	Q5	Presence of mobile reductants in aquifers and along faults, including: • Gaseous or liquid hydrocarbons and/or H_2S that have migrated along faults or aquifers from underlying reservoirs or coal seams • Reduced groundwaters	Essential	Hydrocarbon shows in drilling and at surface; petroleum systems analysis of underlying basins; groundwater chemistry (e.g., low Eh)	District (camp)
Depositional gradient	Q5	U deposition and changes in fluid chemistry caused by gradients in: • Redox • pH • silica saturation • vanadium saturation	Essential	Alteration mineral zoning about ore as follows: oxidized (brown/red) sandstone with total oxidation of pre-existing sulfide minerals→ Se enrichment → U ores±silcrete → Mo and sulfide mineral enrichment/replacement of Fe-bearing silicates and silicates → reduced (green/gray) sandstone± silcrete. Groundwater zonation from upstream to downstream as follows: high (oxidized) Eh → ore → low (reduced) Eh. Redox and related reactions may also be reflected in δD, $\delta^{13}C$, $\delta^{18}O$, $\delta^{34}S$ and U-series disequilibria variations in rock and in groundwater.	District (camp) and deposit

[#]Five Questions (Walshe, et al., 2005; Barnicoat, 2007) are as follows:

Q1: What is the geodynamic and P-T-t history of the system?
Q2: What is the architecture of the system?
Q3: What are the characteristics and sources (reservoirs) of water, metals, lagands and sulfur?
Q4: What are the fluid flow drivers and pathways?
Q5: What are the transport and depositional processes for metals, ligands and sulfur?

REFERENCES

Alley, N. F. and Benbow, M. C., 1995. Interior non-marine basins. *The Geology of South Australia, The Phanerozoic*. J. F. Drexel and W. V. Preiss (eds). South Australia, Geological Survey. Bulletin 54, Volume 2, 187-200 pp.

Alliance Resources, 2009. Quarterly report for the period ended 30 June 2009. Melbourne, Alliance Resources Ltd.

Bampton, K. F., Haines, J. B. and Randell, M. H., 2001. Geology of the Honeymoon uranium project. *Proceedings of the Autralasian Institute of Mining and Metallurgy*, **306**, 1-11 pp.

Barnicoat, A. C., 2007. Mineral Systems and Exploration Science: Linking fundamental controls on ore deposition with the exploration process. *Digging Deeper: Proceedings of the Ninth Biennial SGA meeting*, Dublin, 1407-1411 pp.

Bethke, C. M. and Johnson, T. M., 2008. Groundwater Age and Groundwater Age Dating. *Annual Review of Earth and Planetary Sciences*, **36**, 121–52 pp.

Brugger, J., Long, N., McPhail, D. C. and Plimer, I., 2005. An active amagmatic hydrothermal system: The Paralana Hot Springs, Northern Flinders Ranges, South Australia. *Chemical Geology*, **222**, 35-64 pp.

Brunt, D., 2005. Update on Beverley area exploration. *St Barabara's Day SA Explorers Conference*, Adelaide.

Callen, R. A., 1990. Curnamona, South Australia. 1: 250,000 geological series. Explanatory notes. Sheet SH/54-14. Geological Survey of South Australia, 56.

Callen, R. A., Alley, D. R. and Greenwood, D. R., 1995. Lake Eyre Basin. *The Geology of South Australia, The Phanerozoic*. J. F. Drexel and W. V. Preiss (eds). South Australia, Geological Survey. Bulletin 54, Volume 2, 101-126 pp.

Callen, R. A. and Benbow, M. C., 1995. The Deserts – Playas, Dunefields and Watercourses. *The Geology of South Australia, The Phanerozoic*. J. F. Drexel and W. V. Preiss (eds). South Australia, Geological Survey. Bulletin 54, Volume 2, 244-251 pp.

Callen, R. A., Sheard, M. J., Benbow, M. C. and Belperio, A. P., 1995. Alluvial Fans and Piedmont Slope Deposits. *The Geology of South Australia, The Phanerozoic*. J. F. Drexel and W. V. Preiss (eds). South Australia, Geological Survey. Bulletin 54, Volume 2, 241-243 pp.

Célérier, J., 2002. Neotectonics and intraplate deformation in the Northern Flinders Ranges, South Australia. *Unpublished Honours Thesis, The University of Melbourne*.

Célérier, J., Sandiford, M., Hansen, D. L. and Quigley, M., 2005. Modes of active intraplate deformation, Flinders Ranges, Australia. *Tectonics*, **24**, pp.

Cleverley, J., 2008. Deposition: Reactive transport modelling. *New perspectives: the foundations and future of Australian exploration. Abstracts for the June 2008 pmd*CRC Conference. Geoscience Australia Record 2008/09*. R. J. Korsch and A. C. Barnicoat (eds). 29-37 pp.

Cleverley, J., Hornby, P. and Poulet, T., 2006. Pmd*RT: combined fluid, heat and chemical modelling and its application to Yilgarn geology. *Predictive Mineral Discovery CRC - Extended Abstracts. Geoscience Australia Record 2006/7*. A. C. Barnicoat and R. J. Korsch (eds). 23-28 pp.

Coats, R. P. and Blissett, A. H., 1971. Regional and economic geology of the Mount Painter Province. Adelaide, Department of Mines, Geological Survey of South Australia, 426 p.

Cuney, M. and Kyser, K., 2008. Recent and not-so-recent developments in uranium deposits and implications for exploration. *Mineralogical Association of Canada Shortcourse Series, Quebec City*, **39**, 258 pp.

Curtis, J. L., Brunt, D. A. and Binks, P. J., 1990. Tertiary palaeochannel uranium deposits of South Australia. *Geology of the Mineral Deposits of Australia and Papua New Guinea*. F. E. Hughes (ed). The Australasian Institute of Mining and Metallurgy. 2, 1631–1636 pp.

Dahlkamp, F. J., 1993. Uranium ore deposits. Heidelberg, Springer-Verlag, 460 p.

Daniels, M. D., 2006. Dsitribution and dynamics of large woody debries and organic matter in a low-energy meandering stream. *Geomorophology*, **77**, 286 - 298 pp.

Domenico, P. A. and Schwartz, F. W., 1998. Physical and Chemical Hydrogeology. John Wiley and Sons, Inc., New York.

Drexel, J. F. and Major, R. B., 1990. Mount Painter uranium–rare earth deposits. *Geology of the mineral deposits of Australia and Papua New Guinea*, 993–998pp.

Drexel, J. F., Preiss, W. V. and Parker, A. J., 1993. The geology of South Australia, The Precambrian. South Australia, Geological Survey.

Elburg, M. A., Bons, P. D., Foden, J. and Brugger, J., 2003. A newly defined late Ordovician magmatic-thermal event in the Mt Painter Province, northern flinders Ranges, South Australia. *Australian Journal of Earth Sciences*, **50**, (4), 611-631 pp.

Ellis, G. K., 1976. EL 217 Lake Namba, Evaluation of Previous Drilling and Resistivity Results. South Australian Department of Mines and Energy, 42 p.

Ewers, G. R., Evans, N., Hazell, M. and Kilgour, B., 2002. OZMIN Mineral Deposits Database. *Geoscience Australia*.

Fisher, L., Elmer, F., Cleverley, J., Schaubs, P. and Potma, W., 2008. Deposition: Modelling uranium deposition. *New perspectives: the foundations and future of Australian exploration. Abstracts for the June 2008 pmd*CRC Conference. Geoscience Australia Record 2008/09*. R. J. Korsch and A. C. Barnicoat (eds). 38-42 pp.

Foster, D. A., Murphy, J. M. and Gleadow, A. J. W., 1994. Middle Tertiary hydrothermal activity and uplift of the northern Flinders Ranges, South Australia: Insights from apatite fission-track thermochronology. *Australian Journal of Earth Sciences*, **41**, 11-17 pp.

Freeze, R. A. and Cherry, J., 1979. Groundwater. Prentice-Hall Inc, New Jersey.

FrOG Tech, 2005. OZ SEEBASE™ Phanerozoic Basin study, Public Domain Report to Shell Development Australia. FrOG Tech Propriety Limited.

FrOG Tech, 2006. OZ SEEBASE™ Proterozoic Basin study, Report to Geoscience Australia FrOG Tech Propriety Limited.

Fyodorov, G. V., 1999. Uranium deposits of the Inkai–Mynkuduk ore field, Kazakhstan. *Developments in Uranium Resources, Production, Demand and the Environment*, Vienna, International Atomic Energy Agency Technical Meeting, Vienna, June 1999, 95–112 pp.

Geoscience Australia, 2002. GEODATA 9 Second DEM and D8 Digital Elevation Model Version 3 and Flow Direction Grid. Geoscience Australia. 43 p.

Geoscience Australia, 2005. Gazetteer of Australia 2005 release. Canberra, Geoscience Australia.

Geoscience Australia, 2008. Australia's identified mineral resources 2008. Canberra, Geoscience Australia.

Geoscience Australia, 2009. OZMIN: Uranium resources extracted February 2009. Canberra, Geoscience Australia.

Geuzaine, C. and Remacle, J. F., 2009. Gmsh: a three-dimensional finite element mesh generator with built-in pre- and post-processing facilities. *International Journal for Numerical Methods in Engineering, Accepted for publication*.

Gravestock, D. I. and Cowley, W. M., 1995. Arrowie Basin. *The Geology of South Australia, The Phanerozoic*. J. F. Drexel and W. V. Preiss (eds). South Australia, Geological Survey. Bulletin 54, Volume 2, 20-31 pp.

Gravestock, D. I., Moore, P. S. and Pitt, M., 1986. Contributions to the geology and hydrocarbon potential of the Eromanga Basin. (eds). Geological Society of Australia. Special Publication 12, 384 pp.

Haynes, R. W., 1975. Beverley sedimentary Uranium orebody, Frome embayment, South Australia. *Economic Geology of Australia and Papua New Guinea*. C. L. Knight (ed). AusIMM. AusIMM Monograph 5, 808 - 813 pp.

Heathgate Resources, 1998. Beverley uranium mine: environmental impact statement. Heathgate Resources Pty Ltd.

Heathgate Resources, 2009. Beverley Four Mile project: public environment report and mining lease proposal. Adelaide, Heathgate Resources Pty Ltd.

Hou, B., Zang, W., Fabris, A., Keeling, J., Stoian, L. and Fairclough, M., 2007. Palaeodrainage and Tertiary coastal barriers of South Australia. *Digital geological map of South Australia. South Australia Department of Primary Industries and Resources, Adelaide*.

Idnurm, M. and Heinrich, C. A., 1993. A palaeomagnetic study of hydrothermal activity and uranium mineralization at Mt Painter, South Australia. *Australian Journal of Earth Sciences*, **40**, 87-101 pp.

Jaireth, S., Bastrakov, E. N. and Fisher, L., 2008a. Two types of sandstone uranium systems in the Frome Embayment? Preliminary results of fluid flow and chemical modelling. *AusIMM International Uranium Conference 2008*, Adelaide, 18-19 June 2008.

Jaireth, S., McKay, A. and Lambert, I., 2008b. Association of large sandstone uranium deposits with hydrocarbons. *AusGeo News*, **89**, 8-13 pp.

Janeczek, J. and Ewing, R. C., 1992. Structural formula of uraninite. *Journal of Nuclear Materials*, **190**, 128-132 pp.

Jeuken, B., 2008. Groundwater flow modelling of migration of mining fluids from the proposed Four Mile East mining zone. Final report. *Heathgate Beverley Mine report*.

Jones, A. P., Wall, F. and Williams, C. T., 1996. Rare earth minerals: chemistry, origin and ore deposits. Kluwer Academic Publishers.

Krieg, G. W., 1995. The Mesozoic. *The Geology of South Australia, The Phanerozoic*. J. F. Drexel and W. V. Preiss (eds). South Australia, Geological Survey. Bulletin 54, Volume 2, 92-149 pp.

Krieg, G. W., Alexander, E. M. and Rogers, P. A., 1995. Eromanga Basin. *The Geology of South Australia, The Phanerozoic*. J. F. Drexel and W. V. Preiss (eds). South Australia, Geological Survey. Bulletin 54, Volume 2, 101-126 pp.

Langford, R.P., Wilford, G.E., Truswell, E.M., and Isern, A.R., 1995. Palaeogeographic atlas of Australia. Volume 10 - Cainozoic. Australian Geological Survey Organisation, Canberra.

Lawford, G., Stanley, S. and Kilgour, B., 2007. Drainage network (national geoscience dataset). Canberra, Geoscience Australia.

LeBlanc, R. J., 1972. Geometry of sandstone reservoir bodies. *Underground waste management and environmental implications*. T. D. Cook (ed). Tulsa, The American Association of Petroleum Geologists. Memoir 18, 133 - 189 pp.

Loveley, D. R., Phillips, E. J. P., Gorby, Y. A. and Landa, E. R., 1991. Microbial reduction of uranium. *Nature*, **350**, 413-416 pp.

Ludwig, K. R. and Cooper, J. A., 1984. Geochronology of Precambrian granites and associated U-Ti-Th mineralization, northern Olary province, South Australia. *Contributions to Mineralogy and Petrology*, **86**, 298-308 pp.

Mallet, J. L., 1992. Discrete smooth interpolation in geometric modelling for fields like geology and biology where classical modelling cannot account for all heterogeneous data defining the complex surfaces. *Computer Aided Design*, **24**, 178-191 pp.

Marshall, M. J., 1979. Geochemical exploration studies in the Mount Painter Province. *PIRSA Open File Envelope 3536*.

Marsland-Smith, A., 2005. Geological setting and minerology of uranium mineralisation at the Beverley deposit, Frome Basin, SA. *4th Sprigg Symposium Uranium: exploration, deposits, mines, and minewaste disposal geology*, Adeaide, Geological Society of South Australia.

Martin, H. A., 1990. The palynology of the Namba formation in the Wooltana-1 bore, Callabonna basin (Lake Frome), South Australia and its relevance to Miocene grasslands in central Australia. *Alcheringa*, **14**, 247-255 pp.

McConachy, G., Mcinnes, D. and Paine, J., 2006. Airborne electromagnetic signature of the Beverley Uranium deposit, South Australia. *SEG/New Orleans 2006 Annual Meeting*, New Orleans, 790 - 794 pp.

McCuaig, T. C. and Beresford, S., 2009. Scale dependence of targeting criteria in light of recent advances in understanding mineral systems. *"Smart Science for Exploration and Mining" Proceedings of the Tenth Biennial SGA Meeting*, Townsville.

McKay, A., D and Miezitis, Y., 2001. Australia's uranium resoruces, geology and development of deposits. Canberra, AGSO - Geoscience Australia, 184 p.

McKelson, J., 2000. Geology of the Paralana Hot Spring Area, North Flinders Ranges, South Australia. *Unpublished Honours Thesis, The University of Melbourne*.

McLaren, S., Dunlap, W. J., Sandiford, M. and McDougall, I., 2002. Thermochronology of high heat-producing crust at Mount Painter, South Australia: Implications for tectonic reactivation of continental interiors. *Tectonics*, **21**, 1020 pp.

Miall, A. D., 1992. Alluvial deposits. *Facies models: response to sea level change*. R. G. Walker and N. P. James (ed). St Johns, Geological Association of Canada. 119 - 142 pp.

Mitchell, M. M., Kohn, B. P., O Sullivan, P. B., Hartley, M. J. and Foster, D. A., 2002. Low-temperature thermochronology of the Mt Painter Province, South Australia. *Australian Journal of Earth Sciences*, **49**, (3), 551-563 pp.

Neimanis, M. J. and Hill, S. M., 2006. Plant biogeochemical expression of uranium mineralisation in Australia: Research outline and preliminary results. *Regolith 2006: Consolidation and Dispersion of Ideas (2006: Hahndorf, South Australia)*.

Neumann, N., Sandiford, M. and Foden, J., 2000. Regional geochemistry and continental heat flow: implications for the origin of the South Australian heat flow anomaly. *Earth and Planetary Science Letters*, **183**, (1-2), 107-120 pp.

Payne, T. E. and Airey, P. L., 2006. Radionuclide migration at the Koongarra uranium deposit, northern Australia - lessons from the Alligator Rivers analogue project. *Physics and Earth Chemistry*, **31**, 572-586 pp.

Pillans, B., 2004. Geochronology of the Australian regolith. *Regolith Landscape Evolution Across Australia: A compilation of regolith-landscape case histories and landscape evolution models*, Perth, 41-52 pp.

Preiss, W. V., 1987. The Adelaide Geosyncline: Late Proterozoic stratigraphy, sedimentation, palaeontology and tectonics. *Geological Survey of South Australia Bulletin*, **53**, 438 pp.

Preiss, W. V., 1995. Delamerian Orogeny. *The geology of South Australia*. J. F. Drexel and W. V. Preiss (eds). Geological Survey of South Australia. Bulletin 54. Vol. 2, The Phanerozoic, 45-60 pp.

Quigley, M., Sandiford, M., Fifield, K. and Alimanovic, A., 2007. Bedrock erosion and relief production in the northern Flinders Ranges, Australia. *Earth Surface Processes and Landforms*, **32**, 929-944 pp.

Radke, B. M., Ferguson, J., Cresswell, R. G., Ransley, T. R. and Habermehl, M. A., 2000. Hydrochemistry and implied hydrodynamics of the Cadna-Owie-Hooray aquifer. 248p.

Randell, R. N., 1973. EL 5 and EL 6, Lake Pundalpa and Lake Amerarkoo Areas. Progress and Final Reports to Licence Explirely for the Period 7/9/72 to 6/12/73. Union Corp. (Australia) Pty Ltd., Primary Industries and Resources South Australia.

Raymond, O., 2009. Surface geology of Australia 1:1,000,000 scale [Digital Dataset] Geoscience Australia.

Rutherford, L., Burtt, A. C., Barovich, K. M., Hand, M. and Foden, J., 2007. Billeroo North alkaline magmatic complex: geology and economic significance. *MESA Journal*, **45**, 33-39 pp.

Sandiford, M., Coblentz, D. and Schellart, W. P., 2005. Evaluating slab-plate coupling in the Indo-Australian plate. *Geology*, **33**, 113-116 pp.

Schwab, R. G., Herold, H., Götz, C. and de Oliveira, N. P., 1990. Compounds of the crandallite type: synthesis and properties of pure rare earth element-phosphates. *Neues Jahrb. Mineral., Monatsh*, **6**, 241–254 pp.

Sherman, D. M., Peacock, C. L. and Hubbard, C. G., 2008. Surface complexation of U(VI) on goethite (α-FeOOH). *Geochimica et Cosmochimica Acta*, **72**, 298-310 pp.

Shvarov, Y. V. and Bastrakov, E. N., 1999. HCh: a software package for geochemical equilibrium modelling. User's Guide. Australian Geological Survey Organisation, Record 1999/25. 61 p.

Skidmore, C., 2005. Geology of the Honeymoon uranium deposit. *4th Sprigg Symposium Uranium: Exploration, Deposits, Mines and Minewast Disposal Geology*, Adelaide, Geological Society of South Australia.

Skirrow, R. G., Jaireth, S., Huston, D. L., Bastrakov, E. N., Schofield, A., van der Wielen, S. E. and Barnicoat, A. C., 2009. Uranium mineral systems: Processes, exploration criteria and a new deposit framework. Geoscience Australia Record 2009/20. 44 p.

SKM, 2008. Environmental studies for the Four Mile Project - Conceptual hydrogeological model of the Four Mile region. Sinclair Knight Merz. 44 p.

Smith, M. L., Pillans, B. J. and McQueen, K. G., 2009. Paleomagnetic evidence for periods of intense oxidative weathering, McKinnons mine, Cobar, New South Wales. *Australian Journal of Earth Sciences*, **56**, (2), 201-212 pp.

Southern Cross Resources, 2000. Honeymoon uranium project: environmental impact statement. Toowong.

Sprigg, R. C., 1984. Arkaroola - Mount Painter in the Northern Flinders Ranges, SA: The last billion years. Arkaroola Pty Ltd, Australia.

Sprigg, R. C., 1986. The Eromanga Basin in the search for commercial hydrocarbons. *Contributions to the geology and hydrocarbon potential of the Eromanga Basin*. D. I. Gravestock, P. S. Moore and M. Pitt (ed). Geological Society of Australia. Special Publication 12, 384pp.

Teale, G. S. and Fanning, C. M., 2000. The Portia-North Portia Cu-Au (-Mo) Prospect, South Australia. Timing of mineralisation, albitisation and origin of ore fluid. *Porter, TM (ed), Hydrothermal Iron Oxide Copper-Gold & Related Deposits: A Global Perspective, Australian Mineral Foundation, Adelaide*, 137-147 pp.

Teasdale, J., Pryer, L., Etheridge, M., Romine, K., Stuart-Smith, P., Cowan, J., Loutit, T., Vizy, J. and Henley, P., 2001. Eastern Arrowie Basin SEEBASE* project. *SRK Project PI12*. 36 p.

van der Wielen, S. E., Kirkby, A., Britt, A., Schofield, A., Skirrow, R. G., Bastrakov, E. N., Cross, A., Nicoll, M., Mernagh, T. P. and Barnicoat, A. C., 2009. Large-scale exploration targeting for uranium mineral systems within the Eromanga Basin. *"Smart Science for Exploration and Mining" Proceedings of the Tenth Biennial SGA Meeting*, Townsville, 607-609 pp.

Walshe, J. L., Cooke, D. R. and Neumayr, P., 2005. Five questions for fun and profit: A mineral systems perspective on metallogenic epochs, provinces and magmatic hydrothermal Cu and Au deposits. *Mineral Deposit Research: Meetng the Global Challenge*, 477-480 pp.

Weibel, R. and Friis, H., 2007. Alteration of opaque heavy minerals as a reflection of the geochemical conditions in depositional and diagenetic environments. *Developments in Sedimentology*, **58**, 277-303 pp.

Williams, P. J. and Skirrow, R. G., 2000. Overview of iron oxide-copper-gold deposits in the Curnamona Province and Cloncurry district (Eastern Mount Isa Block), Australia. *Hydrothermal Iron Oxide Copper–Gold and Related Deposits: a Global Perspective*, **1**, 105–122 pp.

Wülser, P.-A., 2009. Uranium metallogeny in the North Flinders Ranges region of South Australia. Adelaide University, unpublished Doctor of Philosophy thesis.

Wülser, P. A., Brugger, J. and Foden, J., 2005. U-Th-REE mobility in and around the Mt Painter & Mt Babbage Inliers, Northern Flinders Ranges (South Australia). *4th Sprigg Symposium-*

Uranium: exploration, deposits, mines and minewaste disposal geology, Adelaide: Geological Society of Australia.

Wyborn, L. A. I., Heinrich, C. A. and Jaques, A. L., 1994. Australian Proterozoic mineral systems: essential ingredients and mappable criteria. *AusIMM Publication Series 5/94*, 109-115 pp.

Appendix 1: Field guide to the Proterozoic Mt Painter Inlier and Mesozoic to Cenozoic basins of the Lake Frome region

Stephen J. Hore and Steven M. Hill

Introduction

The Mount Painter region, incorporating the northern Flinders Ranges and western Lake Frome Plains, is a world-class uranium province. The region hosts historical uranium workings in the Mt Painter - Mt Gee area; one of Australia's three uranium mines at Beverley; as well as the Four Mile Uranium prospect, which is planned to go into production in 2010. The highly prospective region hosts both "brownfields" and "greenfields" exploration opportunities.

The distribution of uranium in the region is a result of 1600 million years of geology including primary U-enrichment within early Mesoproterozoic basement granites and gneisses, uraniferous hematitic breccia systems and subsequent multiple periods of reworking and redistribution up to the present day. Sandstone-hosted uranium deposits within Cenozoic sediments of the Frome Embayment and Callabonna Sub-basin are active mineralising systems within an environment characterised by Neotectonic faulting, sedimentation and fluid flow.

The Mount Painter region is situated in the northeastern section of the Adelaide Geosyncline and forms the northwestern part of the Curnamona Province. The older metasediments and granites (the Mt. Painter and Babbage Inliers) have been assigned a Mesoproterozoic age and are intruded by younger, post-Delamerian granites. The inliers are unconformably flanked by Adelaidean metasediments to the west and south, and by Mesozoic and younger sediments to the east. Historically, the area has been of note more for the diversity of mineralisation (U, Cu, Pb, talc) than its quantity but in recent years there has been active mining of uranium.

Despite the Northern Flinders Ranges – Lake Frome Plains region being one of the state's most prospective areas for mineral exploration (particularly for uranium), there are still major parts of the geological framework that are unresolved including aspects relating to the basement and the surrounding sedimentary basins. Furthermore, the regolith geology and associated landscape history is poorly understood. This is surprising given the dramatic exposures of a wide range of regolith materials and landforms as well as the importance of this part of the geological history for the dispersion, expression and secondary reconcentration of uranium mineralisation. Recent collaborative research by PIRSA and the University of Adelaide, however, has made some major contributions to this geological framework, as well as using this as an important field education and training laboratory.

Uranium has recently increased in importance as an exploration target commodity in Australia. One of the main challenges for this exploration is the detection of buried uranium mineralisation. However, there are increasing environmental and cultural sensitivities related to mineral exploration in areas such as the Frome region, requiring an effective and efficient but also minimal impact approach. So in addition to geological mapping, sampling and interpretation, plant biogeochemistry provides a method for obtaining a surficial expression of buried uranium mineralisation. In general plant roots extend subsurface and chemically interact with sub-surface substrates. Trace elements may then translocate from the substrate through

plant roots and into subaerial plant organs. As a result, samples of subaerial organs have the potential to express the buried substrate. Examples of results from this analysis have been included at a few of the localities.

This excursion guide will introduce some example outcrops of the Mesoproterozoic basement (Locations 4, 5, 6, 8), Adelaidean sediments (Locations 1, 2, 3, 4, 11), uraniferous breccias (Locations 7, 9), neotectonics (Locations 11, 13, 14) and Cenozoic sediments (Locations 11, 13, 14) (Figure 1). It is by no means a comprehensive excursion guide but will serve as an introduction to an interesting area and world-class geological classroom.

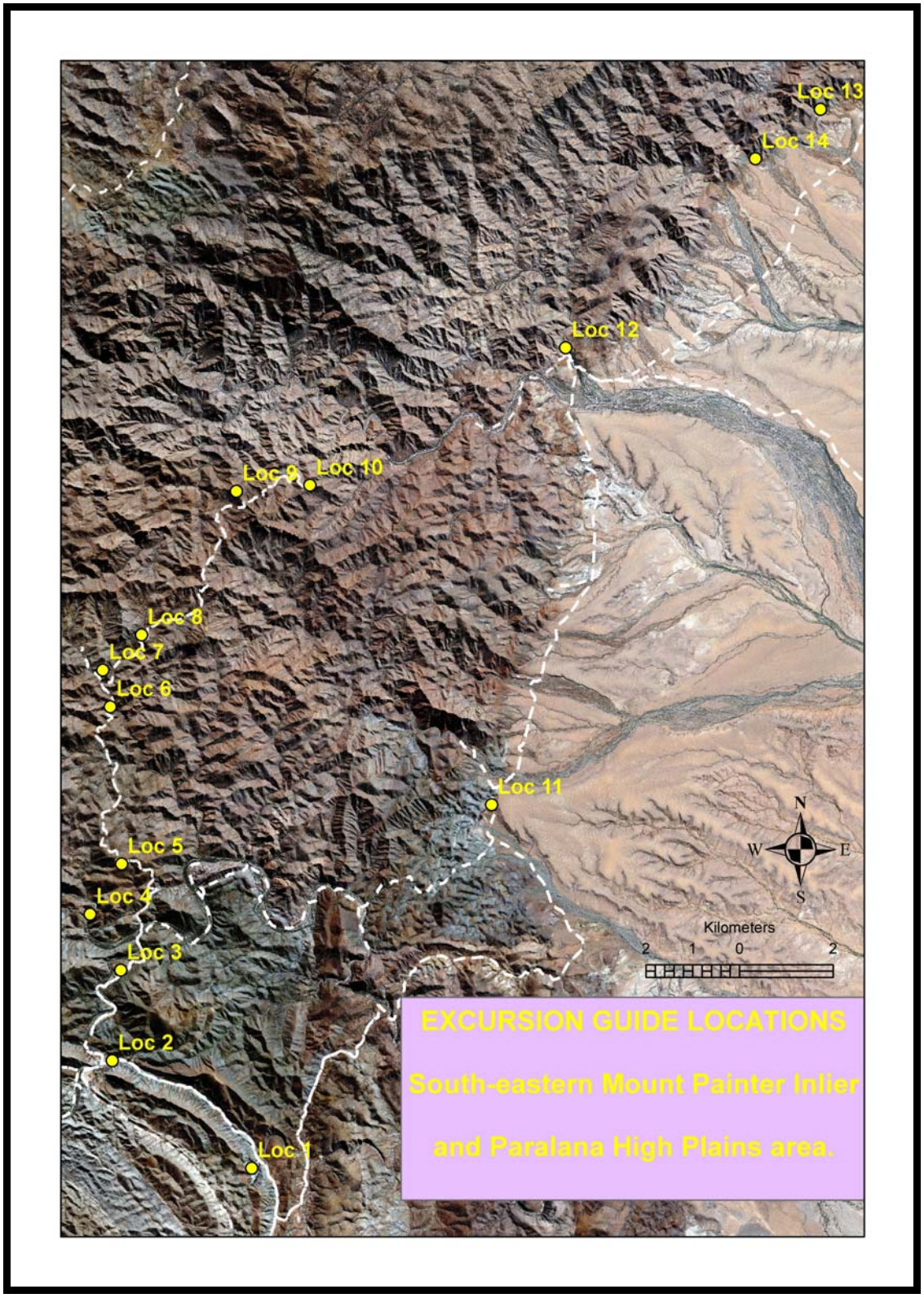

Figure 1: Excursion Guide locations

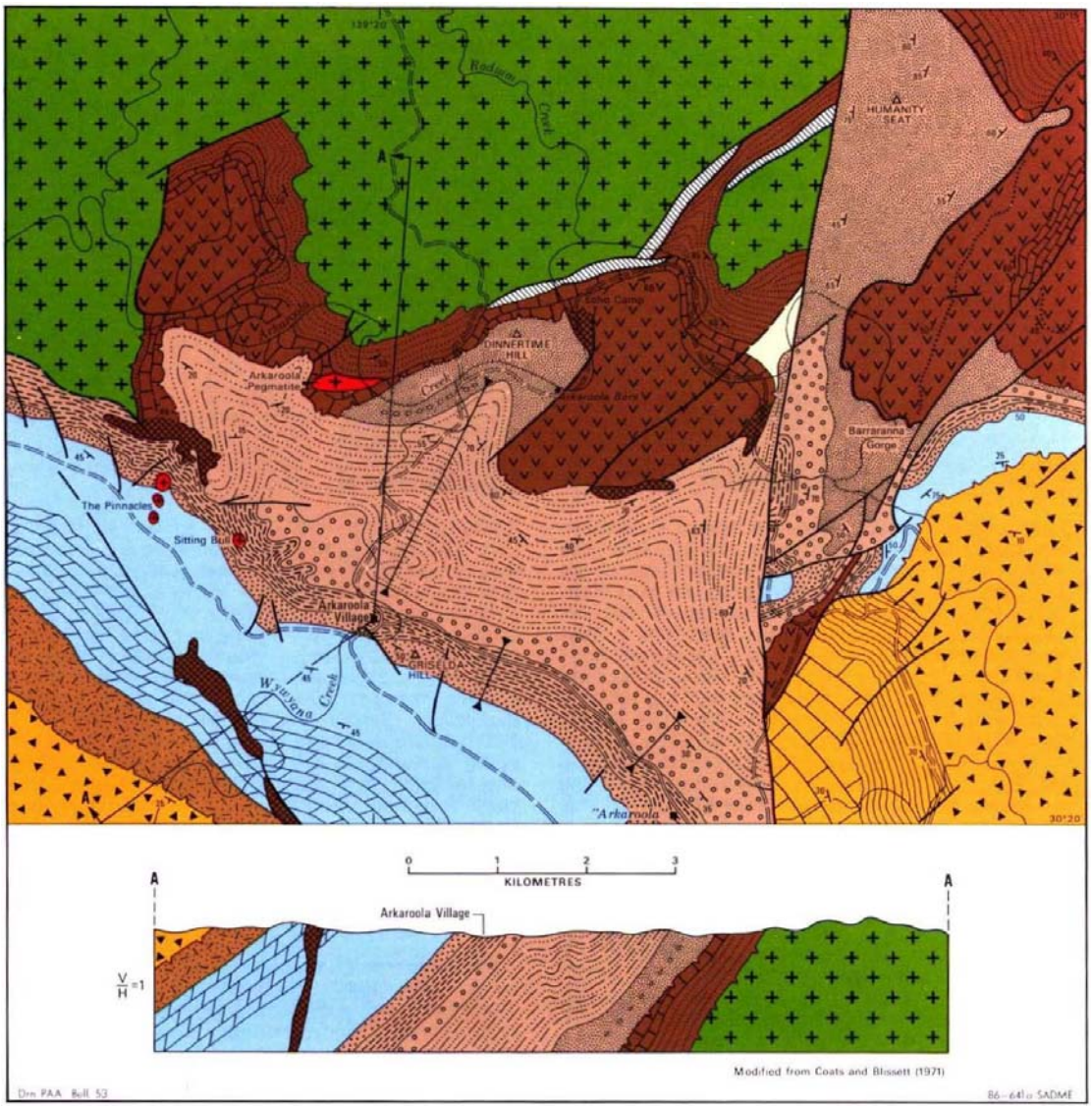

Figure 2: Geological map of the Burra Group in the Arkaroola area (Bulletin 53)

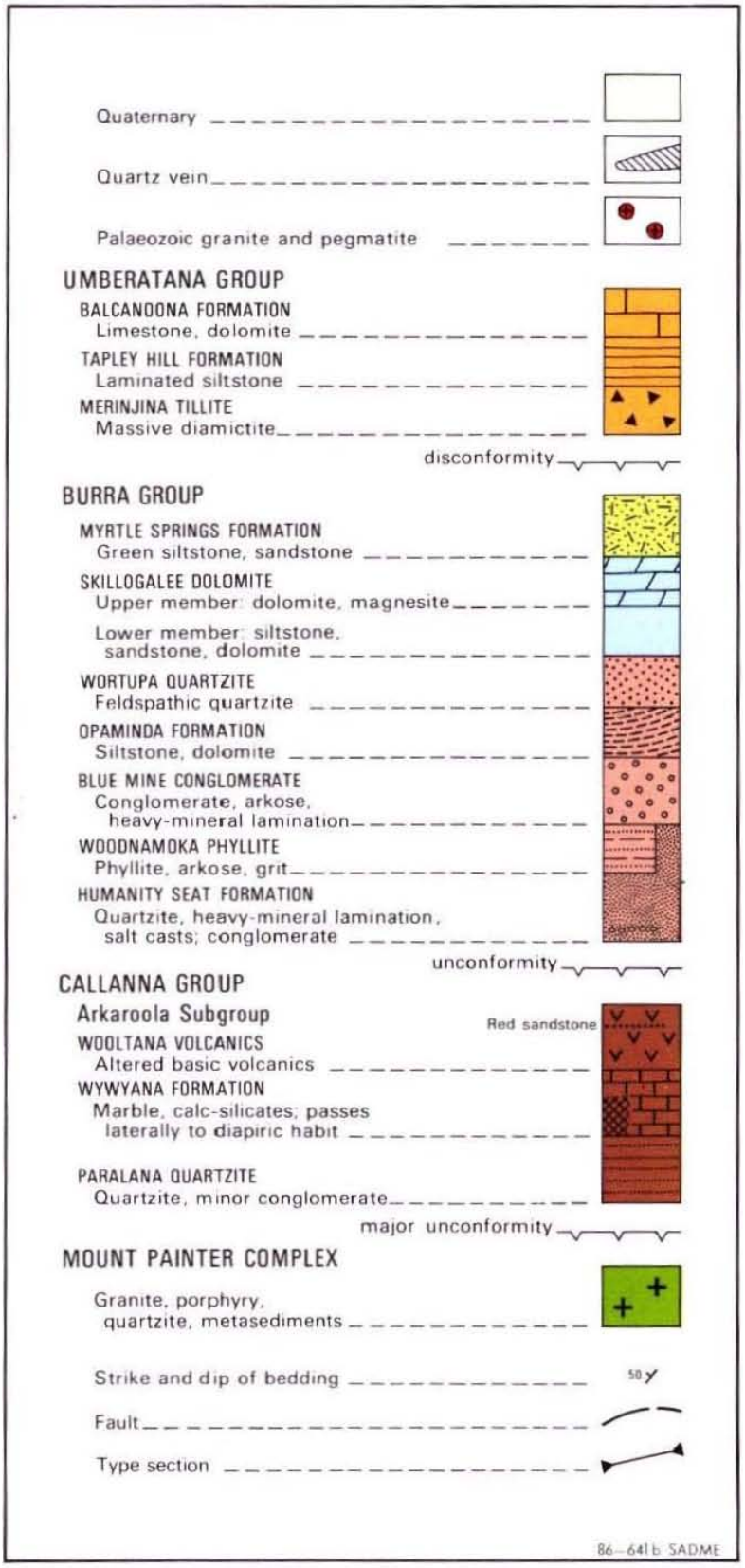

Figure 3 : Geological legend for map of the Burra Group in the Arkaroola area (figure 1)

Locality 1 (343230E ; 6643250N) - Arkaroola Homestead “Helicopter Pad” —

A boudinaged section of the Opaminda Formation (calcsilicate) can be seen in the wall of a cut pad approximately 100m south of the Arkaroola Homestead. The Adelaidean sequence here, and in most other parts of the Flinders Ranges, shows very little evidence of metamorphism associated with the Delamerian Orogeny (~490 Ma). The Opaminda Formation overlays the Blue Mine Conglomerate and is overlain by the Wortupa Quartzite which has a transitional and conformable contact.

The boudinaged section, with subsequent faulting, may be a result of the Delamerian Orogeny or due to subsequent movement of the nearby Paralana Fault. Metamorphic grade is upper greenshist facies.

Locality 2 (340250E ; 6645550N) - Wywyana Creek to the east of the village

Immediately east of Arkaroola Village (approx. 100m) where the main road crosses Wywyana Creek, is another exposure of the Opaminda Formation at the base of Griselda Hill (named after Griselda Sprigg, wife of Reg Sprigg, founder of the Arkaroola Tourist Resort).
Here again the low grade metamorphism (greenshist facies) of the Opaminda Formation is evident.

Locality 3 (340434E ; 6647484N) Mount Oliphant Plaque —

Taking the track from Arkaroola Tourist Resort a few kilometers to the north there is a plaque dedicated to Sir Mark Oliphant.

A walk 50m to the south from the plaque along the track a small cutting exposes a section of the Woodnamoka Phyllite showing retrogressed andalusite crystals, evident as quartz–muscovite aggregates. This indicates amphibolite-facies metamorphism in contrast to little evidence of metamorphism at Arkaroola. The degree of metamorphism has therefore increased markedly over the 3km northwards from Arkaroola, as the basement inlier is approached. Scapolite, tremolite and corderite isograds are essentially concordant with the unconformity.

The increased strain can be seen in the Woodnamoka Phyllite compared to the earlier unit investigated.

Locality 4 (339780E ; 6648681N) Arkaroola Waterhole Unconformity

Continuing along the track is a turn-off to the left to Arkaroola Waterhole. Immediately adjacent to the waterhole, ~50 m out of the creek and hidden in a small gully to the east, is the major unconformity between a probable metavolcanic basement unit (~1575Ma) of the Mt Painter Inlier and the basal Adelaidean Paralana Quartzite. The basement at the unconformity is predominantly a quartz–muscovite–feldspar unit with rounded blue quartz phenocrysts (Mt Neill Granite).

Leaving Arkaroola Waterhole travel back onto the track and take another left turn after 50m.

Drive to the boom gate of the entrance to the Ridgetop Track. Written permission must be obtained for entry from Arkaroola by way of a signed consent form which is given in limited circumstances. The road is blocked to vehicular traffic by a locked gate. A 4WD vehicle and competent driver are absolutely essential from this point on.

Locations 5 to 10 are along the Ridgetop Track which is operated by Arkaroola Tourist Resort who run two daily tours. As the track is single lane and has few turning places co-ordination with the tours is essential.

Locality 5 (340454E ; 6649755N) Coulthard's Lookout

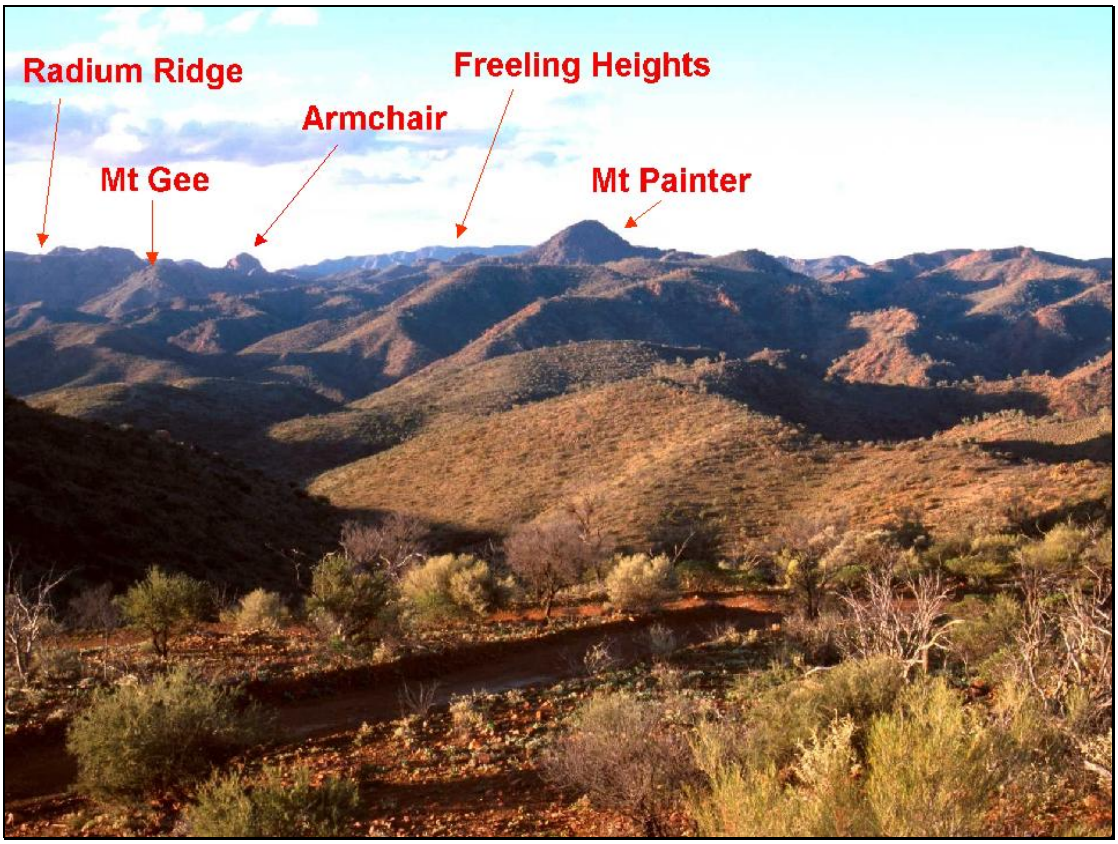

Locality 5 : northerly view from Coulthard's Lookout

The viewing platform built by Arkaroola is positioned on red-brown Mount Neill Granite Porphyry. To the distant south is Benbonyathae Hill, which is capped by Cambrian sediments.

The intervening country exposes the entire Adelaidean sequence of the northern Flinders Ranges. To the east is Lake Frome, and to the north are Mt Painter, Radium Ridge and Mt Gee.

Locality 6 (340210E ; 6653115N) Radium Creek Metamorphics

Situated in Radium Creek along side the track is a prominent outcrop of the pelitic facies of Radium Creek Metamorphics. Observed here is the main north-east trending fabric in this section of the Mount Painter Inlier (S_{main} = probably S_2) which is of pre-Delamerian origin.

Locality 7 (340050E ; 6653900N) No. 6 Mount Painter uranium workings

Access to the No. 6 Mount Painter uranium workings is several 100m north along the track towards the old Exoil Camp off the main Ridgetop Track. From here the historic workings, at the hilltop, can be accessed by hiking up a disused track. The workings are within hematitic breccia which is hosted within granitic breccia. Small amounts of vivid green torbernite coat the hematitic breccia. Biotite schist of the Radium Creek Metamorphics at this location contains occasional, small, bright blue corundum crystals. From top of the hill an overview of the basement, breccias and the sinter of Mt Gee is provided, including a large dyke-like body of siliceous hematitic breccia which crops out on the western side of Mount Gee.

The uranium mined in the original workings in circ 1910 was carried out on camel back for the production of radium. The hematitic breccias of the Mount Painter Inlier have fascinated geoscientists since the first major attempt to understand the geology during and immediately after World War II. At this time, the Australian and British Governments were actively exploring the province for uranium, and a major effort was made in the Mt Gee and East Painter regions. Mt Gee is a prominent hill with a silica rich capping situated amongst the breccias.

After the Governments ceased their operation in the area interest in the uranium waned until the Oilmin Group and Transoil NL carried out an extensive drilling program during 1968–71, and defined a resource (excluding East Painter) of 3.8 Mt at 0.1% U_3O_8 in hematitic and minor granitic breccia. The primary uranium mineral was determined as uraninite. It is these tracks forged into the hillside by this exploration program that we travel on to the following locations. Marathon Resources have undertaken further drilling programs in the area in recent years and in September 2008 Marathon Resources redefined the Mt Gee uranium resource upgrade to 31,400 tonnes of contained U_3O_8 in 51 million tonnes of mineralisation. At a cut-off of 300 ppm U_3O_8 the average grade was 615 ppm.

Locality 8 (340880E ; 6654650N) ‘Waterfall lookout’ — Radium Ridge Breccias

Less than 50 m down the disused portion of the Ridgetop Track, the gradational contact between basement schist–gneiss and granitic breccia is exposed. The valley in the foreground is underlain entirely by a minimum of 300m of granitic, chloritic and haematitic breccias (uraniferous). Radium Ridge, which rises ~200 m above the valley, is also composed entirely of these breccias. Mt Gee is immediate north and just beyond that is Radium Ridge, while Mt Painter is just to the east of this site.

Locality 9 (342900E ; 6657720N) Streitberg Prospect

View of the Armchair prospect, west from Streitberg Ridge

The Streitberg prospect on Streitberg Ridge was drilled by the Exoil consortium in ~1970. Drill chips at the surface include specular hematite and pyrite. Massive granitic breccia and also hematitic breccia crops out in the area. The Streitberg Prospect is on the ridge to the east of the

Armchair uranium prospect. As part of the ongoing plant biogeochemical studies at Adelaide University vegetation has been sampled at this location (table 1).

Hematitic breccia hand sample reported by Marshall (1979) gave a high U/Th ratio of ~6:1 (U = 400ppm, Th = 70ppm), and a high proportion of U (110 ppm) is extractable. Although similar to the Mt Gee deposits, this is a variant in that Ba is low (140ppm) and Pb high (190ppm), (also 420ppm Zn) probably reflecting parent rock composition. Cu is typically high (730ppm), with some Ag (2ppm) and Mo (25ppm).

Selected biogeochemical assays from Streitberg Ridge prospect, Northern Flinders Ranges, taken during April 2006.

Streitberg Ridge prospect	**U (ppm)**	**Cu (ppm)**	**Ag (ppb)**	**Th (ppm)**
Acacia sp.	0.03	4.77	7	0.05
Eremophila freelingii	0.36	19.44	41	0.09
Eucalyptus intertexta	0.81	6.24	5	0.02
Xanthorrhoea quadrangulata	0.02	1.49	<2	0.02

Table 1: Neimanis & Hill (2006).

Locality 10 (344470E ; 6657850N) Sillers Lookout

Spectacular views northeastwards towards (from left to right) Mawson Plateau, Paralana Hot Springs and Paralana Fault, and Beverley Uranium Mine. The lookout was named after Bill Siller (Exoil consortium chief), whose wife Beverley had the mine named after her.

Leaving the Ridge Top Track returning to Arkaroola Tourist Complex. Then follow the track along the Paralana Fault and then to the eastern plains.

Locality 11 (348350E ; 6651020N) Lady Buxton Fault

Immediately alongside the track to East Painter/Paralana Hot Springs and near the Lady Buxton Copper Mine is an exposure of field relationships demonstrating the neotectonic activity of the region. Here the Adelaidean Wywyana Formation has been thrust over Cenozoic sediments.

The footwall of this thrust is composed of partially consolidated ferruginous lithic gravels with sub-angular to sub-rounded pebbles up to 10 cm in diameter. Pebble lithologies include an assortment of Mesoproterozoic and Neoproterozoic rock types. The matrix of this sediment includes granules and coarse sand to silt dominated by quartz and maghemite and minor lithic fragments, with ferruginous and carbonate cement. The hangingwall consists of weathered Neoproterozoic marbles of the Wywyana Formation. The thrust is oriented 070^{o} and dips at 20^{o} toward the north-west. Linear grooves on the fault plane trend down dip, indicating most recently dominantly dip-slip movement. An estimate of displacement along the structure is problematic as the thickness of the footwall sequence is unknown. The age of the thrust is poorly constrained as the footwall lithology is unique within the field area.

The abundance of maghemite granules in the footwall sediment suggest a Neogene age, as maghemite becomes more prevalent in sediments in the region post-dating the Miocene. The moderate degree of consolidation and development of carbonate and ferruginous induration suggest a degree of antiquity but is not inconsistent with a Neogene age. The interpreted environment of deposition for these sediments is proximal colluvial-alluvial fans, which is similar to the local sediments deposited in the contemporary landscape. These sediments may represent a local lithological variation of the Willawortina Formation (Célérier, 2002).

Locality 12 (349930E ; 6660790N) Paralana Hot Springs

The Paralana Hot Springs is on the Paralana Fault near where Hot Springs Creek crosses the rangefront consisting of predominately Mesoproterozoic basement containing uraniferous granites and gneisses. The Paralana Hot Springs result from meteoric water circulating through hot rocks, and are the surface expression of a cyclic, low-temperature, non-volcanic hydrothermal system (Brugger et al., 2005).

The springs flow continuously from the fault zone forming two pools of water adjacent to brecciated and jasperized basement boulders. The temperature of the water is around 60ºC, flowing around 16,000 L/s, has a pH of 7-8, total dissolved salts of 1144 mg/L and contains ~0.07ppb U (Brugger et al., 2005).

This section of the creek is one of the most vegetated in the region, dominated by river red gums (*Eucalyptus camaldulensis*), inland teatrees *(Melaleuca* glomerata) and bulrush *(Typha domingensis*). Large algal blooms are within the hot spring pools and pools within the adjacent stream channel (McKelson, 2000).

Analysis by McKelson (2000) has shown that river gums contain ~1ppm U, the bulrushes ~1ppm U, the inland teatrees ~2-8 ppm U but interestingly the algal mat contains ~24ppm U. Results show that the levels of thorium and lead within the algae are also significantly higher than those of the spring water and the other plant species.

Locality 13 (355368E ; 6665889N) Four Mile Thrust

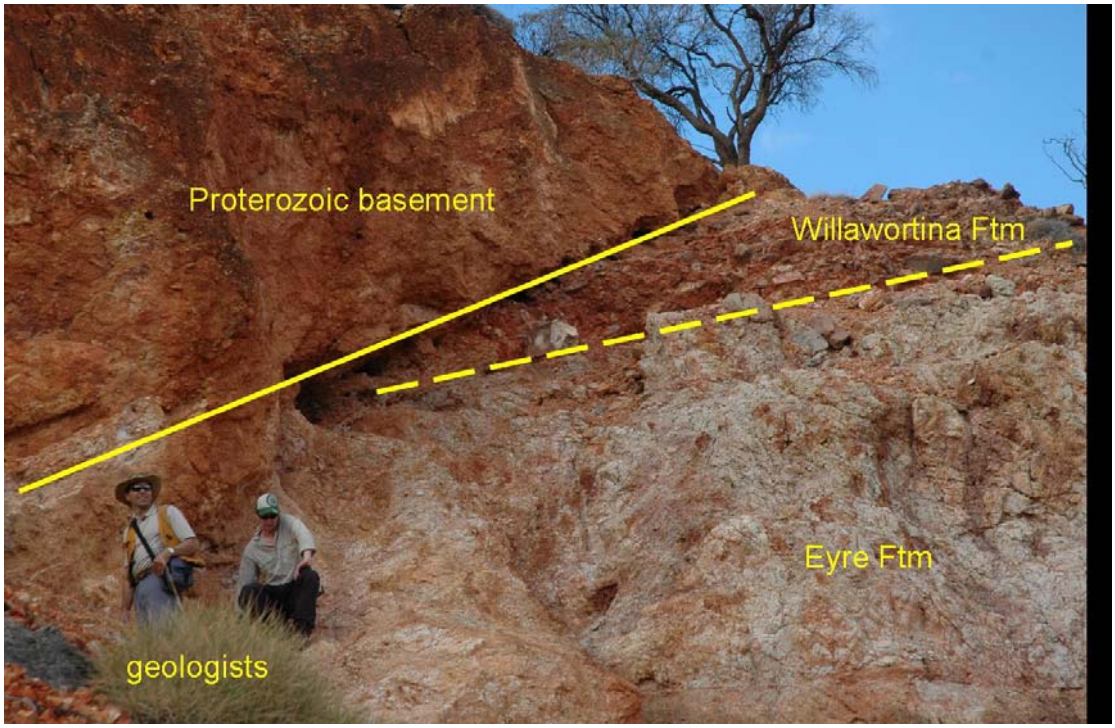

There is no track to this locality and a 30 minute hike is required from the Arkaroola-Wooltana boundary track a few kilometers north of Four Mile Creek.

This site features a dramatic example of young tectonic thrust faulting on the northern side of a small creek on the range front.

Further interpretation of this area is required as a recent re-examination suggests Proterozoic basement thrust over mottled Eyre Formation and poorly consolidated Willawortina Formation. Célérier (Célérier, 2002), however, interprets the footwall of the structure to be entirely Willawortina Formation with the matrix composed of kaolinite and quartz sand, and the mottles defined by variations in abundance of red-brown hematite. Overlying the Willawortina Formation sediments is a wedge of modern red hill scree covering parts of the outcrop. The hangingwall of the outcrop is a complex feature, within which there are several reverse faults with varying orientations consisting of Eyre Formation and Neoproterozoic Paralana Quartzite.

Locality 14 (353980E ; 6664830N) Four Mile Creek - Dead Tree Section

A key stratigraphic section adjacent to the Four Mile West uranium mineralisation has recently been recognised by University of Adelaide and PIRSA researchers within an ephemeral stream tributary of Four Mile Creek. This section includes:

- the basal Mesozoic lithic gravels (possibly equivalent to the Algebuckina Sandstone);
- a complete sequence of Eyre Formation sediments extending from the basal quartzose gravel, through sediments laterally equivalent to those that host the Four Mile mineralisation and the uppermost pedogenic silcrete (equivalent to the 'Cordillo Silcrete'); and,
- Lower energy proximal fluvial sands of the Namba Formation.

The sedimentary section extends for over 150 m and may contain evidence of cryptic signatures relating to fluid migration and residence associated with the Four Mile mineralisation. The exposed sediments are now oxidised and therefore any prospect of hosting significant uranium mineralisation is low. However because parts of this sequence are laterally equivalent to the adjacent Four Mile mineralisation they may have previously hosted mineralisation.

The compilation and description of this section is presently being finalised by Steve Hill (University of Adelaide) and Steve Hore (PIRSA) and is due for submission for publication in 2009.

APPENDIX 2: METADATA FOR 3D GEOLOGICAL MAPS, FIGURES 3.3-3.7.

Map Symbol	Stratigraphic Name	Stratigraphic Description
br	Unnamed GIS Unit - see description	Breccia, undifferentiated.
br3	Unnamed GIS Unit - see description	Diapiric breccia
Cgl	Merrimelia Formation	Conglomerate, polymict, framework supported, massive; fluvio-glacial conglomerate, diamictite and sandstone. Glacigene, deep-water lacustrine rhythmites, fluvio-glacial outwash, etc.
CP-g	Mount Gee Sinter	Quartz-haemetite, rhythmically layered, vuggy
CPgi	Tirrawarra Sandstone	Conglomerate; sandstone, medium to coarse-grained; mudstone.Fluvial, alluvial fans, distal proglacial outwash, backswamp, minor coal.
CP-r	Radium Ridge Breccias	Breccia, granitic, chloritic and haematitic. Included sediments and diamictite blocks.
dl	Unnamed GIS Unit - see description	Dolerite, undifferentiated.
dl1	Unnamed GIS Unit - see description	Dolerite in diapiric breccia. Based on green unit in Callanna Beds on ANDAMOOKA
dl2	Unnamed GIS Unit - see description	Dolerite, quartz porphyry, aplite. Based on "diorite" in Melrose Diapir on ORROROO.
dw	Unnamed GIS Unit - see description	Deep weathering, undifferentiated
E	Unnamed GIS Unit - see description	Undifferentiated Cambrian rocks
ED1	Unnamed GIS Unit - see description	Soda leucogranite, white, medium grained. Based on red unit on COPLEY
Ef	Lake Frome Group	Sandstone; siltstone; shale; limestone; conglomerate.
Efb	Balcoracana Formation	Siltstone, very micaceous; shale; carbonate; sandstone, arkosic, fine-grained and crossbedded. Trilobite tracks.
Efm	Moodlatana Formation	Siltstone, micaceous; shale; arkosic fine to medium-grained sandstone; minor carbonate
Efp	Pantapinna Sandstone	Sandstone, feldspathic, red, white, fine to medium-grained; minor micaceous siltstone and shale
Eh	Hawker Group	Limestone, siltstone, shale; lesser sandstone, greywacke, sandstone.
Ehd	Midwerta Shale	Shale, green-grey to black, argillaceous pyritic and manganiferous
Ehi	Wirrapowie Limestone	Limestone and calcareous siltstone, green and grey, stromatolitic, intraformational conglomerate; minor cross bedded ooid grainstone.
Ehj	Ajax Limestone	Limestone, reefs, flat-topped, keep-up. Lower thick-bedded and upper nodular limestone.
Ehm	Moorowie Formation	Shale; siltstone; shelf margin oolite; reef limestone;
Eho	Oraparinna Shale	Shale, calcareous.
Ehp	Parachilna Formation	Sandstone, upward-fining; with siltstone and minor carbonate interbeds. Trace fossils include Diplocraterion, and Bemella
Ehq	Woodendinna Dolomite	Dolomite; shale; conglomerate.

Map Symbol	Stratigraphic Name	Stratigraphic Description
Ehr	Mernmerna Formation	Limestone; bioherm complexes. Slope, platform bioherm complexes, distal slope environments; turbidites; nodular wackestone; black laminated lime mud.
Ehw	Wilkawillina Limestone	Archaeocyath-calcimicrobe limestone.
E-m	Mooracoochie Volcanics	Tuff; lapilli-tuff; trachyte; rhyolite and crystal tuff; conglomerate and agglomerate.
EO	Unnamed GIS Unit - see description	Undifferentiated Cambrian-Ordovician rocks
Eo	Moralana Supergroup	Sandstone, feldspathic, red, white, minor pyritic shale; siltstone; limestone, fossiliferous, oolitic, stromatolitic, with minor sandstone and siltstone
Eob	Billy Creek Formation	Siltstone, shale, dolomite, with tuff beds. Age 522.8+/-1.8Ma (U-Pb).
Eobc	Coads Hill Member	Sandstone, pale brown,fine to medium-grained; limestone, dark grey; shale, red and green; shaly siltstone. Conglomerate at the base. Some tuff beds.
Eobd	Edeowie Limestone Member	Mudstone, dolomitic, with planar to wavy lamination; limestone, peloidal, sandy, with tuff beds.
EO-k	Kalladeina Formation	Limestone: ooid-oncolite packstone, recrystallised, with silicified trilobites.
EO-k1	Unnamed GIS Unit - see description	Tuff, agglomerate, alkali within-plate basalt: STRZELECKI sheet
Eop	Parara Limestone	Limestone, algal and dolomitic, glauconitic sandstone interbeds.
EOu	Dullingari Group	Shale, black, pyritic; sandstone, grey, white; mudstone, grey, green.
Eow	Wirrealpa Limestone	Limestone, medium grey, micritic; basal dolomite.
fe	Unnamed GIS Unit - see description	Ironstone, ferruginisation, undifferentiated
gb	Unnamed GIS Unit - see description	Gabbro, undifferentiated.
hf	Unnamed GIS Unit - see description	Hornfels, undifferentiated.
J1	Unnamed GIS Unit - see description	Lamprophyric intrusives, including kimberlite.
J-b	Birkhead Formation	Siltstone, dark grey and brown; mudstone; sandstone, buff, fine to medium-grained; minor coal seams
J-h	Hutton Sandstone	Sandstone, white, fine to coarse-grained; with minor dark grey lenticular carbonaceous siltstone and shale interbeds
JK	Unnamed GIS Unit - see description	Undifferentiated Jurassic-Cretaceous rocks
JK-a	Algebuckina Sandstone	Sandstone, fine to coarse-grained, with granule and pebble layers,and shale intraclasts
JK-n	Namur Sandstone	Sandstone, white to pale grey,fine to coarse-grained, crossbedded and quartzose; minor siltstone and mudstone
J-p	Poolowanna Formation	Sandstone, white to pale grey, fine to medium-grained, crossbedded, ripple cross laminated; siltstone, dark grey; shale; coal seams and breccias
K	Unnamed GIS Unit - see description	Undifferentiated Cretaceous rocks
K-a	Allaru Mudstone	Mudstone

Map Symbol	Stratigraphic Name	Stratigraphic Description
Km	Marree Subgroup	Shale, dark grey, bioturbated, fossiliferous; sandstone, fine to very fine grained, calcareous, clayey.
Kmb	Bulldog Shale	Mudstone, grey, bioturbated, fossiliferous and shaly; minor silt to very fine-grained sandstone intervals.
Kmc	Coorikiana Sandstone	Sandstone, fine-grained, calcareous, clayey; sandy siltstone; minor siltstone
Kmo	Oodnadatta Formation	Claystone and siltstone,interbedded; with fine-grained sandstone, calcareous and ferruginous concretions; limestone with celestite and baryte veins.
Knc	Cadna-owie Formation	Sandstone, fine-grained, with coarse-grained sandstone beds, and pale grey siltstone, minor conglomerate.
Knm	Mackunda Formation	Sandstone, calcareous; siltstone; shale
Knr	Parabarana Sandstone	Sandstone, calcareous, with clasts of quartz, quartzite, and porphyry; sand, gravel and shale. U shaped burrows and other fossils
Knw	Winton Formation	Shale; siltstone; sandstone. Non-marine, minor coal horizons
KTa	Unnamed GIS Unit - see description	Undifferentiated Cretaceous-Paleocene rocks
Kta_dw	Unnamed GIS Unit - see description	Undifferentiated deep weathering
K-u	Murta Formation	Siltstone, dark grey, argillaceous and carbonaceous with interbedded fine to very fine-grained sandstone.
K-um	McKinlay Member	Sandstone, buff, very-fine to medium-grained interbedded with dark grey carbonaceous and micaceous siltstone.
L	Unnamed GIS Unit - see description	Undifferentiated Palaeoproterozoic rocks.
L2	Unnamed GIS Unit - see description	Feldspar-hornblende amphibolite. Based on Prot-beta3 on OLARY
LE	Unnamed GIS Unit - see description	Undifferentiated Palaeoproterozoic to Cambrian (Proterozoic to Cambrian) rocks.
LM	Unnamed GIS Unit - see description	Undifferentiated Palaeo-Mesoproterozoic rocks
LN	Unnamed GIS Unit - see description	Undifferentiated Palaeo-Neoproterozoic rocks (Proterozoic undifferentiated)
Lr	Radium Creek Metamorphics	Schist, psammitic to pelitic, garnet-sericite, quartz-feldspar-mica; gneiss, calc-silicate, quartz-feldspar-mica; amphibolite, calc-silicate, siliceous; marble, calc-silicate; quartzite, orthoquartzite, feldspathic; migmatite
Lr1	Unnamed GIS Unit - see description	Calcsilicate-marble. CALLABONNA: interim unit for compilation.
Lw	Willyama Supergroup	Composite gneiss suite; calc-silicate suite; amphibolite; quartzofeldspathic gneiss.
Lw1	Unnamed GIS Unit - see description	Undiff. schist,gneiss,quartzite,migmatite. Based on Prot-ws on CURNAMONA and OLARY
Lw18	Unnamed GIS Unit - see description	Siliceous metasiltstone. Based on unit Prot-wt on CURNAMONA

Map Symbol	Stratigraphic Name	Stratigraphic Description
Lw19	Unnamed GIS Unit - see description	Schist, aluminous/carbonaceous/chloritoid . Based on unit Prot-wk on CURNAMONA
Lw2	Unnamed GIS Unit - see description	Migmatite,gneiss,granitoids. Based on Prot-wm on CURNAMONA and OLARY
Lw9	Unnamed GIS Unit - see description	Quartz-magnetite+/-albite rock,sulfides,barite. Based on unit f on OLARY
Lwb	Broken Hill Group	Ironstone; sulfide rich; marble; plagioclase rich metasediment; calc-silicate; siliciclastic pelite; BIF; amphibolite, variably brecciated.
Lwbmb	Bimba Sulfide Member	Ironstone, sulfide-rich; banded iron silicate formation; thin units and lenses of calcsilicate; marble; calc-albitite; plagioclase-rich metasediment in graphitic psammitic-pelitic metasediment.
Lwt	Thackaringa Group	Gneiss, quartz-feldspar-biotite, foliated; calc-albitite and quartz-plagioclase rich metasediment; metavolcanics 1699+/-10 Ma; ironstone; calc-silicate; minor Pb-Zn-Ag-Cu mineralisation; minor amphibolite.
M	Unnamed GIS Unit - see description	Undifferentiated Mesoproterozoic rocks.
M1	Unnamed GIS Unit - see description	Syn- to late tectonic granite to adamellite; pegmatoids. Based on Prot-gamma on OLARY and CURNAMONA
M4	Unnamed GIS Unit - see description	Undifferentiated amphibolite. Based on Prot-beta1 on OLARY
M5	Unnamed GIS Unit - see description	Metabasalt with pillow structures. Based on Prot-v2 on CURNAMONA
M6	Unnamed GIS Unit - see description	Trachyte metavolcanics, often porphyritic. Based on Prot-v1 on CURNAMONA
M7	Unnamed GIS Unit - see description	Metasiltstone, shale, greywacke. Based on Prot-m on CURNAMONA
M-fc	Corundum Creek Schist Member	Schist, sandy; quartzite; muscovite-biotite and corundum-spinel schists.
Mm	Moolawatana Suite	Felsic intrusive rocks.
mm	Unnamed GIS Unit - see description	Man-made materials: for example fill, dumps, concrete.
Mmb	Box Bore Granite	Granite, coarse-grained, alkaline, potassic and foliated. With fluorite and allanite accessory minerals.
Mmt	Terrapinna Granite	Granite, grey, ovoid K feldspar megacrysts.
M-n	Mount Neill Granite	Granite, red-weathering, K feldspars.
N	Unnamed GIS Unit - see description	Undifferentiated Neoproterozoic rocks.
Nal	Wooltana Volcanics	Metasediments; marble; trachyte;sandstone; schist; phyllite;bsasl conglomerate.
Nau	Cutana beds	Quartzite; schist; siltstone
Naw	Wywyana Formation	Calcsilicate; marble; actinolite amphibolite.
Nb	Burra Group	Siltstone, laminated; shale; sandstone, heavy mineral lamination, quartzose to feldspathic, cross bedding; dolomite, blue-grey to pale pink, lenticular.

Map Symbol	Stratigraphic Name	Stratigraphic Description
Nc	Callanna Group	Siltstone, locally carbonaceous; sandstone, locally stromatolitic, ripple marks, halite casts, heavy mineral lamination; carbonates; evaporites; basalt, minor acid and intermediate volcanics
nd	Unnamed GIS Unit - see description	No description or log available (sample may or may not have been recovered)
Nds	Saddleworth Formation	Mudstone; siltstone; shale, partly carbonaceous.
NE	Unnamed GIS Unit - see description	Undifferentiated Proterozoic and/or Cambrian rocks
Nee	Elatina Formation	Sandstone, arkosic, medium grained, red-brown, slumped, ripple cross laminated; siltstone, sandy, red, dropstones and minor beds of diamictite with cobble to boulder size clasts of dolomite, basalt, dolerite, tuff.
Nia	Angepena Formation	Siltstone, reddish, thin bedded; interbeds of dolomite and minor grey-green shale; pisolitic and algal limestone.
Nib	Amberoona Formation	Shales, green, finely laminated, silty; with purple and grey silty shale.
Nie	Enorama Shale	Shale, grey-green and minor red, laminated; silty shale, rare fine grained sandstone.
Nir	Tarcowie Siltstone	Siltstone, sandy, flaser bedded.
Nirc	Cox Sandstone Member	Sandstone, coarse-grained; sandstone medium to fine-grained, with siltstone.
Niru	Uroonda Siltstone Member	Siltstone, grey-green, coarse; bands of coarse quartzitic siltstone.
Nit	Etina Formation	Limestone, sandy, grey, oolitic, stromatolitic, trough cross bedding; interbedded with siltstone, grey-green. Local diapir derived conglomerate.
Niy	Yankaninna Formation	Siltstone, grey-green, thinly bedded, calcareous, with lenses of dolomite.
Niz	Trezona Formation	Limestone, intraclastic and stromatolitic; with interbeds of calcareous siltstone.
Nk1	Unnamed GIS Unit - see description	Siltstone rafts in diapirs. Based on red-dashed white unit on COPLEY
Nk3	Unnamed GIS Unit - see description	Shale rafts in diapirs. Based on blue-dashed white unit on COPLEY
Nk4	Unnamed GIS Unit - see description	Quartzite/sandstone rafts in diapirs. Based on blue-dotted white unit on COPLEY
Nkn	Niggly Gap beds	Siltstone, micaceous; sandstone; dolomite.
Nl	Belair Subgroup	Siltstone, dark grey, laminated with minor sandstone, dolomite interbeds; quartzite, fine to coarse, feldspathic, cross bedded, minor siltstone interbeds; slate
Nms	Skillogalee Dolomite	Dolomite; marble, with magnesite mud-pellet conglomerates.
Nnb	Balcanoona Formation	Dolomite, pale grey; limestone, dark grey, algal, oolitic.

Map Symbol	Stratigraphic Name	Stratigraphic Description
Nnt	Tapley Hill Formation	Siltstone, grey to black, dolomitic and pyritic grading upwards to calcareous, thinly laminated, locally cross-bedded; dolomite, grey, flaggy to massive; limestone conglomerate, intraformational; greywacke.
Nntc	Mount Caernarvon Greywacke Member	Greywacke, with lenticular diamictite.
Nntt	Tindelpina Shale Member	Shale, pyritic, carbonaceous; thinly laminated grey dolomite beds and lenses.
Noc	Copley Quartzite	Quartzite; siltstone.
Noo	Wortupa Quartzite	Sandstone, grey-green, well bedded; quartzite, pale grey; minor dark grey siltstone; arkosic grit; conglomerate.
Nop	Opaminda Formation	Siltstone, dark grey well bedded; pale green talcose shale; amphibolite; marble.
Nou	Blue Mine Conglomerate	Conglomerate, pink, heavy-mineral laminated, arkosic; minorsandstone; dark grey laminated siltstone.
Nov	River Wakefield Formation	Dolomite; sandstone; siltstone; quartzite.
Np	Pound Subgroup	Sandstone; quartzite; siltstone.
Npb	Bonney Sandstone	Sandstone, fine to medium grained, occasionally coarse, flaggy to medium bedded, silty and feldspathic, cross bedded, ripple marks, small scale slumps, mudcracks, intraclasts; siltstone; quartzite
Npbp	Patsy Hill Member	Limestone, algal-laminated, grey, also wavy/swaley cross-stratified limestone, grading up to thick-bedded calcarenite then to micaceous sandstone. Generally two limestone-sandstone parasequences.
Npr	Rawnsley Quartzite	Quartzite and sandstone, white or light grey, locally flaggy and fossiliferous.
Ns	Sandison Subgroup	Sandstone; mudstone. Marine shelf and slope deposits, some shore face.
ns	Unnamed GIS Unit - see description	No sample: lost in drilling, cavity; sea if offshore.
Nsb	Brachina Formation	Siltstone, shale, red-brown and olive green, laminated, flaggy to medium bedded; alternating with sandstone, fine grained, occasionally coarse grained. All lithologies calcitic in part.
Nsn	Nuccaleena Formation	Dolomite, thin, laminated, micritic, with interbedded shale near the top.
Nu	Umberatana Group	Tillite; sandstone; siltstone; arkose; dolomite; quartzite; conglomerate; shale; greywacke.
Nu1	Unnamed GIS Unit - see description	Undifferentiated Nepouie and Upalinna Subgroups; includes the superseded Farina Subgroup
Nu2	Unnamed GIS Unit - see description	Undifferentiated Upalinna and Yerelina Subgroups; includes the superseded Willochra Subgroup
Nw	Wilpena Group	Quartzite; siltstone; shale; calcareous in part.

Map Symbol	Stratigraphic Name	Stratigraphic Description
Nwb	Bunyeroo Formation	Siltstone, shale, grey-red to grey-green, partly calcitic, minor fine grained sandstone; dolomite, grey; limestone, grey, lenses, thin beds
Nww	Wonoka Formation	Shale, grey, calcareous; flaggy dolomite, limestone and silt.
Ny	Yudnamutana Subgroup	Diamictite; siltstone; pebbly dolomite; orthoquartzite.Glaciomarine.
Ny2	Unnamed GIS Unit - see description	Undifferentiated Sturtian glacial sediments. Based on unit Prot-s on BILLA KALINA
Nya	Appila Tillite	Tillite; quartzite; siltstone. Massive, grey.
Nyf	Fitton Formation	Conglomerate; arkose, pebbly; quartzite, white, massive, interbedded with silty shale.
Nyh	Holowilena Ironstone	Hematitic siltstone, purplish red, thinly bedded; red shale; grey siltstone, minor dolomite, medium, grained quartzite, ironstone lenses.
Nyp	Pualco Tillite	Siltstone, dark grey, calcareous, with scattered quartz grains; quartzite, tillite and minor siltstone; green-grey tillite.
Nyw	Wilyerpa Formation	Siltstone, green. Lower third is fine grained, includes glacial dropstones; middle unit is medium to coarse sandstone; upper unit is siltstone with minor sandstone. Minor diamictite, sandy and pebbly dolomite.
Nyww	Warcowie Dolomite Member	Conglomerate, massive, well rounded pebble and boulder clasts, silty and sandy matrix; dolomite, massive to well bedded, grey and brown; breccia, dolomitic matrix.
O-p	Pando Formation	Sandstone, pale green-grey, laminated, bioturbated, silty. With glauconite.
or	Unnamed GIS Unit - see description	Orebody or ore zone, undifferentiated
pg	Unnamed GIS Unit - see description	Pegmatite, undifferentiated.
Pgd	Daralingie Formation	Sandstone, siltstone and coal. Fluvio-deltaic.
Pge	Epsilon Formation	Shale, siltstone, sandstone and coal.Fluvio-deltaic, lacustrine, with transgressive and regressive successions.
Pgm	Murteree Shale	Siltstone, grey-green, shaly, with thin lenses of fine-grained sandstone. Lacustrine.
Pgp	Patchawarra Formation	Siltstone, coal-swamp; sandstone; minor coal. Fluvio-lacustrine floodplain, minor deltaic environments.
Pgr	Roseneath Shale	Siltstone, shaly, with minor sandstone lenses. Lacustrine, diachronous
Pgt	Toolachee Formation	Sandstone; mudstone; coal. Mixed-load channels,flood-plain and swamp.
PRn	Nappamerri Group	Red beds; mudstone; siltstone; sandstone; lithic sandstone. Fluvial, fluvio-lacustrine, streams, high sinuosity streams,
PRna	Arrabury Formation	Red beds, sandstone, siltstone, mudstone carbonaceous in part. Fluvial, fluvio-lacustrine.
Q	Unnamed GIS Unit - see description	Undifferentiated Quaternary rocks
Qa	Unnamed GIS Unit - see description	Undifferentiated alluvial/fluvial sediments

Map Symbol	Stratigraphic Name	Stratigraphic Description
Qe	Unnamed GIS Unit - see description	Undifferentiated aeolian sediments
Qh	Unnamed GIS Unit - see description	Undifferentiated Holocene rocks
Qha	Unnamed GIS Unit - see description	Undifferentiated alluvial/fluvial sediments
Qha4	Unnamed GIS Unit - see description	Proximal alluvial fan sediments with gilgai. Based on Qh2 on CURNAMONA
Qhe	Unnamed GIS Unit - see description	Undifferentiated aeolian sediments
Ql1	Unnamed GIS Unit - see description	Playa sediments
Qp	Unnamed GIS Unit - see description	Undifferentiated Pleistocene rocks
Qpa	Unnamed GIS Unit - see description	Undifferentiated alluvial/fluvial sediments
Qpa2	Unnamed GIS Unit - see description	Gypcreted/carbonate-cemented gravel. Based on Qpt on WARRINA, CURDIMURKA
Qpae	Eurinilla Formation	Alluvial, lacustrine, lacustrine shoreline. red-brown to yellow-brown sand and gravel.
Qpat	Telford Gravel	Polymict gravel, well rounded, includes boulders. Alluvial fan deposits.
Qpav	Avondale Clay	Clay, grey; sandy clay, with vertical mottling.
Qr	Unnamed GIS Unit - see description	Undifferentiated colluvial/regolith sediments
Qr1	Unnamed GIS Unit - see description	Gibber-mantled colluvium. Based on Q on MURLOOCOPPIE
qz	Unnamed GIS Unit - see description	Quartz veins/bodies, undifferentiated
R	Unnamed GIS Unit - see description	Undifferentiated Triassic rocks
sh	Unnamed GIS Unit - see description	Sheared rocks/shearing, undifferentiated
T	Unnamed GIS Unit - see description	Undifferentiated Cenozoic rocks
T_fe	Unnamed GIS Unit - see description	Undifferentiated ferricrete
Taee	Eyre Formation	Pyritic, carbonaceous sand, grain-size ranges from silt to small cobble, with beds of lignite and clay.Clays are montmorillonite, kaolinite and illite.Braided streams.
Tam	Unnamed GIS Unit - see description	Undifferentiated Paleocene - Miocene rocks
TmQ_si	Unnamed GIS Unit - see description	Undifferentiated silcrete
Tope	Etadunna Formation	White dolomite and limestone with green and grey Mg rich claystone and fine-grained sand.
Topn	Namba Formation	Sand, fine to medium-grained, poorly sorted, angular, silt, thin dolomite, oolitic dolomite interbeds. Shallow, brackish to fresh water lakes.
TpQa	Unnamed GIS Unit - see description	Undifferentiated alluvial/fluvial sediments
TpQaw	Willawortina Formation	Sandy mud; silty dolomite, lacustrine, floodplain. Coarse framework supported gravel, braided flow origin and matrix supported clayey gravels (debris flows).
TQ	Unnamed GIS Unit - see description	Undifferentiated Cenozoic -Pleistocene rocks
we	Unnamed GIS Unit - see description	Weathering/weathered rocks, undifferentiated

Instructions for the CD-ROM

Uranium ore-forming systems of the Lake Frome region, South Australia:
Regional spatial controls and exploration criteria

This CD-ROM contains the above-titled Report as Record 2009-40.pdf

View this .pdf document using Adobe Acrobat Reader (click Adobe.txt for information on readers)

Click on: Record 2009-40.pdf to launch the document.

Directories on this CD-ROM:

Figure 3.3 Record 2009-40
Figure 3.4 Record 2009-40
Figure 3.5 Record 2009-40
Figure 3.6 Record 2009-40
Figure 3.7 Record 2009-40
